

CHEMOENZYMATIC SYNTHESIS OF ISOTOPICALLY LABELLED FOLATES

A thesis submitted to Cardiff University for the degree of
Doctor of Philosophy by

Antonio Angelastro

Supervisor: Prof. Rudolf K. Allemann

2017

DECLARATION

This work has not been submitted in substance for any other degree or award at this or any other university or place of learning, nor is being submitted concurrently in candidature for any degree or other award.

Signed (candidate) Date

STATEMENT 1

This thesis is being submitted in partial fulfilment of the requirements for the degree of Doctor of Philosophy

Signed (candidate) Date

STATEMENT 2

This thesis is the result of my own independent work/investigation, except where otherwise stated, and the thesis has not been edited by a third party beyond what is permitted by Cardiff University's Policy on the Use of Third Party Editors by Research Degree Students. Other sources are acknowledged by explicit references. The views expressed are my own.

Signed (candidate) Date

STATEMENT 3

I hereby give consent for my thesis, if accepted, to be available online in the University's Open Access repository and for inter-library loan, and for the title and summary to be made available to outside organisations.

Signed (candidate) Date

STATEMENT 4: PREVIOUSLY APPROVED BAR ON ACCESS

I hereby give consent for my thesis, if accepted, to be available online in the University's Open Access repository and for inter-library loans **after expiry of a bar on access previously approved by the Academic Standards & Quality Committee.**

Signed (candidate) Date

ABSTRACT

Dihydrofolate reductase (DHFR) is a key enzyme in cellular anabolism. It catalyses the reduction of 7,8-dihydrofolate (H₂F) to 5,6,7,8-tetrahydrofolate (H₄F) *via* hydride transfer from the C4 position of NADPH to the C6 position of H₂F accompanied with protonation at the N5 position of H₂F. Due to the importance of DHFR as an anticancer and antimicrobial target, the catalytic mechanism of DHFR has long been the focus of intense research. Kinetic isotope effect (KIE) measurements can provide insight into the mechanism of DHFR catalysis and guide the rational design of novel anti-DHFR drugs. However, because of a lack of a practical strategy to introduce heavy atoms (¹⁵N, ¹³C) into H₂F, current research is mostly restrained to the study of hydrogen isotope effects. In this thesis, a fourteen step, one-pot chemoenzymatic synthesis of labelled H₂F is reported. The flexibility of this synthetic approach enables the production of various isotopically enriched H₂Fs from simple starting materials such as D-glucose. The labelled substrates were used to measure, for the first time, heavy atom KIEs and to derive information about the transition state of the chemical step during DHFR catalysis. This methodology is widely applicable to other biochemically important substrates and cofactors and it can be used for a wide variety of *in vitro* and *in vivo* investigations.

ACKNOWLEDGEMENTS

This PhD thesis marks the realisation of a dream, the end of a journey started decades ago inside a small chemistry lab from a small town in southern Italy, Solofra.

My dream. My journey.

In every journey you make in life, you meet people along the way. People who are fundamental for making your dreams come true. This is one such case, and I would like to express my deepest gratitude to all who helped, supported and guided me during my PhD studies.

Thank you Prof. Rudolf Allemann for having trusted me. It was you who granted me the honour to be your student, to mature as a scientist within your research group, and the support that shaped my passion for science.

Thank you Dr Louis Luk for the training, help, support and the endless discussions we have had during these years. Your teachings and friendship have been precious and fundamental to me.

Thank you to Dr Rob Jenkins and Thomas Williams for your extensive help with my favourite analytical technique: mass spectrometry.

Thank you to all my colleagues from the Allemann group with whom I have shared my passion for science. To Dr Enas Behiry for her help with the pre-steady state kinetics, to Dr Luke Johnson for his fundamental help with NMR spectroscopy (and checking my English!!), to Dr Veronica Gonzalez for her help with cloning, to Dr Juan Faraldos for the enjoyable discussions on terpenes and organic chemistry, and to Dr Melody Demiray with whom I share the passion for coffee and cigarettes.

Thank you to Marianna Loizzi, a beloved friend, colleague and best-housemate-ever with whom I shared both the joy and pain of the PhD life.

Thank you to all the people from the Luk, Casini and Tsai groups with whom I have enjoyed evenings at the pub.

Thank you to my family. My dad, mum, sister, brother and brother-in-law who always granted me unconditional support in every choice I made in my life, including to pursue a PhD in Wales.

Thank you to my extraordinary fiancée, Cinzia.

Last but not least, I would like to thank God and the Divine Mercy of Jesus from whom I have been given the strength and comfort for realising this dream.

TABLE OF CONTENTS

DECLARATION	i
ABSTRACT.....	ii
ACKNOWLEDGEMENTS.....	iii
LIST OF FIGURES	x
LIST OF TABLES	xv
LIST OF ABBREVIATIONS.....	xvi
1. INTRODUCTION.....	1
1.1 The role of enzymes in biology and drug discovery	2
1.2 Kinetic isotope effect: a powerful tool to dissect transition-states on an atomic scale.....	10
1.3 The role of dihydrofolate reductase (DHFR) in pharmacotherapy and drug design.....	13
1.4 The catalytic mechanism of DHFR from <i>Escherichia coli</i>	19
1.5 Synthesis of isotopically labelled folates	25
1.5.1 Isotopic labelling of folate's pterin moiety	26
1.6 How folates are made by nature: the folate <i>de novo</i> biosynthetic pathway	29
1.7 Aims.....	31
2. A DISULFIDE-BASED NADP⁺ RECYCLING SYSTEM WITH A HIGH TURNOVER NUMBER.....	33
2.1 Preface	34
2.1.1 ATP recycling systems.....	35
2.1.2 NADP ⁺ recycling systems	36
2.1.3 The glutaredoxin (GRX) system: an ideal recycling scheme for NADP ⁺	38
2.2 Construction of the glutaredoxin system for NADP ⁺ recycling	39
2.2.1 Gene expression, purification and characterisation of recombinant glutaredoxin 2 (GRX2) and 6-phosphogluconate dehydrogenase (6PGDH).....	40
2.2.1.1 Characterisation and activity assay of 6PGDH	40
2.2.1.2 Characterisation and activity assay of EcGRX2	41
2.2.2 <i>In vitro</i> assembly of the GRX system and determination of the maximal TTN.....	43
2.3 Conclusion.....	47
3. CHEMO-ENZYMATIC SYNTHESIS OF ISOTOPICALLY LABELLED GUANOSINE NUCLEOTIDES	48
3.1 Preface	49
3.1.1 Background: the <i>de novo</i> and salvage pathway of guanosine nucleotides	50
3.2 Chemo-enzymatic synthesis of guanosine nucleotides	53
3.3 Synthesis of isotopically labelled guanine.....	55

3.3.1	Traube purine synthesis of guanine	55
3.3.1.1	Synthesis of [7- ¹⁵ N] and [6- ¹³ C,7- ¹⁵ N] Guanine.....	57
3.3.2	Synthesis of guanine from 5-amino-4-imidazolecarboxamide	59
3.3.2.1	Synthesis of [2- ¹³ C]-guanine	61
3.4	Chemo-enzymatic synthesis of GMP	61
3.4.1	Synthesis of [1',2',3',4',5'- ¹³ C ₅]-, [1',2',3',4',5'- ¹³ C ₅ ,7- ¹⁵ N]-, [1',2',3',4',5'-8- ¹³ C ₆ ,7- ¹⁵ N]- and [2- ¹³ C]-GMP	63
3.5	Chemo-enzymatic synthesis of GTP	68
3.5.1	Gene expression, purification and characterisation of recombinant guanylate kinase (GK)	68
3.6	Conclusion.....	70
4.	CHEMO-ENZYMATIC SYNTHESIS OF ISOTOPICALLY LABELLED H ₂ Fs AND INVESTIGATION OF EcDHFR CATALYSIS VIA HEAVY-ATOM ISOTOPE EFFECTS*	72
4.1	Preface	73
4.2	Cloning, expression, purification and assay of recombinant enzymes constituting the H ₂ F <i>de novo</i> pathway.	74
4.2.1	Activity assay of recombinant enzymes constituting the H ₂ F pathway	75
4.3	Design of H ₂ F chemo-enzymatic synthesis.....	80
4.3.1	DHNATPase enhances GTP-CH-I activity	82
4.3.2	DHPS substrate tolerance simplifies H ₂ F biosynthesis	84
4.4	Synthesis and characterization of labelled H ₂ Fs	86
4.5	Single and multiple heavy-atom isotope effect studies on EcDHFR	92
4.6	Conclusion.....	96
5.	GENERAL CONCLUSIONS	98
6.	MATERIALS AND METHODS	103
6.1	Materials.....	104
6.2	Preparation of solutions, buffers and growth mediums	105
6.2.1	Luria-Bertani (LB) liquid medium	105
6.2.2	Luria-Bertani (LB) solid medium	105
6.2.3	Sterile glycerol solution (50% v/v).....	105
6.2.4	Sterile antibiotic solutions	105
6.2.5	Bradford reagent	106
6.2.6	Molecular cloning buffers	106
6.2.6.1	Transformation buffer I (Tfb-I)	106
6.2.6.2	Transformation buffer II (Tfb-II)	106
6.2.6.3	Transformation buffer III (Tfb-III)	107
6.2.6.4	Transformation buffer IV (Tfb-IV).....	107
6.2.6.5	Tris-acetate-EDTA (TAE) 50X buffer.....	107

6.2.7	Enzyme purification buffers	107
6.2.7.1	Enzyme purification buffer 1 (EPB-1).....	107
6.2.7.2	Enzyme purification buffer 2 (EPB-2).....	107
6.2.7.3	Enzyme purification buffer 3 (EPB-3).....	108
6.2.7.4	Enzyme purification buffer 4 (EPB-4).....	108
6.2.7.5	Enzyme purification buffer 5 (EPB-5).....	108
6.2.7.6	Enzyme purification buffer 6 (EPB-6).....	108
6.2.7.7	Enzyme purification buffer 7 (EPB-7).....	108
6.2.8	SDS-PAGE buffers	109
6.2.8.1	SDS resolving buffer.....	109
6.2.8.2	SDS stacking buffer	109
6.2.8.3	SDS sample buffer	109
6.2.8.4	10X Running buffer	109
6.3	Molecular cloning.....	110
6.3.1	TAE agarose gel electrophoresis	110
6.3.2	Purification of DNA by agarose gel extraction.....	110
6.3.3	Purification of DNA by spin miniprep column	110
6.3.4	Preparation of XL1-Blue super-competent cells.....	111
6.3.5	Amplification of target genes from E.coli chromosomal DNA by polymerase chain reaction (PCR).....	111
6.3.6	Preparation of pET28-a empty vector	113
6.3.7	Ligation of target genes into pET28-a empty vector	113
6.3.8	Analysis of ligation products	114
6.4	Production and purification of recombinant enzymes.....	115
6.4.1	Preparation of BL21(DE3)pLysS and BL21-CodonPlus(DE3)RP competent cells.....	115
6.4.2	Transformation of competent cells with pET28a-gnd, pET28a-grxB, pET28a-gmk and pET28a-nudB vectors	115
6.4.3	Production of recombinant enzymes	116
6.4.4	Purification of recombinant enzymes	117
6.4.4.1	Purification of recombinant enzymes bearing an hexahistidine tag (His-tag)	117
6.4.4.1.1	Purification of GRX2, 6PGDH, XGPRT, GK, DHNA and HPPK	117
6.4.4.1.2	Purification of PRS	118
6.4.4.2	Purification of recombinant wild-type enzymes	118
6.4.4.2.1	Purification of GTP-CH-I, DHPS and EcDHFR.....	118
6.4.4.3	SDS-PAGE analysis	119
6.4.4.3.1	SDS-PAGE gel preparation.....	119

6.4.4.3.2	SDS-PAGE samples preparation.....	119
6.4.4.3.3	SDS-PAGE running protocol	120
6.4.4.4	Enzymes storage.....	120
6.4.4.5	Determining protein and substrates concentration	120
6.4.4.5.1	Bradford assay.....	120
6.4.4.5.2	Beer-Lambert law.....	121
6.4.5	Enzyme activity assays	121
6.4.5.1	Comparison of GTP-CH-I activity with and without DHNTPase	122
6.3.5.2	DHNA, HPPK, DHPS activity assay	122
6.5	Determining GRX system total turnover number (TTN).....	123
6.6	Synthesis of isotopically labelled guanines.....	124
6.6.1	Traube purine synthesis.....	124
6.6.1.1	Synthesis of [5- ¹⁵ N]-2,4,5-triamino-6-hydroxypyrimidine.....	124
6.6.1.2	Synthesis of [7- ¹⁵ N]-guanine	124
6.6.1.3	Synthesis of [6- ¹³ C,7- ¹⁵ N]-guanine.....	125
6.6.2	Synthesis of guanine from 5-amino-4-imidazolecarboxamide	125
6.6.2.1	Synthesis of [2- ¹³ C]-guanine	125
6.7	General procedure for the synthesis of isotopically labelled GMPs	126
6.8	General procedure for the synthesis of isotopically labelled H ₂ Fs	127
6.9	Characterisation of isotopically labelled GMPs and H ₂ Fs	130
6.9.1	NMR spectroscopy.....	130
6.9.1.1	[1',2',3'4',5'- ¹³ C ₅]-GMP	130
6.9.1.2	[1',2',3'4',5'- ¹³ C ₅ , 7- ¹⁵ N]-GMP	130
6.9.1.3	[1',2',3'4',5',8- ¹³ C ₆ , 7- ¹⁵ N]-GMP	130
6.9.1.4	[2- ¹³ C]-GMP	130
6.9.1.5	[5- ¹⁵ N]-H ₂ F	131
6.9.1.6	[6- ¹³ C]-H ₂ F	131
6.9.1.7	[5- ¹⁵ N][6- ¹³ C]-H ₂ F	131
6.9.1.8	[6,7,9- ¹³ C ₃]-H ₂ F	131
6.9.1.9	[5- ¹⁵ N][6,7,9- ¹³ C ₃]-H ₂ F	132
6.9.2	Liquid chromatography – high resolution mass spectrometry (LC-HRMS) 132	
6.10	Pre-steady state kinetics (PSSK) and heavy-atom kinetic isotope effect measurements on EcDHFR.....	132
6.10.1	Preparation of natural abundance H ₂ F for PSSK measurements	132
6.10.2	Single-turnover experiments	133
6.10.3	Errors and their propagation	134

6.10.3.1	Standard deviation and standard error of the mean	134
6.10.3.2	Propagation of uncertainty	134
7.	REFERENCES	135
8.	APPENDICES	150
8.1	Appendix 1. High-resolution mass spectrometry data	151
8.1.1	HRMS of isotopically labelled guanosine monophosphates.....	151
8.1.2	HRMS of isotopically labelled dihydrofolates	154
8.2	Appendix 2. Pre-steady state kinetic data	157
8.3	Appendix 3. Additional SDS-PAGE analyses	159
8.4	Appendix 4. Sequencing data	162
8.4.1	Sequencing of <i>gmk</i>	162
8.4.2	Sequencing of <i>gnd</i>	166
8.4.3	Sequencing of <i>grxB</i>	173
8.4.4	Sequencing of <i>nudB</i>	177
8.5	Appendix 5. Published articles	181

LIST OF FIGURES

Figure 1.1. Reaction coordinate diagram of an uncatalysed chemical reaction compared to its enzyme-catalysed counterpart. In an enzyme-catalysed reaction, the free energy barrier is lowered by providing an alternative pathway where the activation energy needed to reach the transition state (S^\ddagger) is stabilised by the enzyme through the formation of the enzyme-substrate active complex (ES^\ddagger) which collapsed to yield the product (P).....	3
Figure 1.2. Pharmacological target families according to Imming <i>et al.</i> (4).....	3
Figure 1.3. The process of drug discovery. Small molecules are tested <i>in vitro</i> on a suitable biological entity (e.g. enzyme) for therapeutic intervention. Compounds showing the best selectivity/activity profile progress into <i>in vivo</i> studies as drug candidates. Eventually, the drug candidate will be approved and launched on the market.....	5
Figure 1.4. Mechanism of peptide bond hydrolysis catalysed by HIV-protease and examples of non-cleavable isosteres employed in the development of HIV-protease inhibitors. Figure adapted from ref (14) and (17).....	7
Figure 1.5. Sialic acid cleavage catalysed by neuraminidase (NA). Zanamivir and oseltamivir are proposed to mimic the mimic the NA oxocarbenium ion transition-state intermediate. Figure adapted from ref (19).....	8
Figure 1.6. PNP-catalysed phosphorolysis of inosine and its corresponding transition-state analogue, Immucillin-H.....	9
Figure 1.7. Reaction coordinate diagram illustrating the difference in vibrational energy between light (black) and heavy (red) isotopes to reach the transition-state.....	11
Figure 1.8. Kinetic isotope effects map for human PNP. Isotope effects were measured for PNP-catalysed arsenolysis of inosine. Atoms of which the isotope effect has been measured are highlighted in blue (N) and red (C and H), respectively. Figure adapted from ref (32).....	12
Figure 1.9. Reduction of 7,8-dihydrofolate (H_2F) to 5,6,7,8-tetrahydrofolate (H_4F) catalysed by dihydrofolate reductase (DHFR). The pro- <i>R</i> hydride from C4 of NADPH is transferred to <i>Re</i> -face on C6 accompanied with protonation of N5 of H_2F	14
Figure 1.10. Folate coenzymes constituting the one-carbon metabolism. Connections to key metabolic pathways are highlighted. 1 , Dihydrofolate reductase (DHFR); 2 , 10-Formyl- H_4F synthetase (FTHFS); 3 , 10-Formyl- H_4F dehydrogenase (FDH); 4 , 5,10-Methenyl- H_4F cyclohydrolase (MTHFC); 5 , 5,10-Methylene- H_4F dehydrogenase (MTHFD); 6 , 5,10-Methylene- H_4F reductase (MTHFR); 7 , Methionine synthase (MS); 8 , Serine hydroxymethyltransferase (SHMT); 9 , Thymidylate synthase (TS); 10 , 5,10-Methenyl- H_4F synthetase (MTHFS); 11 , Formimino- H_4F cyclodeaminase (FTCD). Figure adapted from ref (49).....	16
Figure 1.11. Antifolate drugs employed in the treatment of cancer, malaria and bacterial diseases.....	17
Figure 1.12. Cartoon representation of the neutron crystal structure of EcDHFR ternary complex with $NADP^+$ and folate (PDB 4PDJ). (A) EcDHFR secondary structure β -sheets (blue) and α -helices (orange) moieties are highlighted. (B) The adenosine binding domain (brown) as well as M20 (red), F-G (blue), G-H (purple) moieties from the loop domain are highlighted.....	20
Figure 1.13. EcDHFR kinetic scheme adapted from (77). Five intermediate species (Michaelis complex, product ternary complex, product binary complex, product release complex and holoenzyme) constituting the catalytic cycle are highlighted. E = enzyme; H_2F = dihydrofolate.....	21

Figure 1.14. Closed (green) and occluded (red) conformations of the M20 loop adopted during EcDHFR catalytic cycle. Both holoenzyme and Michaelis complex are in the closed conformation, whereas the product ternary, binary and release complexes are in the occluded conformation. Structures representing closed and occluded conformations are adapted from PDB 1RX2 and 1RX6, respectively.....	22
Figure 1.15. EcDHFR reaction mechanism proposed by Wan <i>et al.</i> Figure readapted from ref (88).....	24
Figure 1.16. Synthesis of [2- ¹³ C]-folic acid by Cocco <i>et al.</i> (116). The reported overall yield is ~13%.....	27
Figure 1.17. Synthetic route for the production of [5- ¹⁵ N]-folic acid or [6- ¹³ C]-folic acid reported by Selinsky <i>et al.</i> (89). The overall yield is ~5%.....	28
Figure 1.18. Folate <i>de novo</i> biosynthetic pathway.....	30
Figure 1.19. Sequence of chemical reactions catalysed by GTP cyclohydrolase I (GTP-CH-I) from <i>Escherichia coli</i>	30
Figure 2.1. (A) Recycling systems for ATP from ADP. (B) Recycling system for ATP from AMP by coupling of pyruvate kinase (PK) with myokinase (MK).....	36
Figure 2.2. Current recycling systems for NADP ⁺ . Figure adapted from ref (179).....	37
Figure 2.3. The glutaredoxin system. Figure taken from ref (179).....	38
Figure 2.4. (A) SDS-PAGE of purified 6PGDH (MW = 53.6 kDa; fractions 1-4) compared to cell lysate (Lys) before and after (FT) purification. (B) Activity assay of 6PGDH through UV-vis spectroscopy by monitoring NADPH increase at 340 nm. Freeze dried 6PGDH (black) shows a marked activity loss compared to fresh (or 50% glycerol stock) 6PGDH. 6PGDH assay principle is shown in (C)	41
Figure 2.5. (A) SDS-PAGE of purified GRX2 (MW = 26.4 kDa; fractions 1-3) compared to cell lysate (Lys) before and after (FT) purification. (B) GRX2 activity monitored by UV-vis spectroscopy following NADPH decrease at 340 nm. Because GRX2 does not directly oxidise NADPH, GR is coupled to the recombinant enzyme in presence of catalytic quantities of GSH. Oxidation of GSH to GSSG is therefore directly linked to GRX2 resulting into the reduction of HED to β-ME concomitant to the oxidation of NADPH to NADP ⁺ . The assay principle is shown on panel (C) . Compared to fresh (or 50% glycerol stock) GRX2, freeze dried GRX2 (green) suffers of activity loss.....	42
Figure 2.6. Positive ESI-MS of purified GRX2. Deconvoluted experimental molecular weight of the recombinant enzyme was 26,383 amu (calculated 26,368 amu).....	43
Figure 2.7. (A) Conversion of D-glucose to 6-phosphogluconate (6-PG) by hexokinase (HK) and glucose 6-phosphate dehydrogenase (6GPDH). The ATP/ADP and the NADP ⁺ recycling (highlighted in red) systems are composed of pyruvate kinase (PK), glutathione reductase (ScGR) and glutaredoxin 2 (EcGRX2). Conversion of substrate to product has been monitored by ¹³ C-NMR spectroscopy using ¹³ C ₆ -D-glucose as starting material (B) . While at TTN = 5 x 10 ⁵ there was a complete conversion of ¹³ C ₆ -D-glucose to ¹³ C ₆ -6-PG (C) , at TTN = 8 x 10 ⁵ residual peaks from G6P at 96 and 92 ppm indicate an incomplete conversion (D)	45
Figure 2.8. Conversion of D-glucose to ribulose-5-phosphate (Ru5P) by hexokinase (HK), glucose 6-phosphate dehydrogenase (6GPDH) and phosphogluconate dehydrogenase (6PGDH).....	46
Figure 3.1. (A) Structure of guanosine and deoxyguanosine nucleotides. (B) Cofactors such as tetrahydrobiopterin, dihydrofolate, riboflavin and molybdopterin are biosynthetically derived from guanosine triphosphate (GTP). Atoms derived from GTP are highlighted in red.....	50
Figure 3.2. Biosynthesis of GTP through the purine <i>de novo</i> pathway.....	52
Figure 3.3. Biosynthesis of GMP through the purine salvage pathway.....	53
Figure 3.4. General scheme of guanine assembly from either (A) , a substituted pyrimidine, or (B) , an imidazole derivative.....	55

Figure 3.5. (A) Traube purine synthesis of guanine (207). (B) Experimental conditions and yields for cyclisation of (8) to guanine. (C) Ring closure mechanism proposed by Sharma <i>et al.</i> (207) for the morpholine-catalysed reaction.....	56
Figure 3.6. (A) Positive ESI-MS of (A) natural abundance and (B) ¹⁵ N-labelled 2,4,5-triamino-6-hydroxypyrimidine (9)	57
Figure 3.7. (A) Positive ESI-MS and ¹ H-NMR of (A) natural abundance and (B) ¹⁵ N-labelled guanine.....	58
Figure 3.8. (A) Positive ESI-MS, (B) ¹ H-NMR and (C) ¹ H- ¹⁵ N-HMBC of [7- ¹⁵ N,8- ¹³ C]-guanine.....	59
Figure 3.9. (A) Mechanism proposed by Yamazaki <i>et al.</i> (210) for the cyclisation of 5-(N'-benzoyl-S-methylisothiocarbamoyl)amino-4-imidazolecarboxamide (10) to guanine through the <i>in situ</i> formation of 5-cyanoamido-4-imidazolecarboxamide (11) . (B) Synthesis of guanine from 5-amino-4-imidazolecarboxamide (14)	60
Figure 3.10. Positive ESI-MS of [2- ¹³ C]-guanine.....	61
Figure 3.11. Chemo-enzymatic synthesis of guanosine monophosphate (GMP).....	62
Figure 3.12. (A) Syringe-pump system for controlling guanine concentration. Comparison between (B) GMP synthesised by controlled flow of alkaline guanine into the reaction mixture and (C) without syringe pump.....	63
Figure 3.13. (A) ¹ H-NMR and (B) ¹³ C-NMR of [1',2',3',4',5'- ¹³ C ₅]-GMP.....	65
Figure 3.14. (A) ¹ H-NMR of [1',2',3',4',5'- ¹³ C ₅ ,7- ¹⁵ N]-GMP. (B) Purine C8 proton splits as a doublet for the spin-spin coupling to N7 (² J _{NH} = 12 Hz). (C) Isotopically labelled carbons from the ribose moiety are shown by ¹³ C-NMR, while (D) ¹ H- ¹⁵ N-HMBC experiment shows a correlation between C8 proton (δ = 8.00 ppm) to the N7 at 235 ppm.....	66
Figure 3.15. (A) ¹ H-NMR of [1',2',3',4',5',8- ¹³ C ₆ ,7- ¹⁵ N]-GMP. (B) Purine C8 proton splits as a doublet of doublets for the spin-spin coupling to both C8 and N7 atoms (¹ J _{CH} = 213 Hz, ² J _{NH} = 12 Hz). (C) Isotopically labelled carbons from the ribose moiety are shown by ¹³ C-NMR between 100 ppm and 50 ppm, while C2 of the purine ring resonates at 135 ppm. (D) ¹ H- ¹⁵ N-HMBC experiment shows a correlation between C8 proton to the N7 at 235 ppm.....	67
Figure 3.16. (A) ¹ H-NMR and (B) ¹³ C-NMR of [2- ¹³ C]-GMP.....	67
Figure 3.17. Continuation of guanosine monophosphate (GMP) biosynthesis illustrated in figure 3.11 to the formation of guanosine triphosphate (GTP).....	68
Figure 3.18. ESI-MS ⁺ of purified GK R152G mutant. Deconvoluted experimental molecular weight of the recombinant enzyme was 25,526 amu (calculated 25,525 amu).....	69
Figure 3.19. (A) SDS-PAGE of purified GK (MW = 25.5 kDa; fractions 1-2) compared to cell lysate (Lys) before and after (FT) purification. (B) GK activity monitored by UV-vis spectroscopy following NADH decrease at 340 nm. The assay principle is shown on panel (C) . Compared to fresh (or 50% glycerol stock, red) GK, freeze dried GK (green) suffers of activity loss.....	70
Figure 4.1. SDS-PAGE of purified DNTPase by affinity chromatography (fractions 1-2) compared to cell lysate (Lys) before and after (FT) purification. After prolonged heating (right panel) the recombinant enzyme (MW = 19.5 kDa) shifts nearby the 18.4 kDa band of the marker.....	75
Figure 4.2. Formation of DHNTP from GTP catalysed by GTP-CH-I by UV-vis spectroscopy. UV spectra of starting material (blue) and product (red) are highlighted.....	76
Figure 4.3. Anion exchange chromatograms of GTP (A) incubated with GTP-CH-I and (B) GTP-CH-I and DHNTPase.....	77
Figure 4.4. Positive ESI LC-MS of dihydroneopterin (DHN; MW = 255 amu) generated by GTP-CH-I, DHNTPase and ALP.....	78
Figure 4.5. Positive ESI LC-MS of 6-hydroxymethyl-7,8-dihydropterin (HMDP; MW = 195 amu) by GTP-CH-I, DHNTPase, ALP and DHNA.....	78
Figure 4.6. Anion exchange chromatogram of 6-hydroxymethyl-7,8-dihydropterin pyrophosphate (HMDPpp) generated by GTP-CH-I, DHNTPase, ALP, DHNA and HPPK.....	79

Figure 4.7. Positive ESI LC-MS of H ₂ Pte generated from 6-hydroxymethyl-7,8-dihydropterin pyrophosphate (HMDPpp) and p-aminobenzoic acid (pABA) by dihydropteroate synthase (DHPS).....	79
Figure 4.8. Biosynthetic strategy for the synthesis of H ₂ F. Glucose and guanine are processed into the key intermediate guanosine triphosphate (GTP, Chapter 3), which is then reorganized into DHN by GTP-CH-I, DHNTPase and ALP. DHNA, HPPK and DHPS combine DHN with pABA-Glu to yield the final product H ₂ F. Additionally, myokinase (MK), glutathione reductase (GR) and glutaredoxin 2 (GRX2), are used to constitute cofactor regeneration systems for ATP and NADP ⁺ (171, 179).....	81
Figure 4.9. Anion exchange analysis of GTP incubated with GTP-CH-I reveals a partial conversion of GTP into DHNTP. Formation of guanosine monophosphate (GDP) is due to the non-enzymatic hydrolysis of GTP the assay.....	82
Figure 4.10. Comparison of GTP-CH-I activity in absence (black) and presence (red) of DHNTPase monitoring 7,8-dihydropterin formation absorbance at 330 nm by UV-Vis spectroscopy.....	83
Figure 4.11. Anion exchange analysis of GTP incubated with GTP-CH-I and DHNTPase shows total conversion of GTP into DHNMP.....	84
Figure 4.12. (A) In nature, H ₂ F is assembled from HMDPpp, pABA and Glu by dihydropteroate synthase (DHPS) and dihydrofolate synthase (DHFS). (B) <i>In vitro</i> , a shorter route to H ₂ F is made possible by DHPS tolerance to alternative substrates like pABAGlu.....	85
Figure 4.13. (A) ¹ H- ¹³ C HMBC of [6- ¹³ C]-H ₂ F and (B) ¹ H- ¹⁵ N HMBC (right panel) of [5- ¹⁵ N]-H ₂ F.....	88
Figure 4.14. ¹ H- ¹³ C HMBC (left panel) and ¹ H- ¹⁵ N HMBC (right panel) of [5- ¹⁵ N][6- ¹³ C]-H ₂ F.....	88
Figure 4.15. ¹ H- ¹³ C HMBC (left panel) and ¹ H- ¹⁵ N HSQC (right panel) of [6,7,9- ¹³ C ₃]-H ₂ F.....	89
Figure 4.16. ¹ H- ¹³ C HMBC (left panel) and ¹ H- ¹⁵ N HMBC (right panel) of [5- ¹⁵ N][6,7,9- ¹³ C ₃]-H ₂ F.....	89
Figure 4.17. (A) ¹ H-NMR spectrum of natural abundance H ₂ F. (B) 2D-NMR NOESY experiment allows to unambiguously assign H7 and H9 protons, as highlighted in panels (C) and (D) . In the NOESY experiment, H7 protons strongly correlate through space to 5' and 3' protons from pABA moiety whereas cross-correlations between H9 protons and 5'/3' are weaker or not detectable.....	90
Figure 4.18. Sections from ¹ H-NMR spectra of isotopically labelled H ₂ Fs. (A) In ¹ H-NMR spectrum of [5- ¹⁵ N]-H ₂ F, both H7 and H9 are singlets as in natural abundance H ₂ F. (B) When H ₂ F C6 position is ¹³ C-enriched, as in [6- ¹³ C]- and [5- ¹⁵ N,6- ¹³ C]-H ₂ F, H7 and H9 protons split as a doublet (² J _{CH} = 6 Hz) due to the long-range coupling to C6 (C) . In addition to C6, further isotopic enrichment of C7 and C9 positions results in additional splitting of H7 and H9 protons as doublet of doublets because of the short-range coupling of C7 to H7 (¹ J _{CH} = 144 Hz) and C9 to H9 (¹ J _{CH} = 132 Hz).....	91
Figure 4.19. Possible scenarios for the EcDHFR catalysed reaction. (A) Hydride from C4 of NADPH is transferred to C6 of H ₂ F, followed by protonation in a stepwise fashion. (B) Hydride transfer is concomitant to protonation. (C) H ₂ F is firstly protonated, then hydride transfer occurs.....	94
Figure 4.20. (A) SDS-PAGE and (B) positive ESI-MS of recombinant EcDHFR (theoretical MW = 17,999 amu, found = 18,000 amu) used for pre-steady-state kinetic measurements.....	94
Figure 4.21. Heavy-atom KIEs measured on EcDHFR using (A) [5- ¹⁵ N]-H ₂ F, (B) [6- ¹³ C]-H ₂ F and (C) [5- ¹⁵ N][6- ¹³ C]-H ₂ F. (D) Comparison between heavy-atom KIEs indicate a substantial difference between relative contributions of N5 and C6 positions in stabilizing the transition state during hydride transfer.....	96
Figure A.1. Positive TOF HRMS of natural abundance GMP.....	152
Figure A.2. Positive TOF HRMS of [1',2',3',4',5'- ¹³ C ₅]-GMP.....	153
Figure A.3. Positive TOF HRMS of [1',2',3',4',5',8- ¹³ C ₆ ,7- ¹⁵ N]-GMP.....	153

Figure A.4. Positive TOF HRMS of [1',2',3',4',5'- ¹³ C ₅ ,7- ¹⁵ N]-GMP	154
Figure A.5. Positive TOF HRMS of [2- ¹³ C]-GMP.....	154
Figure A.6. Positive TOF HRMS of natural abundance H ₂ F.....	155
Figure A.7. Positive TOF HRMS of [5- ¹⁵ N]-H ₂ F.....	155
Figure A.8. Positive TOF HRMS of [6- ¹³ C]-H ₂ F.....	156
Figure A.9. Positive TOF HRMS of [6- ¹³ C,5- ¹⁵ N]-H ₂ F.....	156
Figure A.10. Positive TOF HRMS of [6,7,9- ¹³ C ₃]-H ₂ F.....	157
Figure A.11. Positive TOF HRMS of [6,7,9- ¹³ C ₃ ,5- ¹⁵ N]-H ₂ F.....	157
Figure A.12. SDS-PAGE of purified PRS (MW = 34,2 kDa; fractions 1-3) compared to cell lysate (Lys) before and after (FT) purification.....	160
Figure A.13. SDS-PAGE of purified XGPRT (MW = 16,8 kDa; fractions 1-2) compared to cell lysate (Lys) before and after (FT) purification.....	160
Figure A.14. SDS-PAGE of purified GTP-CH-I (MW = 24,8 kDa; fractions 1-6) compared to cell lysate (Lys) after size exclusion chromatography.....	161
Figure A.15. SDS-PAGE of purified DHNA (MW = 13,6 kDa; fractions 1) compared to cell lysate (Lys) before and after (FT) purification.....	161
Figure A.16. SDS-PAGE of purified HPPK (MW = 18,1 kDa; fractions 1-3) compared to cell lysate (Lys) before and after (FT) purification.....	161
Figure A.17. SDS-PAGE of purified DHPS (MW = 30,6 kDa; fractions 5-8) compared to cell lysate (Lys) after size exclusion chromatography.....	162

LIST OF TABLES

Table 1.1. Enzymes as pharmacological targets and their modulators in clinical use (shown in bold) (6).....	4
Table 2.1. Experimental TTN value of the GRX system tested for NADP ⁺ recycling determined by ¹³ C-NMR spectroscopy.....	45
Table 3.1. Isotopically labelled GMPs synthesised in this work. ¹³ C is highlighted in red.....	65
Table 4.1. Isotopically labelled H ₂ Fs synthesised in this work. ¹³ C is highlighted in red.....	86
Table 4.2. Heavy-atom KIEs measured on EcDHFR using [6- ¹³ C]-H ₂ F, [5- ¹⁵ N]-H ₂ F and [5- ¹⁵ N][6- ¹³ C]-H ₂ F.....	95
Table 6.1. Primers designed for PCR amplification. Restriction sites for <i>Nde</i> I (CATATG) and <i>Xho</i> I (CTCGAG) are shown in bold.....	112
Table 6.2. PCR protocol for the amplification of <i>gnd</i> , <i>grxB</i> , <i>gmk</i> and <i>nudB</i> genes. After the initial denaturation step, denaturation, annealing and elongations (highlighted) were repeated 30 times before the final elongation.....	113
Table 6.3 Recombinant enzymes used in this work overproduced in <i>E. coli</i> strains.....	117
Table A.1. Pre-steady-state kinetic data for determining ¹⁵ N-KIE on EcDHFR using [5- ¹⁵ N]-H ₂ F.....	158
Table A.2. Pre-steady-state kinetic data for determining ¹³ C-KIE on EcDHFR using [6- ¹³ C]-H ₂ F.....	158
Table A.3. Pre-steady-state kinetic data for determining ¹⁵ N, ¹³ C-KIE on EcDHFR using [5- ¹⁵ N][6- ¹³ C]-H ₂ F.....	159

LIST OF ABBREVIATIONS

5-Methyl-H₄F	5-Methyl-tetrahydrofolate
5,10-Methylene-H₄F	5,10-Methylene-tetrahydrofolate
6PGDH	6-Phosphogluconate dehydrogenase
10-Formyl-H₄F	10-Formyl-tetrahydrofolate
AICART	Aminoimidazole carboxamide ribonucleotide formyltransferase
ATP	Adenosine triphosphate
ADP	Adenosine diphosphate
AMP	Adenosine monophosphate
AK	Acetate kinase
AICAR	5-Aminoimidazole-4-carboxamide ribonucleotide
AIR	5-Aminoimidazole ribonucleotide
ALP	Alkaline phosphatase
ABD	Adenosine binding domain
amu	Atomic mass unit
β-ME	β-Mercaptoethanol
CarK	Carbamate kinase
CreK	Creatine kinase
CAIR	Carboxy-amino-imidazole ribonucleotide
DHN	7,8-Dihydroneopterin
DHNTase	7,8-Dihydroneopterin triphosphate pyrophosphatase

DHNMP	7,8-Dihydroneopterin monophosphate
DHNTTP	7,8-Dihydroneopterin triphosphate
DHPS	Dihydropteroate synthase
DHFR	Dihydrofolate reductase
DHFS	Dihydrofolate synthase
dTMP	Deoxythymidine monophosphate
dUMP	Deoxyuridine monophosphate
EcDHFR	<i>Escherichia coli</i> dihydrofolate reductase
EcGRX2	<i>Escherichia coli</i> glutaredoxin 2
ES[‡]	Enzyme-substrate active complex
FGAR	Formylglycineamide ribonucleotide
FGAM	Formylglycinamide ribonucleotide
FAICAR	N-Formylaminoimidazole-4-carboxamide ribonucleotide
FTHFS	10-Formyl-H ₄ F synthetase
FDH	10-Formyl-H ₄ F dehydrogenase
FTCD	5,10-Methenyl-H ₄ F synthetase
FA	Folic acid
G6PDH	Glucose 6-phosphate dehydrogenase
GTP	Guanosine triphosphate
GMP	Guanosine monophosphate
GDP	Guanosine diphosphate

GDH	Glutamate dehydrogenase
GR	Glutathione reductase
GSH	Glutathione (reduced form)
GSSG	Glutathione (oxidised form)
GRX	Glutaredoxin
G6P	Glucose 6-phosphate
GPAT	Glutamine phosphoribosylpyrophosphate amidotransferase
GAR	Glycinamide ribonucleotide
GARS	Glycinamide ribonucleotide synthetase
GARTFase	GAR transformylase
GK	Guanylate kinase
GTP-CH-I	GTP cyclohydrolase I
GART	Glycinamide ribonucleotide formyltransferase
H₂F	Dihydrofolate
H₄F	Tetrahydrofolate
HED	2-Hydroxyethyl disulphide
HMDP	6-Hydroxymethyl-7,8-dihydropterin
HMDPpp	6-Hydroxymethyl-7,8-dihydropterin pyrophosphate
HPPK	6-Hydroxymethyl 7,8-dihydropterin pyrophosphokinase
HR-MS	High-resolution mass spectrometry

H₂Pte	7,8-dihydropteroate
HK	Hexokinase
IMP	Inosinate monophosphate
IMPDH	IMP dehydrogenase
<i>k</i>_{cat}	Turnover number
<i>K</i>_M	Michaelis constant
KIE	Kinetic isotope effect
<i>k</i>	Rate constant
<i>K</i>_i	Inhibition constant
LP	Loop domain
MS	Mass spectrometry
MS	Methionine synthase
MTHFC	5,10-Methenyl-H ₄ F cyclohydrolase
MTHFD	5,10-Methylene-H ₄ F dehydrogenase
MTHFR	5,10-Methylene-H ₄ F reductase
MTX	Methotrexate
NA	Neuraminidase
NMR	Nuclear magnetic resonance
NADPH	Nicotinamide adenine dinucleotide (reduced form)
NADP⁺	Nicotinamide adenine dinucleotide (oxidised form)
NOX	NADPH oxidase

P	Product
pABA	p-Aminobenzoate
pABA-Glu	p-Aminobenzoyl-L-glutamic acid
PEP	Phosphoenolpyruvate
PK	Pyruvate kinase
PNP	Purine nucleoside phosphorylase
PRPP	Phosphoribose pyrophosphate
PRS	Ribose-phosphate pyrophosphokinase
PRA	5-Phospho-β-D-ribosylamine
PRI	Phosphoriboisomerase
PCR	Polymerase chain reaction
QM/MM	Quantum mechanics/molecular mechanics
Ru5P	Ribulose-5-phosphate
R5P	Ribose 5-phosphate
S	Substrate
S[‡]	Transition state
SAM	S-adenosylmethionine
SHMT	Serine hydroxymethyltransferase
SDS-PAGE	Sodium dodecyl sulfate polyacrylamide gel electrophoresis
ScGR	<i>Saccharomyces cerevisiae</i> glutathione reductase

SAICAR	N-succinyl-5-aminoimidazole-4-carboxamide ribonucleotide
SKIE	Solvent kinetic isotope effect
TS	Thymidylate synthase
TTN	Total turnover number
XGPRT	Xanthine-guanine phosphoribosyl transferase

1. INTRODUCTION

1.1 The role of enzymes in biology and drug discovery

Life is defined as a “condition that distinguishes animals and plants from inorganic matter, including the capacity for growth, reproduction, functional activity, and continual change preceding death” (1). Chemistry underpins all the phenomena observed in life. A countless number of finely tuned chemical reactions occur at precise points inside a living cell. Nucleic acid and protein biosynthesis, production and storage of energy, CO₂ fixation and glucose metabolism are a few examples of all chemistry that takes place inside an organism. For life to be sustainable, a chemical reaction must also occur within a reasonable time scale. Hence, as catalysts designed by nature, enzymes are the foundation of the hierarchy of life. Whereas under neutral conditions the half-times of chemical reactions that have biological importance range between 5 s (CO₂ hydration) and 1.1 billion years (amino acid decarboxylation), enzymes are capable of accelerating the reaction rates up to a factor of 10¹⁹ with an average turnover number (k_{cat}) of ~ 10 s⁻¹ and a catalytic efficiency (k_{cat}/K_M) of $\sim 10^5$ M⁻¹ s⁻¹ (2, 3) by providing a reaction path that has a lower overall energy barrier (Figure 1.1).

Considering that nearly all fundamental cellular events with tight spatial and temporal control are dictated by enzymes, it is not surprising that nearly half (47%) of the drugs currently employed in medicine are enzyme modulators (Figure 1.2) (4, 5). Depending on the source (human, bacterial, parasitic, viral) and role of an enzyme in a determined physio-pathological condition, small-molecules modulating enzymatic activity can be used to address a broad range of disorders. Some examples include inflammatory, cancerous, cardiovascular and neurodegenerative diseases as well as bacterial, parasitic and viral infections (Table 1.1).

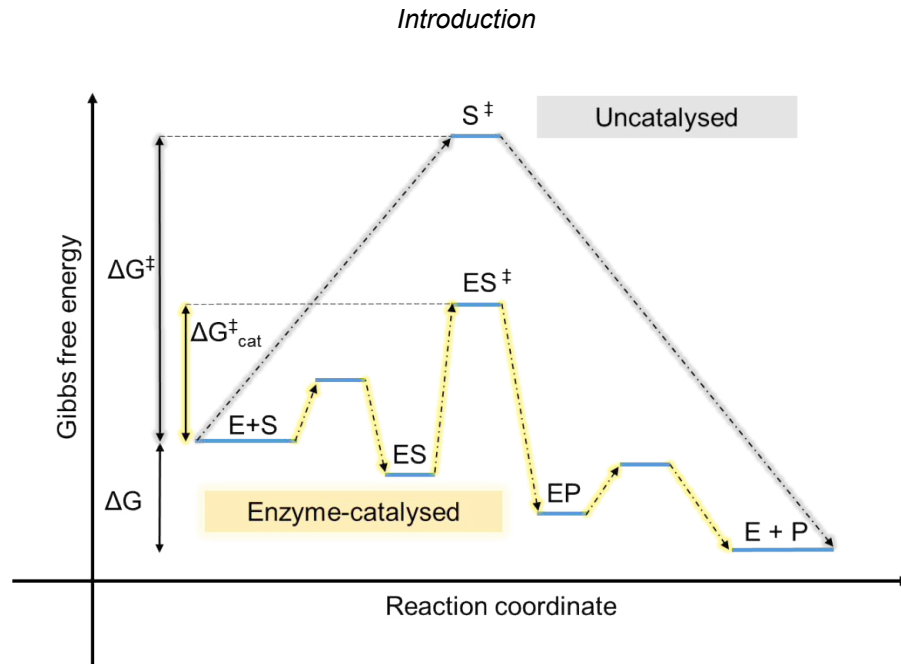


Figure 1.1. Reaction coordinate diagram of an uncatalysed chemical reaction compared to its enzyme-catalysed counterpart. In an enzyme-catalysed reaction, the free energy barrier is lowered by providing an alternative pathway where the activation energy needed to reach the transition state (S^\ddagger) is stabilised by the enzyme through the formation of the enzyme-substrate active complex (ES^\ddagger) which collapsed to yield the product (P).

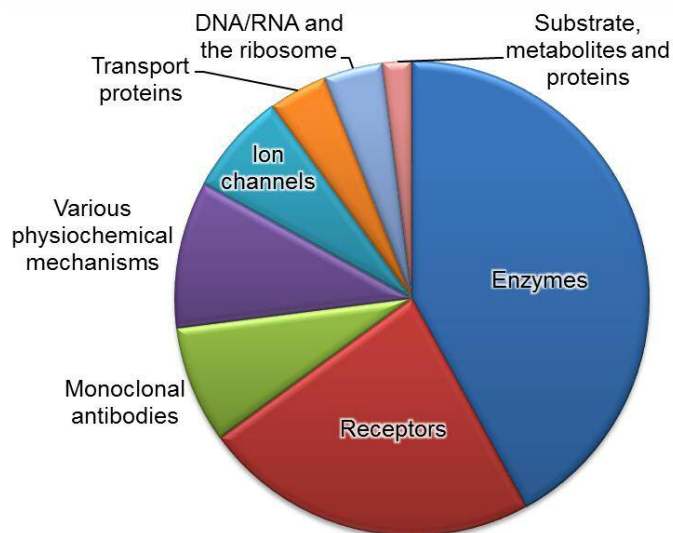


Figure 1.2. Pharmacological target families according to Imming *et al.* (4).

Table 1.1. Enzymes as pharmacological targets and their modulators in clinical use
(shown in bold) (6).

HUMAN
Acetylcholinesterase (Physostigmine), Aldehyde dehydrogenase (Disulfiram), Angiotensin-converting enzyme (Captopril), Carbonic anhydrase (Dorzolamide), Dihydrofolate reductase (Methotrexate), Hydrogen potassium ATPase (Omeprazole), Lipase (Orlistat), GABA transaminase (Valproic acid), DOPA decarboxylase (Levodopa), Tyrosine kinase (Imatinib), Phosphodiesterase III (Milrinone), Phosphodiesterase V (Sildenafil), DNA polymerase (Fluorouracil), HMG-CoA reductase (Lovastatin), Vitamin K epoxide reductase (Warfarin), Cyclooxygenase (Aspirin), Lipoxygenase (Mesalazine), 5 α -testosterone reductase (Finastereide)
BACTERIAL
Alanine racemase (D-cycloserine), Enoyl reductase (Isoniazid), Serine protease (Amoxicillin), Dihydrofolate reductase (Trimethoprim), Peptidyl transferase (Phosphomycin), Dihydropteroate synthase (Sulphamethoxazole), Phosphoenolpyruvate transferase (Chloramphenicol), DNA gyrase (Fluoroquinolones)
VIRAL
Aspartyl protease (Darunavir), Reverse transcriptase (Efavirenz), Glycosidase (Zanamivir), RNA polymerase (Sofosbuvir), DNA polymerase (Acyclovir)
PARASITIC
Δ^{14} -Sterol reductase (Amorolfin), Dihydrofolate reductase (Proguanil)

To transform an enzymatic modulator into a drug, there are three pharmacological requirements: efficacy, tolerability and safety. Ideally, a drug must be specific acting only on its biological target and restoring homeostasis from a pathological condition (efficacy). Any side (tolerability) or toxic (safety)

effects arising from the disruption of other concomitant biological processes must be avoided. In other words, selectivity is an exceptionally crucial issue in drug development, as it dictates whether or not a biologically active compound will be a potential drug candidate (7, 8). In early stages of drug discovery (Figure 1.3), efforts are primarily focused on optimising an active molecule's selectivity and suppressing its undesirable off-target effects through the design, synthesis and screening of compound libraries. This is in general a cost-demanding process with low success rate (8). To reduce the costs and increase the probabilities of developing a drug suitable for the pharmaceutical market, a detailed knowledge on how the target enzyme functions in its own physiological framework by physical, chemical and biological investigations is fundamental.

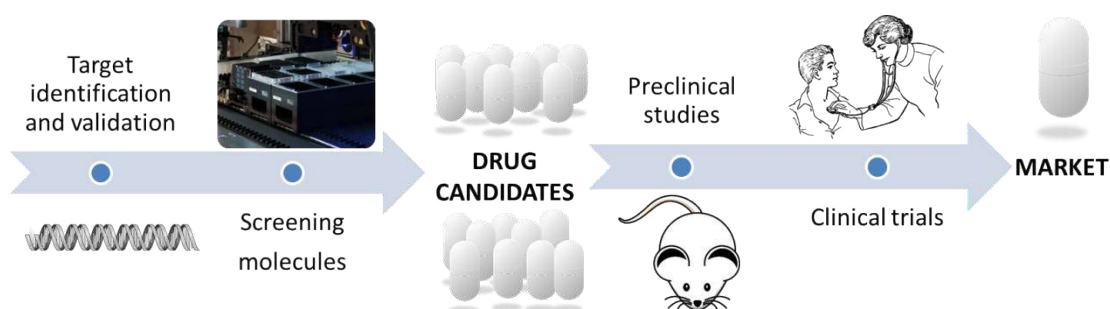


Figure 1.3. The process of drug discovery. Small molecules are tested *in vitro* on a suitable biological entity (e.g. enzyme) for therapeutic intervention. Compounds showing the best selectivity/activity profile progress into *in vivo* studies as drug candidates. Eventually, the drug candidate will be approved and launched on the market.

In modern drug discovery, inhibition is the most common approach to modulate enzymes for therapeutic intervention. Linus Pauling in 1946 was first to point out that “many chemotherapeutic agents exercise their activity by acting as inhibitors to an enzymatic reaction through competition with an essential metabolite of

similar structure” (9). Today, this remark has matured into the general concept that a small-molecule mimicking the transition-state of an enzyme-catalysed reaction provides both powerful inhibition and high selectivity required for a drug candidate that is suitable to progress throughout clinical investigations (10, 11). In the reaction pathway from substrate (S) to product (P) of an enzyme-catalysed reaction (Figure 1.1), the transition-state (ES^\ddagger) represents the highest energy and most unstable transient structure involved. Enzyme active sites, by providing the optimal shape and electrostatic environment, bind to S^\ddagger structure to form the ES^\ddagger complex with high selectivity and dissociation constants estimated between 10^{-14} and 10^{-23} M, significantly lower than those for S and P (12). Consequently, a stable molecule that is most structurally and electrostatically similar to S^\ddagger is expected to bind tightly to the enzyme’s active site.

Information derived from mechanistic studies of enzyme catalysis has been directly used in the design of clinically used drug molecules. This includes the development of HIV-protease inhibitors (e.g. darunavir) (13, 14). Being used during the maturation of essential viral enzymes from their inactive polyprotein precursors, including reverse transcriptase, RNase H and integrase (15), HIV-protease has a pivotal role in the progression of the life cycle of HIV and hence is an anti-viral target (16). This enzyme is an aspartyl protease that cleaves a peptide bond through a general acid-base mechanism where a water molecule, activated by an aspartate residue, performs a nucleophilic attack at the carbonyl group of the peptide bond (Figure 1.4) (14). The consequential tetrahedral intermediate collapses to yield a carboxylate and amine as hydrolysis products. In the rational design of HIV-protease inhibitors, the sp^3 carbon of the oxyanion intermediate can be mimicked by replacing it with noncleavable isosteres such as hydroxyethylene, reduced amide and dihydroxyethylene moieties (14).

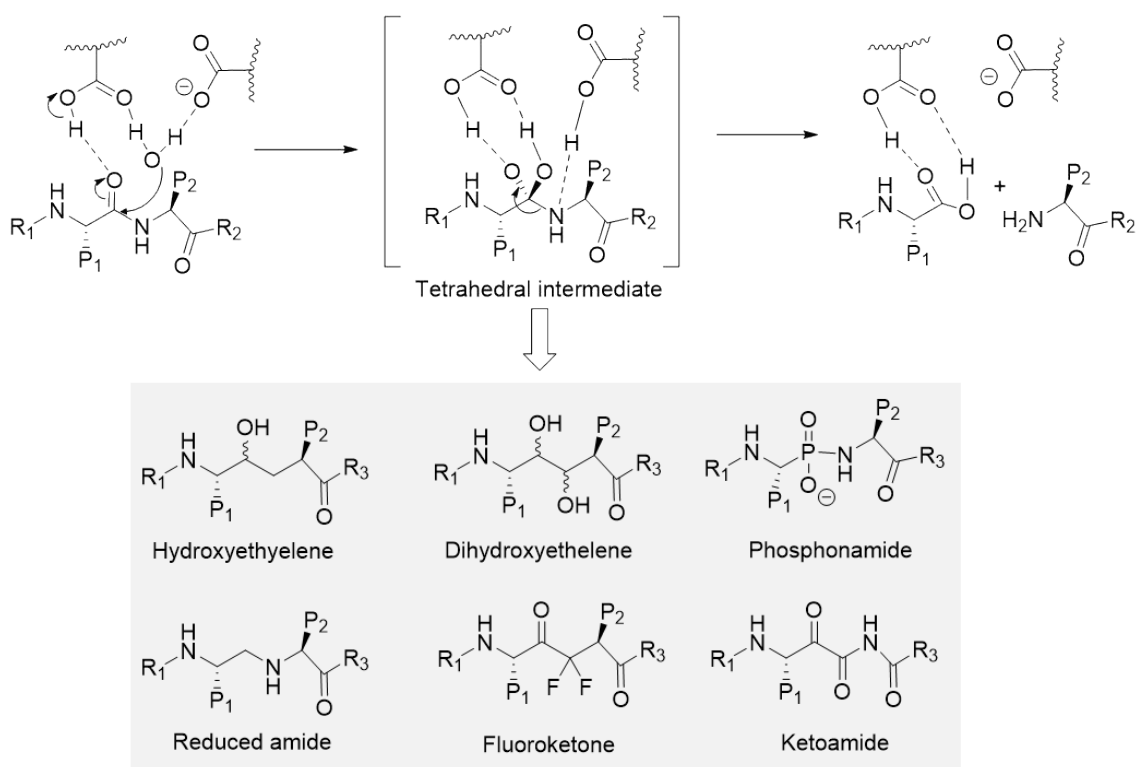


Figure 1.4. Mechanism of peptide bond hydrolysis catalysed by HIV-protease and examples of non-cleavable isosteres employed in the development of HIV-protease inhibitors. Figure adapted from ref (14) and (17).

The transition-state analysis approach has also been used in the development of zanamivir and oseltamivir which target neuraminidase (NA) from influenza virus (18, 19). NA is a glycosidase (or sialidase) needed to remove sialic acid from glycoproteins through the cleavage of an α -ketosidic bond (Figure 1.5). Because this reaction is fundamental to spread virions from infected cells to healthy hosts, inhibition of NA eventually results in halting of the influenza virus life cycle. Zanamivir and oseltamivir are proposed to mimic the NA oxocarbenium ion transition-state intermediate the existence of which was first hypothesised based

on the results obtained from kinetic isotope effect (KIE) measurements, nuclear magnetic resonance (NMR) and molecular dynamics studies (19, 20).

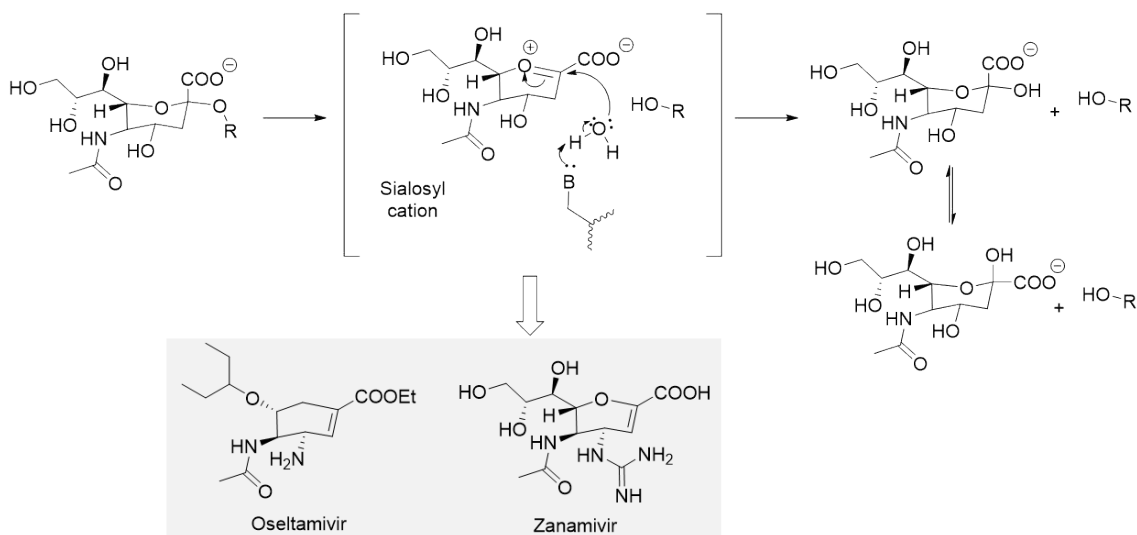


Figure 1.5. Sialic acid cleavage catalysed by neuraminidase (NA). Zanamivir and oseltamivir are proposed to mimic the NA oxocarbenium ion transition-state intermediate. Figure adapted from ref (19).

The discovery of immucillin-H (Forodesine), a powerful purine nucleoside phosphorylase (PNP) inhibitor with picomolar affinity, is a classic example of the full potential of inventing drug candidates by combining fundamental enzymology with drug discovery (21, 22). PNP catalyses the phosphorolysis of ribonucleosides (*e.g.* inosine) or deoxyribonucleosides (*e.g.* deoxyguanosine) to ribose- or deoxyribose-1-phosphate and the respective purine base (23). It was established that a complete inhibition of PNP in human T-cells causes an accumulation of deoxyguanosine, which eventually leads to cell death due to altered DNA metabolism (24). Because in human tissues only T-cells undergo apoptosis upon PNP inhibition, this represents an opportunity to address the

treatment of malignant and autoimmune diseases including T-cell lymphomas (25). However, PNP inhibition must be exceptionally tight for deoxyguanosine to reach toxic intracellular concentrations (26). To this end, Schramm and co-workers, guided by a detailed transition-state map of PNP structural and electronic features, designed the transition-state analogue immucillin-H, which inhibits human PNP with a pM inhibition constant (K_i) (Figure 1.6) (22). Immucillin-H showed a good safety and tolerability profile even at high dosage during phase I and II clinical trials (27, 28), providing an important proof of concept about the potential applications of transition-state analysis to drug design.

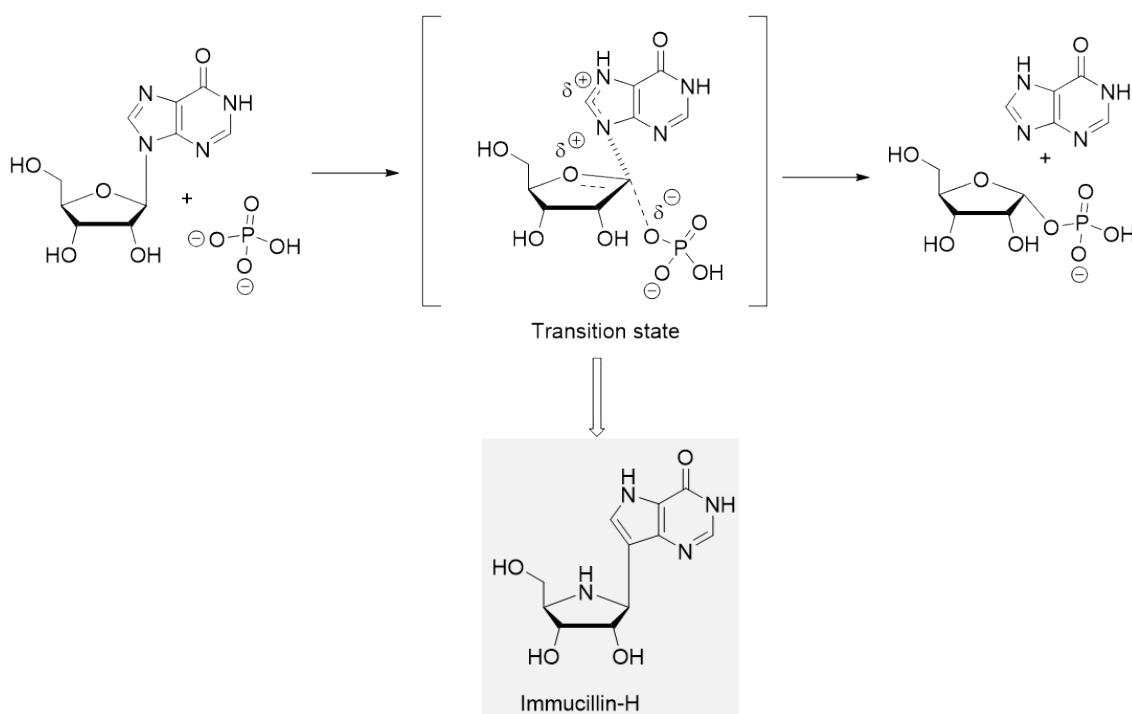


Figure 1.6. PNP-catalysed phosphorolysis of inosine and its corresponding transition-state analogue, Immucillin-H.

1.2 Kinetic isotope effect: a powerful tool to dissect transition-states on an atomic scale.

The transition-state of an enzyme-catalysed reaction is a metastable, short-lived species with a lifetime of $\sim 10^{-14}$ s (12), and thus its characterisation is a non-trivial task. Its features, including the structural and electronic rearrangements occurring in the ES^\ddagger complex, need to be experimentally verified under nearly physiological conditions. Because of these strict requirements, the measurement of kinetic isotope effects (KIEs) is the physical technique that can provide accurate information about the transition state species. KIE is defined as “the effect on the rate constant of two reactions that differ only in the isotopic composition of one or more of their otherwise chemically identical components” (29). This difference in reaction rates reflects the different contribution to the stabilization of the transition state between “light” (e.g. ^1H , ^{12}C , ^{14}N) and “heavy” (e.g. ^2H , ^{13}C , ^{15}N) isotopes in terms of vibrational energies at the zero point (Figure 1.7), and it is defined as:

—

where k_L and k_H denote the reaction rate constants for the light and heavy isotope, respectively. When reactants approach the transition state, there is progressive distortion of their atomic framework with altered bond lengths and electrostatics. In general, atoms directly involved in the formation and/or breakage of chemical bonds during the transition-state yield relatively high KIE values and they are therefore defined as “primary”. Although to a lesser extent, atoms directly adjacent to the reaction centre contribute to stabilization as well, and they are defined as “secondary”. Hydrogen KIEs are measured by replacing ^1H with either

deuterium (^2H) or tritium (^3H), and they are relatively easy to measure because of the significant mass difference between the isotopes. Isotope effect involving $^{12}\text{C}/^{13}\text{C}$, $^{14}\text{N}/^{15}\text{N}$, $^{16}\text{O}/^{18}\text{O}$ are generally referred to as heavy-atom KIEs and they are more difficult to detect compared to hydrogen KIEs (30).

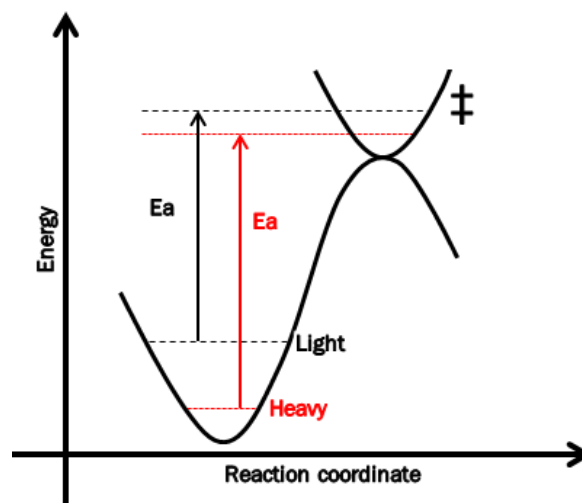


Figure 1.7. Reaction coordinate diagram illustrating the difference in vibrational energy between light (black) and heavy (red) isotopes to reach the transition-state.

In the transition-state analysis of the PNP-catalysed reaction, hydrogen and heavy-atom KIEs were measured for each atomic position participating to the formation of the transition state with an accuracy of better than 0.5% (Figure 1.8) (31). This required the synthesis of isotopically labelled substrates to probe the KIE for each position. Although KIE values do not represent a direct observation of the transition-state, they can be used to construct a computational model, using both quantum mechanical and semi-empirical approaches, by matching bond length and atoms to the experimental KIEs. The electronic distribution at the van der Waals surface was computed for the resulting structure, which has eventually been used in the design of immucillin-H (22, 32).

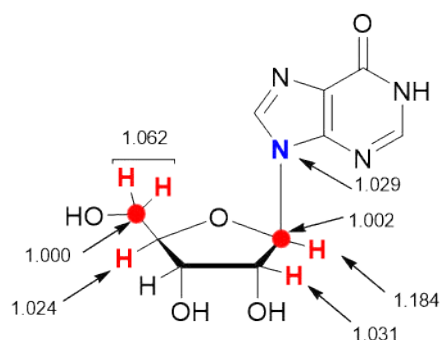


Figure 1.8. Kinetic isotope effect map for the reaction catalysed by human PNP. Isotope effects were measured for the PNP-catalysed arsenolysis of inosine. Atoms for which the isotope effects were measured are highlighted in blue (N) and red (C and H), respectively. Figure was adapted from ref (32).

In addition to the construction of transition-state models, results obtained from KIE measurements can provide a diverse range of information that is useful in drug discovery. The investigation of neuraminidase (NA) by KIE measurements has revealed that the substrate contains significant oxocarbenium character during the chemical transformation; based on these findings, an oxocarbenium intermediate, zanamivir, was designed (18-20). KIE measurements are also valuable in understanding mechanistic aspects related to drug resistance. Resistance against HIV-protease inhibitors is an emblematic example. More than 10 HIV-protease inhibitors with a K_i between nano- and picomolar concentration have been developed and marketed from 1995. However, because of the high viral replication rate combined to a poor proof-reading ability of HIV reverse transcriptase (33), the use of these inhibitors has selected HIV-protease variants that are resilient to inhibition (34). It is estimated that mutation of approximately 37 residues out of the 99-residue sequence can yield an HIV-protease variant resistant to protease inhibitors (35). Most importantly, these mutations may be

additive, implying an impressive combination of possible cross mutations. Hence, it has become difficult to define a common mechanism of resistance on a molecular level (35). Although X-ray crystallography studies helped to spot altered inhibitor-enzyme interactions (34), comparing transition-state maps between wild-type HIV-protease and its mutants based on KIE measurements showed that resistance is not related to the catalytic mechanism itself, but rather to a different stabilization of intermediates along the reaction pathway (17).

1.3 The role of dihydrofolate reductase (DHFR) in pharmacotherapy and drug design.

Though often found to be useful in drug discovery, rational design of enzymatic inhibitors aided by KIE interpretation and transition-state analysis remains an underexploited approach (36, 37), mainly because the synthesis of specifically isotopic labelled substrates needed for KIE measurements is challenging. Accordingly, this render to the use of inhibitors not resembling the transition-state or not capturing any transition-state binding energy; instead, they are small-molecules occupying the active site with an affinity constant higher than the natural substrate. Although a systematic and scientifically acceptable approach to the discovery of new drugs began in the early 1900s (38, 39), the use of rational design for drug development is relatively recent. In 1980s, when protein crystallography and computational chemistry were established methodologies, the design of a small-molecules using enzyme's active sites as a footprint became the dominant strategy to the discovery of new drugs by structure-based, computer-aided and fragment-based drug design approaches (40-42). Before these advancements, drugs were mostly discovered either serendipitously or

through blind screening, that is without any useful knowledge about the enzymatic target to allow a rational design approach (43).

The development of inhibitors of the pharmacological target dihydrofolate reductase (DHFR) highlights the need of producing isotopically labelled substrates for KIE measurement. Found in almost all organisms – from bacteria and protozoa to mammals – DHFR catalyses the reduction of dihydrofolate (H₂F) to tetrahydrofolate (H₄F) *via* hydride transfer from C4 of NADPH to C6 of H₂F and protonation of N5 of H₂F (Figure 1.9) (44).

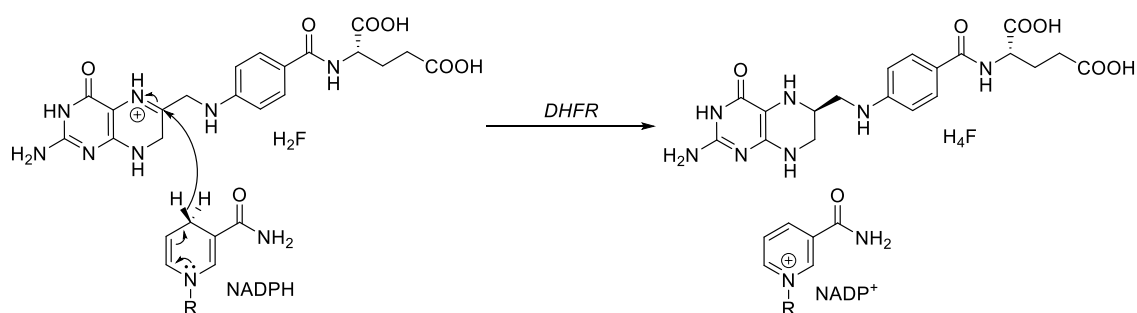


Figure 1.9. Reduction of 7,8-dihydrofolate (H₂F) to 5,6,7,8-tetrahydrofolate (H₄F) catalysed by dihydrofolate reductase (DHFR). The *pro-R* hydride from C4 of NADPH is transferred to the *Re*-face on C6 accompanied with protonation of N5 of H₂F.

H₄F is the source of a series of structurally-related coenzymes involved in the one-carbon metabolism, in which single carbon units activated in different oxidation states are shuttled within a cell to sustain fundamental anabolic processes (Figure 1.10) (45). 5-Methyl-tetrahydrofolate (5-methyl-H₄F) is the cofactor needed by methionine synthase (MS) to regenerate methionine from homocysteine, which is required for S-adenosylmethionine (SAM) biosynthesis. In the cell, SAM acts as donor for methyl group transfer reactions, including DNA

and histones methylation (46). Folate metabolism also has an important role in keeping a balanced pool of serine and glycine amino acids (47). Because cancerous cells are highly dependent on serine, it is hypothesised that carbon units shuttled in the folate metabolism are mainly provided by this amino acid (48). Notably, the one-carbon cycle is essential to sustain nucleic acid production. 5,10-Methylene-tetrahydrofolate (5,10-methylene-H₄F) is needed in pyrimidine biosynthesis by thymidylate synthase (TS) to generate deoxythymidine monophosphate (dTMP) from deoxyuridine monophosphate (dUMP). 10-Formyl-tetrahydrofolate (10-formyl-H₄F) is employed in two biochemical reactions catalysed by glycinamide ribonucleotide (GART) and aminoimidazole carboxamide ribonucleotide (AICART) formyltransferases for the *de novo* biosynthesis of purines. Given the central importance of the one-carbon metabolism in sustaining cellular proliferation, disruption of the DHFR catalytic cycle has life-threatening consequences for a cell.

Introduction

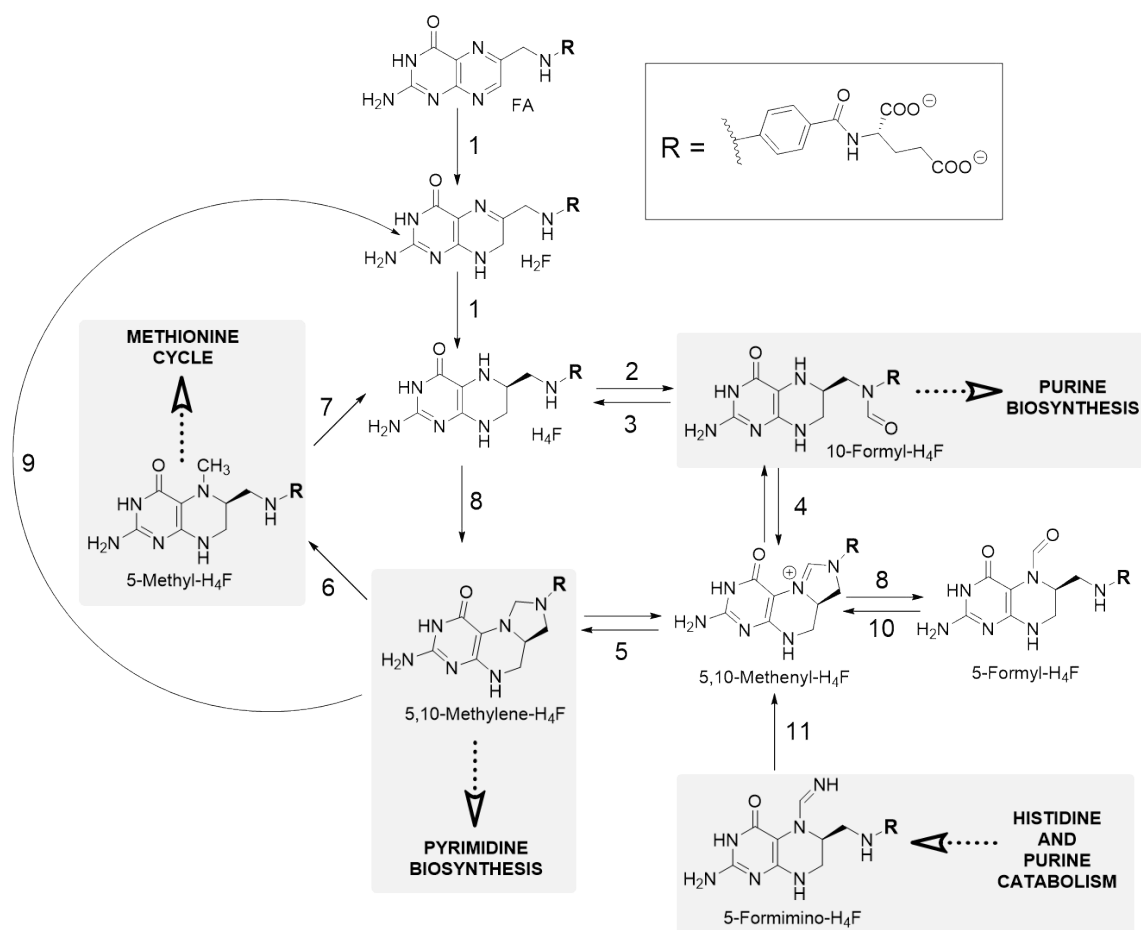


Figure 1.10. Folate coenzymes constituting the one-carbon metabolism. Connections to key metabolic pathways are highlighted. **1**, Dihydrofolate reductase (DHFR); **2**, 10-Formyl-H₄F synthetase (FTHFS); **3**, 10-Formyl-H₄F dehydrogenase (FDH); **4**, 5,10-Methenyl-H₄F cyclohydrolase (MTHFC); **5**, 5,10-Methenyl-H₄F dehydrogenase (MTHFD); **6**, 5,10-Methylene-H₄F reductase (MTHFR); **7**, Methionine synthase (MS); **8**, Serine hydroxymethyltransferase (SHMT); **9**, Thymidylate synthase (TS); **10**, 5,10-Methenyl-H₄F synthetase (MTHFS); **11**, Formimino-H₄F cyclodeaminase (FTCD). Figure adapted from ref (49).

Inhibition of human or microbial DHFR is an effective strategy to stem uncontrolled cellular growth typical of malignancies as well as eradicate microbial infections. Indeed, DHFR was the first enzymatic target to be exploited in cancer therapy, since aminopterin was reported in 1948 to reverse childhood acute

leukaemia (50). A decade later, methotrexate (MTX) was introduced to treat choriocarcinoma (51, 52), and it remains one of the most used anticancer drugs to date. A series of small-molecules targeting parasitic DHFRs were reported as well. Proguanil, developed through a British research programme during the Second World War, was shown to have antimalarial properties (53, 54); this was followed by the discovery of pyrimethamine in 1951 (55). Trimethoprim, introduced in the late 1960s, preferentially inhibits bacterial DHFRs (56). It is worthwhile to point out that all antifolate drugs (aminopterin, MTX, proguanil, pyrimethamine, trimethoprim) discussed here (Figure 1.11) are neither the result of rational drug design nor was their mechanism of action fully understood at the time of their discovery (57). It was only during 1990s, with the aim to tackle resistance to MTX, that a “next generation” antifolates, including pemetrexed, were (at least in part) rationally designed (58-61).

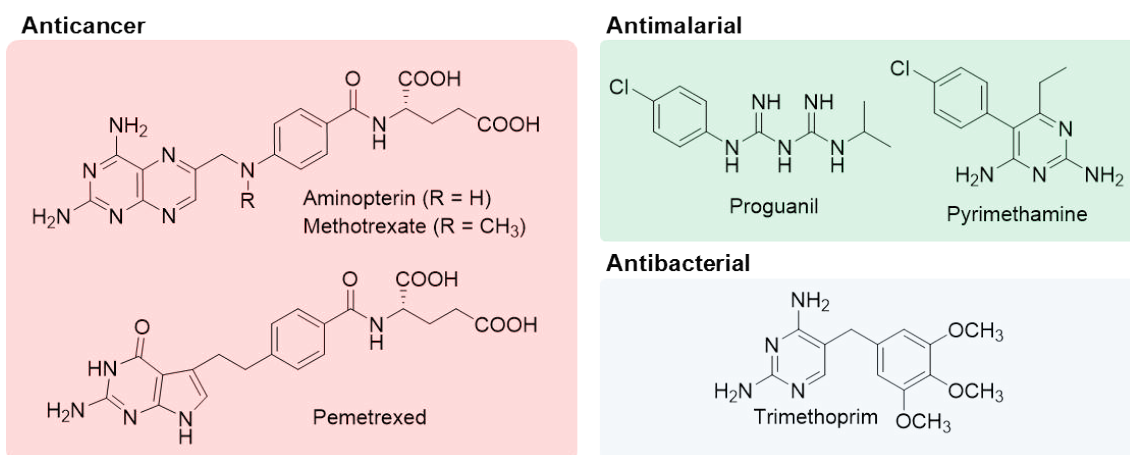


Figure 1.11. Antifolate drugs employed in the treatment of cancer, malaria and bacterial diseases.

Drug resistance is one of the socioeconomic and health challenges that drives the scientific community to design new antifolate drugs (60, 61). Unfortunately, this issue is not only related to the increasing failure of MTX in treating cancer, but it is common to all anti-DHFR drugs. While in the last decades there has been a satisfactory output of novel antifolates for anticancer therapy (60), new generation of drugs targeting malarial and bacterial DHFRs has yet to come (62). In general, mechanisms of antimicrobial resistance are classified in three main categories (63): (1) reduction of an antibiotic's intracellular concentration either by preventing its cell uptake through a reduced permeability or by increasing cellular expulsion through efflux pumps located in the cell's membrane; (2) antibiotic metabolism to inactive compounds *via* enzyme-catalysed biochemical modifications including hydrolysis and phosphorylation; and (3) mutations of the gene codifying the target enzyme.

Resistance against microbial anti-DHFR drugs predominantly occurs by mutations of the chromosomal gene resulting in an enzyme having decreased affinity to the inhibitor (62, 64). Additionally, bacteria can also acquire plasmid-encoded resistant DHFR through the horizontal transfer of exogenous DNA (65). To minimise the development of drug resistance, trimethoprim or proguanil are commonly co-administered with other drugs that act on other targets, *e.g.* dihydropteroate synthase (DHPS, figure 1.13). Because DHPS is involved in the *de novo* biosynthesis of H_2F (section 1.6), its inhibition causes a sharp fall of the intracellular H_2F concentration which negatively affects the one-carbon metabolism. Combination of trimethoprim with DHPS-targeting sulfamethoxazole (Co-trimoxazole) is used in the treatment of urinary, lung and ear infections (66). Association of proguanil with the DHPS-targeting drug dapsone is instead a valid option for prophylaxis and treatment of malaria (67).

1.4 The catalytic mechanism of DHFR from *Escherichia coli*

DHFR from *E. coli* (EcDHFR) is one of the most investigated enzymes. While the first X-ray crystal structure of EcDHFR was reported in 1977 (68), to date about 90 structures, including enzyme-ligand complexes with NADP⁺, folic acid and various inhibitors (e.g. MTX, trimethoprim), are available in the Protein Data Bank. The wealth of structural details prompted the use of EcDHFR as a preferred model in the discovery of antimicrobial DHFR inhibitors, including structure-based drug design (69-72) and high-throughput screening campaigns of large compound libraries (73, 74).

EcDHFR is a monomeric protein composed of 159 amino acids (17,999 amu) (UniProtKB – P0ABQ4) folded into an eight-stranded β -sheet (β A - β H) and four α -helices (α B, α C, α E and α F) (Figure 1.12) (75). Strands β A - β G are parallel whereas β H is antiparallel (75). Two structural subdomains divided by the active site cleft, the adenosine binding domain (ABD) and loop domain (LP), were identified (76). ABD (residues 38-88) binds the adenosine moiety of NADPH, while three loops, M20 (residues 9-24), F-G (residues 116-132) and G-H (residues 142-150), constitute overall the LD region interacting with H₂F. Within the active site, at the interface between ABD and LP subdomains, H₂F pterin ring lies in between helices α B and α C, close to NADPH nicotinamide moiety.

The binding of EcDHFR to its ligands (NADPH, NADP⁺, H₂F and H₄F) was determined by pre-steady state kinetics studies, allowing to depict its catalytic cycle under physiological conditions (Figure 1.13) (77). E:NADPH:H₂F is the catalytically productive Michaelis complex, where NADPH C4 hydride is transferred to H₂F C6 yielding the product ternary complex (E:NADP⁺:H₄F). After hydride transfer, NADP⁺ is first released forming the product binary complex

(E:H₄F). Subsequently, NADPH binds to the enzyme forming the product release complex (E:NADPH:H₄F) where H₄F is thereafter discharged to produce the E:NADPH holoenzyme. EcDHFR holoenzyme eventually loads the next H₂F substrate starting a new catalytic cycle.

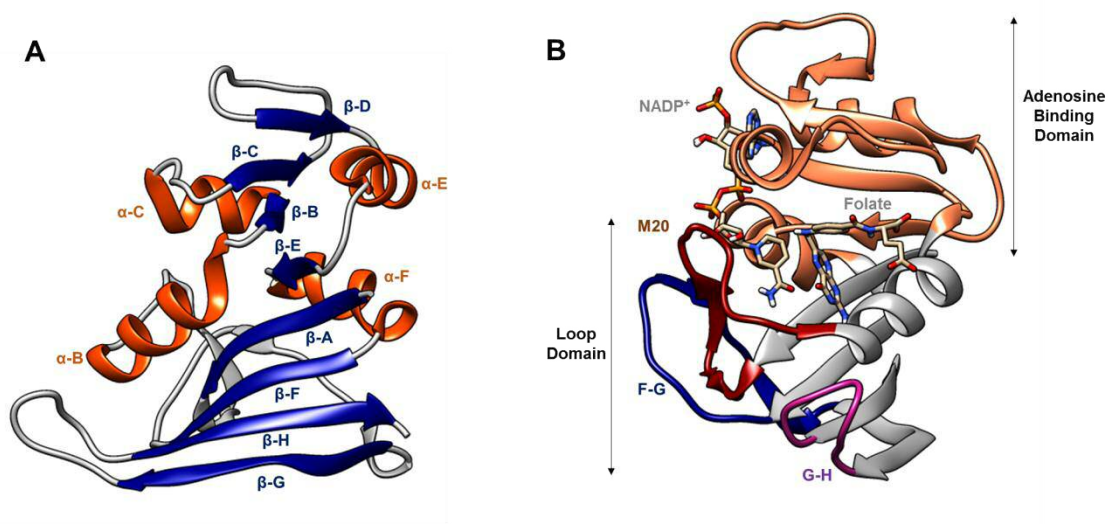


Figure 1.12. Cartoon representation of the neutron crystal structure of EcDHFR ternary complex with NADP⁺ and folate (PDB 4PDJ). **(A)** EcDHFR secondary structure β -sheets (blue) and α -helices (orange) moieties are highlighted. **(B)** The adenosine binding domain (brown) as well as M20 (red), F-G (blue), G-H (purple) moieties from the loop domain are highlighted.

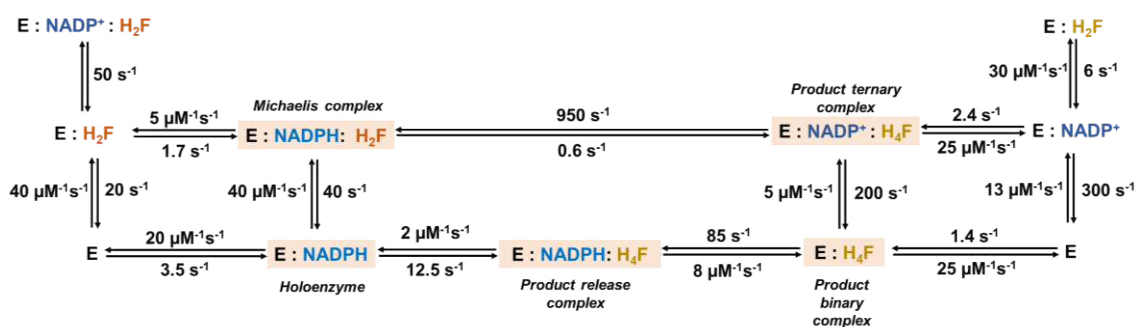


Figure 1.13. EcDHFR kinetic scheme adapted from ref (77). Five intermediate species (Michaelis complex, product ternary complex, product binary complex, product release complex and holoenzyme) constituting the catalytic cycle are highlighted. E = enzyme; H₂F = dihydrofolate.

X-ray crystallography and NMR studies of the five enzyme-substrate intermediates participating in the catalytic cycle revealed that major conformational changes occur during EcDHFR catalysis (78, 79). In particular, the M20 loop switches from a “closed” conformation in the Michaelis complex to an “occluded” conformation in the product ternary complex (Figure 1.14) (79). The M20 loop is in the closed conformation in the Michaelis complex and shields both substrates from solvent interference, forming a microenvironment where the nicotinamide moiety of NADPH and the pterin ring of H₂F are juxtaposed for hydride transfer. The reduction of H₂F to H₄F concomitant to oxidation of NADPH to NADP⁺ is accompanied by a conformational change of the M20 loop from the closed to the occluded state, in which Met16 partially occupies the active site of EcDHFR by replacing NADP⁺ pyridine ring (78). Such conformational changes were shown to be essential to EcDHFR catalysis, and it has been proposed that M20 loop movements contribute to the stabilization of the transition state (78, 80, 81). Because of this relationship between protein motions and catalysis, EcDHFR is extensively used as a model in fundamental enzymology (82).

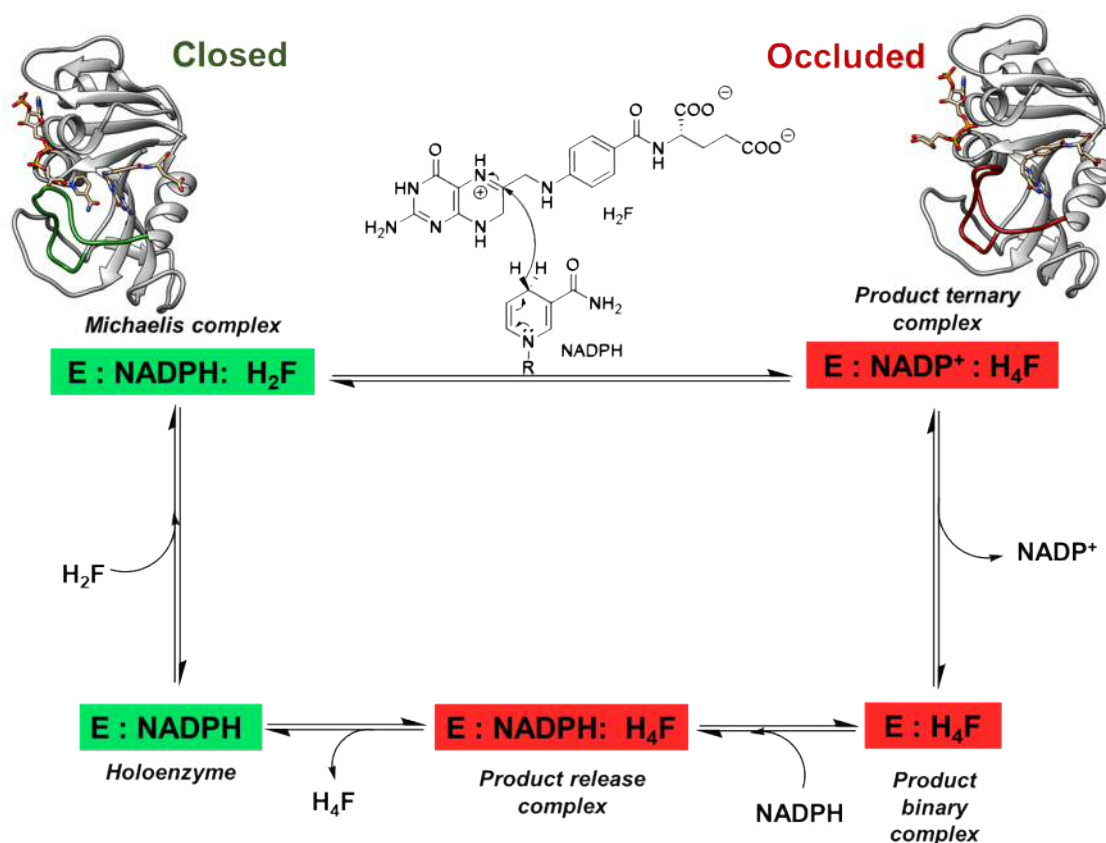


Figure 1.14. Closed (green) and occluded (red) conformations of the M20 loop adopted during EcDHFR catalytic cycle. Both holoenzyme and Michaelis complex are in the closed conformation, whereas the product ternary, binary and release complexes are in the occluded conformation. Structures representing closed and occluded conformations are adapted from PDB 1RX2 and 1RX6, respectively.

During EcDHFR catalysis, protonation of H_2F N5 is a chemical event intimately connected to NADPH *pro-R* hydride transfer to C6 H_2F *Re*-face, and pH-dependency of enzymatic kinetic parameters underlines the importance of N5 protonation for catalytic efficiency (83). Interestingly, all DHFRs contain a single ionisable carboxylic acid residue within their active site, being either glutamic acid in vertebrates or aspartic acid in bacteria (84). While H_2F N5 pK_a is 6.5 in EcDHFR Michaelis complex (77), mutation of Asp27 to Ser, the only acidic residue within the active site, causes a dramatic shift of the pK_a value to 3.8,

resulting in impaired catalysis at neutral pH (85). Nevertheless, Asp27-mutated EcDHFR can still function at a sufficiently acidic pH, suggesting that protonated H₂F (H₃F⁺) coming from the solvent is the active species required for catalysis (85). This hypothesis was further supported by the increase of k_{cat} value with decreasing pH for both wild-type and Asp27-mutated EcDHFRs (85). It is also worthwhile to note that at physiological conditions H₄F release is the rate limiting step in EcDHFR catalysis, whilst at pH > 9 hydride transfer becomes rate limiting (77).

Since Asp27 is the only acidic residue inside the active site cavity, it is reasonable to propose that this residue acts as the proton source during catalysis. However, X-ray crystallographic studies performed by Bystroff *et al.* showed that Asp27 stabilises the pterin ring of H₂F *via* hydrogen bonding to N3 and the amino group attached to C2 rather than being in proximity of H₂F N5 (86). In an attempt to explain the role of Asp27 in catalysis, an indirect protonation mechanism was initially proposed where Asp27 promotes enolisation of H₂F pterin from keto- to enol-form, so that a water molecule buried within the active site can donate a proton to H₂F N5 (86). However, energy minimisations and molecular dynamics simulation studies performed by Shrimpton & Allemann did not support such a mechanism (87). Recently, Wan *et al.* solved the ultra-high-resolution X-ray structure of the EcDHFR pseudo-Michaelis complex with folate and NADP⁺, providing experimental evidences that definitely exclude the keto-enol mechanism proposed by Bystroff *et al.* (88). In Wan *et al.* work, Asp27 was shown to be negatively charged while the folate pterin ring lies within the active site in the keto-form. Folate N5 position was found protonated by a nearby water molecule, of which access into the active site is facilitated by M20 loop movements (Figure 1.15). To date, it is accepted EcDHFR facilitates H₂F

protonation through the modulation of H₂F N5 pK_a rather than providing an acidic proton within the active site, and this is consistent with the fact H₂F N5 pK_a is elevated from 2.6 to 6.5 when bound to EcDHFR (89, 90).

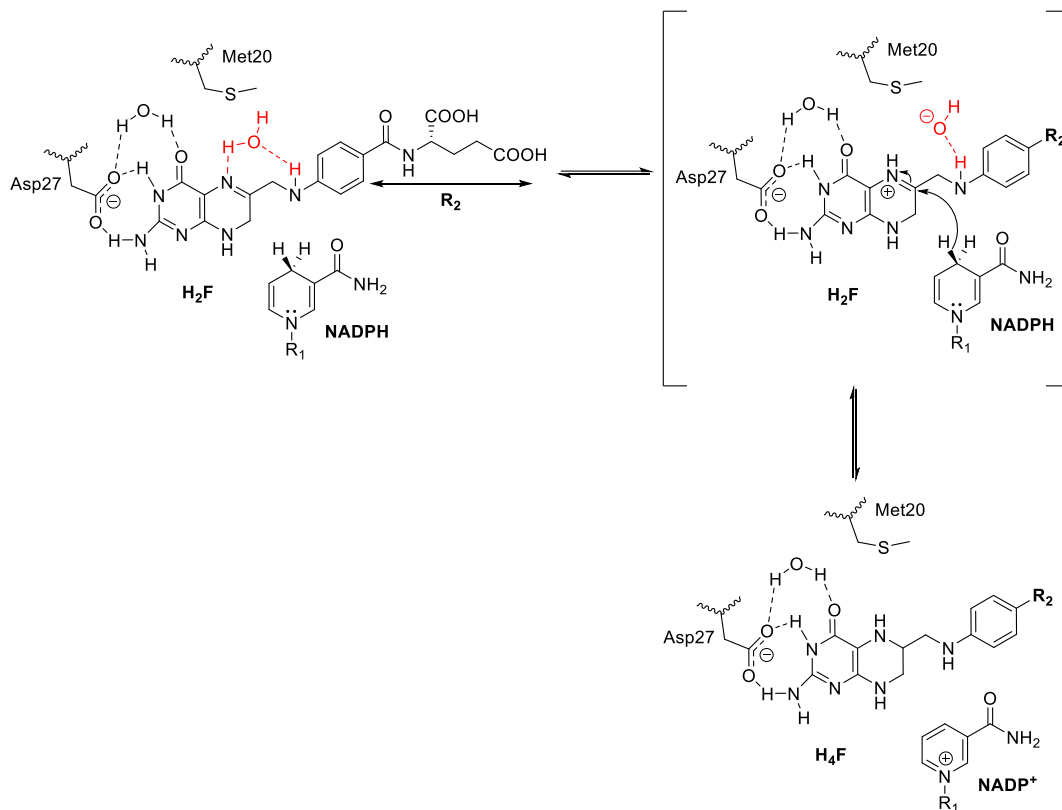


Figure 1.15. EcDHFR reaction mechanism proposed by Wan *et al.* Figure readapted from Ref (88).

Even though the protonation mechanism has been sufficiently explained, the evolution of transition-state during EcDHFR catalysis needs to be further investigated. Based on the chronological order of protonation and hydride transfer, three mechanistic possibilities can be deduced (chapter 4, section 4.5, figure 4.19). In the simplest case, protonation and hydride transfer occur in a concerted fashion. Alternatively, these chemical events are separated from each other, where hydride transfer precedes N5 protonation of H₂F or *vice versa*. More than three decades ago, Stone & Morrison provided experimental evidences that

support the stepwise mechanism in which H_3F^+ is effectively the reacting species during hydride transfer (83); these conclusions were mainly based on the interpretation of primary hydrogen and solvent isotope effect (SKIE) data at pH values from 7.0 to 10.0. Analyses of EcDHFR catalysis by quantum mechanics/molecular mechanics (QM/MM) and molecular dynamics simulations also suggest N5 protonation precedes the step of hydride transfer (91-95). Liu *et al.* has recently provided further experimental evidences supporting this model, by probing and comparing solvent and hydrogen KIEs of Asp27- and Tyr100-mutated EcDHFRs to the wild-type enzyme at pH values from 4.0 to 12.0 (96). Although experimental evidences provided by Liu *et al.* are more convincing than those by Stone & Morrison, the use of mutated EcDHFRs in the experimental design inevitably raises the question on whether the catalytic behaviour of these mutated unnatural enzymes produces an altered reaction path (97). Furthermore, D_2O was used in the SKIE measurement and it is known to modify the enzyme catalytic behaviour by changing solvent viscosity (98, 99). To unambiguously verify the catalytic mechanism of the DHFR reaction, heavy atom KIE measurement is therefore essential.

1.5 Synthesis of isotopically labelled folates

In addition to KIE measurement, isotopic labelling of natural products such as H_2F can be used as an approach to gain insights into folate metabolism (44, 77, 83, 90, 96, 100-125) and physiology (126-132). In a molecule, replacement of natural abundant atoms with their heavy counterparts confers the unique advantage to collect atomic-scale information on a given system under investigation with a negligible effect on its chemistry. This is because neutron number differences between isotopes reflect on their physical properties which

can be probed by techniques such as KIE, NMR, mass spectrometry, and IR. While the first chemical synthesis of [¹⁴C]-folic acid ([¹⁴C]-FA) was reported in 1951 (133), preliminary *in vivo* investigations of human folate metabolism with [³H]-FA were described nearly a decade later (126). Since then, about thirty synthetic procedures designated to label folates with either radioactive or stable isotopes have been reported (110, 112, 115-117, 134-156). Such a large number of procedures is justified by folate's chemical complexity and the lack of highly selective reactions, as each synthetic strategy would only allow a discrete pattern of isotopic substitutions. Besides, these syntheses are often laborious and costly due to the shortage of suitable labelled starting materials, and the picture is further complicated when reduced folates (e.g. H₂F) are considered, as most of them are notoriously unstable towards oxygen, light, heat and non-physiological pH values (157-160). Consequently, despite half a century of remarkable efforts, only small number of folate isotopologues are easily accessible, and this perhaps explains why many paths of research in folate biology are still unexplored.

1.5.1 Isotopic labelling of folate's pterin moiety

During the reduction of H₂F to H₄F catalysed by DHFR, both key chemical events (protonation and hydride transfer) and enzyme-substrate interactions occur on folate's pterin moiety, particularly at positions N5, C6, C7 and C9. The use of folates with isotopic label specifically located in the pterin moiety is therefore essential in studying DHFR catalysis. However, the synthesis of labelled folates remains non-trivial, and isotopic enrichment of atoms constituting the pterin moiety (e.g. N5, C6, C7 and C9) is a challenging task.

Folate and its derivatives, in general, can be synthesised by connecting pterin, *p*-aminobenzoate (*p*ABA) and glutamate in a sequential order. To incorporate an

isotope label into pterin in a regio-specific manner, various synthetic strategies have been derived. Cocco *et al.* reported the synthesis of [2-¹³C]-FA to probe the protonation state of folate's pterin moiety in complex with DHFR by ¹³C-NMR spectroscopy (116). In this synthetic procedure (Figure 1.16), ¹³C-guanidine is condensed with 2-amino-3-cyano-5-(acetoxymethyl)pyrazine (**1**) to yield 2,4-diamino pteridine-6-methanol (**2**). 2,4-Diamino-6-(bromoethyl)pteridine (**3**), generated *in situ* by bromination of **2**, is subsequently condensed to *p*-aminobenzoyl-L-glutamic acid (*p*ABA-Glu) yielding [2-¹³C]-aminopterin. Alkaline hydrolysis of [2-¹³C]-aminopterin eventually produces [2-¹³C]-FA with 13% overall yield.

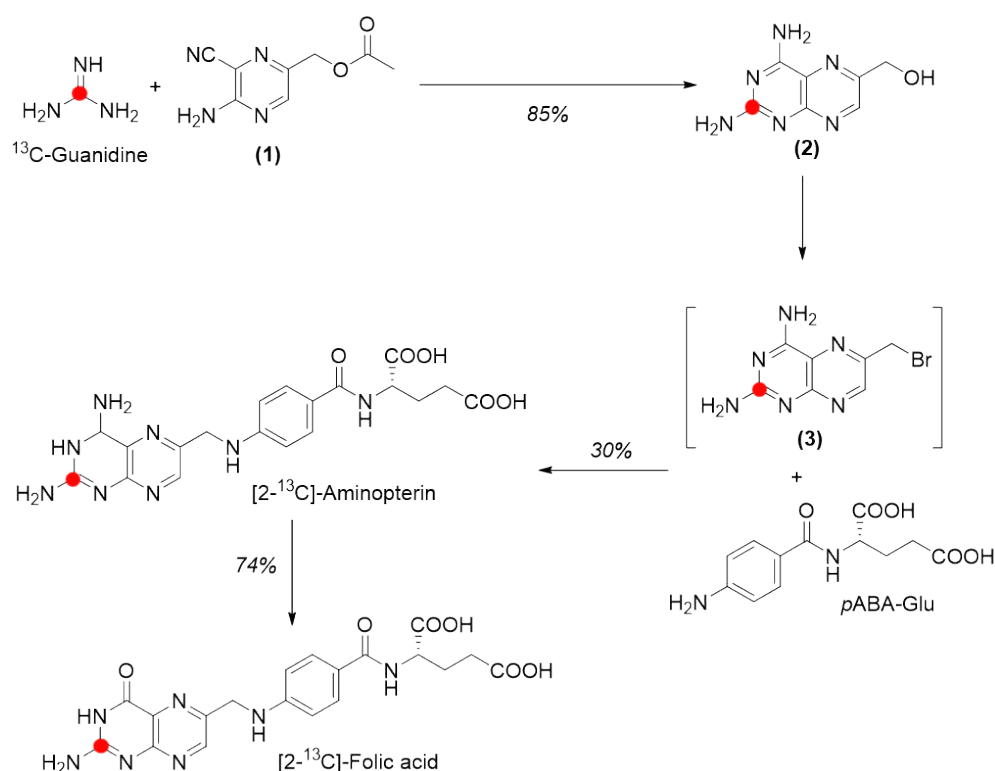


Figure 1.16. Synthesis of [2-¹³C]-folic acid by Cocco *et al.* (116). The reported overall yield is ~13%.

To further probe the protonation state of folic acid bound to DHFR by means of NMR spectroscopy, [5-¹⁵N]- and [6-¹³C]-folic acid were synthesised as well by Selinsky *et al.* (117). In this synthetic route (Figure 1.17), the pteridine ring is assembled by condensing 2,4,5,6-tetraminopyridine (**5**) with dihydroxyacetone to yield **2**. Similar to the procedure described by Cocco *et al.*, isotopically labelled folic acid is synthesised from **2** in three additional chemical steps with an overall yield of ~5%. To synthesise [5-¹⁵N]-FA, **5** was prepared from 2,3,6-triaminopyrimidine (**4**) using isotopically labelled sodium nitrite (Na¹⁵NO₂), while [2-¹³C]-dihydroxyacetone needed for the synthesis of [6-¹³C]-FA was produced from [2-¹³C]-glucose following a chemoenzymatic procedure (161).

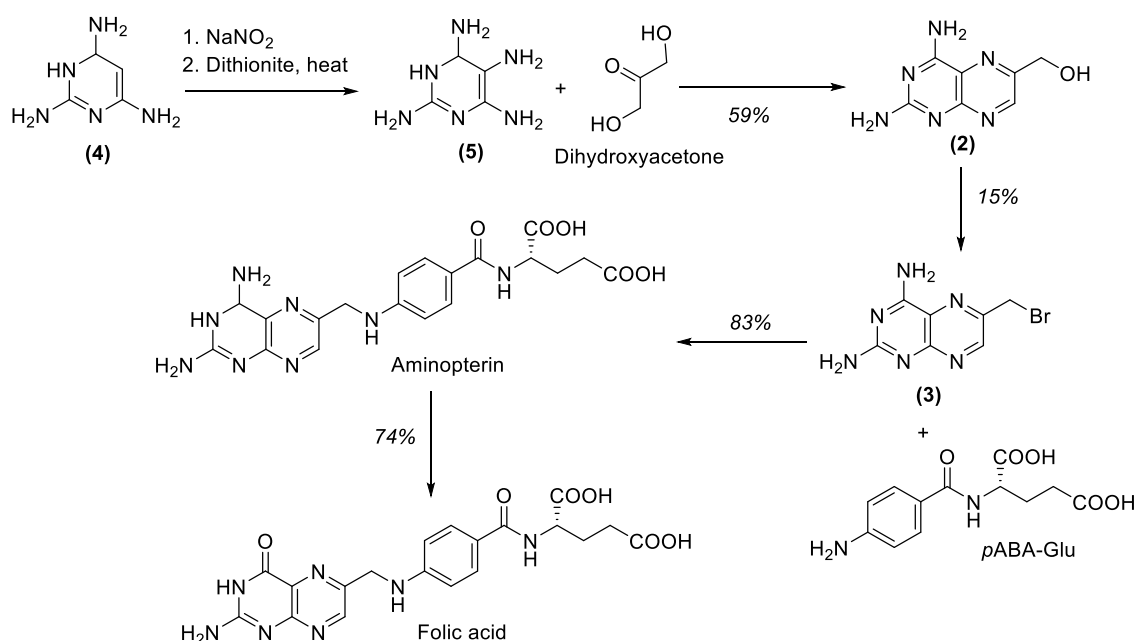


Figure 1.17. Synthetic route for the production of [5-¹⁵N]-folic acid or [6-¹³C]-folic acid reported by Selinsky *et al.* (89). The overall yield is ~5%.

To date, folate specifically labelled with ¹⁵N and ¹³C at the respective N5, C2 and C6 positions have been made using the synthetic routes described by Cocco *et al.*

al. and Selinsky *et al.* Nevertheless, because symmetric reagents guanidine and dihydroxyacetone are used in these pathways, regioselective isotope labelling of other positions of FA's pterin moiety, including C7 and C9, cannot be achieved.

1.6 How folates are made by nature: the folate *de novo* biosynthetic pathway

A fundamental difference in folate metabolism between mammals, parasites and bacteria is that mammalian cells do not possess a biosynthetic machinery to produce H₂F, which is supplied through dietary intake as folic acid (vitamin B9). On the other hand, microbes in general synthesise H₂F from guanosine triphosphate (GTP) in 7 biochemical reactions catalysed by the folate *de novo* biosynthetic pathway enzymes (Figure 1.18). Assuming the folate *de novo* pathway from *E. coli* as a general model, the first committed biosynthetic step in folate biosynthesis is rearrangement of GTP into 7,8-dihydroneopterin triphosphate (DHNTTP) through four tandem reactions: hydrolysis of C8 in the purine ring yielding a formyl intermediate, consequential deformylation, Amadori rearrangement of the ribose moiety, followed by a ring closure reaction (Figure 1.19). DHNTTP is then dephosphorylated to 7,8-dihydroneopterin (DHN) in two steps, the first specifically catalysed by 7,8-dihydroneopterin triphosphate pyrophosphatase (DHNTPase) while the intermediate 7,8-dihydroneopterin monophosphate (DHNMP) is believed to be hydrolysed into DHN by a non-specific phosphatase (162, 163). Dihydroneopterin aldolase (DHNA) then transforms DHN into 6-hydroxymethyl-7,8-dihydropterin (HMDP), which is then pyrophosphorylated to 6-hydroxymethyl-7,8-dihydropterin pyrophosphate (HMDPpp) by 6-hydroxymethyl 7,8-dihydropterin pyrophosphokinase (HPPK). HMDP pyrophosphorylation serves the forthcoming nucleophilic substitution catalysed by dihydropteroate synthase (DHPS), where HMDPpp is combined

Introduction

with *p*ABA to yield 7,8-dihydropteroate (H₂Pte). Dihydrofolate synthase (DHFS) eventually synthesises H₂F by forming a peptide bond between the α-amino group of glutamic acid (Glu) and the carboxylic group of H₂Pte.

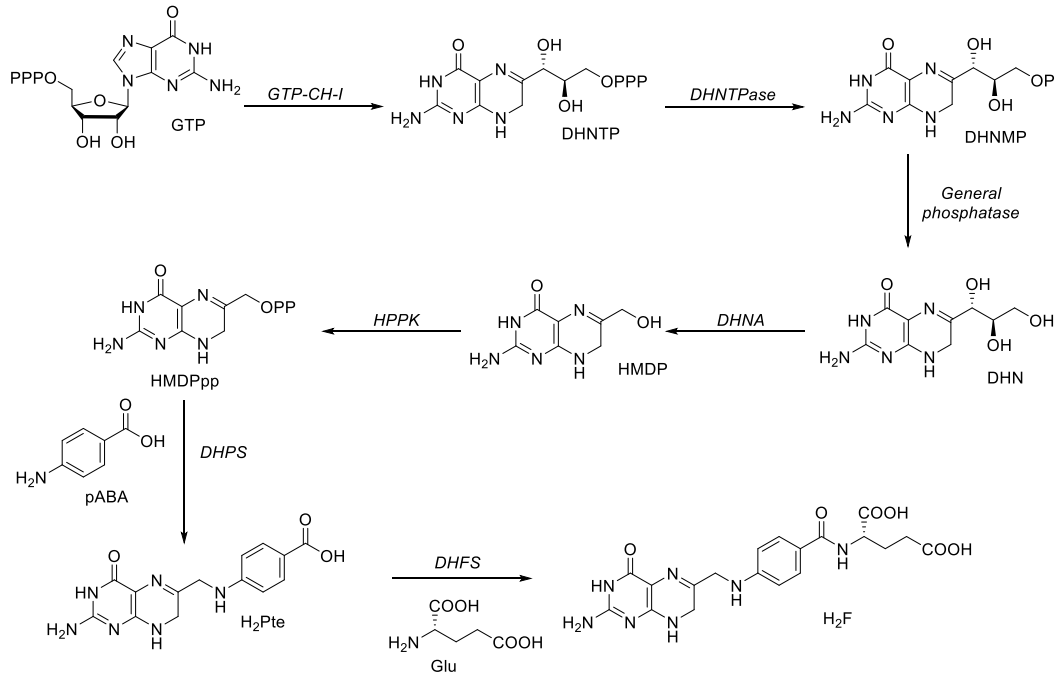


Figure 1.18. Folate *de novo* biosynthetic pathway.

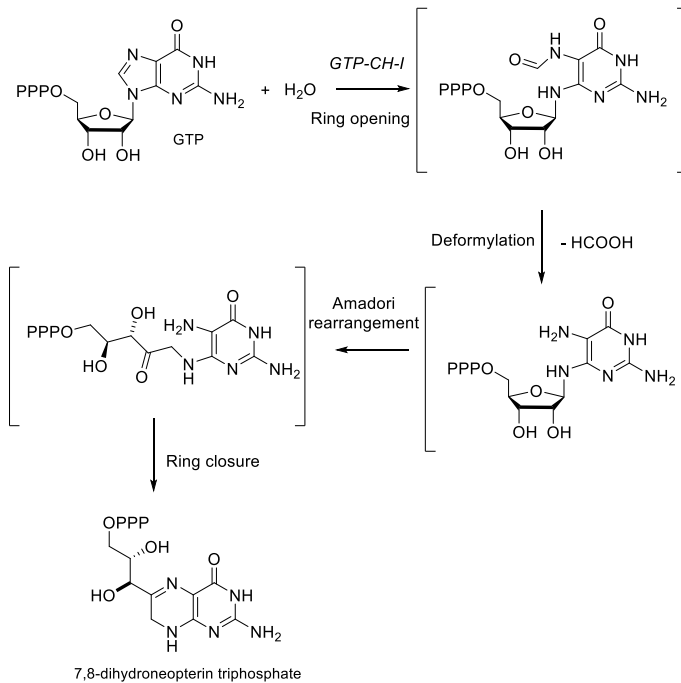


Figure 1.19. Sequence of chemical reactions catalysed by GTP cyclohydrolase I (GTP-CH-I) from *Escherichia coli*.

1.7 Aims

The main goal of this investigation is to provide insight into DHFR catalysis through heavy-atom KIE measurements using isotopically labelled H₂Fs. Heavy-atom KIE data provides unambiguous information about the chronological order of protonation and hydride transfer in DHFR catalysis, and it is crucial to build a transition-state model for the design of novel anti-DHFR drugs. Because of its prominent role in drug discovery and fundamental enzymology, heavy-atom KIE studies will be conducted firstly on EcDHFR. It is worthwhile to note that both N5 and C6 position of H₂F have never been investigated *via* heavy-atom KIE, mainly because current synthetic routes to introduce heavy atoms (¹⁵N, ¹³C) into H₂F pterin moiety are laborious and costly (section 1.5) (116, 117). Therefore, there is a need to develop a practical synthetic procedure to produce site-specifically labelled H₂F at any position of the pterin moiety by using simple and readily-available starting materials.

In vitro metabolic engineering offers a cost-effective way to produce high-value complex natural products through the appropriate combination of enzymes from different organisms (164, 165). Enzymes are designed by nature to perform chemical transformations with unmatched chemo-, regio- and enantio-selectivity, making their use to site-specific isotopic labelling particularly attractive (166, 167). Nevertheless, their application to folate chemistry is surprisingly restricted to a small number of examples (135, 138, 140, 142, 156), that is a rational approach fully exploiting the many inherited benefits of biocatalysis (mild conditions, eco-compatibility, versatility, easier product separation) for the site-specific isotopic labelling of folates must be addressed.

Introduction

In this work, a one-pot chemo-enzymatic synthesis to the production of H₂Fs labelled at N5, C6, C7 and C9 positions of the pterin ring using enzymes from the folate *de novo* biosynthetic pathway is reported. Because guanosine triphosphate (GTP) is the key intermediate to locate isotopic labels on H₂F pterin moiety, efforts were primarily focused on establishing a biosynthetic procedure to generate guanosine nucleotides that is compatible to the folate *de novo* pathway enzymes to yield H₂F. Additionally, an efficient and versatile cofactor regeneration system for NADP⁺ based on glutaredoxin/glutathione reductase redox couple has been developed.

2. A DISULFIDE-BASED NADP⁺ RECYCLING SYSTEM WITH A HIGH TURNOVER NUMBER*

**This chapter summarises the work published on ACS Catal., 2017, 7 (2), pp 1025-1029 (DOI: 10.1021/acscatal.6b03061). Authors of this article include Antonio Angelastro, William M. Dawson, Louis Y. P. Luk, and Rudolf K. Allemann. AA, the author of this PhD thesis, is the only first author for this article.*

2.1 Preface

Cofactor recycling is an essential aspect of biocatalysis, as many enzymes such as transferases and oxidoreductases, which are often employed in the manufacturing of high-value chemicals in both industrial and laboratory settings, require cofactors. Cofactors are additional chemical components employed by an enzyme to perform a range of chemical transformations such as reductions, oxidations and phosphorylation. Implementing cofactor regeneration schemes reduces the use of these structurally complex and expensive compounds from stoichiometric to catalytic quantities. Importantly, as many cofactor-dependent enzymes catalyse reversible reactions, cofactor recycling systems drive biochemical reactions to completion by preventing accumulation of their bioproducts that may inhibit enzymatic activity, according to Le Chatelier's principle. A practical parameter to quantify the efficiency of a cofactor recycling system is the total turnover number (TTN), which is the total number of moles of product formed per mole of cofactor (168-170) :

The TTN value puts in relationship the cost of mole of cofactor needed for each mole of product formed, and it should be in the range of 10^4 to 10^6 for a recycling system to be considered efficient on a laboratory scale and economically viable on an industrial scale (168-170).

In the biosynthetic works described in chapters 3 and 4, at least six enzymes require the use of adenosine triphosphate (ATP) or oxidised adenine dinucleotide

nicotinamide phosphate (NADP⁺) as cofactors. Hexokinase (HK), ribose-phosphate pyrophosphokinase (PRS), guanylate kinase (GK) and 6-hydroxymethyl 7,8-dihydropterin pyrophosphokinase (HPPK) utilise ATP to donate either a phosphate or diphosphate group to their substrates, generating respectively adenosine diphosphate (ADP) and adenosine monophosphate (AMP) as by-products. ATP regeneration was achieved as previously described (169, 170). On the other hand, glucose 6-phosphate dehydrogenase (G6PDH) and 6-phosphogluconate dehydrogenase (6PGDH) reduce NADP⁺ while performing their catalytic function. This chapter describes a new NADP⁺ regeneration system which has a TTN significantly higher than those reported previously in the literature.

2.1.1 ATP recycling systems

Several enzymatic procedures for regenerating ATP from ADP have been reported, including the use of acetate kinase (AK), pyruvate kinase (PK), carbamate kinase (CarK) and creatine kinase (CreK) (Figure 2.1 A) (169, 170). Among those, regeneration of ATP fuelled by phosphoenolpyruvate (PEP) under the action of PK is considered one of the most efficient (169). ATP recycling from AMP can be accomplished by coupling an additional enzyme to PK, myokinase (MK), which produces 2 ADP molecules from ATP and AMP, that are further phosphorylated by PK to regain ATP (Figure 2.1 B) (171).

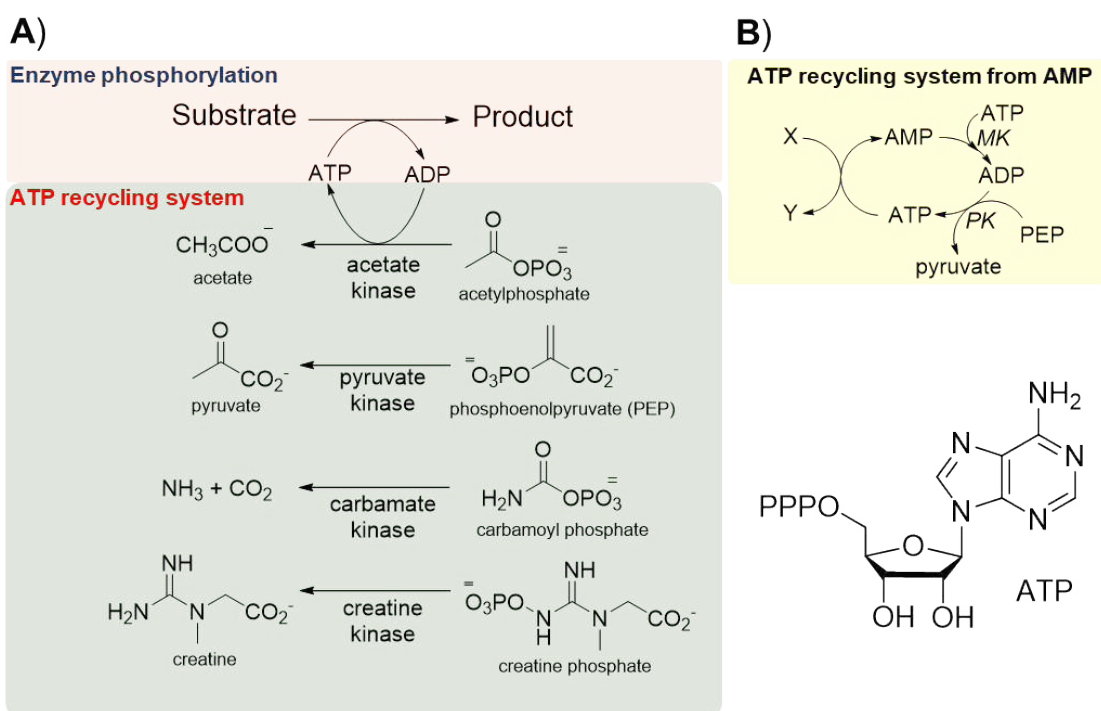


Figure 2.1. (A) Recycling systems for ATP from ADP. (B) Recycling system for ATP from AMP by coupling of pyruvate kinase (PK) with myokinase (MK).

2.1.2 NADP⁺ recycling systems

While ATP regeneration systems are well established, recycling of NADP⁺ from NADPH is significantly less developed as few recycling schemes have been reported. Use glutamate dehydrogenase (GDH), one of the first regeneration methods for NADP⁺, is still the most used notwithstanding its drawbacks (166, 167, 172, 173). This enzyme oxidises NADPH to NADP⁺ to convert α-ketoglutarate and ammonium to glutamate (Figure 2.2). Unfortunately, GDH has an maximal steady-state turnover number of only ~40 s⁻¹ thus limiting its recycling efficiency (173, 174). Moreover, its maximal TTN is less than 10³ (171). Accordingly, other regeneration schemes, including the D-lactate dehydrogenase (LDH) (175), NADPH oxidase (NOX)(176, 177) and the laccase/mediator system

(178), have been developed in attempts to replace GDH. However, the TTNs determined for LDH and NOX (from 100 to 300) are even lower than those for GDH, whereas the laccase/mediator system was not tested for recycling NADP⁺ (178).

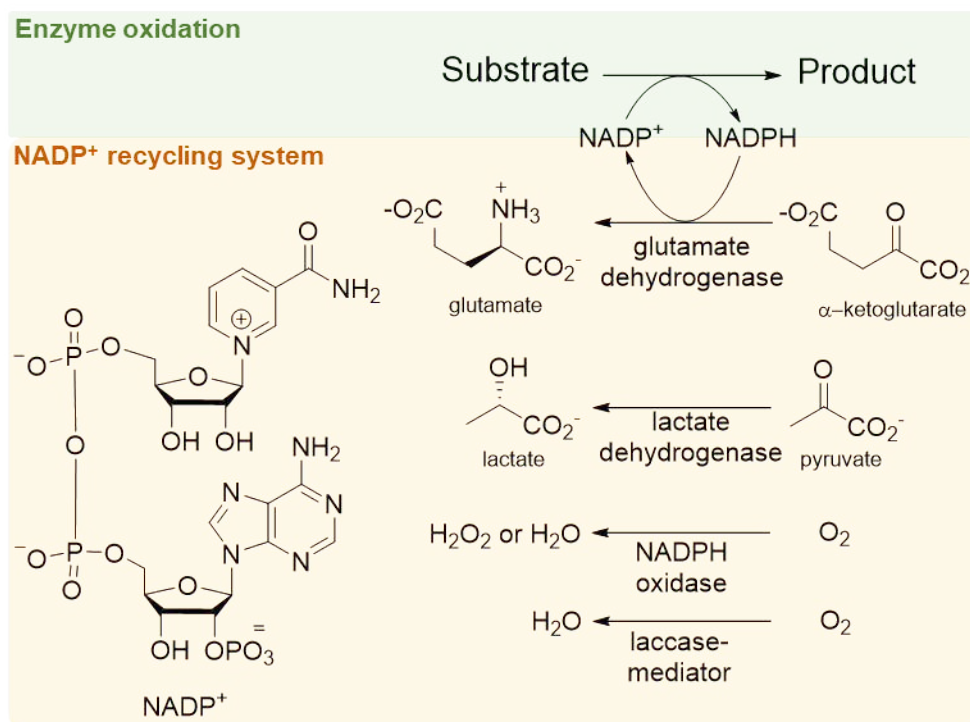


Figure 2.2. Current recycling systems for NADP⁺. Figure adapted from ref (179).

In evaluating a possible implementation of these NADP⁺ recycling schemes for the *in vitro* biosynthesis of H₂F, both the NOX and laccase/mediator system would be incompatible due to their oxygen-dependency, as reduced pterins including H₂F are prone to oxygen-dependent oxidation (157, 158). Additionally, reduced pterins easily degrade in acidic conditions (157), but the laccase/mediator system functions only at acidic pH (between 3.0 and 6.0) with an optimum of 3.5 (178). Therefore, only the GDH and LDH recycling systems would be an option for the

chemo-enzymatic synthesis of H₂F, but their low TTNs pose a serious limit to the overall biosynthetic efficiency.

2.1.3 The glutaredoxin (GRX) system: an ideal recycling scheme for NADP⁺

A recycling system characterised by a high TTN that uses simple and inert oxidising reagents is ideally needed for NADP⁺ regeneration in the chemo-enzymatic synthesis of H₂F. In nature, NADP⁺ is mainly regenerated through the enzymatic reduction of disulfide bonds (180). One such example is the glutaredoxin (GRX) system, which is composed of a pair of tandem enzymes, glutaredoxin (GRX) and glutathione reductase (GR), which react with a pair of redox reagents, glutathione (GSH) and its oxidized counterpart GSSG (181). In the GRX system, GRX reduces the disulfide bonds to yield thiols using the reducing power of GSH, which is then oxidised to GSSG (182, 183). GSSG is recycled back to GSH in the concomitant oxidation of NADPH to NADP⁺ by GR (Figure 2.3).

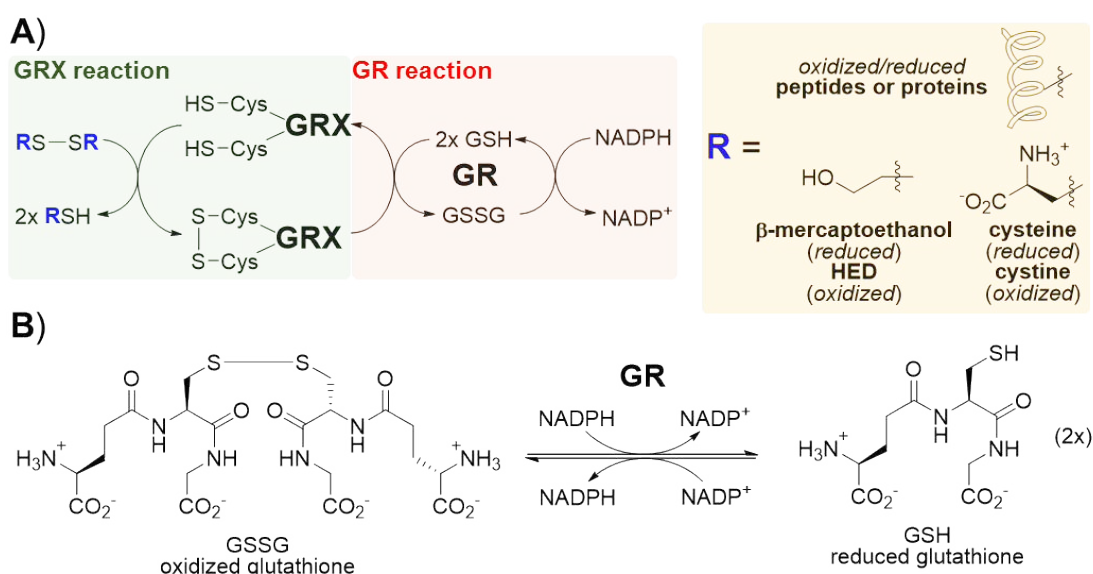


Figure 2.3. The glutaredoxin system. Figure taken from ref (179).

The GRX system is an appropriate NADP⁺ recycling scheme for H₂F biosynthesis, as glutathione and its oxidised counterpart are relatively inert compared to oxygen. Importantly, the GRX system can employ a wide range of disulfide compounds including 2-hydroxyethyl disulfide (HED or oxidised β-mercaptoethanol) and cystine (Figure 2.3 A) as the latent oxidising reagent (184, 185). Such substrate promiscuity is particularly attractive, as the latent oxidising reagent can be in general tailored for the biocatalytic system under investigation. This therefore avoids any possible complications related to chemical incompatibilities or product isolation. The reduced thiol by-product generated by the GRX system can also serve as a reducing agent protecting both substrates and biocatalysts from oxidative damages. Though this system requires the use of two coupling enzymes, it provides competitive advantages that cannot be offered by the currently available NADP⁺ recycling systems.

2.2 Construction of the glutaredoxin system for NADP⁺ recycling

Because of their favourable kinetic properties, glutathione reductase from *Saccharomyces cerevisiae* (ScGR) and glutaredoxin 2 from *Escherichia coli* (EcGRX2) were employed in this work to reconstitute *in vitro* the GRX system for means of NADP⁺ recycling (186-189). ScGR shows a high steady-state turnover number (k_{cat}) of 240 s⁻¹ at pH 7.0 (187) whereas the experimental k_{cat} for EcGRX2 is ~550 s⁻¹ for HED at pH 7.0 (188). Based on these kinetic parameters, the GRX system formed by the ScGR/EcGRX2 pair is expected to recycle NADP⁺ 8.64 x 10⁵ times (240 s⁻¹ x 60 x 60) per hour.

To test its efficiency, ribulose-5-phosphate (Ru5P) was generated *in situ* from glucose by coupling HK to the two NADP⁺-dependent enzymes that will be required for both of guanosine phosphates (chapter 3) and H₂F (chapter 4) chemo-enzymatic syntheses, G6PDH and 6PGDH. The TTN of the GRX system was determined by ¹³C-NMR spectroscopy using ¹³C₆-D-glucose as starting material.

2.2.1 Gene expression, purification and characterisation of recombinant glutaredoxin 2 (GRX2) and 6-phosphogluconate dehydrogenase (6PGDH)

While HK, G6PDH and GR are readily available from commercial sources, recombinant EcGRX2 and 6PGDH were produced from the genes for GRX2 and 6PGDH, *grxB* and *gnd* respectively. The constructs were amplified by PCR reaction using *E.coli* K-12 chromosomal DNA as template and subsequently cloned into the NdeI and XhoI sites of pET28-a vector (chapter 6, section 6.2). Recombinant enzymes, bearing a N-terminal hexahistidine tag, were overproduced in *E. coli* BL21(DE3) and purified by Ni²⁺ affinity chromatography (chapter 6, section 6.3).

2.2.1.1 Characterisation and activity assay of 6PGDH

Production and purification of recombinant 6PGDH was followed by sodium dodecyl sulfate polyacrylamide gel electrophoresis (SDS-PAGE) analysis (Figure 2.4 A). 6PGDH catalyses the decarboxylative oxidation of 6-phosphogluconate (6-PG) to ribulose-5-phosphate (Ru5P) and CO₂/bicarbonate using NADP⁺ as the final electron acceptor (Figure 2.4 C). Accordingly, enzymatic activity can be measured by UV-vis spectroscopy by following NADPH absorbance at 340 nm (Figure 2.4 B). To assess the most appropriate way for storing purified 6PGDH

without causing any activity loss, enzymatic activities of fresh, 50% glycerol stock and freeze dried 6PGDH were compared (Figure 2.4 B). While 6PGDH stored in 50% glycerol at -20°C retains an enzymatic activity comparable to that of the freshly purified enzyme, freeze dried 6PGDH suffers of substantial activity loss.

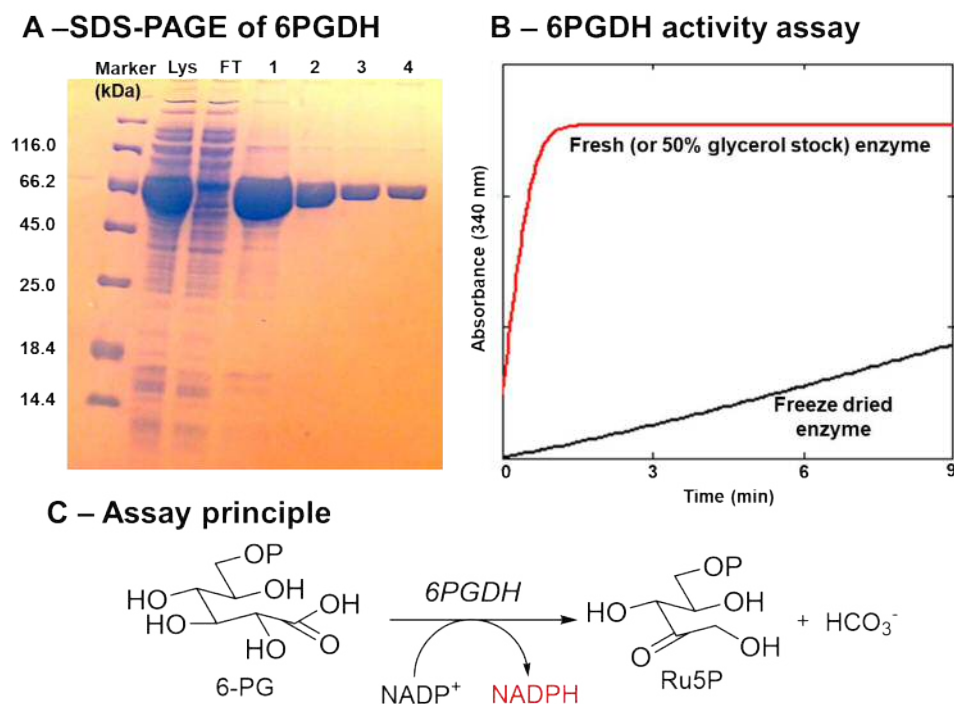


Figure 2.4. (A) SDS-PAGE of purified 6PGDH (MW = 53.6 kDa; fractions 1-4) compared to cell lysate (Lys) before and after (FT) purification. (B) Activity assay of 6PGDH through UV-vis spectroscopy by monitoring NADPH increase at 340 nm. Freeze dried 6PGDH (black) shows a marked activity loss compared to fresh (or 50% glycerol stock) 6PGDH. 6PGDH assay principle is shown in (C).

2.2.1.2 Characterisation and activity assay of EcGRX2

Recombinant EcGRX2 was analysed by SDS-PAGE (Figure 2.5 A). In addition, pure recombinant enzyme was subjected to mass spectrometry analysis (Figure 2.6). Because EcGRX2 activity cannot be directly assayed by UV-vis

spectroscopy, the recombinant enzyme was coupled to ScGR using a procedure described by Holmgren which monitors the consumption of NADPH by measuring UV absorbance at 340 nm (Figure 2.5 B and C) (190). To ensure that NADPH consumption was a direct consequence of EcGRX2 activity, ScGR activity was monitored before addition of EcGRX2 into the same reaction mixture. Activity of freeze dried EcGRX2 was found significantly lower than its glycerol stock counterpart, therefore the enzyme was routinely stored at -20°C in 50% glycerol.

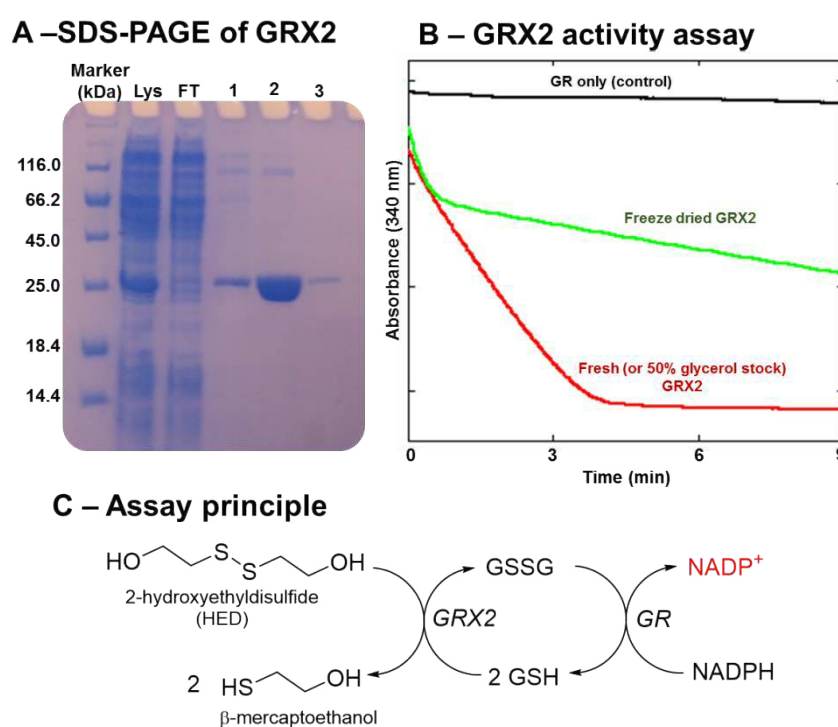


Figure 2.5. (A) SDS-PAGE of purified GRX2 (MW = 26.4 kDa; fractions 1-3) compared to cell lysate (Lys) before and after (FT) purification. (B) EcGRX2 activity monitored by UV-vis spectroscopy following NADPH decrease at 340 nm. Because GRX2 does not directly oxidise NADPH, ScGR is coupled to the recombinant enzyme in presence of catalytic quantities of GSH. Oxidation of GSH to GSSG is therefore directly linked to EcGRX2 resulting into the reduction of HED to β -ME concomitant to the oxidation of NADPH to NADP⁺. The assay principle is shown on panel (C). Compared to fresh (or 50% glycerol stock) EcGRX2, freeze dried EcGRX2 (green) suffers of activity loss.

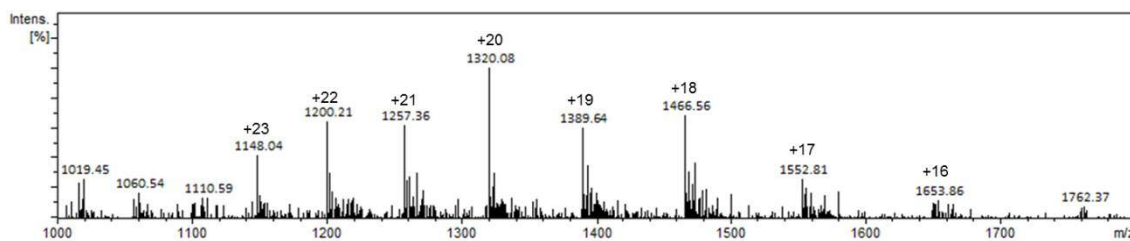


Figure 2.6. Positive ESI-MS of purified EcGRX2. Deconvoluted experimental molecular weight of the recombinant enzyme was 26,383 amu (calculated 26,368 amu).

2.2.2 *In vitro* assembly of the GRX system and determination of the maximal TTN

To determine the experimental TTN of the ScGR/EcGRX2 redox couple, HK and G6PDH were combined to oxidise D-glucose into 6-PG in two biochemical steps (Figure 2.7 A). In the first HK-catalysed reaction, ATP donates a phosphate group to D-glucose to yield glucose-6-phosphate (G6P) and ADP. Therefore, PK and stoichiometric amounts of PEP were included to recycle ATP. G6PDH mediates the oxidation of G6P by NADP⁺ to generate one equivalent of 6-PG and NADPH in each catalytic cycle; this enzymatic reaction merits the use of the GRX system to regenerate NADP⁺. Accordingly, the NADP⁺ regenerating system was included by adding ScGR and EcGRX2, catalytic GSH and a stoichiometric amount of the latent oxidizing reagent HED (or cystine). Use of ¹³C₆-D-glucose allowed to precisely monitor the course of the reaction by NMR spectroscopy. When NADP⁺ was added to the reaction mixture, the substrate was efficiently converted to the product 6-PG, in which the corresponding C1 signal in the ¹³C-NMR spectrum shifted from ~96 and 92 ppm (64% β- and 36% α-anomer, respectively) to ~178 ppm (Figure 2.7 C).

To assess the maximal number of TTN that could be achieved by the ScGR/EcGRX2 system, different concentrations of NADP⁺ were used ranging from 0.1 mM to 1 nM (Table 2.1). Noticeably, full conversion of substrate to product was observed when the concentration of NADP⁺ decreased to 10 nM corresponding to a TTN of 5×10^5 (Figure 2.7 C). On the other hand, D-glucose/NADP⁺ ratios corresponding to a TTN value superior to 5×10^5 lead to a partial conversion of starting material into product (Figure 2.7 D). Consequently, it is concluded that the TTN of the ScGR/EcGRX2 recycling system can reach a TTN up to 5×10^5 , a value that has not been achieved by other existing NADP⁺ recycling systems. It should also be noted that this enzyme pair is compatible with the PK/PEP ATP-recycling system used for adding the phosphate at the C-6 position of glucose (171). Additionally, cystine, though sparingly soluble, can act as a latent oxidizing reagent as well.

A disulfide-based NADP⁺ recycling system with a high turnover number

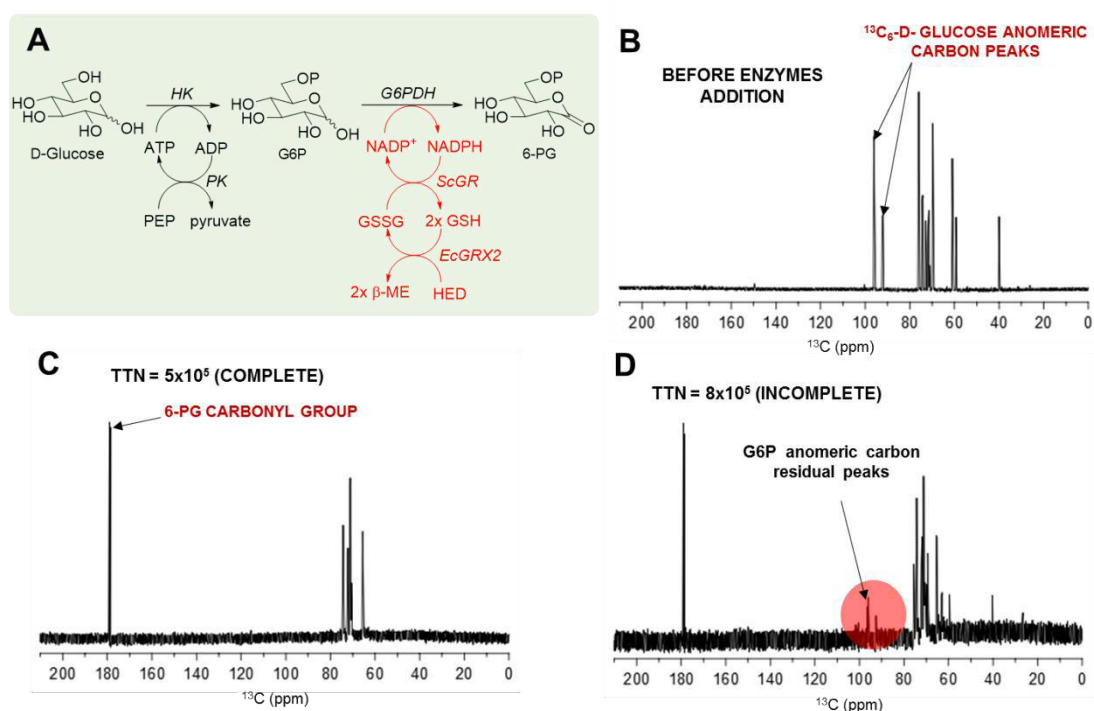


Figure 2.7. (A) Conversion of D-glucose to 6-phosphogluconate (6-PG) by hexokinase (HK) and glucose 6-phosphate dehydrogenase (G6PDH). The ATP/ADP and the NADP⁺ recycling (highlighted in red) systems are composed of pyruvate kinase (PK), glutathione reductase (ScGR) and glutaredoxin 2 (EcGRX2). Conversion of substrate to product has been monitored by ¹³C-NMR spectroscopy using ¹³C₆-D-glucose as starting material (B). While at TTN = 5 × 10⁵ there was a complete conversion of ¹³C₆-D-glucose to ¹³C₆-6-PG (C), at TTN = 8 × 10⁵ residual peaks from G6P at 96 and 92 ppm indicate an incomplete conversion (D).

Table 2.1. Experimental TTN value of the GRX system tested for NADP⁺ recycling determined by ¹³C-NMR spectroscopy.

NADP ⁺ concentration	TTN	Conversion of ¹³ C ₆ -glucose to ¹³ C ₆ -PG
0.1 mM	50	Complete
5 μM	10 ³	Complete
0.5 μM	10 ⁴	Complete
50 nM	10 ⁵	Complete
10 nM	5 × 10 ⁵	Complete
6 nM	8 × 10 ⁵	Incomplete
1 nM	1 × 10 ⁶	Incomplete

To further examine the compatibility of the ScGR/EcGRX2 recycling system, 6PGDH was incorporated to the model pathway as an additional NADP^+ -dependent enzyme. Upon the addition of 6PGDH, the intermediate 6PG underwent a complete oxidative decarboxylation; the two characteristic downfield chemical shifts correspond to the C3 of Ru5P ($\delta = 160$ ppm) and the byproduct bicarbonate ($\delta = 213$ ppm). This indicated that the ScGR/EcGRX2 recycling system can readily double its workload by incorporating another set of NADP^+ -dependent enzyme (Figure 2.8).

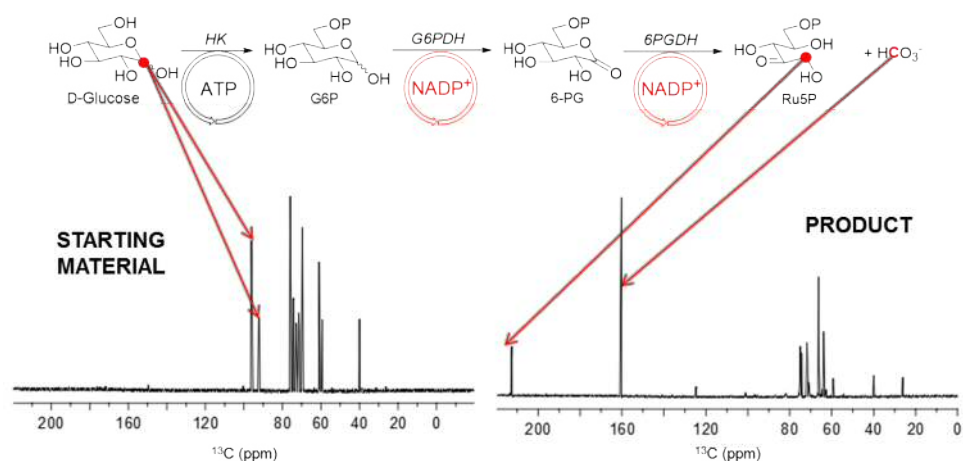


Figure 2.8. Conversion of D-glucose to ribulose-5-phosphate (Ru5P) by hexokinase (HK), glucose 6-phosphate dehydrogenase (6GPDH) and phosphogluconate dehydrogenase (6PGDH).

2.3 Conclusion

A novel NADP⁺ recycling system based on the ScGR/EcGRX2 redox couple was developed. The GRX system showed its ability to drive a glucose-utilising biosynthetic pathway yielding important synthons including 6-PG and Ru5P. By using small organic sulfides as latent oxidising reagents, the ScGR/EcGRX2 pair could regenerate NADP⁺ using hydride ions from NADPH to produce thiols *via* glutathione. Although this system is composed of two enzymes, GRX accepts organic disulfides including HED and cystine, converting them into β -mercaptoethanol and cysteine, both of which are useful 'byproducts' protecting the enzymes, reagents and products from unwanted oxidative damage. Moreover, GRX is known to enhance protein stability by preventing them from oxidative misfolding and aggregation (191-193). Accordingly, this system is atomically economical, as there are reagents (e.g. HED) serving more than one role. Unlike the NAD(P)H oxidases (NOXs) and the laccase/mediator system, the ScGR/EcGRX2 are functional in both aerobic and anaerobic environment, so that these enzymes can operate with oxygen-sensitive biocatalysts and biosynthetic intermediates such as reduced pterins and H₂F. Indeed, the durable antioxidant environment built on NADPH is one of the main advantages of GRX system. Most importantly, both ScGR and EcGRX2 are highly active offering TTNs of up to 5 x 10⁵ outperforming the currently available NADP⁺ recycling systems. Accordingly, the NADP⁺ recycling system sustained by ScGR/EcGRX2 is superior than all of the currently available systems and offers many advantages for commercial and academic users.

**3. CHEMO-ENZYMATIC SYNTHESIS OF ISOTOPICALLY
LABELLED GUANOSINE NUCLEOTIDES**

3.1 Preface

Guanosine is one of the four natural nucleosides comprising of a purine base (guanine) covalently linked to ribose at the C1 via a β -N₉-glycosidic bond. In living organisms, guanosine is mainly found as guanosine monophosphate (GMP), guanosine diphosphate (GDP) or guanosine triphosphate (GTP). Additionally, deoxyguanosine nucleotides (dGMP, dGDP and dGTP), where the 2'-hydroxyl is reduced, are commonly present within the cellular environment (Figure 3.1 A). Both guanosine and deoxyguanosine nucleotides participate in a wide range of biological and biosynthetic processes, including cell signalling, RNA and DNA biosynthesis.

GTP is perhaps the most important phosphorylated derivative of guanosine from a biosynthetic point of view. In addition to being employed in RNA biosynthesis, GTP is the first intermediate of many biosynthetic pathways from various organisms to the production of a variety of natural products including pigments (194, 195), toxins (196), non-canonical nucleotides (197) and cofactors (196, 198-201). Notably, GTP participates in the first committed step in the biosynthesis of flavin (201), molybdopterin (196, 198), tetrahydrobiopterin (199), and dihydrofolate (H₂F, section 1.6) cofactors (Figure 3.1 B).

For the scope of this thesis, production of site-specifically labelled GTP is fundamental to the enzymatic synthesis of isotopically enriched H₂F for heavy-atom KIE studies on DHFR. Besides, isotopically enriched guanosine nucleotides have many applications in biochemical studies including RNA structural and functional analysis (202-204). In this chapter, a simplified approach to the chemo-enzymatic synthesis of guanine nucleotides is described. The biosynthetic procedure reported herein, which includes the newly developed cofactor

recycling scheme reported in Chapter 2, has been designed for being highly compatible to H₂F biosynthesis.

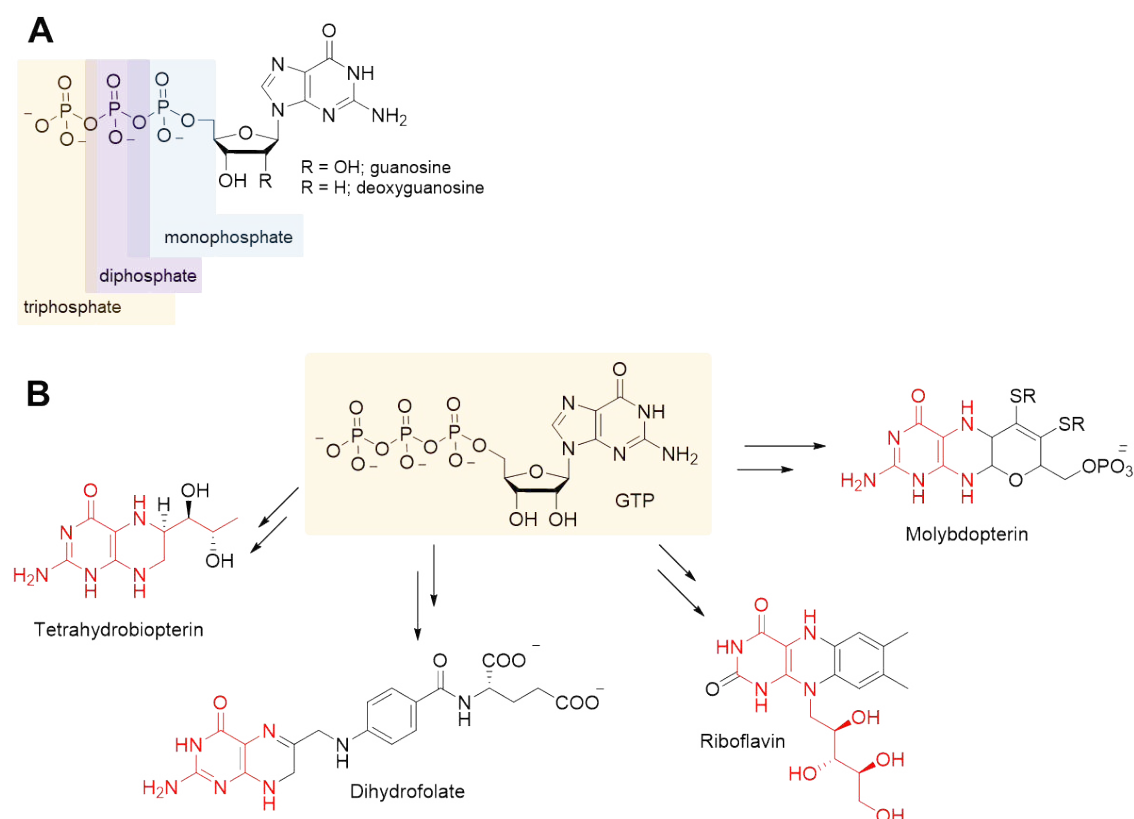


Figure 3.1. (A) Structure of guanosine and deoxyguanosine nucleotides. (B) Cofactors such as tetrahydrobiopterin, dihydrofolate, riboflavin and molybdopterin are biosynthetically derived from guanosine triphosphate (GTP). Atoms derived from GTP are highlighted in red.

3.1.1 Background: the *de novo* and salvage pathway of guanosine nucleotides

In cells, guanosine nucleotides are mainly biosynthesised *de novo* from ribose-5-phosphate (R5P), which is provided by the pentose phosphate pathway from D-glucose (Figure 3.2). In the first step of purine *de novo* biosynthesis, the anomeric carbon of R5P is pyrophosphorylated to phosphoribose pyrophosphate (PRPP) with consumption of ATP by ribose-phosphate pyrophosphokinase

(PRS). PRPP is then converted into 5-phospho- β -D-ribosylamine (PRA) by glutamine phosphoribosylpyrophosphate amidotransferase (GPAT) where an amino group from glutamine is donated to PRPP. Glycine is subsequently connected to PRA to yield glycinamide ribonucleotide (GAR) by glycinamide ribonucleotide synthetase (GARS). A one-carbon unit provided by 10-formyl-H₄F is transferred to GAR by GAR transformylase (GARTFase) to form formylglycineamide ribonucleotide (FGAR). FGAR is converted into formylglycinamide ribonucleotide (FGAM) by FGAR amidotransferase with consumption of glutamine and ATP. FGAM is then cyclised to 5-aminoimidazole ribonucleotide (AIR) by FGAM cyclase. Addition of CO₂ to AIR by AIR carboxylase leads to the formation of carboxyamino-imidazole ribonucleotide (CAIR). An aspartate residue is added to CAIR to yield N-succinyl-5-aminoimidazole-4-carboxamide ribonucleotide (SAICAR) by the action of the enzyme SAICAR synthetase. SAICAR lyase removes a fumarate molecule from SAICAR to yield 5-aminoimidazole-4-carboxamide ribonucleotide (AICAR). A second carbon unit from N¹⁰-formyl-H₄F is donated to AICAR by AICAR transformylase to yield N-formylaminoimidazole-4-carboxamide ribonucleotide (FAICAR). Cyclisation of FAICAR to inosinate by IMP synthase yields inosinate monophosphate (IMP). Conversion of IMP to GMP is achieved in two biochemical steps catalysed by IMP dehydrogenase (IMPDH) and XMP-glutamine amidotransferase.

Chemo-enzymatic synthesis of isotopically labelled guanosine nucleotides

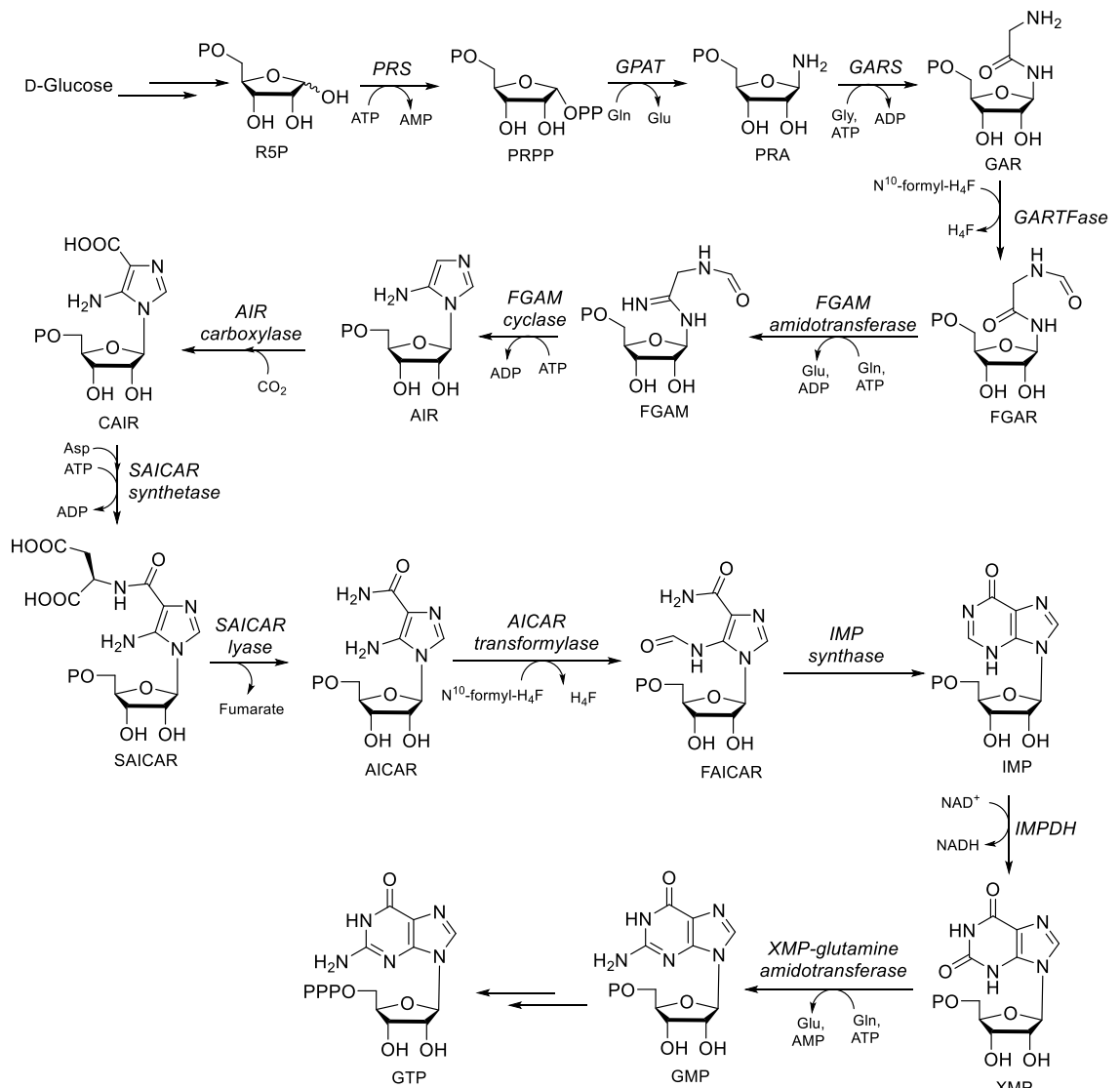


Figure 3.2. Biosynthesis of GTP through the purine *de novo* pathway.

GMP can also be produced from R5P using the preformed guanine base (Figure 3.3) *via* the salvage pathway. Similar to the *de novo* pathway, R5P is added with a diphosphate group yielding PRPP. The guanine base is then combined to PRPP by a specific enzyme, xanthine-guanine phosphoribosyl transferase (XGPRT), to yield GMP in a single biochemical step. While 6 ATP, 3 Gln, 2 N¹⁰-formyl-H₄F, NAD⁺, Gly, Asp and CO₂ are needed for assembling the purine ring *de novo* from R5P, only one ATP molecule and guanine are needed in the

corresponding salvage pathway. Considering that nucleotide biosynthesis is in general an energetically demanding process, it is not surprising that nature has developed such a system to recover preformed purine bases from cellular degradation processes.

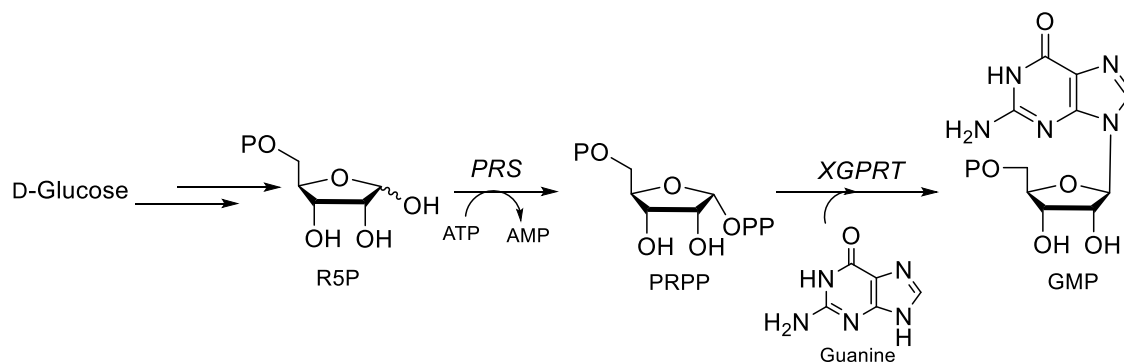


Figure 3.3. Biosynthesis of GMP through the purine salvage pathway.

3.2 Chemo-enzymatic synthesis of guanosine nucleotides

Site-specific isotopic labelling of guanosine nucleotides has been investigated previously, particularly for structural and functional analysis of ribonucleic acids through NMR spectroscopy (166, 167, 202-207). Production of specifically labelled GMP, GDP and GTP *via* chemoenzymatic procedures is particularly attractive for the unmatched chemo-, regio- and enantio-selectivity of enzymatic catalysts.

Because it would be simple to reproduce the purine salvage pathway *in vitro*, the logical option to produce purine nucleotides chemo-enzymatically is by employing the purine salvage enzymes, as previously reported by Tolbert *et al.* (205). Unfortunately, guanine has low solubility which turned out to be a limiting factor for an efficient GMP biosynthesis. In an attempt to minimise this problem, it was proposed to combine an excess of the insoluble purine base with high amounts

of enzymes and long reaction times, ranging between 4 h and 70 h (202, 205). Nevertheless, this biosynthetic route remains impractical due to a lack of reproducibility. To circumvent the problem, Schultheisz *et al.* engineered the purine *de novo* biosynthetic pathway in a one-pot synthesis (166). In this elegant work, purine nucleotides isotopically labelled at specific positions were produced using very simple starting materials (*e.g.* D-glucose) with yields up to 66%. However, the synthetic procedure requires a minimum of 28 enzymes, 5 cofactor recycling systems and various reagents making it difficult to be expanded for the synthesis of other relevant natural products such as folate.

Because the main goal of this research is to develop an enzymatic one-pot synthesis of site-specifically labelled folate through the generation of the key intermediate GTP from D-glucose, the enzymatic assembly of the guanosine nucleotide must be simple, yet efficient. Due to the complex setup, a hypothetical implementation of the *de novo* purine synthesis described by Schultheisz *et al.* to the H₂F biosynthetic pathway is difficult (166). Consequently, in this work efforts were focused on synthesising isotopically labelled GMP by combining the pentose phosphate and purine salvage pathways enzymes. Accordingly, it will allow us to further extend the biosynthetic pathway to produce other natural products including H₂F. Moreover, given the importance of labelled guanosine nucleotides have for biochemical studies, the scientific community would benefit from a facile chemo-enzymatic procedure for the synthesis of isotopically labelled GMP/GDP/GTP.

3.3 Synthesis of isotopically labelled guanine

In the chemo-enzymatic assembly of GMP that uses purine salvage pathway enzymes, D-glucose and guanine are employed as starting materials. While D-glucose isotopically enriched on various positions is available from commercial sources, site-specifically labelled guanine can be synthesised in house following well-established procedures (208). In general, guanine is assembled through the cyclisation of either a substituted pyrimidine (Figure 3.4 A) or an imidazole derivative (Figure 3.4 B).

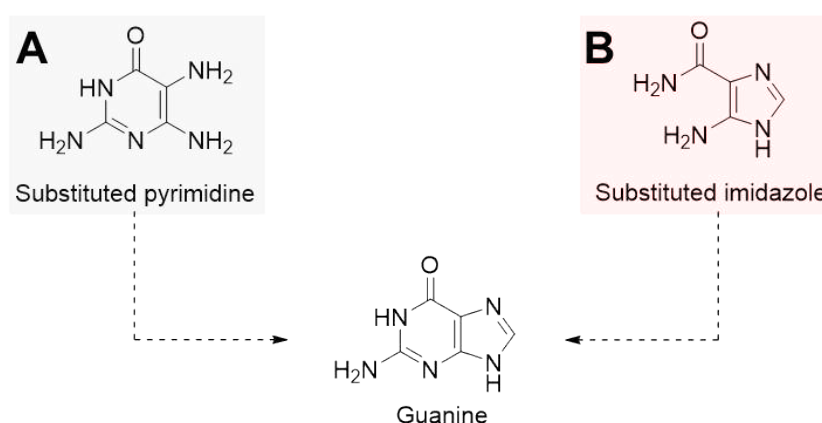


Figure 3.4. General scheme of guanine assembly from either (A), a substituted pyrimidine, or (B), an imidazole derivative.

3.3.1 Traube purine synthesis of guanine

The first method to synthesise guanine was developed by Wilhelm Traube in 1900 (209). The “Traube purine synthesis” (Figure 3.5 A) involves the nitrosation of 2,4-diamino-6-hydroxypyrimidine (**6**) at C5 to yield the intermediate 2,4-diamino-6-hydroxy-5-nitrosopyrimidine (**7**). Reduction with sodium dithionite

under aqueous conditions leads to 2,4,5-triamino-6-hydroxypyrimidine (**8**) which is subsequently cyclised to guanine with formic acid under reflux.

In addition to the use of formic acid reported in the original work, other procedures involving the use of reagents such as formamide, trimethylorthoformate and morpholine for the ring closure step were described (208, 210). Aiming to achieve the highest possible yield, all these reported modifications have been tested (Figure 3.5 B). Cyclisation of **8** with either formamide or trimethylorthoformate under conditions reported in (208) did not yield the desired product. Ring closure using formic acid resulted in 40% guanine whilst a mixture of formic acid and morpholine doubled the yield to 85%. It has been proposed that formation of 4-formylmorpholine facilitates the formylation step required for **8** to be transformed in guanine (Figure 3.5 C) (210).

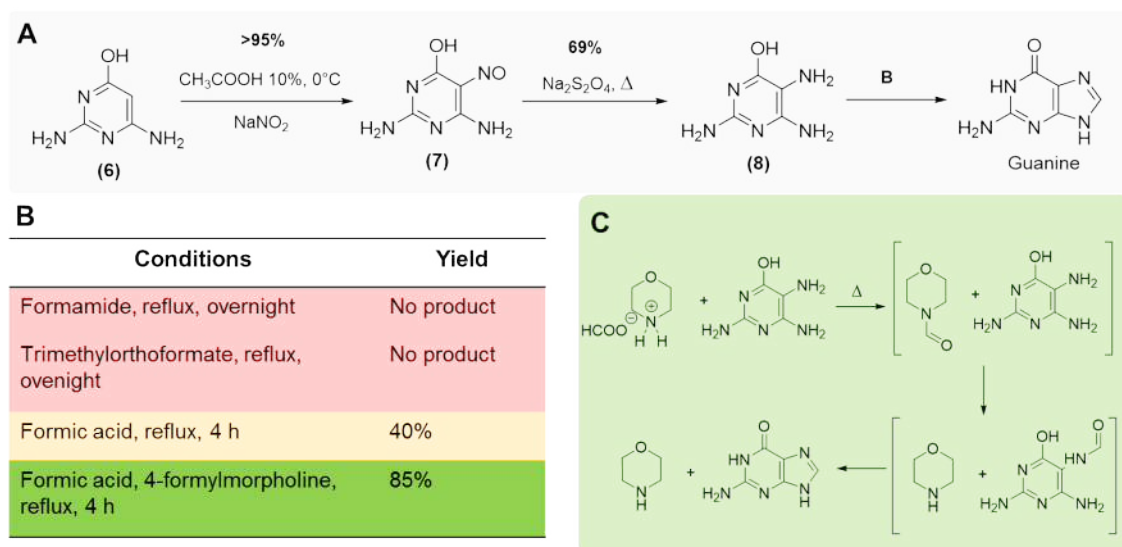


Figure 3.5. (A) Traube purine synthesis of guanine (209). (B) Experimental conditions and yields for cyclisation of (**8**) to guanine. (C) Ring closure mechanism proposed by Sharma *et al.* (210) for the morpholine-catalysed reaction.

3.3.1.1 Synthesis of [7-¹⁵N] and [6-¹³C,7-¹⁵N] Guanine

Because simple starting materials such as sodium nitrite and formic acid are employed the Traube synthesis, [7-¹⁵N]- and [6-¹³C,7-¹⁵N]-guanine can be cost-effectively synthesised (chapter 6, section 6.6.1). The use of Na¹⁵NO₂ during nitrosation of **6**, followed by reduction with dithionite, leads to the intermediate [5-¹⁵N]-2,4,5-triamino-6-hydroxypyrimidine (**9**), which has been characterised by both ¹⁵N-NMR spectroscopy (δ = 24 ppm, singlet) and MS (Figure 3.6). The labelled compound shows a mass increase of ~1 amu compared to that with isotopes of natural abundance.

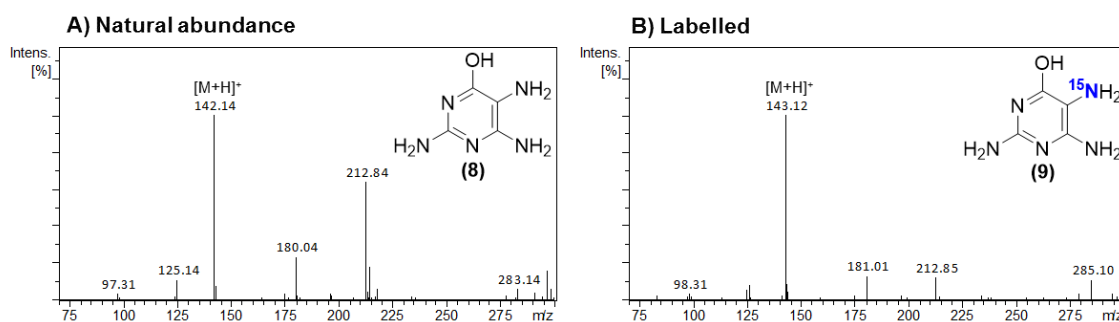


Figure 3.6. (A) Positive ESI-MS of (A) natural abundance and (B) ¹⁵N-labelled 2,4,5-triamino-6-hydroxypyrimidine (**9**).

Cyclisation of **9** with formic acid in morpholine yields guanine labelled at N7 (Figure 3.7). This is evident by the mass increase of ~1 amu in the spectrum and the spin-spin long range coupling between ¹⁵N and the C8 proton which leads a doublet at 7.56 ppm (²J_{NH} = 10 Hz). Additionally, the ¹⁵N-NMR spectrum shows a peak at 214 ppm.

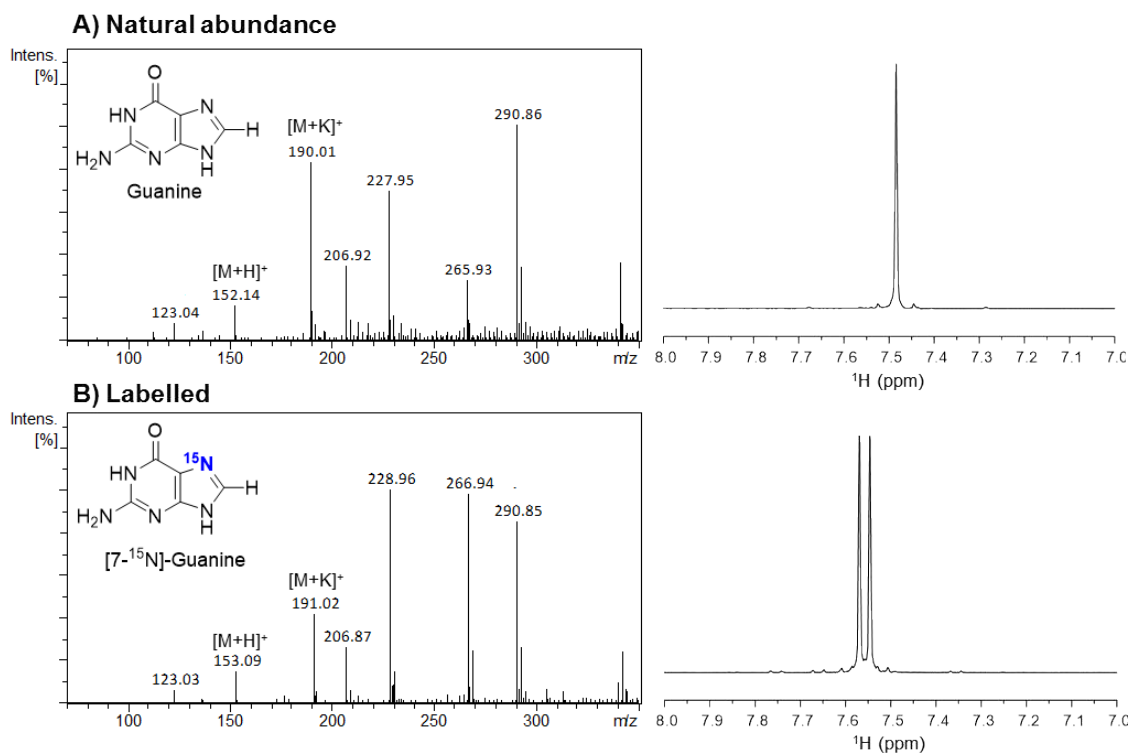


Figure 3.7. (A) Positive ESI-MS and ^1H -NMR of (A) natural abundance and (B) ^{15}N -labelled guanine.

Condensation of **9** with ^{13}C formic acid in morpholine as solvent results in $[\text{6-}^{13}\text{C}, \text{7-}^{15}\text{N}]\text{-guanine}$ (Figure 3.8). Compared to guanine with isotopes of natural abundance, positive ESI-MS of the double-labelled compound shows a mass increase of ~ 2 amu (Figure 3.8 A). The proton attached to C8 appears at ~ 7.5 ppm as a doublet of doublets ($^1J_{\text{CH}} = 186$ Hz, $^2J_{\text{NH}} = 10$ Hz) in the ^1H -NMR spectrum, due to the spin-spin coupling to both N7 and C8 (Figure 3.8 B). ^{13}C -NMR shows a doublet at 148 ppm ($^2J_{\text{CN}} = 3.0$ Hz) while in the ^1H - ^{15}N -HMBC experiment N7 correlates to the C8 proton at 219.3 ppm (Figure 3.8 C).

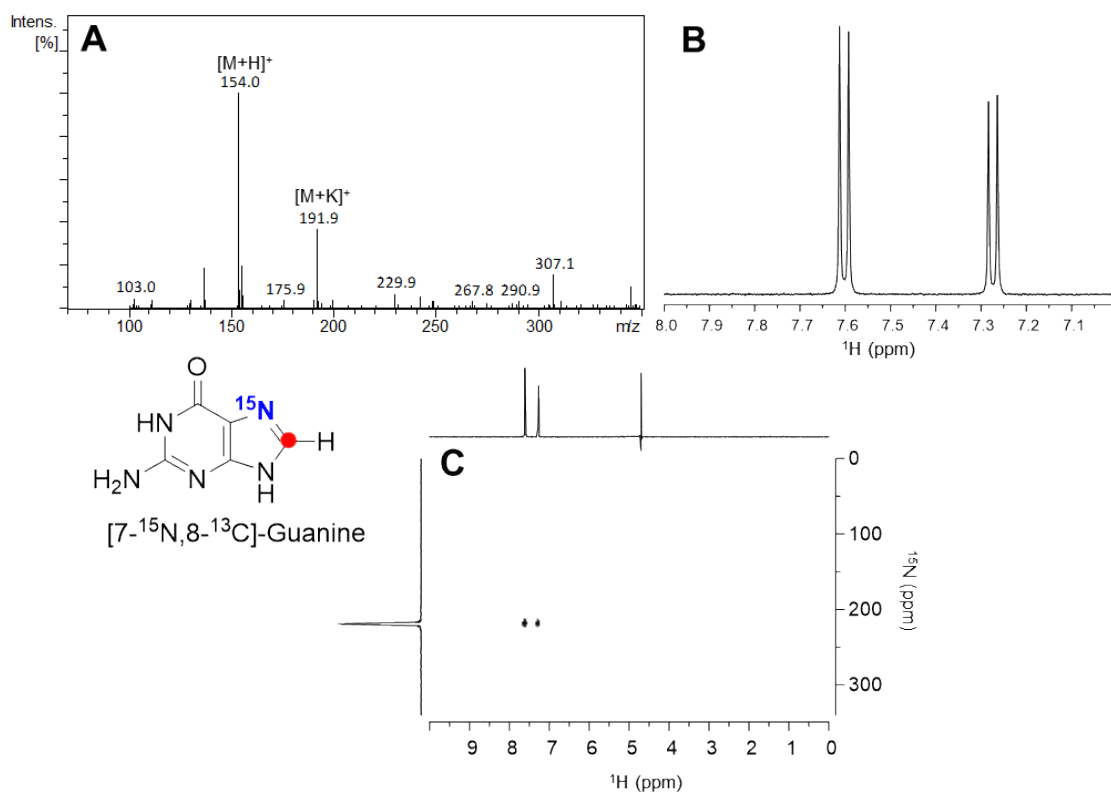


Figure 3.8. (A) Positive ESI-MS, (B) ^1H -NMR and (C) ^1H - ^{15}N -HMBC of $[7\text{-}^{15}\text{N},8\text{-}^{13}\text{C}]$ -guanine.

3.3.2 Synthesis of guanine from 5-amino-4-imidazolecarboxamide

Yamazaki *et al.* developed an approach to prepare guanine from 5-amino-4-imidazolecarboxamide (**14**) through the intramolecular cyclisation of 5-cyanoamido-4-imidazolecarboxamide (**11**), which is generated *in situ* by heating of 5-(N'-benzoyl-S-methylisothiocarbamoyl)amino-4-imidazolecarboxamide (**10**) in strong alkaline conditions (Figure 3.9) (211, 212). Benzoyl isothiocyanate (**13**), freshly prepared by reacting benzoyl chloride (**12**) and KSCN, is added to **14** yielding 5-(N'-benzoylisothiocarbamoyl)amino-4-imidazolecarboxamide (**15**). Treatment of **15** with methyl iodide leads to the formation of **10** which is subsequently heated at 100°C in 6M NaOH to trigger the cyclisation to guanine. In the original synthetic strategy, both intermediates **10** and **15** were purified before proceeding to the

next synthetic step. In this work, a modified version of this synthetic route was developed where only the final product was purified with an overall yield of 29%, similar to that of Yamazaki *et al.* (31% overall) (211, 212).

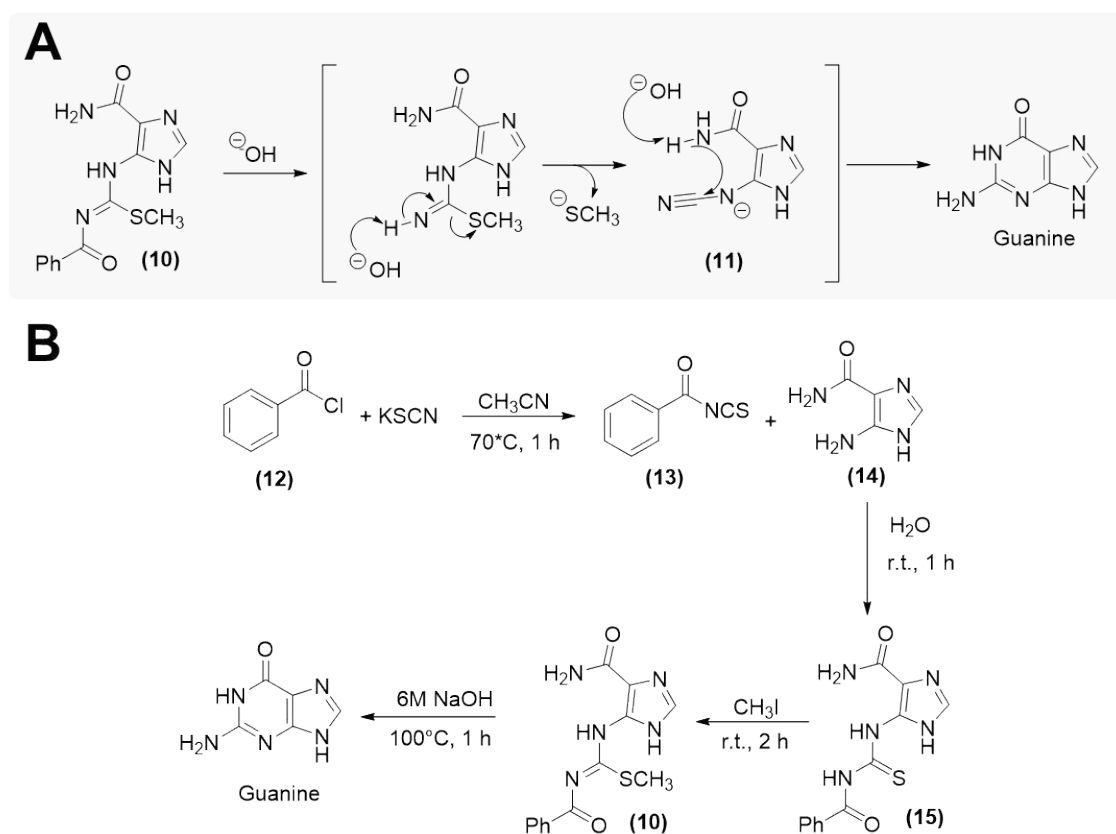


Figure 3.9. (A) Mechanism proposed by Yamazaki *et al.* (212) for the cyclisation of 5-(N'-benzoyl-S-methylisothiocarbamoyl)amino-4-imidazolecarboxamide (**10**) to guanine through the *in situ* formation of 5-cyanoamido-4-imidazolecarboxamide (**11**). (B) Synthesis of guanine from 5-amino-4-imidazolecarboxamide (**14**).

3.3.2.1 Synthesis of [2-¹³C]-guanine

[2-¹³C]-guanine was prepared following the synthetic route described in section 3.3.2 by replacing natural abundance KSCN with its ¹³C counterpart (chapter 6, section 6.6.2.1). Similar to [7-¹⁵N]-guanine (section 3.3.1.1), MS characterisation of [2-¹³C]-guanine showed a mass increase of ~1 amu (Figure 3.10). ¹³C-NMR experiment showed a singlet peak at 159 ppm.

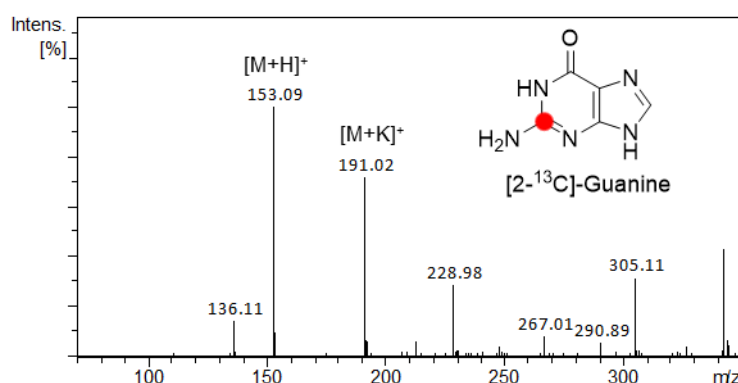


Figure 3.10. Positive ESI-MS of [2-¹³C]-guanine.

3.4 Chemo-enzymatic synthesis of GMP

A total of 10 enzymes have been combined for the biosynthesis of GMP described in this work. As discussed in chapter 2, D-glucose is converted into the intermediate Ru5P by the action of enzymes from the pentose phosphate pathway, namely HK, G6PDH and 6PGDH (Figure 3.11). Here, the biosynthetic cascade continues with the isomerisation of Ru5P to R5P catalysed by phosphoriboisomerase (PRI). R5P is the connection between the pentose phosphate and purine salvage pathways, where PRRP is linked to the purine moiety by XGPRT to yield the final product GMP. The newly developed NADP⁺ recycling system based on the GR/GRX2 redox couple (chapter 2) was used in this biosynthetic procedure.

Chemo-enzymatic synthesis of isotopically labelled guanosine nucleotides

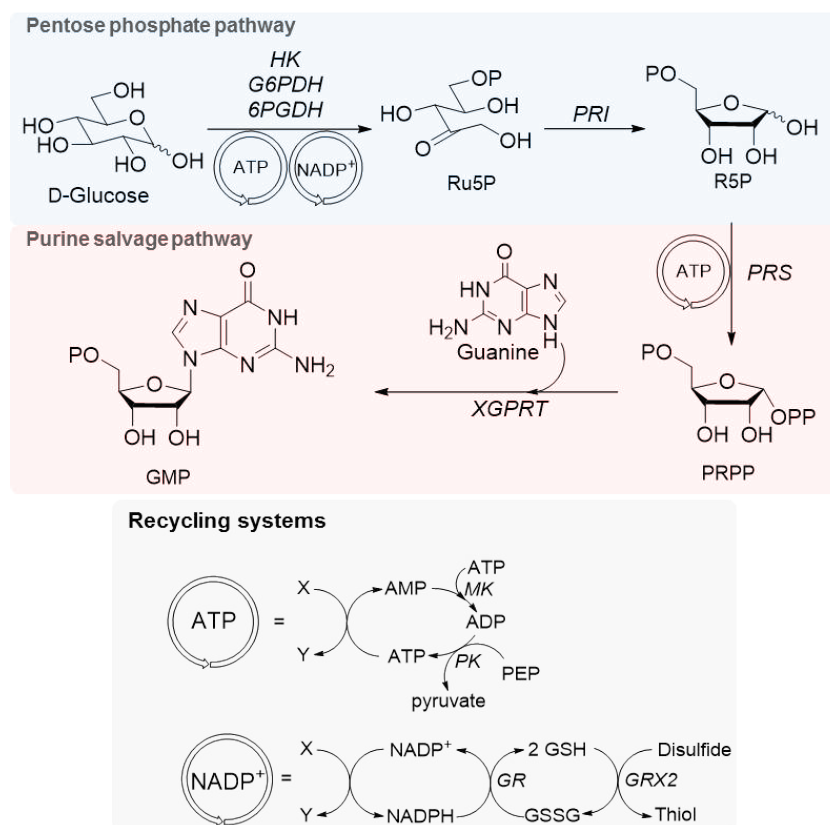


Figure 3.11. Chemo-enzymatic synthesis of guanosine monophosphate (GMP).

A serious issue regarding GMP biosynthesis is the low solubility of guanine. Here, a system where the guanine concentration is kept just below saturation has been developed (Figure 3.12 A). A reservoir of the purine base dissolved in alkali solution (50 mM KOH) is flowed into the reaction mixture with a syringe pump. The guanine injected into the system is then converted into soluble GMP. To maintain the pH of the reaction mixture within the optimum range, the ratio between amounts of alkali needed to dissolve guanine and buffer was determined experimentally. With this approach, substrates are employed in stoichiometric amounts, reaction times are shortened and there is no need for high amounts of enzymes to shift the equilibrium towards product formation.

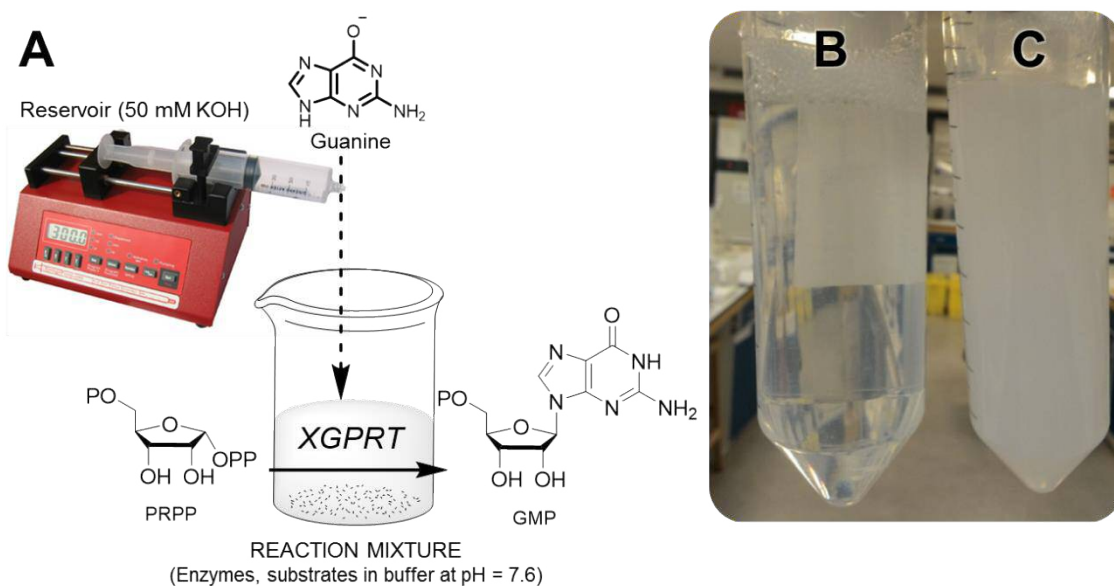


Figure 3.12. (A) Syringe-pump system for controlling guanine concentration. Comparison between (B) GMP synthesised by controlled flow of alkaline guanine into the reaction mixture and (C) without syringe pump.

3.4.1 Synthesis of $[1',2',3',4',5'-^{13}\text{C}_5]$ -, $[1',2',3',4',5'-^{13}\text{C}_5,7-^{15}\text{N}]$ -, $[1',2',3',4',5'-8-^{13}\text{C}_6,7-^{15}\text{N}]$ - and $[2-^{13}\text{C}]$ -GMP

The guanine biosynthetic pathway assembled in this work allowed us to synthesise various isotopically labelled GMPs (Table 3.1) in one day with yields ranging between 70% and 80%. In addition to 6PGDH and GRX2 (chapter 2, section 2.2.1), recombinant PRS and XGPRT were employed. Genes cloned in a pET expression system have been expressed and purified as previously reported (166, 213). Because the GRX recycling system for NADP^+ may use either HED or cystine as the final electron acceptor (chapter 2), the biosynthetic efficiency for GMP synthesis was tested by varying those reagents; in either case yields were similar, and no substantial difference was found.

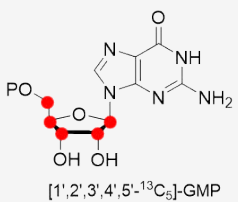
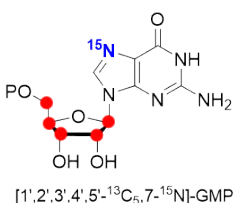
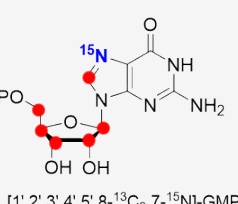
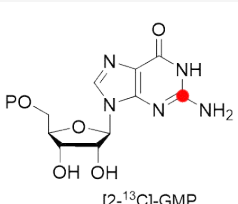
All synthesised compounds were purified by anion exchange chromatography (chapter 6, section 6.6) and quantified through the Beer-Lambert law (chapter 6, section 6.3.4.5.2). All compounds were characterised by high-resolution mass spectrometry (HR-MS); accurate masses are listed in Table 3.1 whereas full spectra are reported in chapter 8. Use of D- $^{13}\text{C}_6$ -glucose and guanine as starting material lead to $[1',2',3',4',5'-^{13}\text{C}_5]$ -GMP. This was shown by ^{13}C -NMR spectroscopy, where carbons C1' (doublet, 86 ppm), C2' (triplet, 74 ppm), C3' (triplet, 71 ppm), C4' (triplet, 84 ppm), C5' (doublet, 63 ppm) couple to each other between 100 ppm and 50 ppm (Figure 3.13 B).

While in $[1',2',3',4',5'-^{13}\text{C}_5,7-^{15}\text{N}]$ -GMP the ^{13}C -NMR spectrum is identical to that of $[1',2',3',4',5'-^{13}\text{C}_5]$ -GMP (Figure 3.14 C), the C8 proton at 8.00 ppm on ^1H -NMR splits as a doublet for the spin-spin coupling to ^{15}N ($^2J_{\text{NH}} = 12$ Hz, Figure 3.14 A and B). Additionally, the ^1H - ^{15}N -HMBC experiment shows the long-range correlation between C8 proton ($\delta = 8.00$ ppm) to the N7 at 235 ppm (Figure 3.14 D).

The C8 proton $[1',2',3',4',5',8-^{13}\text{C}_6, 7-^{15}\text{N}]$ -GMP further splits as a doublet of doublets ($^1J_{\text{CH}} = 213$ Hz, $^2J_{\text{NH}} = 12$ Hz) in the ^1H -NMR spectrum (Figure 3.15 A and B), and this pattern of splitting is also evident in the corresponding ^1H - ^{15}N -HMBC spectrum (Figure 3.15 D) due to the high $^1J_{\text{CH}}$ coupling constant. ^{13}C -NMR spectrum shows the C8 carbon at 135 ppm along with C1', C2', C3', C4' and C5' ribose carbons (Figure 3.15 C).

Because no spin active atom is near C2 of $[2-^{13}\text{C}]$ -GMP, the ^{13}C -label can only be seen through ^{13}C -NMR at 161 ppm as a singlet (Figure 3.16 B).

Table 3.1. Isotopically labelled GMPs synthesised in this work. ^{13}C is highlighted in red

Starting Material	Labelled GMP	Accurate Mass $[\text{M}+\text{H}]^+$ (amu)
D- $^{13}\text{C}_6$ -Glucose + Guanine	 [1',2',3',4',5'- $^{13}\text{C}_5$]-GMP	369.0811
D- $^{13}\text{C}_6$ -Glucose + [7- ^{15}N]-Guanine	 [1',2',3',4',5'- $^{13}\text{C}_5$,7- ^{15}N]-GMP	370.0795
D- $^{13}\text{C}_6$ -Glucose + [7- ^{15}N ,8- ^{13}C]-Guanine	 [1',2',3',4',5',8- $^{13}\text{C}_6$,7- ^{15}N]-GMP	371.0793
D-Glucose + [2- ^{13}C]-Guanine	 [2- ^{13}C]-GMP	365.0674

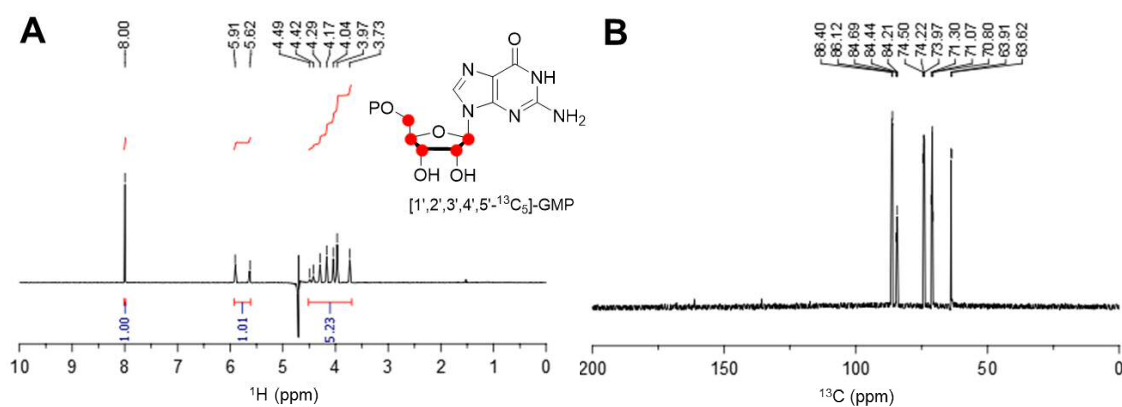


Figure 3.13. (A) ^1H -NMR and (B) ^{13}C -NMR of [1',2',3',4',5'- $^{13}\text{C}_5$]-GMP.

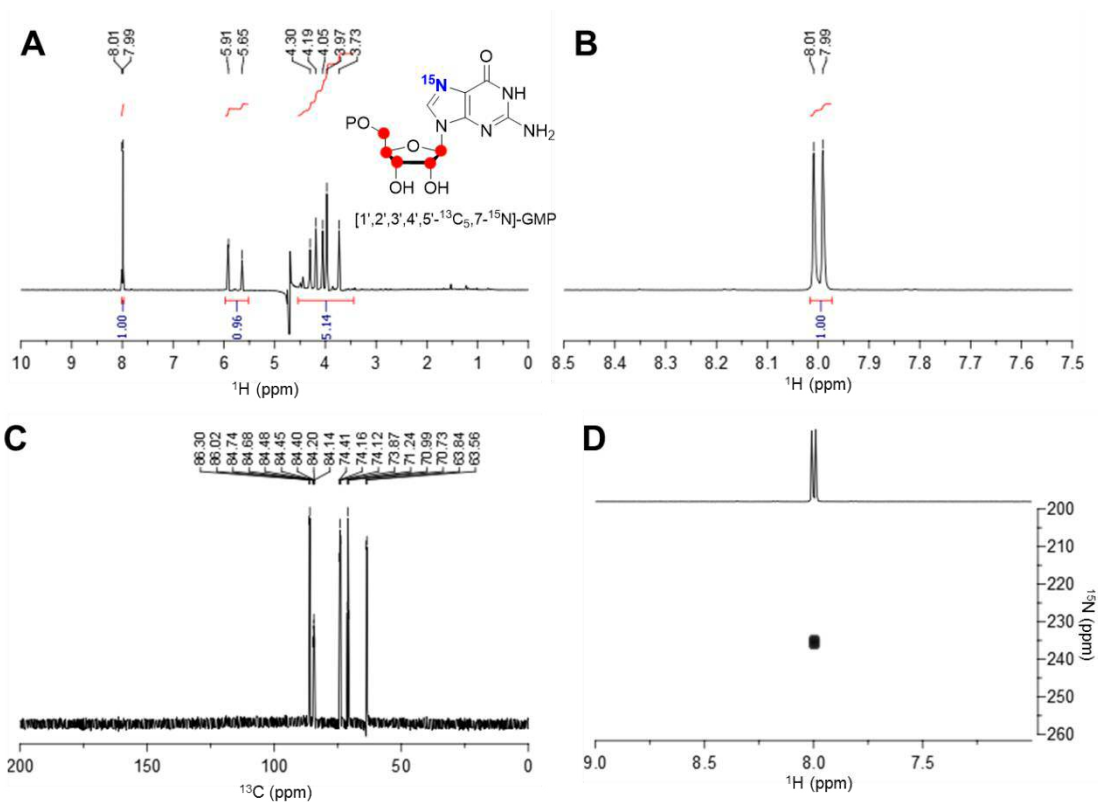


Figure 3.14. (A) ¹H-NMR of [1',2',3',4',5'-¹³C₅,7-¹⁵N]-GMP. (B) Purine C8 proton splits as a doublet for the spin-spin coupling to N7 (²J_{NH} = 12 Hz). (C) Isotopically labelled carbons from the ribose moiety are shown by ¹³C-NMR, while (D) ¹H-¹⁵N-HMBC experiment shows a correlation between C8 proton (δ = 8.00 ppm) to the N7 at 235 ppm.

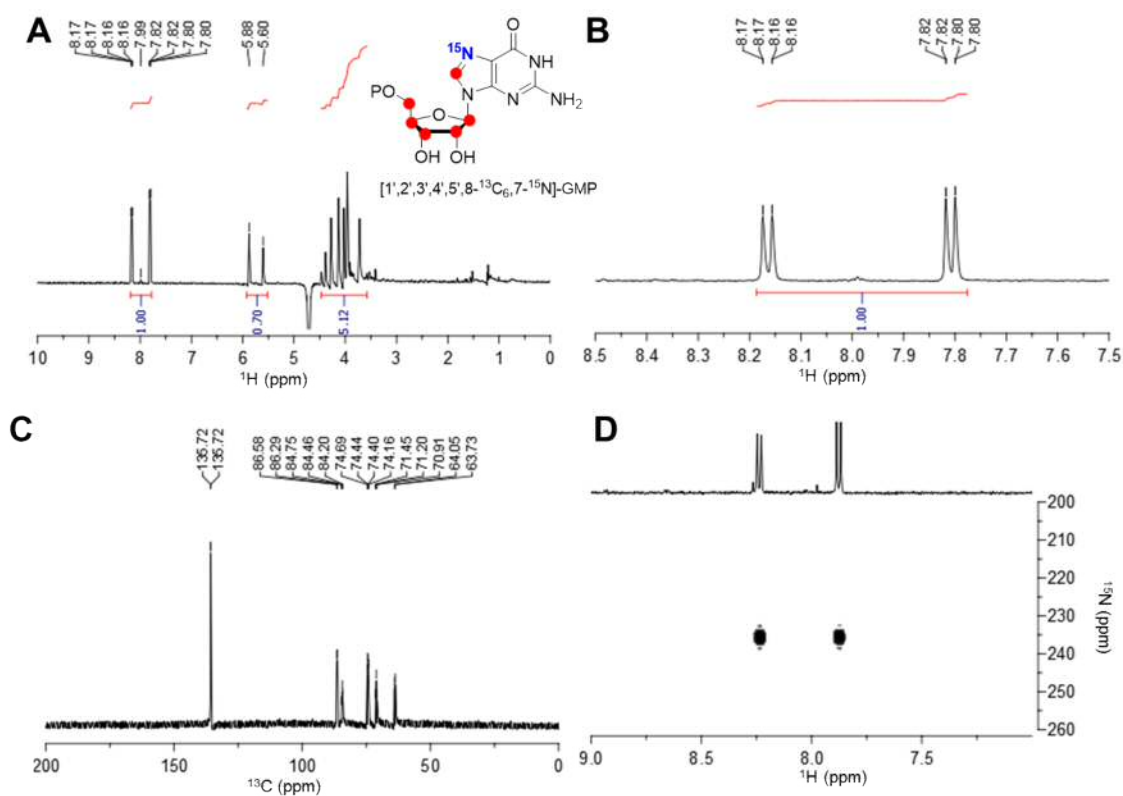


Figure 3.15. (A) ^1H -NMR of $[1',2',3',4',5',8\text{-}^{13}\text{C}_6,7\text{-}^{15}\text{N}]\text{-GMP}$. (B) Purine C8 proton splits as a doublet of doublets for the spin-spin coupling to both C8 and N7 atoms ($^1J_{\text{CH}} = 213$ Hz, $^2J_{\text{NH}} = 12$ Hz). (C) Isotopically labelled carbons from the ribose moiety are shown by ^{13}C -NMR between 100 ppm and 50 ppm, while C2 of the purine ring resonates at 135 ppm. (D) ^1H - ^{15}N -HMBC experiment shows a correlation between C8 proton to the N7 at 235 ppm.

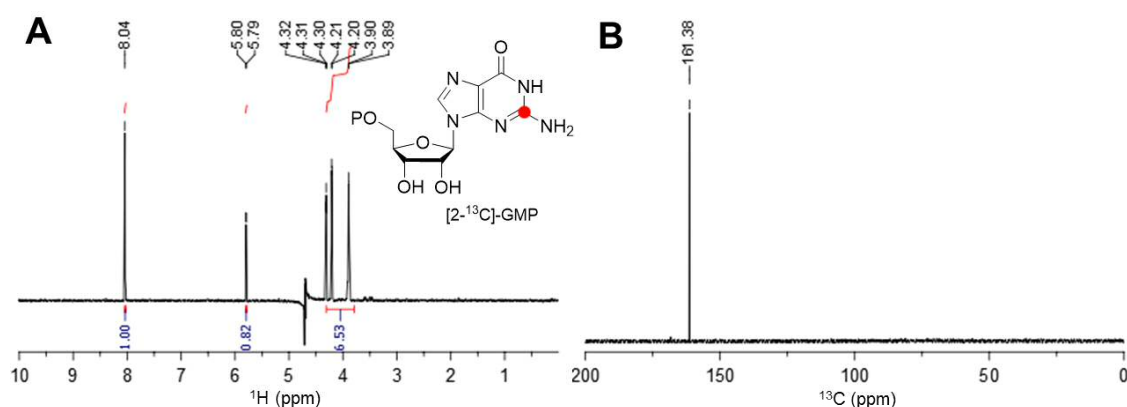


Figure 3.16. (A) ^1H -NMR and (B) ^{13}C -NMR of $[2\text{-}^{13}\text{C}]\text{-GMP}$.

3.5 Chemo-enzymatic synthesis of GTP

Synthesis of GTP is a continuation of GMP biosynthesis where two additional phosphate groups on GMP C5' position are added stepwise (figure 3.17). Consequently, the experimental setup for synthesising GTP is essentially identical to that described for GMP (section 3.4) except for the presence of an additional enzyme, guanylate kinase (GK), which transfers a phosphate group from ATP to GMP yielding ADP and GDP. The GDP intermediate is then further phosphorylated into GTP by the action of the ATP-recycling enzyme PK, which in this case also functions as a biosynthetic enzyme.

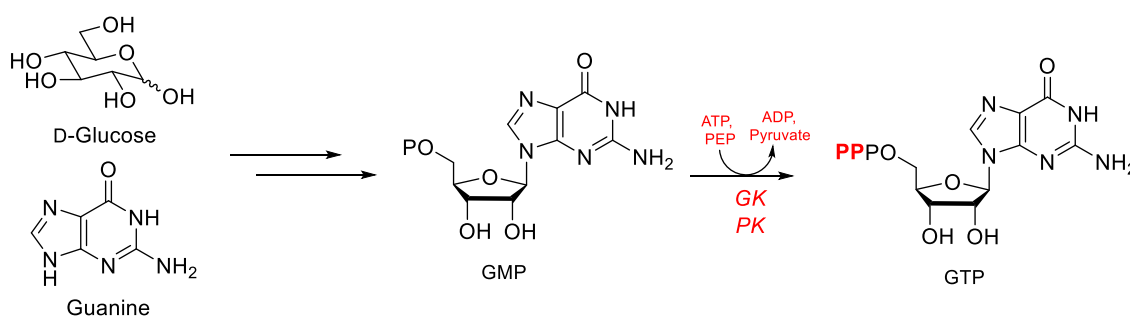


Figure 3.17. Continuation of guanosine monophosphate (GMP) biosynthesis illustrated in figure 3.11 to the formation of guanosine triphosphate (GTP).

3.5.1 Gene expression, purification and characterisation of recombinant guanylate kinase (GK)

The gene codifying for guanylate kinase (*gmk*) was amplified by PCR reaction using *E. coli* K-12 chromosomal DNA as template and subsequently cloned into the NdeI and XhoI sites of pET28-a vector (chapter 6, section 6.2). The recombinant enzyme, bearing a N-terminal hexahistidine tag, was overproduced in *E. coli* BL21(DE3) and purified by affinity chromatography (chapter 6, section

6.3.4.1). Sequencing of the cloned *gmk* gene revealed a point mutation of causing the shift of the Arg152 codon in Gly (R152G), and this was confirmed by mass spectrometry analysis (Figure 3.18). Nevertheless, the mutated enzyme was found active (Figure 3.19) and it therefore did not cause any difference for purposes of the work described here. GK activity has been tested by UV-vis spectroscopy by coupled assay with PK and lactate dehydrogenase (LDH) as previously described (214) (Figure 3.19 B and C). Briefly, ATP consumed by GK is regenerated by PK which in turn produces pyruvate as a by-product. In the presence of NADH, LDH reduces pyruvate to lactate, and this enzymatic step can be detected by following the decrease of NADH absorbance at 340 nm.

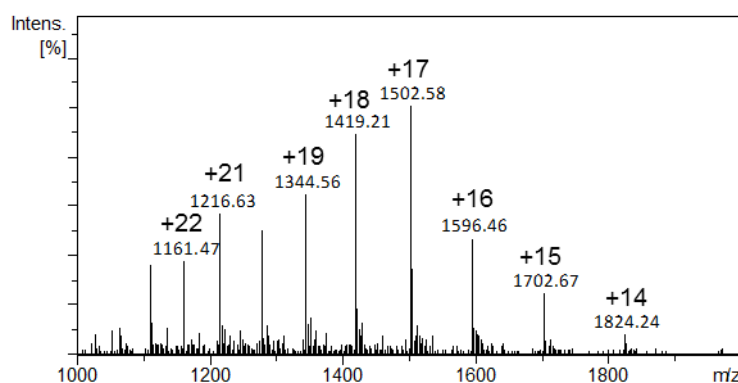


Figure 3.18. ESI-MS⁺ of purified GK R152G mutant. Deconvoluted experimental molecular weight of the recombinant enzyme was 25,526 amu (calculated 25,525 amu).

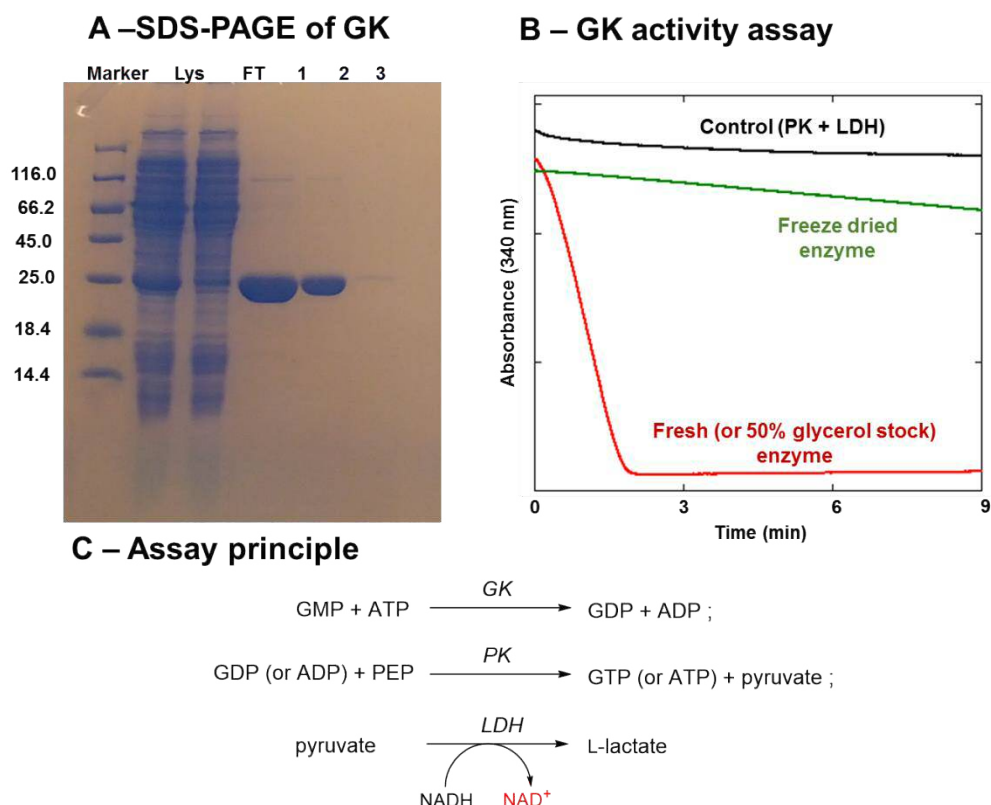


Figure 3.19. (A) SDS-PAGE of purified GK (MW = 25.5 kDa; fractions 1-2) compared to cell lysate (Lys) before and after (FT) purification. (B) GK activity monitored by UV-vis spectroscopy following NADH decrease at 340 nm. The assay principle is shown on panel (C). Compared to fresh (or 50% glycerol stock, red) GK, freeze dried GK (green) suffers of activity loss.

3.6 Conclusion

In this chapter, a simple procedure for the biosynthesis of isotopically labelled guanosine nucleotides (GMP and GTP) is reported. Compared to previous procedures, two major modifications were made. Firstly, the highly efficient recycling system for NADP⁺ based on the GR/GRX redox couple (chapter 2) was implemented. By using small organic sulfides as latent oxidizing reagents, the GR/GRX system is able to produce useful ‘byproducts’ such as β-mercaptoethanol to protect enzymes, reagents and products from unwanted

oxidative damage. Unlike other NADP⁺ recycling schemes such as the NOX and laccase/mediator systems, the GR/GRX pair is not dependent on oxygen and it is therefore functional under both aerobic and anaerobic conditions.

A second modification is related to formation of GMP through the combination of PRPP with insoluble guanine by the purine salvage pathway enzyme XGPRT. Although it has been described that the reaction can proceed using guanine as a slurry (205), such reaction conditions require long reaction times and have poor reproducibility. Hence, in this work, guanine was stored in an alkaline buffer (50 mM KOH) and added to the reaction dropwise with a syringe pump. Under these modifications, approximately 70-80% of GMP can be obtained within 60 mins. [1',2',3',4',5'-¹³C₅]-, [1',2',3',4',5'-¹³C₅,7-¹⁵N]-, [1',2',3',4',5'-8-¹³C₆,7-¹⁵N]- and [2-¹³C]-GMP were synthesised and characterised. These compounds are currently in use in our lab to conduct *in vivo* experiments on *Escherichia coli*.

4. CHEMO-ENZYMATIC SYNTHESIS OF ISOTOPICALLY LABELLED H₂Fs AND INVESTIGATION OF E_cDHFR CATALYSIS VIA HEAVY-ATOM ISOTOPE EFFECTS*

**This chapter summarises the work published on J. Am. Chem. Soc., 2017, 139 (37), pp 13047–13054 (DOI: 10.1021/jacs.7b06358). Authors of this article include Antonio Angelastro, William M. Dawson, Louis Y. P. Luk, E. Joel Loveridge and Rudolf K. Allemann. AA, the author of this PhD thesis, is the only first author for this article.*

4.1 Preface

Mapping the transition-state of the DHFR-catalysed reduction of H₂F by measuring heavy-atom isotope effects is fundamental to dissect the reaction mechanism on an atomic scale and to assist the rational design of novel DHFR inhibitors. To reach this goal, a set of H₂Fs site-specifically labelled on N5, C6, C7 and C9 positions of the pterin moiety with either stable (¹⁵N, ¹³C) or radioactive isotopes (¹⁴C) must be synthesised. To date, despite half a century of efforts and nearly 30 synthetic procedures reported in the literature, synthesis of folates labelled on the pterin moiety can only be partially achieved through laborious and cost-demanding procedures (Chapter 1, section 1.5). This is mainly due to the shortage of suitably labelled starting materials and lack of regio-, stereo- and enantio-selectivity of key chemical reactions. The picture is further complicated when reduced folates (*e.g.* H₂F) are considered as they are unstable toward oxygen, light, heat and non-physiological pH values (157-160).

In this work, the folate *de novo* biosynthetic pathway of *E. coli* was redesigned *in vitro* in a one-pot chemo-enzymatic synthesis. This allows us to produce isotopically labelled folates from D-glucose, guanine and *p*-aminobenzoyl-L-glutamic acid (*p*ABA-Glu). Using this biosynthetic route, H₂Fs enriched with stable isotopes at specific positions were synthesised in less than a week. The high degree of purity and isotopic enrichment (>97%) of these compounds has allowed us to perform, for the first time, single and multiple heavy-atom KIE measurements for EcDHFR catalysis and to derive unambiguous information about the chronological order of protonation and hydride transfer.

4.2 Cloning, expression, purification and assay of recombinant enzymes constituting the H₂F *de novo* pathway.

The folate *de novo* pathway (Chapter 1, section 1.6, figure 1.18) is constituted overall by 6 known enzymes: GTP cyclohydrolase I (GTP-CH-I), 7,8-dihydroneopterin triphosphate pyrophosphatase (DHNTPase), dihydroneopterin aldolase (DHNA), 6-hydroxymethyl 7,8-dihydropterin pyrophosphokinase (HPPK), dihydropteroate synthase (DHPS) and dihydrofolate synthase (DHFS). None of these enzymes is commercially available and therefore they have all been produced in-house through molecular biology techniques (Chapter 6, section 6.2). Genes encoding for GTP-CH-I, DHNA, HPPK and DHPS were cloned by Dr William Dawson (213) and corresponding recombinant enzymes were overproduced in *E. coli* strains as previously reported (213). Additionally, the gene encoding for DHNTPase (*nudB*) has been amplified from *E. coli* K-12 chromosomal DNA and cloned into the NdeI and XhoI sites of pET28-a vector (Chapter 6, Section 6.2). DHNTPase was overproduced in *E. coli* BL21(DE3)RP and purified by affinity chromatography (Chapter 6, section 6.3.4.1) (Figure 4.1).

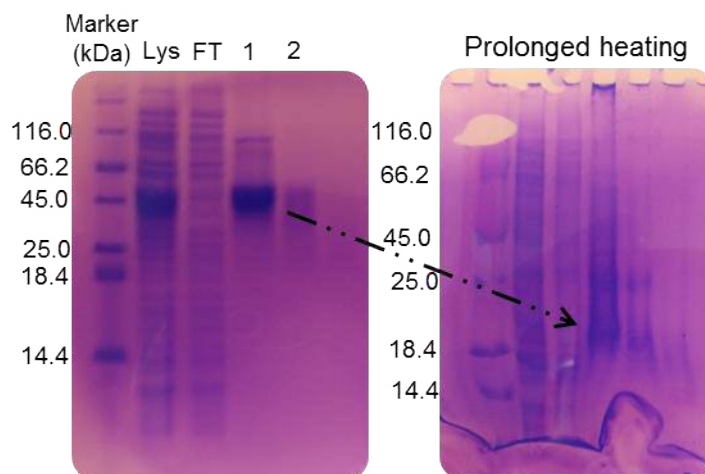


Figure 4.1. SDS-PAGE of purified DNTase by affinity chromatography (fractions 1-2) compared to cell lysate (Lys) before and after (FT) purification. After prolonged heating (right panel) the recombinant enzyme (MW = 19.500 kDa) shifts nearby the 18.4 kDa band of the marker.

4.2.1 Activity assay of recombinant enzymes constituting the H_2F pathway

GTP-CH-I activity can be monitored by following the increase of absorbance at 330 nm which corresponds to the formation of dihydropterin. Alternatively, the conversion of guanosine triphosphate (GTP) to 7,8-dihydroneopterin triphosphate (DHNTP) by GTP-CH-I can be visualised by acquiring UV spectra at defined intervals. As illustrated in Figure 4.2, the UV-vis spectrum at the beginning of the reaction (which corresponds to GTP) has profoundly transformed at the end of the reaction (which corresponds to DHNTP).

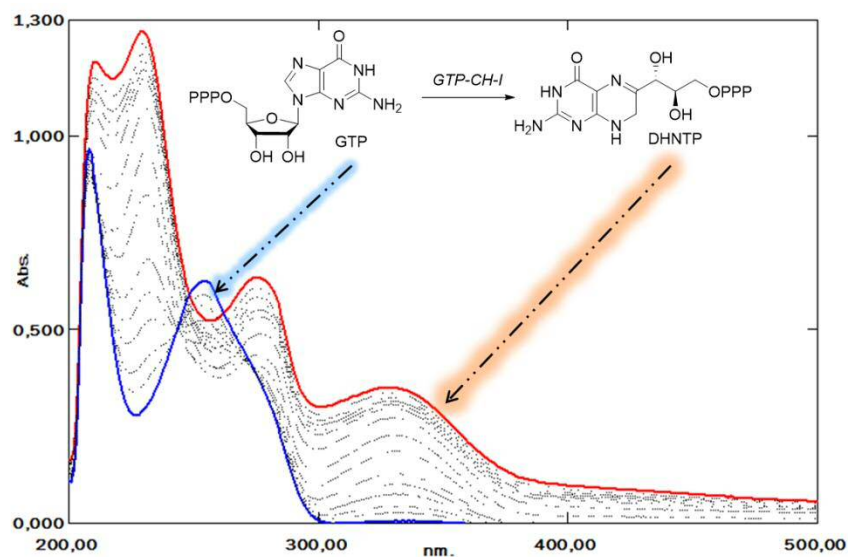


Figure 4.2. Formation of DHNTP from GTP catalysed by GTP-CH-I by UV-vis spectroscopy. UV spectra of starting material (blue) and product (red) are highlighted.

Assaying recombinant DHNTPase, DHNA, HPPK and DHPS activities was particularly problematic as all the corresponding product intermediates DHNTP, 7,8-dihydroneopterin monophosphate (DHNMP), 7,8-dihydroneopterin (DHN), 6-hydroxymethyl-7,8-dihydropterin (HMDP) and 6-hydroxymethyl-7,8-dihydropterin pyrophosphate (HMDPpp) are chemically unstable and have not been clearly characterised. This problem was also reported by Dr William Dawson who could not prove activity for recombinant HPPK and DHPS because DHN oxidised to neopterin under his experimental conditions (213). In this work, the issue was circumvented by sequential coupling of each enzyme to GTP-CH-I without isolating intermediates. Furthermore, reduced pterins were found to be sufficiently stable in the presence of oxygen for a day when protected from light and in presence of radical scavengers such as thiols, allowing analytical characterisation of each intermediate. DHNTP and DHNMP possess a triphosphate and monophosphate group, respectively, and thus can be analysed

Chemo-enzymatic synthesis of isotopically labelled H₂Fs and investigation of EcDHFR catalysis via heavy-atom kinetic isotope effects

by anion exchange chromatography (Figure 4.3). Coupling of DHNTPase with GTP-CH-I results in the formation of DHNMP from GTP (Figure 4.3 B). Dephosphorylation of DHNMP with alkaline phosphatase (ALP) yields the intermediate DHN which was identified by LC-MS (Figure 4.4). Addition of DHNA leads to the formation of HMDP from DHN, as indicated by LC-MS analysis (Figure 4.5). Similar to DHNTP and DHNMP, pyrophosphorylation of HMDP to HMDPpp by HPPK can be monitored by anion exchange chromatography (Figure 4.6). Production of dihydropteroate (H₂Pte) from HMDPpp and *p*ABA mediated by DHPS catalysis was proven by LC-MS (Figure 4.7).

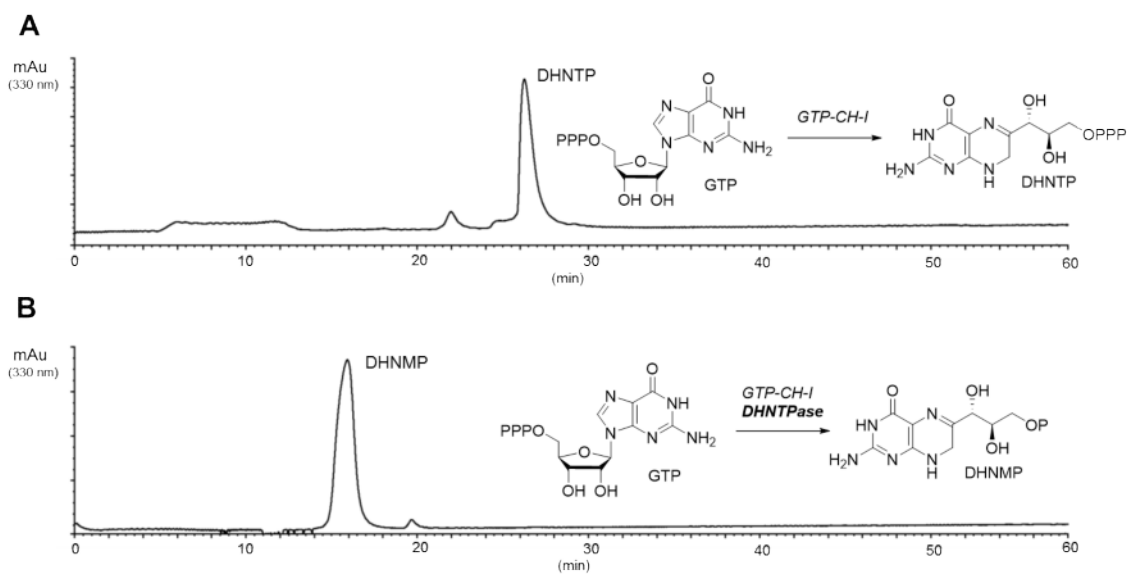


Figure 4.3. Anion exchange chromatograms of GTP (A) incubated with GTP-CH-I and (B) GTP-CH-I and DHNTPase.

Chemo-enzymatic synthesis of isotopically labelled H_2Fs and investigation of *EcDHFR* catalysis via heavy-atom kinetic isotope effects

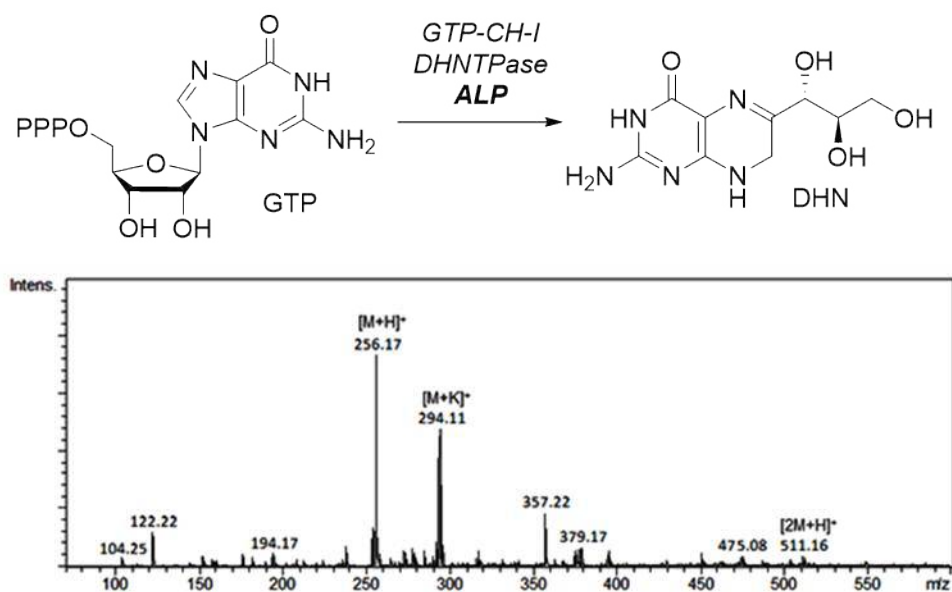


Figure 4.4. Positive ESI LC-MS of dihydroneopterin (DHN; MW = 255 amu) generated by GTP-CH-I, DHNTPase and ALP.

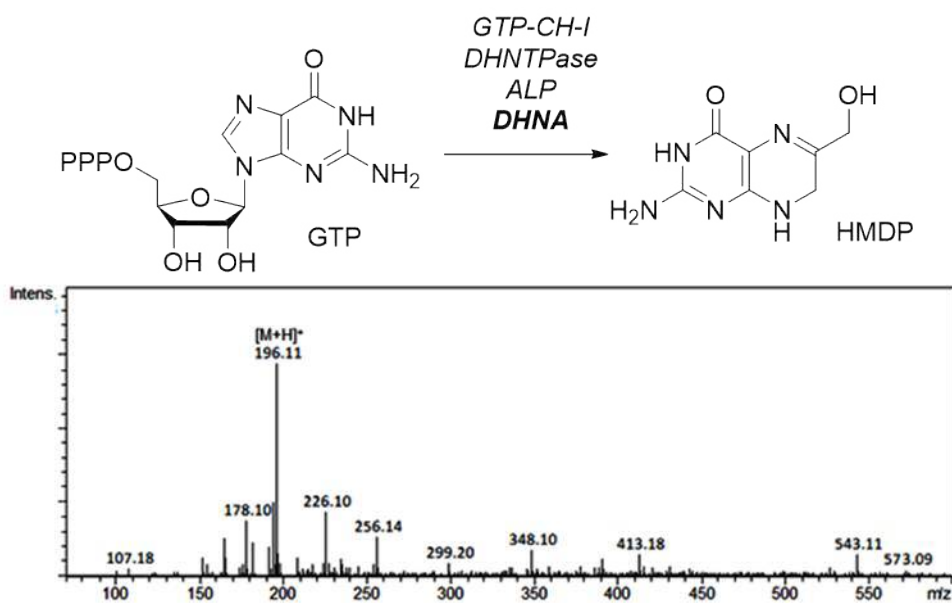


Figure 4.5. Positive ESI LC-MS of 6-hydroxymethyl-7,8-dihydropterin (HMDP; MW = 195 amu) by GTP-CH-I, DHNTPase, ALP and DHNA.

Chemo-enzymatic synthesis of isotopically labelled H_2Fs and investigation of *EcDHFR* catalysis via heavy-atom kinetic isotope effects

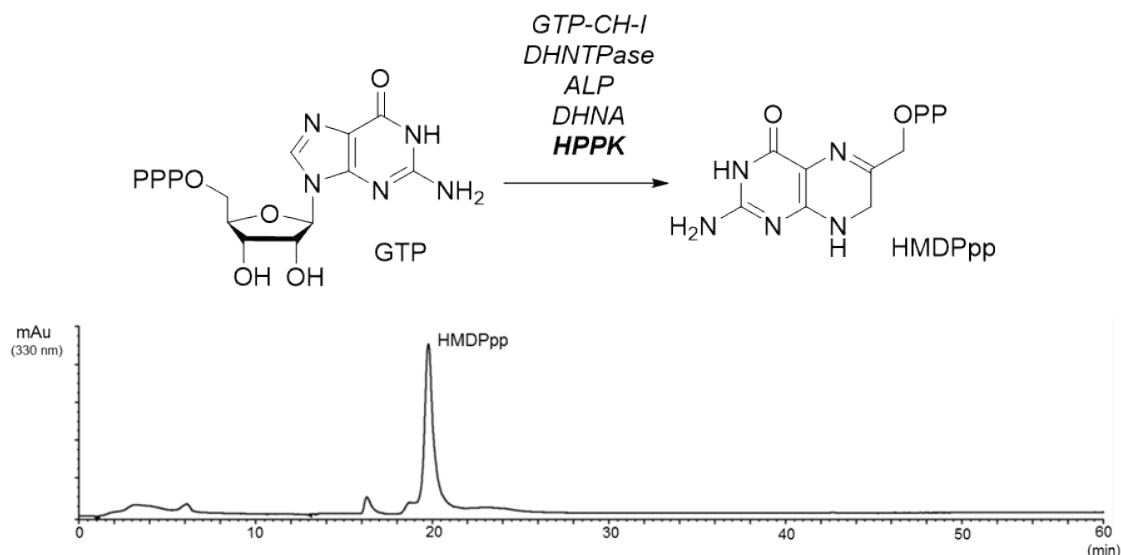


Figure 4.6. Anion exchange chromatogram of 6-hydroxymethyl-7,8-dihydropterin pyrophosphate (HMDPpp) generated by GTP-CH-I, DHNTPase, ALP, DHNA and HPPK.

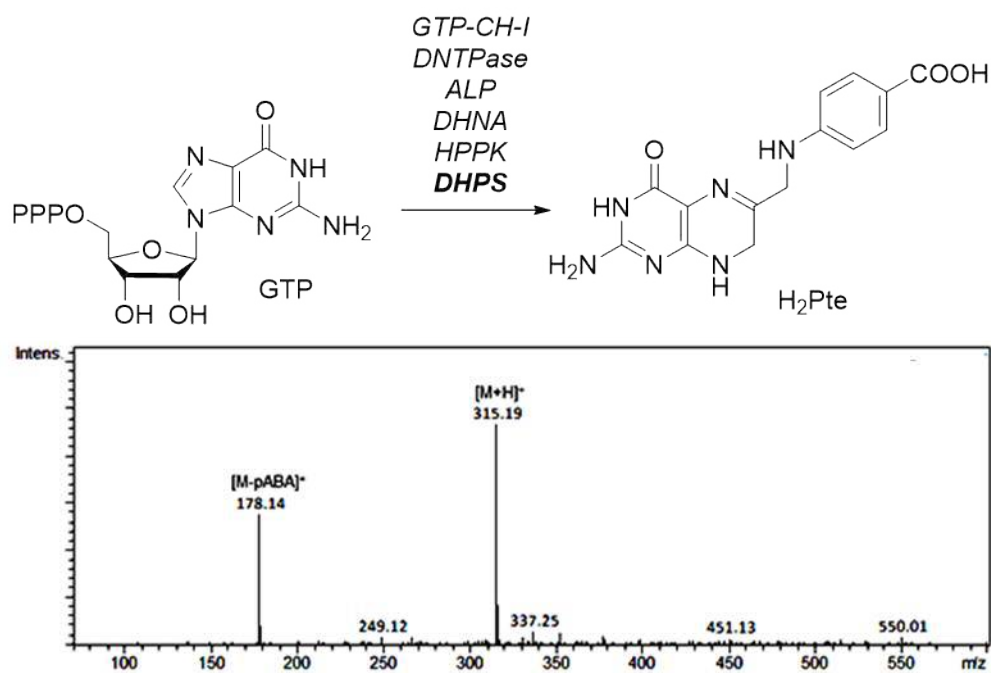


Figure 4.7. Positive ESI LC-MS of H₂Pte generated from 6-hydroxymethyl-7,8-dihydropterin pyrophosphate (HMDPpp) and p-aminobenzoic acid (pABA) by dihydropteroate synthase (DHPS).

4.3 Design of H₂F chemo-enzymatic synthesis

In the design of the enzymatic synthesis of H₂F, two key issues had to be considered: (1) use of simple building block of which isotopically labelled counterparts can be obtained; (2) establish a simple, versatile and fast procedure avoiding isolation of reaction intermediates. Attention was focused on labelling H₂F N5, C6, C7 and C9 of the pterin moiety as these positions are directly involved in the formation of the transition-state during the DHFR-catalysed reduction of H₂F to H₄F (Chapter 1, section 1.3). All atoms composing the pterin moiety are derived from GTP, the first intermediate of the folate *de novo* pathway (Figure 4.8). Precisely, C1', C2', C3', N1, C2, N3, C4, C5, C6, N7 and N9 positions of GTP correspond to the C7, C6, C9, N3, C2, N1, C4b, C4a, C4, N5 and N8 positions of H₂F. The use of isotopically labelled GTP is crucial to produce H₂F enriched on the positions of interest (N5, C6, C7 and C9), and site-specific isotopically labelled GTPs need to be synthesised. As discussed in chapter 3, a biosynthetic procedure for generating isotopically labelled GTP from D-glucose and guanine is available (Figure 4.8). The labelled nucleotides were generated to prepare the corresponding H₂Fs by combining a total of 17 enzymes. In this biosynthetic cascade, no intermediate needs to be isolated due to the general high substrate specificity of each enzyme. Also, because H₂F and other pterin intermediates are prone to oxygen-dependent degradation (158), the biosynthesis was performed in an anaerobic environment, with an overall yield of 30%.

Chemo-enzymatic synthesis of isotopically labelled H_2Fs and investigation of *EcDHFR* catalysis via heavy-atom kinetic isotope effects

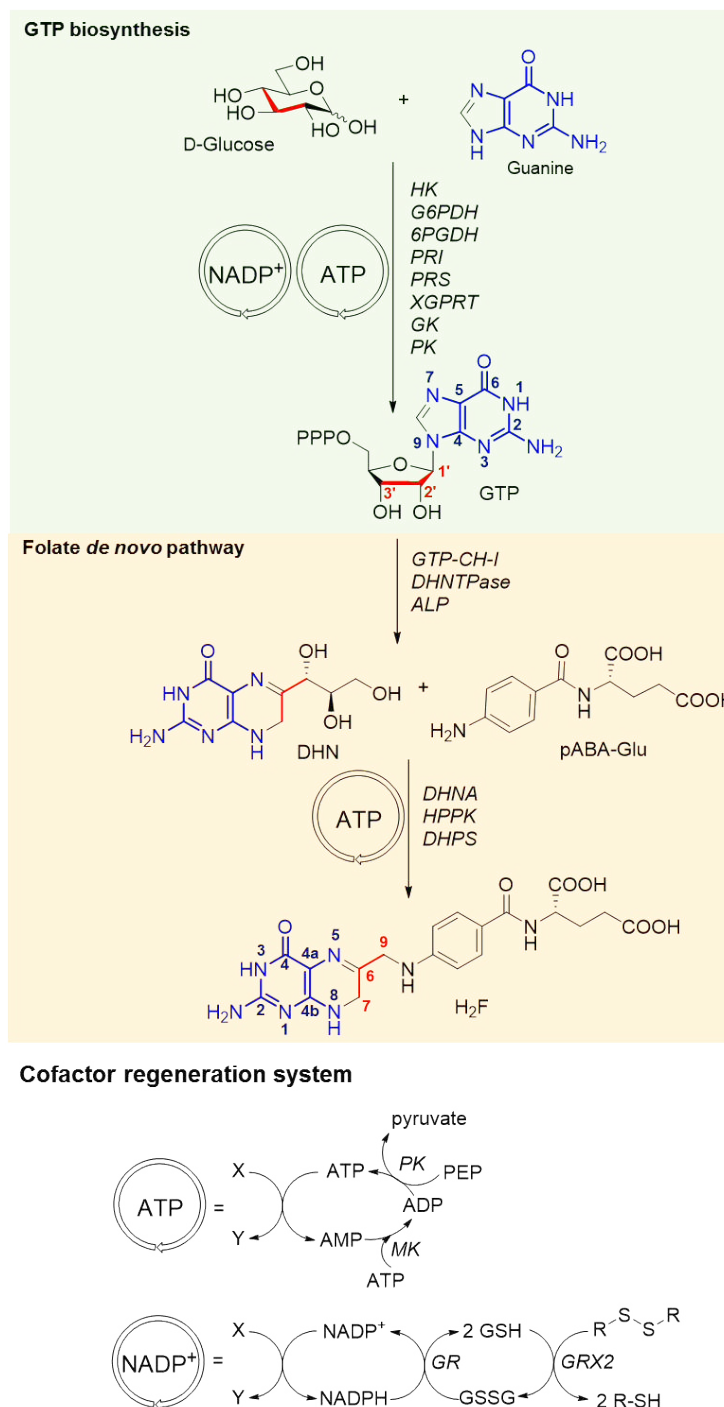


Figure 4.8. Biosynthetic strategy for the synthesis of H_2F . Glucose and guanine are processed into the key intermediate guanosine triphosphate (GTP, Chapter 3), which is then reorganized into DHN by GTP-CH-I, DHNTPase and ALP. DHNA, HPPK and DHPS combine DHN with *p*ABA-Glu to yield the final product H_2F . Additionally, myokinase (MK), glutathione reductase (GR) and glutaredoxin 2 (GRX2), are used to constitute cofactor regeneration systems for ATP and $NADP^+$ (171, 179).

4.3.1 DHNATPase enhances GTP-CH-I activity

Reorganisation of GTP into DHNTP by GTP-CH-I is a metabolic branch point connecting the purine biosynthetic pathway to H₂F *de novo* synthesis (215). *In vitro* manipulation of GTP-CH-I was challenging, mainly because of its low turnover constant ($k_{\text{cat}} = 0.05 \text{ s}^{-1}$) (216) and the inherent chemical instability of DHNTP. Positive allosteric effectors like potassium and magnesium cations were reported to increase the GTP-CH-I rate up to 5-fold and they were included in the reaction buffer (217), whereas oxygen removal stabilises DHNTP allowing longer reaction times. Despite these adjustments, conversion of GTP to DHNTP remained incomplete (Figure 4.9).

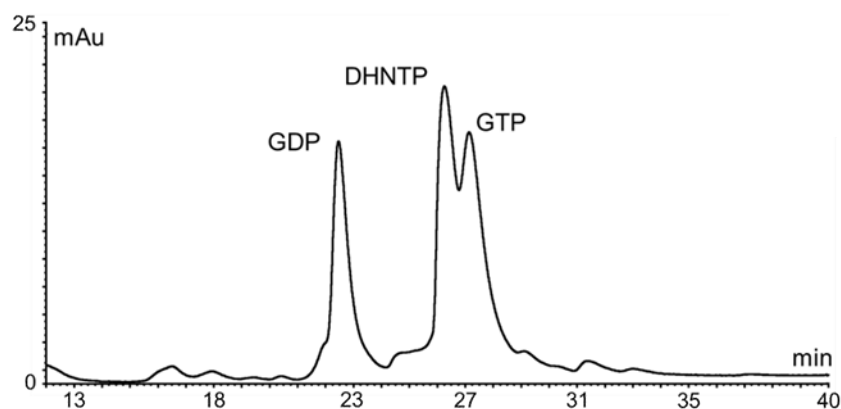


Figure 4.9. Anion exchange analysis of GTP incubated with GTP-CH-I reveals a partial conversion of GTP into DHNTP. Formation of guanosine monophosphate (GDP) is due to the non-enzymatic hydrolysis of GTP the assay.

The second chemical transformation in folate biosynthesis is a partial dephosphorylation of DHNTP to DHNMP by DHNTPase (163, 218). Interestingly, deletion of the gene that encodes DNTase strongly impairs *E. coli* folate metabolism (163). This therefore suggests that DHNTP hydrolysis is involved in

folate metabolic flux regulation. Considering that guanosine monophosphate (GMP) does not influence GTP-CH-I kinetics (219), it is plausible that DHNTPase acts as a positive effector on GTP-CH-I. That is, GTP-CH-I is inhibited by DHNTP but not DHNMP. To test the hypothesis, GTP-CH-I was assayed *in vitro* either in the absence or presence of DHNTPase (Figure 4.10). When coupled to DHNTPase, GTP-CH-I showed a marked rate enhancement and complete conversion to DHNMP (Figure 4.10 and 4.11).

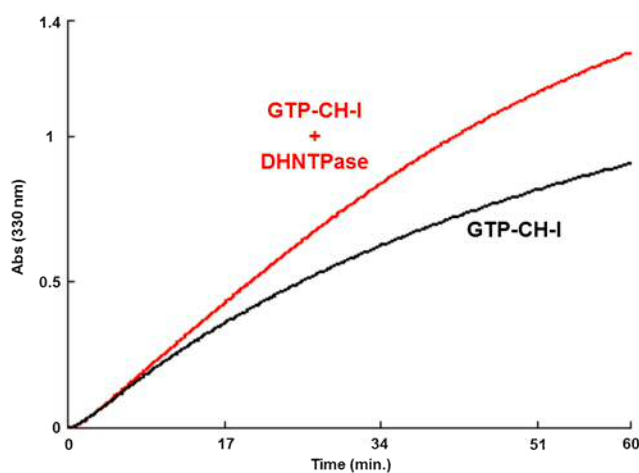


Figure 4.10. Comparison of GTP-CH-I activity in absence (black) and presence (red) of DHNTPase monitoring 7,8-dihydroneopterin formation absorbance at 330 nm by UV-Vis spectroscopy.

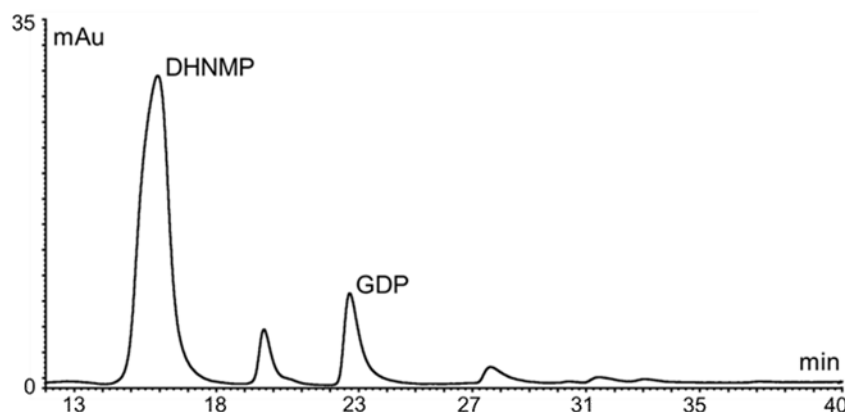


Figure 4.11. Anion exchange analysis of GTP incubated with GTP-CH-I and DHNTPase shows total conversion of GTP to DHNMP.

4.3.2 DHPS substrate tolerance simplifies H_2F biosynthesis

In H_2F biosynthesis, DHNMP needs to be dephosphorylated to DHN. Currently, the natural enzyme responsible for converting DHNMP to DHN is not known (162, 163). Non-specific alkaline phosphatase (ALP) was therefore used. DHN is then refined to HMDP by DHNA through a retro-aldol reaction. Then, HPPK catalyses the pyrophosphorylation of DHN to form HMDPpp with consumption of ATP (220). In *E. coli*, HMDPpp is first added with *pABA* and subsequently glutamate by the actions of two separate enzymes, DHPS and DHFS. These reactions yield dihydrofolate (H_2F) as the product (Figure 4.12). DHPS has a relaxed substrate specificity and is also capable of accepting pre-assembled *pABA*-Glu instead of *pABA* (221), and therefore DHFS was omitted in the reaction pathway. This synthesis requires only one purification step as no intermediate needs to be isolated. However, ALP needed to be removed from the reaction mixture by ultrafiltration before the addition of DHNA, HPPK and DHPS, because ALP can remove phosphate groups from ATP and HMDPpp. All reduced pterins compounds (DHNTP, DHNMP, DHN, HMDP, HMDPpp), including the final

Chemo-enzymatic synthesis of isotopically labelled H₂Fs and investigation of EcDHFR catalysis via heavy-atom kinetic isotope effects

product H₂F, are oxygen-sensitive, therefore the synthetic pathway was performed within a N₂-filled glove box system to ensure the removal of oxygen (<0.5 ppm). Additionally, generation of antioxidant thiols by the NADP⁺ recycling system based on the GRX system (Chapter 2) helped to stabilise intermediates that are unstable in the presence oxygen (e.g. H₂F). For the H₂F biosynthetic pathway, cysteine is preferred over HED (oxidised β-mercaptoethanol) for the GR/GRX2 NADP⁺ regeneration system. Perhaps, β-mercaptoethanol made from the reduction of HED can interfere with other enzymatic reactions, such as the chelation of Zn²⁺ in GTP-CH-I. 6.6 mg of H₂F were produced from 9 mg of glucose with an overall yield of 30%.

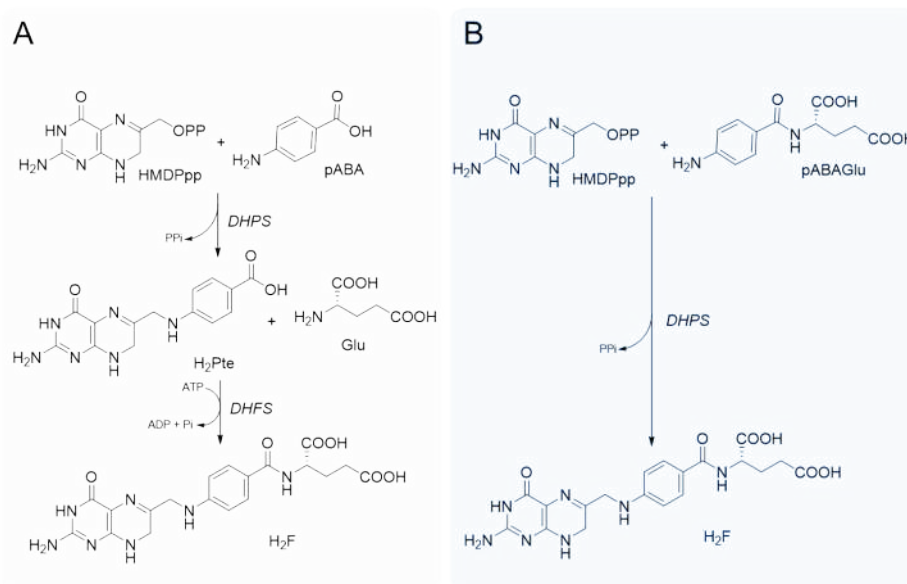
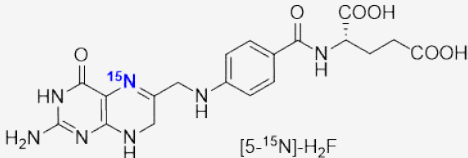
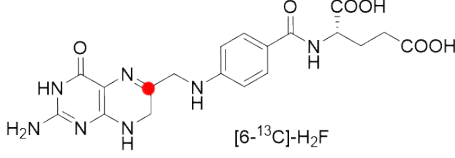
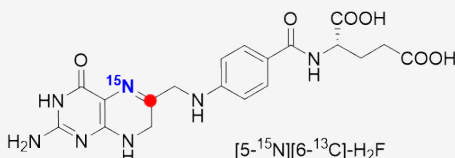
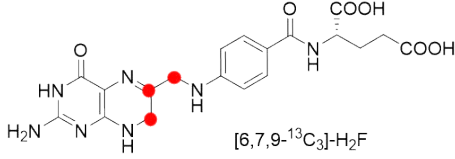
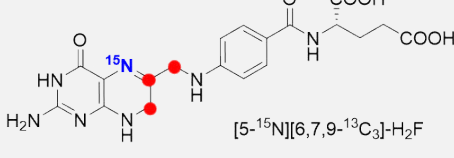


Figure 4.12. (A) In nature, H₂F is assembled from HMDPpp, pABA and Glu by dihydropteroate synthase (DHPS) and dihydrofolate synthase (DHFS). (B) *In vitro*, a shorter route to H₂F is made possible by DHPS tolerance to alternative substrates like pABAGlu.

4.4 Synthesis and characterization of labelled H₂Fs

Five isotopically labelled H₂Fs were synthesised using the H₂F chemo-enzymatic synthesis described in this chapter (Table 4.1). All compounds were characterised by a combination of NMR spectroscopy and high-resolution mass spectrometry (HR-MS).

Table 4.1. Isotopically labelled H₂Fs synthesised in this work. ¹³C is highlighted in red.

Starting Material	Labelled H ₂ F	Accurate Mass [M+H] ⁺ (amu)
D-Glucose [7- ¹⁵ N]-Guanine pABA-Glu	 [5- ¹⁵ N]-H ₂ F	445.1624
[3- ¹³ C]-D-Glucose Guanine pABA-Glu	 [6- ¹³ C]-H ₂ F	445.1624
[3- ¹³ C]-D-Glucose [7- ¹⁵ N]-Guanine pABA-Glu	 [5- ¹⁵ N][6- ¹³ C]-H ₂ F	446.1575
D- ¹³ C ₆ -Glucose Guanine pABA-Glu	 [6,7,9- ¹³ C ₃]-H ₂ F	447.1721
D- ¹³ C ₆ -Glucose [7- ¹⁵ N]-Guanine pABA-Glu	 [5- ¹⁵ N][6,7,9- ¹³ C ₃]-H ₂ F	448.1694

HRMS spectrum of [6-¹³C]-H₂F produced from from [3-¹³C]-D-glucose shows an increase of molecular weight of ~1 amu, and ¹³C-NMR spectroscopic

characterisation reveals a singlet at 152 ppm. Additionally, ¹H-¹³C-HMBC spectroscopy illustrates long-range couplings between 6-¹³C and hydrogens attached to C7 and C9 positions (H7 and H9) (figure 4.13 A). To incorporate a ¹⁵N label into the pterin moiety, the labelled substrate [7-¹⁵N]-guanine was used; the resulting product also showed ~1 amu increase in HRMS analysis and a ¹⁵N signal at 285 ppm coupling with H7 and H9 in the ¹H-¹⁵N HMBC experiment (Figure 4.13 B). When [3-¹³C]-D-glucose and [7-¹⁵N]-guanine are combined in the biosynthetic pathway, both the N5 and C6 positions of H₂F are isotopically enriched. This is evident by a mass increase of ~2 amu and ¹³C-NMR which shows a doublet at ~152 ppm with a coupling constant ¹J_{CN} of 7.5 Hz. ¹H-¹³C HMBC and ¹H-¹⁵N HMBC spectroscopic characterisation also reveals the anticipated long range C7 and C9 hydrogens coupling (Figure 4.14). Similarly, [6,7,9-¹³C₃]-H₂F and [5-¹⁵N][6,7,9-¹³C₃]-H₂F have been made using ¹³C₆-D-glucose and [7-¹⁵N]-guanine and verified by HRMS and NMR spectroscopy analyses (Figures 4.15 and 4.16).

All isotopically labelled H₂Fs were also characterised by ¹H-NMR (Figure 4.17 and 4.18). While ¹H-NMR spectrum of [5-¹⁵N]-H₂F is identical to that of natural abundance H₂F (Figure 4.17 A), chemical shift of both H7 (3.95 ppm) and H9 (3.87 ppm) result perturbed in [6-¹³C]-H₂F, [5-¹⁵N, 6-¹³C]-H₂F, [6-¹³C₃]-H₂F and [5-¹⁵N, 6-¹³C₃]-H₂F (Figure 4.18). When the C6 position of H₂F is ¹³C-enriched ([6-¹³C]-H₂F and [5-¹⁵N, 6-¹³C]-H₂F), both H7 and H9 split as doublets on ¹H-NMR spectrum with a coupling constant ²J_{CH} of 6 Hz (Figure 4.18 B). In addition to the C6 long-range coupling, when C6, C7 and C9 are all ¹³C-labelled, such as in [6-¹³C₃]-H₂F and [5-¹⁵N, 6-¹³C₃]-H₂F, H7 and H9 further split as doublet of doublets (Figure 4.18 C).

Chemo-enzymatic synthesis of isotopically labelled H₂Fs and investigation of EcDHFR catalysis via heavy-atom kinetic isotope effects

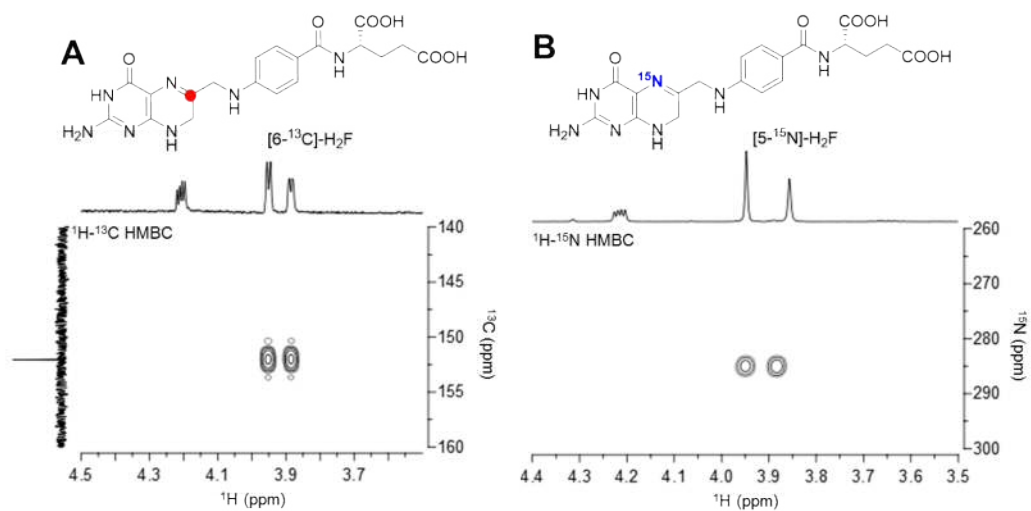


Figure 4.13. (A) ¹H-¹³C HMBC of [6-¹³C]-H₂F and (B) ¹H-¹⁵N HMBC (right panel) of [5-¹⁵N]-H₂F.

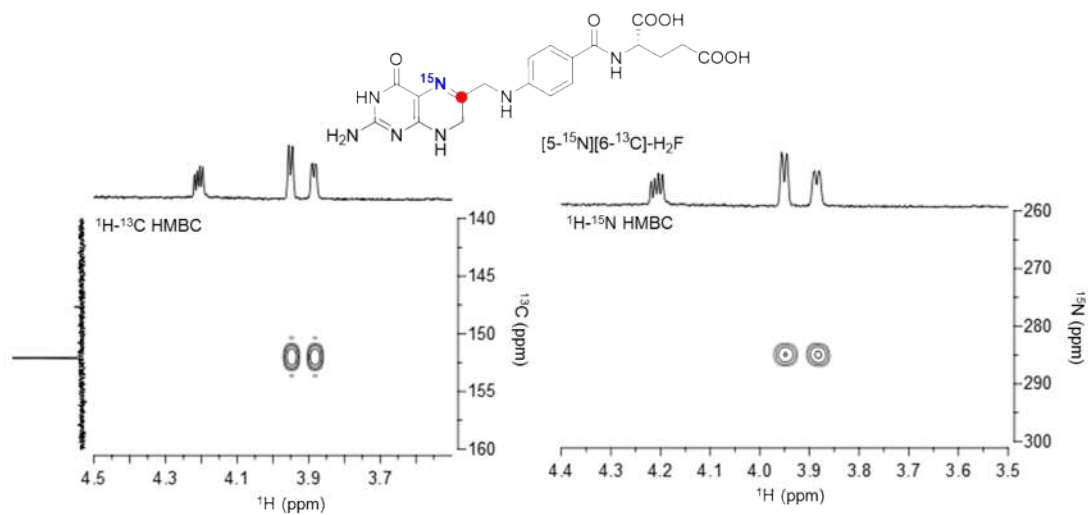


Figure 4.14. ¹H-¹³C HMBC (left panel) and ¹H-¹⁵N HMBC (right panel) of [5-¹⁵N][6-¹³C]-H₂F.

Chemo-enzymatic synthesis of isotopically labelled H_2Fs and investigation of *EcDHFR* catalysis via heavy-atom kinetic isotope effects

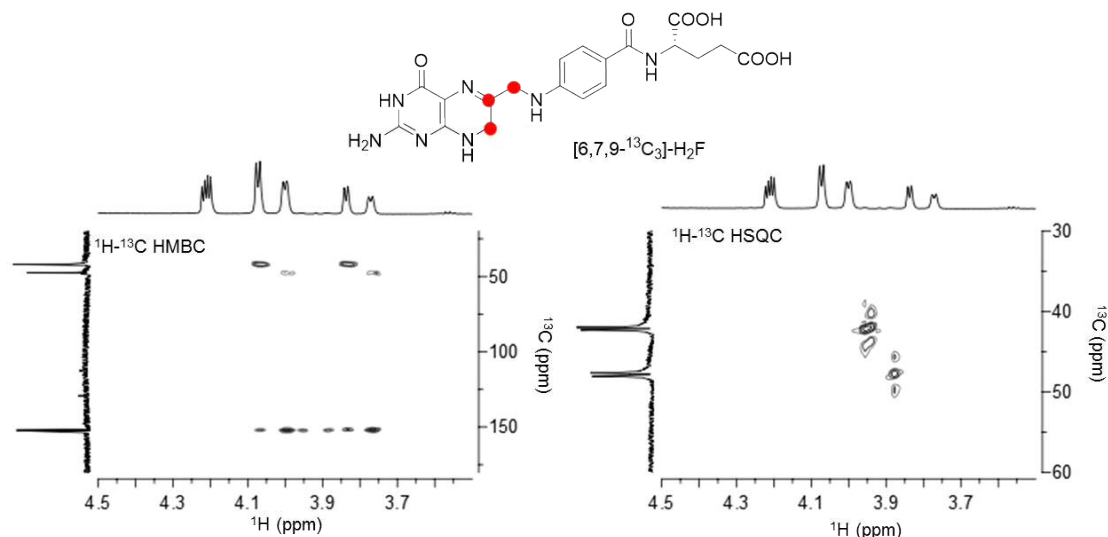


Figure 4.15. $^1H-^{13}C$ HMBC (left panel) and $^1H-^{15}N$ HSQC (right panel) of $[6,7,9-^{13}C_3]-H_2F$.

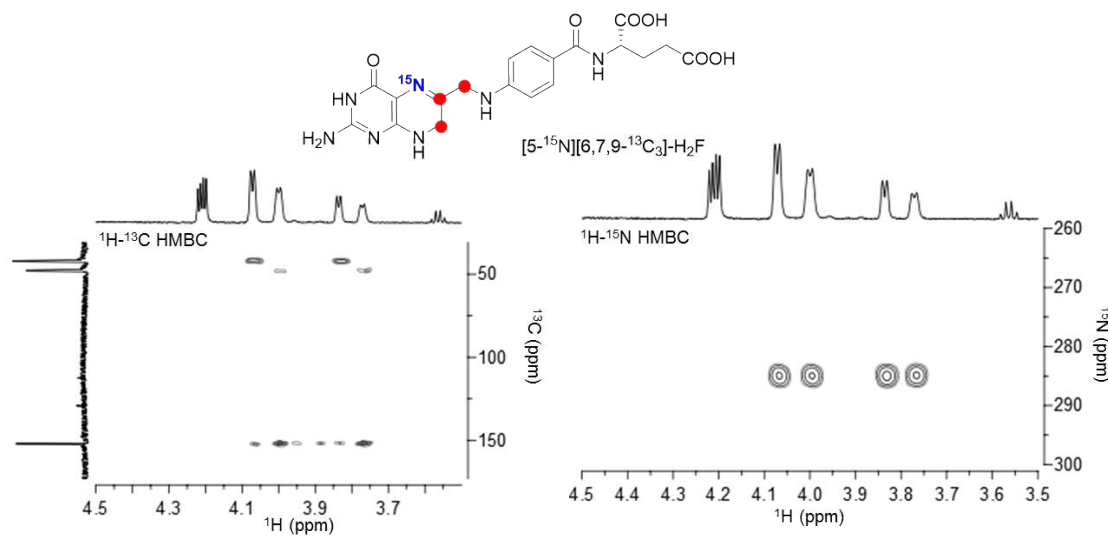


Figure 4.16. $^1H-^{13}C$ HMBC (left panel) and $^1H-^{15}N$ HMBC (right panel) of $[5-^{15}N][6,7,9-^{13}C_3]-H_2F$

Chemo-enzymatic synthesis of isotopically labelled H_2Fs and investigation of *EcDHFR* catalysis via heavy-atom kinetic isotope effects

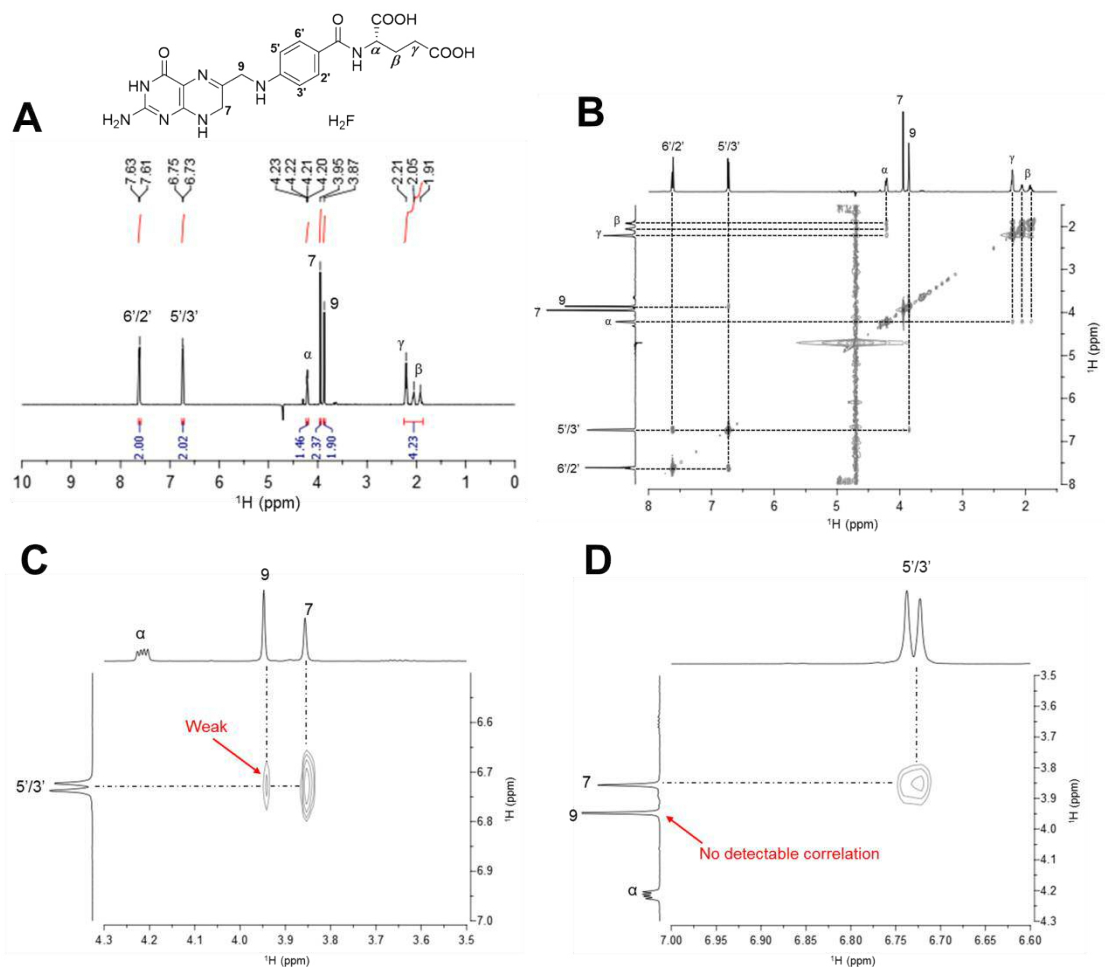


Figure 4.17. (A) 1H -NMR spectrum of natural abundance H_2F . (B) 2D-NMR NOESY experiment allows to unambiguously assign H7 and H9 protons, as highlighted in panels (C) and (D). In the NOESY experiment, H7 protons strongly correlate through space to 5' and 3' protons from *pABA* moiety whereas cross-correlations between H9 protons and 5'/3' are weaker or not detectable.

Chemo-enzymatic synthesis of isotopically labelled H_2Fs and investigation of *EcDHFR* catalysis via heavy-atom kinetic isotope effects

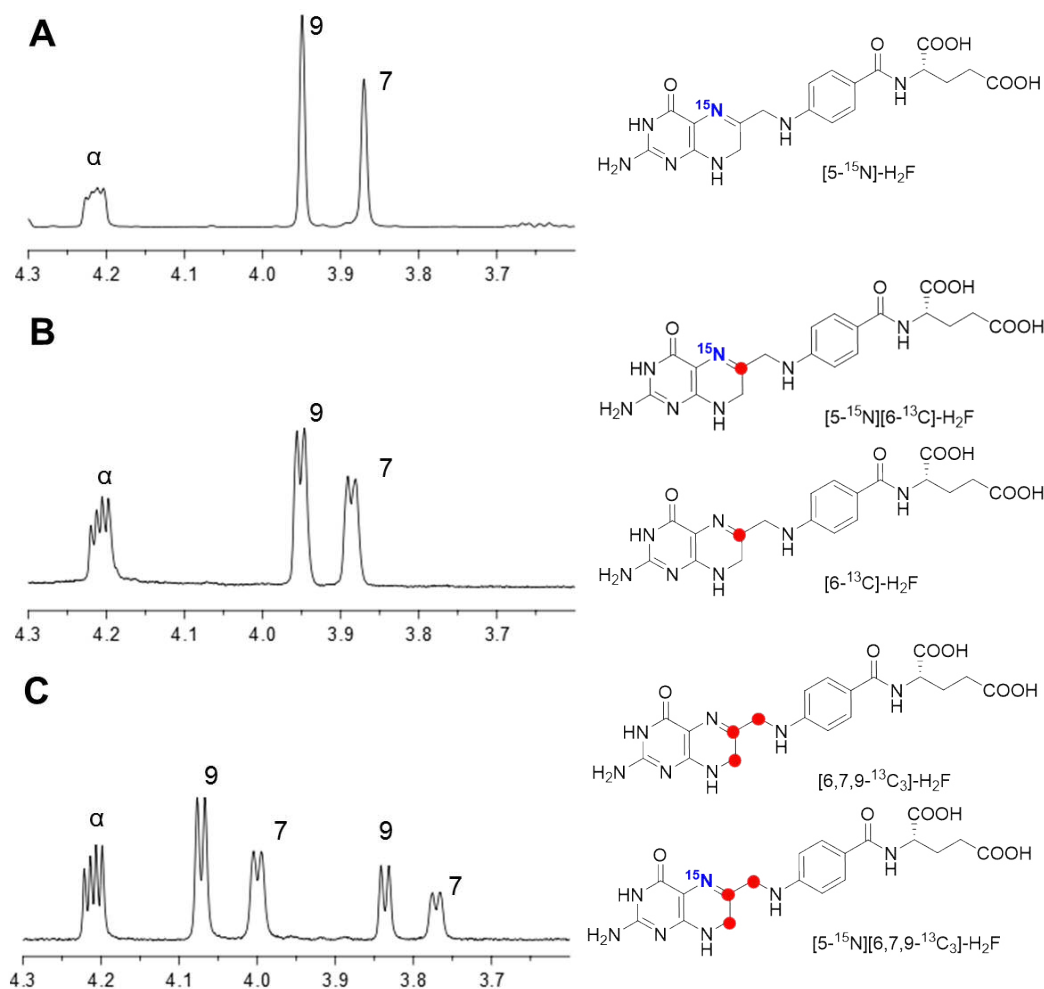


Figure 4.18. Sections from ^1H -NMR spectra of isotopically labelled H_2Fs . **(A)** In ^1H -NMR spectrum of $[5-^{15}\text{N}]-H_2F$, both H7 and H9 are singlets as in natural abundance H_2F . **(B)** When H_2F C6 position is ^{13}C -enriched, as in $[6-^{13}\text{C}]-$ and $[5-^{15}\text{N},6-^{13}\text{C}]-H_2F$, H7 and H9 protons split as a doublet ($^2J_{\text{CH}} = 6$ Hz) due to the long-range coupling to C6 **(C)**. In addition to C6, further isotopic enrichment of C7 and C9 positions results in additional splitting of H7 and H9 protons as doublet of doublets because of the short-range coupling of C7 to H7 ($^1J_{\text{CH}} = 144$ Hz) and C9 to H9 ($^1J_{\text{CH}} = 132$ Hz).

4.5 Single and multiple heavy-atom isotope effect studies on EcDHFR

EcDHFR, the enzyme sustaining the one-carbon metabolic cycle in *E. coli* by catalysing the reduction of H₂F to H₄F (Figure 4.19), is one of the most investigated natural catalyst in enzymology and a well-established model for the discovery of antimicrobial drugs (Chapter 1, section 1.4). Nevertheless, several aspects of its reaction mechanism remain unclear as the transition state structure(s) and the order of chemical transformation events have not been fully elucidated (87, 222). Solvent and hydrogen KIE measurements combined with site-directed mutagenesis have suggested a stepwise mechanism where protonation precedes hydride transfer (Figure 4.19 C) (83, 96).

However, D₂O increases the viscosity of the reaction buffer relative to H₂O (98, 99) and site-directed modification can alter the catalytic behaviour of an enzyme (97). Accordingly, to derive unambiguous information about the nature of the transition-state, [5-¹⁵N]-H₂F, [6-¹³C]-H₂F and [5-¹⁵N][6-¹³C]-H₂F were used to measure the ¹⁵N- and ¹³C-KIE. Recombinant EcDHFR used for pre-steady-state kinetics was overproduced in BL21-Star(DE3) cells (Chapter 6, section 6.3.4.2.1) and purified by a combination of anion exchange and size-exclusion chromatography techniques to ensure high purity (Figure 4.20).

Pre-steady-state kinetic measurements by fluorescence resonance energy transfer from a tryptophan nearby the active site to the reduced cofactor yields hydride transfer rate constants (k_H) with an accuracy up to 0.7%. While the measured ¹⁵N-KIE is one at all temperatures (Table 4.2 and Figure 4.21 A), the corresponding average ¹³C-KIE value at the same temperature range is 1.022 (Table 4.2 and Figure 4.21 B). The double labelled [5-¹⁵N][6-¹³C]-H₂F yielded an

average heavy-atom isotope effect of 1.018, close to that obtained with ¹³C-labeled substrate.

Considering the three possible scenarios for the reduction pathway of H₂F in the EcDHFR catalysed reaction (Figure 4.19), if the reduction proceeds through a concerted mechanism, where the N5 of H₂F is protonated concomitantly to the step of hydride transfer from the C4 of NADPH to the C6 of H₂F (Figure 4.19 B), isotopic labelling of either the reacting nitrogen or carbon atoms in H₂F would lead to a measurable kinetic difference from that of natural abundance substrate. Additionally, a concerted transition state would be reflected in the multiple heavy-atom KIE measurement when using the double labelled [5-¹⁵N][6-¹³C]-H₂F. Instead, as the measured ¹³C- and ¹⁵N¹³C-KIEs yield similar values and the observed ¹⁵N-KIE is close to unity, the heavy-atom isotope effect data reported in this PhD thesis rules out the possibility of a concerted mechanism. The KIE data strongly supports that the steps of protonation and hydride transfer are largely independent of each other and occur in a stepwise fashion. Whether the N5 protonation event occurs either after (Figure 4.19 A) or before (Figure 4.19 C) the hydride transfer step, previous experimental (77, 83, 85, 88-90, 96) and computational (91, 93-95) evidences indicate that N5 protonation is required for hydride transfer to occur but not *vice versa*. Notably (as mentioned in Chapter 1, section 1.4), while H₂F N5 pKa raises within EcDHFR Michaelis complex from 2.6 to 6.5 (77, 89, 90), the Asp27-mutated enzyme is still capable to function at acidic pH although catalytically compromised (85). In addition, Wan *et al.* recently proved through neutron and ultrahigh-resolution X-ray crystallography that folate N5 atom is indeed protonated when bound to EcDHFR (88).

Chemo-enzymatic synthesis of isotopically labelled H_2Fs and investigation of *EcDHFR* catalysis via heavy-atom kinetic isotope effects

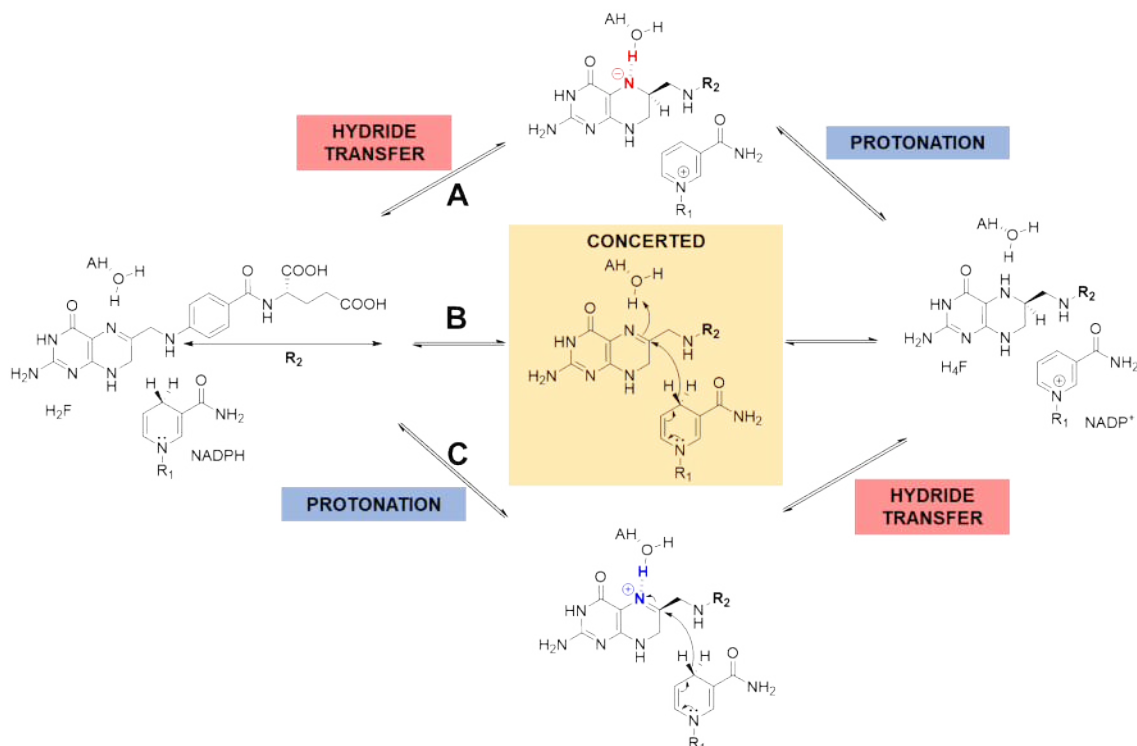


Figure 4.19. Possible scenarios for the *EcDHFR* catalysed reaction. **(A)** Hydride from C4 of NADPH is transferred to C6 of H_2F , followed by protonation in a stepwise fashion. **(B)** Hydride transfer is concomitant to protonation. **(C)** H_2F is firstly protonated, then hydride transfer occurs.

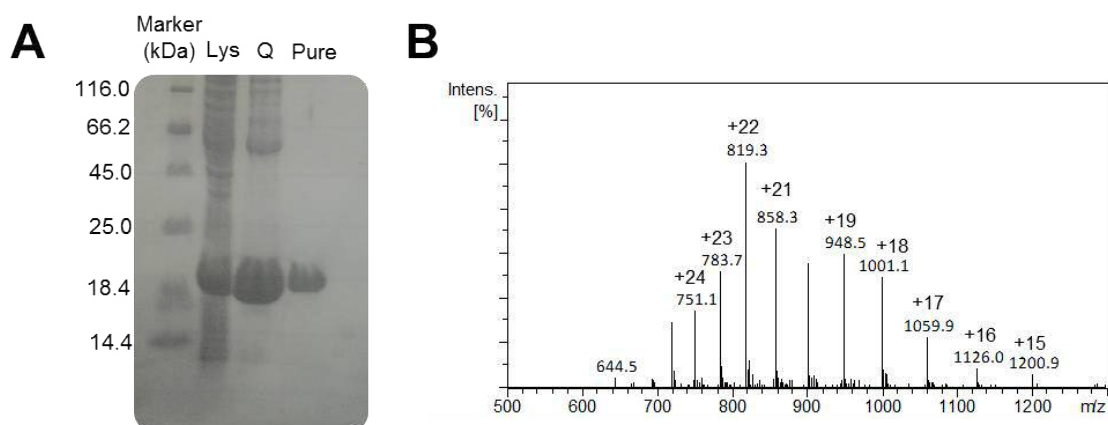


Figure 4.20. **(A)** SDS-PAGE and **(B)** positive ESI-MS of recombinant *EcDHFR* (theoretical MW = 17,999 amu, found = 18,000 amu) used for pre-steady-state kinetic measurements.

Table 4.2. Heavy-atom KIEs measured on EcDHFR using [6-¹³C]-H₂F, [5-¹⁵N]-H₂F and [5-¹⁵N][6-¹³C]-H₂F.

T (°C)	k_H^{14N}/ k_H^{15N}	k_H^{12C}/ k_H^{13C}	k_H^{14N12C}/ k_H^{15N13C}
5	0.996 ± 0.018	1.018 ± 0.009	1.020 ± 0.011
10	0.995 ± 0.018	1.018 ± 0.011	1.023 ± 0.010
15	0.999 ± 0.005	1.015 ± 0.006	1.014 ± 0.008
20	1.000 ± 0.009	1.021 ± 0.013	1.011 ± 0.007
25	0.993 ± 0.009	1.028 ± 0.007	1.018 ± 0.006
30	1.000 ± 0.022	1.023 ± 0.012	1.011 ± 0.009
35	1.000 ± 0.016	1.029 ± 0.012	1.034 ± 0.016

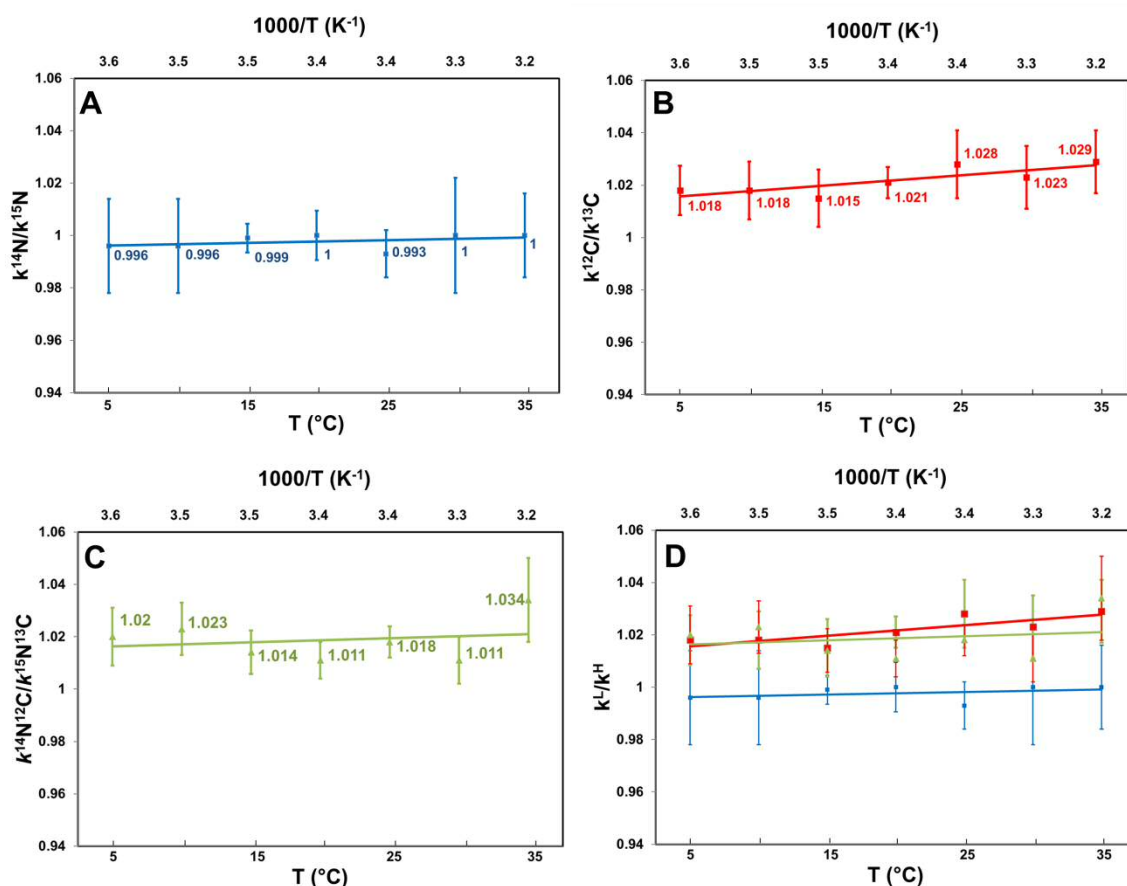


Figure 4.21. Heavy-atom KIEs measured on *EcDHFR* using (A) $[5-^{15}N]-H_2F$, (B) $[6-^{13}C]-H_2F$ and (C) $[5-^{15}N][6-^{13}C]-H_2F$. (D) Comparison between heavy-atom KIEs indicate a substantial difference between relative contributions of N5 and C6 positions in stabilizing the transition state during hydride transfer.

4.6 Conclusion

Isotopically labelled folate derivatives are useful, non-invasive probes to gain insight into the mechanism of DHFR, which may lead to improved design of drugs (Chapter 1). Previous chemical syntheses of folate are low yielding, require multiple purification steps and are characterized by poor regio- and stereo-selectivity (116, 117, 146, 147). Here, H_2F was produced enzymatically in a one-pot reaction from D-glucose, guanine and *pABA*-Glu, whose isotopically labelled counterparts are either commercially available or can be prepared easily (150,

208); only the final product was purified. Due to the improved reaction setup for GTP-CH-I, which converts GTP to DHNTF *via* four chemical steps, the cascade reaction which involves 17 enzymes, is also high yielding (223). The synthesis developed here shows the enormous potential of using enzymes in multistep reactions for the efficient synthesis of complex molecular structures. H₂Fs labelled in specific positions with stable isotopes could be prepared with an average overall yield of 30%. With this powerful biochemical setup, five isotopically labelled H₂Fs were synthesised including [5-¹⁵N]-H₂F, [6-¹³C]-H₂F and [5-¹⁵N][6-¹³C]-H₂F. These compounds were used to measure, for the first time, heavy-atom kinetic isotope effects for the reaction catalysed by EcDHFR, providing strong evidence that protonation at the N5 position of H₂F and hydride transfer to the C4 position occur in a stepwise mechanism.

With this newly developed synthesis it is possible to measure a wide range of primary and secondary heavy-atom isotope effects on DHFR and to derive transition-state maps for the catalysed reaction. However, accuracy of the non-competitive method used in this work is 0.7% whereas it should fall below 0.5% to have an accurate map of the transition-state (31). Accordingly, development of an alternative methodology to yield more accurate heavy-atom isotope effects is currently under progress in our research group. Besides the investigation of DHFR catalysis, labelled folates have many potential applications in both mechanistic enzymology and cell biology (90, 116, 117, 146, 224, 225). The work described here can be applied in nutritional, medical and cell biological research to address *in vivo* bioavailability and to perform kinetic investigation of folate metabolism in whole organisms including humans (119, 123, 225-228).

5. GENERAL CONCLUSIONS

DHFR, one of the most studied enzymes in chemical biology, serves as model in both fundamental enzymology and drug discovery research. Nevertheless, its mechanism of catalysis is not fully understood, mainly because information about the transition-state is missing. Measuring heavy-atom KIEs is the only technique available that can unambiguously provide detailed knowledge about the transition-state of the DHFR-catalysed reaction. However, current synthetic strategies to produce site-specific isotopically labelled H₂Fs are impractical and allow only a restrained pattern of isotopic substitutions.

This PhD programme has developed a versatile and cost-effective strategy for the production of H₂F labelled with stable isotopes (¹⁵N, ¹³C) at precise positions by re-designing the *de novo* folate biosynthetic pathway from *E. coli in vitro*. This methodology, which employs seventeen enzymes in a one-pot system, enables the production of highly purified labelled H₂Fs from D-glucose, guanine and *p*ABA-Glu in less than a week, with a single purification step and 30% overall yield.

In the process of developing the *in vitro* biosynthetic pathway of H₂F, we have addressed several technical issues which are also frequently encountered in the scientific community. A novel NADP⁺ recycling scheme based on the GR/GRX enzymatic redox couple was developed. The previously reported regeneration systems of NADP⁺ are either oxygen-dependent (NOX, laccase/mediator system) or poorly efficient (GDH and LDH system), and so they are not applicable in folate biosynthesis. The GR/GRX system was engineered to overcome these issues, enabling NADP⁺ to be recycled in the absence of oxygen with an improved total turn-over number (TTN). We discovered a maximal TTN of 5×10^5 , noticeably higher than those of other NADP⁺-recycling systems (TTN = $10^2 - 10^3$). NADP⁺

recycling *via* the GRX system also provides other significant advantages. The GRX system utilises electrons from NADPH to reduce small organic disulfides (e.g. cystine and HED) into thiols, with the possibility to choose the latent oxidising reagent on a case-by-case basis. Production of thiol is an additional benefit to the biosynthetic process, as it established a reducing environment preventing both enzymes and oxygen-sensitive intermediates (e.g. H₂F) from oxidative damages. Importantly, the GRX system does not depend on oxygen to function, implying that it can be used both in aerobic and anaerobic conditions. Overall, the development of GR/GRX system represents a substantial advance in the biocatalysis field and it will have wide applications in both academic and industrial settings.

In chapter 3, the synthesis of isotopically labelled GTP, a key branching intermediate to multiple biosynthetic pathways was reported (166, 205). Previous procedures of guanine nucleotides using enzymes from the salvage pathway are considered inadequate because of the poor reproducibility (205). Herein, a chemo-enzymatic approach to the synthesis of labelled guanine nucleotides using a combination of enzymes from the pentose phosphate and purine salvage pathways was reported with two major modifications: (1) GDH was replaced by GRX to recycle the NADP⁺ cofactor; (2) the formation of GMP from PRPP and insoluble guanine was optimised in an automated and reproducible way. Various isotopically labelled GMPs were produced with overall yields ranging between 70% and 80%. The optimised biosynthetic setup described in this thesis is not only beneficial to the synthesis of isotopically labelled H₂Fs, but also to a wide range of biochemical investigations. Isotopically labelled guanosine nucleotides are extensively used for biochemical studies, notably nucleic acids characterisation (202-204). Also, isotopically labelled GMPs synthesised in this

work are currently being used for studying flavin coenzymes including flavin adenine dinucleotide (FAD) (229).

The optimised biosynthetic setup of guanine nucleotides has allowed the synthesis of isotopically labelled H₂Fs in a one-pot procedure. Operating in an oxygen-free environment helped to stabilise reduced pterins, while DHNTPase was found to improve the overall yield by enhancing GTP-CH-I activity. Also, DHPS substrate tolerance permitted to further simplify H₂F synthesis by avoiding an additional biosynthetic step. Site-specific labelled D-glucose, guanine and *p*ABA-Glu are relatively simple to be either obtained from commercial sources or produced in-house. With the research described here it is now possible to prepare folate isotopically-enriched at any desired position using the same biosynthetic strategy. In this work, attention was focused at positions N5, C6, C7 and C9 of H₂F, as these atoms are involved into the formation of the transition-state in the DHFR-catalysed reaction. [5-¹⁵N]-, [6-¹³C]- and [5-¹⁵N,6-¹³C]-H₂F were produced to measure, for the first time, single and multiple heavy-atom kinetic isotope effects on EcDHFR. Our data obtained here strongly support a step-wise mechanism where H₂F N5 is protonated before a hydride from NADPH C4 is transferred to H₂F C6.

Because we aim to map the transition-state of the DHFR-catalysed reaction to design novel anti-DHFR drugs, we have developed a one-pot 14-steps *in vitro* chemo-enzymatic pathway of isotopically labelled H₂F for heavy atom KIE measurement. Whilst gaining important insights into the DHFR reaction, our work has also allowed us to develop a versatile NADP⁺-recycling system and a reproducible high-yielding GMP synthetic pathway. These achievements have created new opportunities in other areas research. The mechanistic

General conclusions

characterisations of other one-carbon enzymes, such as SHMT and TS, both of which are also important antiproliferative targets. This work also allows us to develop new high-yielding synthesis of isotopically labelled nucleotide-derived biomolecules, such as DNA, RNA, cofactors such as FAD and other pterin-containing natural products, including pigments and natural “sun-screen” like biopterin- α -glucoside (230). In conclusion, the completion of this PhD programme has opened the doors for many new research ideas and opportunities.

6. MATERIALS AND METHODS

6.1 Materials

L-Ascorbic acid (99%), 2,4-diamino-6-hydroxypyrimidine, 2-hydroxyethyl disulfide, L-cystine, D-($^{13}\text{C}_6$)-glucose, D-(3- ^{13}C)-glucose (99 atom%), L-glutathione (reduced), guanosine 5'-monophosphate disodium salt hydrate (from yeast, >99%), deuterium oxide (99.9 atom%), guanine, sodium dithionite, sodium nitrite- ^{15}N ($\text{Na}^{15}\text{NO}_2$, 98 atom%), were purchased from Sigma-Aldrich. NADP^+ monosodium salt (>98%) and ATP disodium salt trihydrate (>98%) were purchased from Apollo Scientific Ltd (UK). Phosphoenolpyruvic acid monopotassium salt, 99% was purchased from Alfa Aesar. 6-Phosphogluconic acid dihydrate and isopropyl- β -D-thiogalactopyranoside (IPTG) were obtained from Melford Laboratories Ltd (Ipswich, UK). 4-Aminobenzoic acid (99%), NADPH tetrasodium salt hydrate and guanosine 5'-triphosphate disodium salt hydrate (90%, for biochemistry) were purchased from ACROS Organics. Alkaline phosphatase from bovine intestinal mucosa (ALP, buffered aqueous glycerol solution), pyruvate kinase from rabbit muscle (PK, type II, ammonium sulfate suspension), myokinase from rabbit muscle (MK, ammonium sulfate suspension), glutathione reductase from baker's yeast (GR, *S. cerevisiae*, ammonium sulfate suspension), hexokinase from *S. cerevisiae* (HK, type F-300, lyophilized powder), glucose-6-phosphate dehydrogenase from *L. mesenteroides* (G6PDH, recombinant, expressed in *E. coli*, ammonium sulfate suspension) and phosphoriboisomerase from spinach (PRI, type I, partially purified powder) were purchased from Sigma-Aldrich. Crimson Taq DNA polymerase was purchased from New England Biolabs.

6.2 Preparation of solutions, buffers and growth mediums

6.2.1 Luria-Bertani (LB) liquid medium

Tryptone (10 g), NaCl (10 g) and yeast extract (5.0 g) were dissolved in 950 mL of deionised water (dH₂O). When the solutes have dissolved, volume of the solution was adjusted to 1 L. The final solution was sterilised by autoclaving at 121°C for 20 min. The sterile solution was stored at 4°C.

6.2.2 Luria-Bertani (LB) solid medium

Tryptone (10 g), NaCl (10 g) and yeast extract (5.0 g) were dissolved in 950 mL dH₂O. When the solutes have dissolved, volume of the solution was adjusted to 1 L and agar (15.0 g) was added. The suspension was sterilised by autoclaving at 121°C for 20 min. After sterilisation, the resulting homogeneous solution was cooled to 40°C and added with the appropriate antibiotic (e.g. kanamycin) before being poured into sterile petri dishes. Further cooling at room temperature resulted into solidification of the medium which has been stored at 4°C.

6.2.3 Sterile glycerol solution (50% v/v)

A 50% v/v glycerol solution was prepared by mixing 50 mL of glycerol to 50 mL of dH₂O. The resulting solution was sterilised by autoclaving at 121°C for 20 min and stored at 4°C.

6.2.4 Sterile antibiotic solutions

Three antibiotics (tetracycline, ampicillin and kanamycin) were used as selection markers for molecular cloning or gene expression into *E. coli* hosts. Tetracycline solution was prepared by dissolving 100 mg of the antibiotic in 10 mL of 70% ethanol solution. All remaining antibiotic sterile solutions (ampicillin and kanamycin) were made by dissolving 200 mg of the appropriate antibiotic in 4 mL

of dH₂O and sterilised by filtration using a 0.2 µm syringe filter. Sterile solutions were stored at -20°C.

6.2.5 Bradford reagent

20 mg brilliant blue G250 dissolved in a small amount of ethanol were mixed with 20 mL of 80% H₃PO₄. The solution was diluted to 200 mL with dH₂O, filtered and stored at 4°C protected from light.

6.2.6 Molecular cloning buffers

6.2.6.1 Transformation buffer I (Tfb-I)

0.588 g of potassium acetate (30 mM), 2.42 g of rubidium chloride (100 mM), 0.294 g of calcium chloride (10 mM) and 2.0 g of manganese chloride (50 mM) are dissolved in 100 mL of dH₂O and the pH adjusted with diluted acetic acid to 5.8. 30 mL of glycerol (15% v/v) are thereafter added and the volume adjusted to 200 mL with additional dH₂O. The final solution is sterilised by filtration using a 0.2 µm syringe filter and stored at +4°C

6.2.6.2 Transformation buffer II (Tfb-II)

0.21 g of 3-(N-Morpholino)propanesulfonic acid (MOPS, 10 mM), 1.1 g of calcium chloride (75 mM) were dissolved in 50 mL of dH₂O and the pH adjusted with diluted NaOH to 6.5. 15 mL of glycerol (15% v/v) are thereafter added and the volume adjusted to 100 mL with additional dH₂O. The final solution is sterilised by filtration using a 0.2 µm syringe filter and stored at +4°C.

6.2.6.3 Transformation buffer III (Tfb-III)

1.11 g of calcium chloride (100 mM) was dissolved in 90 mL of dH₂O. After dissolution, the volume was adjusted to 100 mL and the final solution sterilised by autoclaving at 121°C for 20 min. Sterile buffer was stored at 4°C.

6.2.6.4 Transformation buffer IV (Tfb-IV)

1.11 g of calcium chloride (100 mM) was dissolved in 50 mL of dH₂O. After dissolution, 15 mL of glycerol (15% v/v) were added and the volume was adjusted to 100 mL with dH₂O. The final solution sterilised by autoclaving at 121°C for 20 min. Sterile buffer was stored at 4°C.

6.2.6.5 Tris-acetate-EDTA (TAE) 50X buffer

242 g of Tris free base, 18.61 g of EDTA disodium salt were added to 700 mL of dH₂O under stirring. When Tris and EDTA fully dissolved, 57.1 mL of glacial acetic acid were added and the volume adjusted to 1 L.

6.2.7 Enzyme purification buffers

6.2.7.1 Enzyme purification buffer 1 (EPB-1)

6.1 g Tris free base (50 mM), 17.5 g NaCl (300 mM) and 1.4 g imidazole (20 mM) were dissolved in 900 mL of dH₂O. After dissolution, pH was adjusted to 8.00 with diluted HCl. The volume was to 1 L with addition dH₂O and the solution was filtered and degassed before use.

6.2.7.2 Enzyme purification buffer 2 (EPB-2)

6.1 g Tris free base (50 mM), 17.5 g NaCl (300 mM) and 17 g imidazole (250 mM) were dissolved in 900 mL of dH₂O. After dissolution, pH was adjusted to 8.00 with diluted HCl. The volume was to 1 L with addition dH₂O and the solution was filtered and degassed before use.

6.2.7.3 Enzyme purification buffer 3 (EPB-3)

EBF-3 was prepared as for EPB-1 (section 6.2.7.1) but for the addition of 50 mL of 1M KH_2PO_4 (50 mM) before adjusting the pH.

6.2.7.4 Enzyme purification buffer 4 (EPB-4)

EBF-4 was prepared as for EPB-2 (section 6.2.7.2) but for the addition of 50 mL of 1M KH_2PO_4 (50 mM) before adjusting the pH.

6.2.7.5 Enzyme purification buffer 5 (EPB-5)

30.75 mL of 1M K_2HPO_4 , 19.25 mL of 1M KH_2PO_4 and 350 μL β -mercaptoethanol (β -ME) were added to 800 mL of dH_2O . The pH was therefore adjusted to 7.00 and the solution diluted to 1 L yielding a 50 mM PO_4 , 5 mM β -ME solution. The solution was filtered and degassed before use.

6.2.7.6 Enzyme purification buffer 6 (EPB-6)

6.06 g Tris free base (100 mM), 7.45 g KCl (100 mM), 350 μL β -ME (5 mM) were added to 800 mL of dH_2O . The pH was therefore adjusted to 8.00 and the solution diluted to 1 L. The solution was filtered and degassed before use.

6.2.7.7 Enzyme purification buffer 7 (EPB-7)

61.5 mL of 1M K_2HPO_4 , 38.5 mL of 1M KH_2PO_4 , 5.84 g NaCl, 350 μL β -ME were added to 800 mL of dH_2O . The pH was therefore adjusted to 7.00 and the solution diluted to 1 L yielding a 100 mM PO_4 , 100 mM NaCl, 5 mM β -ME solution. The solution was filtered and degassed before use.

6.2.8 SDS-PAGE buffers

6.2.8.1 SDS resolving buffer

6.0 g Tris free base (0.5 M) was dissolved in 80 mL of dH₂O. After dissolution, pH was brought to 6.8 with diluted HCl and the volume was adjusted to 100 mL with dH₂O.

6.2.8.2 SDS stacking buffer

27.23 g Tris free base (1.5 M) was dissolved in 80 mL of dH₂O. After dissolution, pH was brought to 8.8 with diluted HCl and the volume was adjusted to 150 mL with dH₂O.

6.2.8.3 SDS sample buffer

1.25 mL SDS resolving buffer (section 6.2.8.1), 2.5 mL glycerol, 2 mL 10% (w/v) SDS, 0.2 mL 0.5% (w/v) bromophenol blue and 3.55 mL dH₂O were mixed together and stored at room temperature.

6.2.8.4 10X Running buffer

30.3 g of Tris free base, 144.0 g glycine and 10.0 g of sodium-dodecyl sulphate (SDS) were dissolved in 900 mL of dH₂O at 37°C. After dissolution, volume was adjusted to 1 L with dH₂O.

6.3 Molecular cloning

6.3.1 TAE agarose gel electrophoresis

1X TAE buffer diluted from 50X stock solution (section 6.1.6.5) was mixed with agarose at percentages ranging between 0.8% (large fragments separation) and 1.5% (small fragments separation), depending on the size of the DNA fragment to be separated. The mixture was heated near the boiling point until agarose fully dissolved and resulting solution poured on gel-caster system and left to solidify at room temperature. The gel was placed in an electrophoresis chamber immersed in 1X TAE buffer. DNA samples were loaded on the gel and separated by applying a constant electric current (80 mA) for 40 min. When separation was complete, the agarose gel was stained with dilute ethidium bromide solution and DNA fragments were visualised using a UV light box compared to a 100 bp and 1 kb standard size marker.

6.3.2 Purification of DNA by agarose gel extraction

The target DNA fragment separated by agarose gel electrophoresis (section 6.2.1) was cut with a scalpel and separated from agarose using an agarose gel extraction kit (QIAGEN, UK) following instruction provided by the supplier.

6.3.3 Purification of DNA by spin miniprep column

EconoSpin All-in-1 mini prep spin columns (Epoch Biolabs, USA), QIAprep spin miniprep kit (QIAGEN, UK) and QIAquick purification kit (QIAGEN, UK) were used to isolate either plasmid or PCR DNA following instruction provided by the manufacturer.

6.3.4 Preparation of XL1-Blue super-competent cells

XL1-Blue cells from a 50% glycerol stock solution stored at -80°C were incubated in 50 mL of LB medium containing tetracycline (50 mg/L) overnight at 37°C . The day after, 100 mL of fresh LB medium with tetracycline (50 mg/L) was inoculated with 1 mL from the overnight culture and incubated at 37°C . Cell growth was monitored by measuring optical density at 600 nm (OD_{600}). When OD_{600} reached 0.6-0.7, 50 mL of culture was cooled on ice for 15 min and cells were separated from the medium by centrifugation at 3400 g for 6 min. The supernatant was discarded and cells were gently resuspended in 5 mL of Tfb-I buffer (section 6.1.6.1). Cells were left on ice for 15 min, centrifuged, and resuspended in 4 mL of Tfb-II buffer (section 6.1.6.2). Cells were left on ice for further 15 min to be then aliquoted in sterilised Eppendorf tubes (100 μL each tube) and stored at -80°C .

6.3.5 Amplification of target genes from *E.coli* chromosomal DNA by polymerase chain reaction (PCR)

Genes encoding for 6-phosphogluconate dehydrogenase (*gnd*), glutaredoxin 2 (*grxB*), guanylate kinase (*gmk*), 7,8-dihydroneopterin triphosphate pyrophosphatase (*nudB*) were amplified from *E.coli* chromosomal DNA prepared following to the method described by Syn *et al.* (231). All genes were amplified using Crimson Taq polymerase (New England Biolabs) according to the instructions provided by the supplier. Gene sequences for primers design were obtained through GenBank database (Table 6.1). In a typical PCR reaction setup, 10 μL of 5X Crimson Taq buffer, 1 μL of deoxynucleotide triphosphates (final concentration 200 μM), 2.5 μL of forward and 2.5 μL of reverse complement primers (final concentration 1.25 μM), 0.3 μL of chromosomal DNA, 0.3 μL of Crimson Taq polymerase and 33.4 μL of sterilised dH_2O were mixed together in

a PCR tube. PCR reactions were performed using a Biometra thermocycler (Germany). Optimal annealing temperatures were determined experimentally through gradient PCRs. To ensure maximum selectivity, PCR products were all purified through DNA agarose gel extraction (section 6.2.2) to be then digested with *NdeI* and *XhoI* fast-digest restriction enzymes (Thermo Scientific, UK). Digested amplicons were then separated from the restriction fragments through DNA spin miniprep column (section 6.2.3).

Table 6.1. Primers designed for PCR amplification. Restriction sites for *NdeI* (CATATG) and *XhoI* (CTCGAG) are shown in bold.

Enzyme	<i>E. coli</i> gene (NCBI ID)	PCR Primers
6-Phosphogluconate dehydrogenase (6PGDH)	<i>gnd</i> (946554)	Fwd: 5'-GTTGTT CATATG TCCAAGCAACAGATCG-3' Bwd: 5'-CACCAC CTCGAG TTATTATCCAGCCATTCGG-3'
Glutaredoxin 2 (GRX2)	<i>grxB</i> (946926)	Fwd: 5'-GTTGTT CATATG AAGCTATACATTTACGATCACTGC-3' Bwd: 5'-CACCAC CTCGAG TAAATCGCCATTGATGAT-3'
Guanylate kinase (GK)	<i>gmk</i> (948163)	Fwd: 5'-GTTGTT CATATG GGCTCAAGGCAC-3' Bwd: 5'-CACCAC CTCGAG TCAGTCTGCCAACAATTT-3'
7,8-Dihydroneopterin triphosphate pyrophosphatase (DHNTPase)	<i>nudB</i> (946383)	Fwd: 5'-GTTGTT CATATG AAGGATAAAGTGTATAAGCGTC-3' Bwd: 5'-CACCAC CTCGAG TCAGGCAGCGTTAATTACAAACTG-3'

Table 6.2. PCR protocol for the amplification of *gnd*, *grxB*, *gmk* and *nudB* genes. After the initial denaturation step, denaturation, annealing and elongations (highlighted) were repeated 30 times before the final elongation.

	Target gene			
	<i>gnd</i>	<i>grxB</i>	<i>gmk</i>	<i>nudB</i>
Initial denaturation	180 s, 95°C			
Denaturation	20 s, 95°C			
Annealing	30 s, 61°C	30 s, 55°C	30 s, 57°C	30 s, 63°C
Elongation	120 s, 68°C			
Final elongation	300 s, 68°C			

6.3.6 Preparation of pET28-a empty vector

XL1-Blue cells containing a pET28-a vector were grown overnight in 100 mL of LB medium containing 50 mg/L kanamycin. The day after, cells were separated by centrifugation at 3400 g for 5 min. The supernatant was discarded and the pET28-a plasmid was purified from the cell pellet using QIAprep spin miniprep kit (QIAGEN, UK) following instructions from the supplier. Purified pET28-a was then digested with NdeI and XhoI fast-digest restriction enzymes (Thermo Scientific, UK) following the protocol described by the supplier. Digested pET28-a was then purified by agarose gel extraction (Section 6.2.2).

6.3.7 Ligation of target genes into pET28-a empty vector

gnd, *grxB*, *gmk* and *nudB* genes (section 6.2.5) were all ligated into a pET28-a empty vector at NdeI and XhoI restriction sites using T4 DNA ligase (Thermo Scientific, UK). In a typical ligation reaction, 60 µg of the empty vector were mixed with the DNA insert in 1:3 and 1:7 ratio in the buffer provided by supplier reaching

10 μ L final volume. After addition of the T4 ligase enzyme, the reaction mixture was incubated at 37°C overnight. The day after, the ligation product was used to transform XL1-Blue super-competent cells. Briefly, 100 μ L of thawed XL1-Blue super-competent cells (section 6.2.4) were incubated on ice with 10 μ L of the ligation reaction mixture for at least 30 min. Cells were then transformed with the exogenous DNA by heat-shock at 40°C for 44 s. 1 mL of LB medium antibiotic-free was added and heat-shocked cells were incubated at 37°C for 1 hour under shaking. Cells were then centrifugated for 1 minute at 3300 g and 900 μ L of the supernatant were discarded. The remaining 100 μ L of supernatant left into the Eppendorf tube were used to gently resuspend cells into the media. Resuspended cells were then plated on LB solid medium containing kanamycin as the selection maker and incubated at 37°C overnight. A successful ligation will provide after the overnight incubation small XL1-Blue colonies bearing the kanamycin-resistant pET28-a plasmid ligated with the target gene.

6.3.8 Analysis of ligation products

A single colony deriving by the transformation of XL1-Blue cells with the pET28-a ligation product (section 6.2.7) was inoculated in 50 mL of LB liquid medium containing 50 mg/L of kanamycin and grown overnight. The day after, ½ mL from the culture was mixed with a solution of 50% sterile glycerol (section 6.1.3) and stored at -80°C. The remaining part was harvested and the plasmid extracted. Sequencing analysis of pET28a-gnd, pET28a-grxB, pET28a-gmk and pET28a-nudB was performed by Eurofins Genomics.

6.4 Production and purification of recombinant enzymes

6.4.1 Preparation of BL21(DE3)pLysS and BL21-CodonPlus(DE3)RP competent cells

BL21(DE3)pLysS or BL21-CodonPlus(DE3)RP cells from a 50% glycerol stock solution stored at -80°C were incubated in 50 mL of LB medium overnight at 37°C with 35 µg/mL of chloramphenicol or without antibiotic, respectively. The day after, 100 mL of fresh LB medium was inoculated with 1 mL from the overnight culture and incubated at 37°C. Cell growth was monitored by measuring optical density at 600 nm (OD₆₀₀). When OD₆₀₀ reached 0.6-0.7, 50 mL of culture was cooled on ice for 15 min and cells were separated from the medium by centrifugation at 3400 g for 6 min. The supernatant was discarded and cells were gently resuspended in 5 mL of Tfb-III buffer (section 6.1.6.3). Cells were left on ice for 15 min, centrifugated, and resuspend in 4 mL of Tfb-IV buffer (section 6.1.6.4). Cells were left on ice for further 15 min to be then aliquoted in sterilised Eppendorf tubes (100 µL each tube) and stored at -80°C.

6.4.2 Transformation of competent cells with pET28a-gnd, pET28a-grxB, pET28a-gmk and pET28a-nudB vectors

BL21(DE3)pLysS competent cells were transformed with pET-28a-gnd, pET-28a-grxB and pET-28a-gmk plasmids, while BL21-CodonPlus(DE3)-RP cells were transformed with pET28a-nudB. 1 µL of plasmid was incubated with BL21(DE3) competent cells (section 6.3.1) on ice for at 30 min. Transformation with the exogenous DNA was performed by heat shocking at 44°C for 45 s. 1 mL of LB medium antibiotic-free was then added and heat-shocked cells were incubated at 37°C for 1 hour under shaking. Cells were then centrifugated for 1 minute at 3300 g and 900 µL of the supernatant were discarded. The remaining 100 µL of

supernatant left into the Eppendorf tube were used to gently resuspend cells into the media. Resuspended cells were then plated on LB solid medium containing kanamycin as the selection maker and incubated at 37°C overnight. The day after, a single colony is inoculated in 50 mL of LB liquid medium containing kanamycin (50 mg/L) and incubated at 37°C under shaking. ½ mL from the overnight culture was mixed with a solution of 50% sterile glycerol (section 6.1.3) and stored at -80°C.

6.4.3 Production of recombinant enzymes

All recombinant enzymes were overproduced in *E. coli* strains at optimised temperatures and induction times (table 6.3). All *E. coli* strains for gene expression were prepared as described in Section 6.3.2. In a typical procedure, the *E. coli* strain transformed with a given pET plasmid carrying the target gene to express (e.g. pET-28a-grxB) is incubated at 37°C overnight in 50 mL LB liquid medium containing the appropriate antibiotic. The day after, 5 mL from the overnight culture are used to inoculate 1 L of LB liquid medium containing the appropriate antibiotic. The resulting culture is incubated at 37°C until OD₆₀₀ reaches 0.6. Depending on the recombinant enzyme, temperature of the culture was adjusted according to the values reported in Table 6.3 and 120 mg of isopropyl-β-D-1-thiogalactopyranoside (IPTG, 0.5 mM) was added to induce expression of the target gene. After addition of IPTG, cells were left to produce the recombinant enzymes according to the times reported in Table 6.3. Cells were then harvested through centrifugation at 3400 g for 10 min. The supernatant was discarded and the pellet was used either to extract the recombinant enzyme as described in section 6.3.4 or conserved at -20°C.

Table 6.3 Recombinant enzymes used in this work overproduced in *E. coli* strains.

Enzyme (plasmid-gene)	<i>E. coli</i> strain	Temperature and induction time
GRX2 (pET-28a- <i>grxB</i>)	BL21(DE3)pLysS	37°C, 4 h
6PGDH (pET-28a- <i>gnd</i>)	BL21(DE3)pLysS	37°C, 4 h
PRS (pET-22HT- <i>prsA</i>)*	BL21-Star(DE3)pLysS	37°C, 4 h
XGPRT (pET-28a- <i>gpt</i> **)	BL21(DE3)pLysS	25°C, Overnight
GK (pET-28a- <i>gmk</i>)	BL21(DE3)pLysS	37°C, 4 h
GTP-CH-I (pET-21d- <i>folE</i> **)	BL21-Star(DE3)	25°C, Overnight
DHNTase (pET-28a- <i>nudB</i>)	BL21-CodonPlus(DE3)RP	30°C, Overnight
DHNA (pET-28a- <i>folB</i> **)	BL21-CodonPlus(DE3)RP	37°C, 4 h
HPPK (pET28a- <i>folK</i> **)	BL21-CodonPlus(DE3)RP	37°C, 4 h
DHPS (pET-21a- <i>folP</i> **)	BL21-Star(DE3)	25°C, Overnight
EcDHFR (pET-11c- <i>folA</i> ***)	BL21-Star(DE3)	37°C, Overnight

GRX2 = glutaredoxin 2, 6PGDH = 6-phosphogluconate dehydrogenase, PRS = ribose-phosphate pyrophosphokinase, XGPRT = xanthine-guanine phosphoribosyl transferase, GK = guanylate kinase, GTP-CH-I = GTP-cyclohydrolase I, DHNTase = 6-hydroxymethyl 7,8-dihydropterin pyrophosphokinase, DHNA = 7,8-dihydroneopterin aldolase, HPPK = 6-hydroxymethyl 7,8-dihydropterin pyrophosphokinase, DHPS = dihydropteroate synthase, EcDHFR = *Escherichia coli* dihydrofolate reductase.

*Gene cloned by Schultheisz *et al.* (166)

** Gene cloned by Dr. William Dawson (213)

*** Gene cloned by Swanwick *et al.* (232)

6.4.4 Purification of recombinant enzymes

6.4.4.1 Purification of recombinant enzymes bearing an hexahistidine tag (His-tag)

6.4.4.1.1 Purification of GRX2, 6PGDH, XGPRT, GK, DHNA and HPPK

Recombinant enzymes bearing an hexahistidine tag, including GRX2, 6PGDH, XGPRT, GK, DHNA and HPPK, were all purified through affinity chromatography. A pellet of cells containing the overproduced recombinant enzyme (section 6.3)

was resuspended in 20 mL of EBF-1 (section 6.1.7.1) and lysed by sonication on ice. Cell debris were removed by centrifugation at 4 °C, 24300 *g* for 30 min. The supernatant was filtered with a 0.2 µm syringe filter and loaded on a Ni-NTA Agarose resin (Qiagen) pre-equilibrated with the Hig-Tag washing buffer. The resin was then washed three times with EBF-1. The recombinant enzyme bound to the resin was eluted with 20 mL of EBF-2 (section 6.1.7.2). Samples of lysate, flow-through and eluted enzyme were taken for SDS-PAGE analysis (section 6.3.4.3).

6.4.4.1.2 Purification of PRS

PRS was found to aggregate if purified through the method described in section 6.4.4.1.1. However, presence phosphate was found to prevent precipitation of the recombinant enzyme. Accordingly, the purification procedure described in section 6.4.4.1.1 was modified by replacing EBF-1 (section 6.1.7.1) and EBF-2 (section 6.1.7.2) with EBF-3 (section 6.1.7.3) and EBF-4 (section 6.1.7.4), respectively.

6.4.4.2 Purification of recombinant wild-type enzymes

6.4.4.2.1 Purification of GTP-CH-I, DHPS and EcDHFR

Recombinant wild-type GTP-CH-I and DHPS were purified by anion exchange followed by size exclusion chromatography. Cells containing the overproduced enzyme (section 6.3) were re-suspended in EBF-5 (section 6.1.7.5) and lysed by sonication on ice. Cell debris was removed by centrifugation at 4 °C, 24300 *g* for 30 min. The supernatant solution was then loaded onto a Q-sepharose fast flow resin (GE Healthcare Life Sciences) and the recombinant enzyme eluted with a linear gradient from 0 to 1 M NaCl. Fractions containing the enzyme were merged and concentrated by ultrafiltration using a 10 kDa cut-off membrane (Merck Millipore). Ion-exchanged GTP-CH-I and DHPS were further purified using

Superdex 200 and Superdex 75 prep grade size exclusion resin (GE Healthcare Life Sciences), respectively, equilibrated with EBF-6 (section 6.1.7.6). Size-exclusion chromatography purification of EcDHFR was instead performed on a Superdex 75 grade size exclusion resin equilibrated with EBF-7 (section 6.1.7.7). Samples from lysate and fractions were taken for SDS-PAGE analysis.

6.4.4.3 SDS-PAGE analysis

6.4.4.3.1 SDS-PAGE gel preparation

Resolving gel (10%) was prepared by mixing 3.3 mL acrylamide/bis-acrylamide solution, 2.5 mL SDS resolving buffer (section 6.1.8.1), 100 μ L 10% (w/v) SDS and 4.1 mL dH₂O. 50 μ L of 10% (w/v) ammonium persulfate and 20 μ L N,N,N',N'-tetramethylethylenediamine (TEMED) were then added to trigger polymerisation, and the resolving gel solution was poured into the gel caster. The solution was covered with a layer of isopropanol and left to polymerise for 15 min. After polymerisation, the isopropanol layer was removed and the stacking gel (4%) solution, made by mixing 1.3 mL 30% acrylamide/bis-acrylamide solution, 2.5 mL SDS stacking buffer (section 6.1.8.2), 100 μ L 10% (w/v) SDS, 6.1 mL dH₂O, 50 μ L 10% APS and 20 μ L TEMED, was poured. A comb was used to shape 14 wells where samples can be loaded.

6.4.4.3.2 SDS-PAGE samples preparation

50 μ L BME were mixed with 950 μ L of SDS sample buffer (section 6.1.8.3). For each sample to be analysed, 50 μ L of the resulting solution were mixed with 50 μ L of protein sample and heated at 95°C for 4 min.

6.4.4.3.3 SDS-PAGE running protocol

SDS-PAGE gel, prepared as described in section 6.4.4.3.1, was loaded with 7 μL of unstained protein molecular weight marker (Thermo Scientific) and 5 μL of samples to be analysed (section 6.4.4.3.2). The gel was put in a chamber containing 10X SDS running buffer (section 6.1.8.4) diluted to 1X with dH_2O . The gel was run by applying a current at 150 V for 45 min.

6.4.4.4 Enzymes storage

Recombinant GRX2, 6PGDH, GK, DHNTPase, DHNA and HPPK from affinity chromatography purification (section 6.3.4.1.1) were dialysed against 50 mM Tris (pH = 7.6), 50 mM NaCl and 5 mM β -ME buffer and stored in 50% glycerol solution at 20°C maximum for maximum three months. Recombinant PRS (section 6.3.4.1.2) was instead dialysed against 50 mM PO_4 (pH = 7.6), 50 mM NaCl and 5 mM β -ME and stored at -20°C in 50% glycerol for maximum 3 months. Recombinant GTP-CH-I and DHPS from size exclusion chromatography purification (section 6.3.4.2.1) were stored in 50% glycerol as well for maximum 1 month.

6.4.4.5 Determining protein and substrates concentration

6.4.4.5.1 Bradford assay

The principle of the assay developed by Bradford (233) is based on Coomassie dye color change upon binding to a protein under acidic conditions. Bovine serum albumine (BSA) diluted with the Bradford reagent (section 6.1.5) in six samples ranging between 10 $\mu\text{g}/\text{mL}$ and 100 $\mu\text{g}/\text{mL}$ were used to determine a standard calibration curve. UV-vis spectra were collected for each sample between 600 nm and 400 nm, and variation of absorbance at 590 nm and 450 nm were extrapolated to determine the calibration curve. Protein samples of unknown

concentration were then prepared by mixing them with 1 mL of Bradford reagent and their respective absorbance at 590 nm and 450 nm were compared to the standard curve to calculate the concentration. All recombinant enzymes concentration was determined using the Bradford assay except for EcDHFR, which concentration was determined applying the Beer-Lambert law (section 6.4.4.5.2),

6.4.4.5.2 Beer-Lambert law

The Beer-Lambert law establishes a relationship between UV-vis absorption of a given sample and its concentration through the formula:

where A is the absorption, C is the analyte concentration (M) and ϵ is the extinction coefficient ($M^{-1} \text{ cm}^{-1}$) and l is the path length (cm). The value of ϵ is wavelength dependent and it can be used to determine samples concentration by measuring A at the given wavelength. EcDHFR ($\epsilon = 31117 \text{ M}^{-1} \text{ cm}^{-1}$ at $\lambda = 280$ nm), GMP ($\epsilon = 17300 \text{ M}^{-1} \text{ cm}^{-1}$ at $\lambda = 253$ nm), H_2F ($\epsilon = 28000 \text{ M}^{-1} \text{ cm}^{-1}$ at $\lambda = 280$ nm) and NADPH ($\epsilon = 28000 \text{ M}^{-1} \text{ cm}^{-1}$ at $\lambda = 340$ nm) concentrations were determined applying the Beer-Lambert law by measuring A at the given wavelength in 50 mM PO_4 buffer (pH = 7.00).

6.4.5 Enzyme activity assays

GRX2, 6PGDH, PRS, XGPRT, GK and GTP-CH-I activities were assayed following published procedures (171, 190, 205, 214, 234, 235) All anion exchange chromatography analyses were performed using a ProPac SAX-10 analytical or semi-preparative column (Fisher Scientific) with a linear gradient from 0 to 400 mM NaCl over 60 min in 20 mM bicarbonate buffer (pH 8.0). Liquid

chromatography – mass spectrometry (LC-MS) analyses were performed using a Bruker amaZon SL ion-trap mass spectrometer equipped with an ultra-performance liquid chromatography (UPLC) system. All UPLC separations were performed with a linear gradient of 5% to 95% aqueous acetonitrile containing 0.1% HCOOH over 20 min using a C18 analytical column.

6.4.5.1 Comparison of GTP-CH-I activity with and without DHNTPase

0.2 mg of GTP were incubated with GTP-CH-I in 1 mL of 50 mM Tris (pH 7.6), 100 mM KCl, 5 mM MgCl₂, 5 mM β-ME at 37 °C. Formation of 7,8-dihydroneopterin triphosphate (DHNTP) was monitored by UV-vis spectroscopy at 330 nm for 1 h. After 2 h, the mixture was analysed by anion exchange chromatography. DHNTPase was assayed by coupling with GTP-CH-I following the same procedure described above.

6.3.5.2 DHNA, HPPK, DHPS activity assay

Because 7,8-dihydroneopterin (DHN), 6-hydroxymethyl-7,8-dihydropterin (HMDP) and 6-hydroxymethyl-7,8-dihydropterin pyrophosphate (HMDPpp) are chemically unstable, substrates were generated enzymatically from GTP. 1 mg of GTP placed in a 1.5 mL Eppendorf tube was incubated with GTP-CH-I and DHNTPase in 1 mL of 50 mM Tris (pH 8.0), 100 mM KCl, 5 mM MgCl₂, 5 mM BME at 37 °C for 3 h. ALP was added and the mixture left to react for further 30 min. Enzymes were removed using a 10 kDa spin column (GE Healthcare Life Sciences); the filtrate containing DHN was analysed by LC-MS and used to assay DHNA, HPPK and DHPS activities in a sequential order. Addition of DHNA triggers conversion of DHN to HMDP which was detected by LC-MS. 100 µL of ATP solution (10 mg/mL, pH ~7.6) was then added together with HPPK, and formation of HMDPpp was monitored by anion exchange chromatography.

Addition of DHPS to 100 μ L solution of containing *p*-aminobenzoic acid (2 mg/mL) leads to the formation of dihydropteroic acid as detected by LC-MS.

6.5 Determining GRX system total turnover number (TTN)

In a falcon tube 0.05 mmol of $^{13}\text{C}_6$ -D-glucose (9.3 mg), 0.11 mmol of HED (17 mg), 0.06 mmol (13 mg) of PEP were mixed in 10 mL of 50 mM potassium phosphate, 50 mM NaCl, 10 mM MgCl_2 , 2 mM GSH buffer at 37°C, and the pH was adjusted to 7.6 with $\text{NaOH}_{(\text{aq})}$. 0.005 mmol ATP (3 mg) was then added together with 10 nmol PK, 20 nmol GRX2, 5 nmol GR and 5 nmol G6PDH. NADP^+ concentration was varied in order to assess the TTN at 50 (0.001 mmol), 10^3 (5×10^{-5} mmol), 10^4 (5×10^{-6} mmol), 10^5 (5×10^{-7} mmol), 5×10^5 (10^{-7} mmol) and 10^6 (5×10^{-8} mmol) respectively. Formation of $^{13}\text{C}_6$ -PG was triggered by addition of HK (10 nmol) and the progress of the enzymatic reaction was monitored by ^{13}C -NMR spectroscopy by mixing 450 μ L from the reaction mixture with 50 μ L of D_2O .

6.6 Synthesis of isotopically labelled guanines

6.6.1 Traube purine synthesis

6.6.1.1 Synthesis of [5-¹⁵N]-2,4,5-triamino-6-hydroxypyrimidine

A solution of 2,4-diamino-6-hydroxypyrimidine (1.64 g, 12.99 mmol) in 10% acetic acid (30 mL) was cooled on ice and Na¹⁵NO₂ (1 g, 14.29 mmol) dissolved in a small amount of deionized water (dH₂O) was added dropwise under stirring. [5-¹⁵N]-2,4-diamino-5-nitroso-6-hydroxypyrimidine precipitated as a purple solid. The precipitate was centrifuged, washed twice with cold dH₂O and re-suspended in hot dH₂O. When the suspension was close to boil, sodium dithionite (9.95 g, 57.16 mmol) divided in four portions were added every 15 min. The reaction mixture discolored as the nitroso compound reduced to [5-¹⁵N]-2,4,5-triamino-6-hydroxypyrimidine. The solution was then cooled to room temperature. Addition of conc. H₂SO₄ caused precipitation of the final compound. The solid was filtered and crystallized in 1 N H₂SO₄. Crystals were collected and dried under vacuum yielding 2.36 g (9.86 mmol, 69% yield) of [5-¹⁵N]-2,4,5-triamino-6-hydroxypyrimidine sulphate salt.

¹³C NMR (125 MHz, 90% H₂O + 10% D₂O) δ 168.87 (s), 157.92 (s), 154.07 (s), 101.12 (d, *J*_{C-N} = 8.9 Hz) ppm.

6.6.1.2 Synthesis of [7-¹⁵N]-guanine

[5-¹⁵N]-2,4,5-triamino-6-hydroxypyrimidine (2.27 g, 9.49 mmol) were mixed with 4-formylmorpholine (9.45 mL, 94.4 mmol) and refluxed in 98% HCOOH (15 mL) under nitrogen for 3 hours. After this time, the mixture was cooled to room temperature and then put on ice. Ammonium hydroxide was slowly added until the pH reached 9.0. [5-¹⁵N]-guanine precipitated out and was collected by

centrifugation, washed three times with cold dH₂O then twice with acetone, and dried under vacuum to yield 1.23 g of off-white powder (8.06 mmol, 85% yield).

¹H NMR (500 MHz, 90% H₂O + 10% D₂O) δ 7.56 (d, 1H, *J*_{C-N} = 10 Hz) ppm. ¹³C NMR (125 MHz, H₂O + 10% D₂O) δ 167.22 (d, *J*_{C-N} = 3.8 Hz), 159.96 (s), 159.44 (s), 146.61 (s), 117.19 (d, *J*_{C-N} = 3.8 Hz) ppm.

6.6.1.3 Synthesis of [6-¹³C,7-¹⁵N]-guanine

Synthesis of [6-¹³C,7-¹⁵N]-guanine was performed as for [7-¹⁵N]-guanine (section 6.5.1.2) using [5-¹⁵N]-2,4,5-triamino-6-hydroxypyrimidine (1.07 g, 4.25 mmol) and H¹³COOH (1 g, 0.85 mmol) as starting material. 1 mL morpholine was used as solvent.

¹H NMR (600 MHz, 90% H₂O + 10% D₂O) δ 7.43 (dd, 1H, ¹*J*_{C-H} = 198 Hz, ²*J*_{N-H} = 12 Hz) ppm. ¹³C NMR (150 MHz, 90% H₂O + 10% D₂O) δ 147.89 (d, *J*_{C-N} = 3 Hz) ppm.

6.6.2 Synthesis of guanine from 5-amino-4-imidazolecarboxamide

6.6.2.1 Synthesis of [2-¹³C]-guanine

Benzoyl chloride (592 μL, 5.09 mmol) and KS¹³CN (495 mg, 5.09 mmol) were placed in a round bottom flask and put under a stream of N₂. ~10 mL of anhydrous CH₃CN was added, and the mixture was stirred at 70°C. A white solid, KCl, precipitated. After 1 h, the solid was filtered and the solvent was evaporated under reduced pressure. Crude ¹³C-benzoyl isothiocyanate formed during the reaction appeared as a faint yellow oil. 5-amino-4-imidazolecarboxamide (642, 5.09 mmol) dissolved in ~ 50mL dH₂O was mixed with crude ¹³C-benzoyl isothiocyanate, and the solution was stirred at room temperature overnight. The

day after, 1 mL of NaOH 6M was added to the reaction mixture to dissolve 5-(N'-benzoyl-isothiocarbamoyl)amino-4-imidazolecarboxamide precipitated from the solution in the course of the reaction. The solution was filtered and methyl iodide (1.3 mL, 20 mmol) was added. The solution was vigorously stirred for 2 h at room temperature, and 5-(N'-benzoyl-S-methylisothiocarbamoyl)amino-4-imidazolecarboxamide appeared as a white solid. The precipitate was filtered and washed twice with water to be then put in a round bottom flask. 15 mL of 6M NaOH were added and the mixture was heated at 100°C for 1 h. The solution was left to cool at room temperature to be then put on ice. Concentrated HCl was added with caution into the mixture until the pH reached ~7.00. [2-¹³C]-guanine precipitated. The solid was separated from the solution by centrifugation, washed with water, ethanol and then dried under vacuum to yield 226 mg (29 % overall) of final product.

¹H NMR (600 MHz, 90% H₂O + 10% D₂O) δ 7.52 (1H, s) ppm. ¹³C NMR (150 MHz, 90% H₂O + 10% D₂O) δ 159.17 (s) ppm.

6.7 General procedure for the synthesis of isotopically labelled GMPs

In a falcon tube 0.05 mmol ¹³C₆-D-glucose (9.3 mg), 0.11 mmol HED (17 mg) or cystine (26 mg), 0.2 mmol PEP (41 mg) were mixed in 5 mL of 100 mM Tris, 50 mM NaCl, 10 mM MgCl₂, 2 mM GSH buffer at 37°C, and the pH was thereafter adjusted to 7.6 with NaOH_(aq). 0.005 mmol ATP (3 mg) and 0.001 mmol NADP⁺ (0.8 mg) were then added together with 10 nmol PK, 10 nmol MK(171), 20 nmol GRX2, 5 nmol GR, 5 nmol G6PDH and 5 nmol PRI, and the volume adjusted to 10 mL with further addition of reaction buffer. The enzymatic cascade was triggered by addition of HK (10 nmol) which was monitored by UV-vis spectroscopy following NADPH absorbance at 340 nm. When the absorbance

declined to the baseline (or solid cystine was fully dissolved to reduced cysteine), PRS (10 nmol) and XGPRT (30 nmol) were added. The reaction was left to proceed for further 15 min. in order to generate sufficient amounts of the intermediate PRPP *in situ*. 0.05 mmol of guanine (7.6 mg) dissolved 50 μ L of KOH (5.0 M) were diluted to 10 mL with deionized water and loaded in a 10 mL syringe. Alkaline guanine was then flowed into the reaction mixture at the rate of 0.2 mL/min (1 μ mol/min). After 50 min., when addition of guanine was complete, the reaction mixture was allowed to proceed for further 10 min. The pH shifted from 7.6 to \sim 8.0. The final product was purified from the crude mixture by anion exchange chromatography with a linear gradient from 0 to 40% of 1M NaCl in 60 min in 20 mM bicarbonate buffer (pH = 8.0) using a ProPac SAX-10 preparative column (Fisher Scientific). GMP eluted after \sim 16 min. Fractions containing the product were merged and, prior to freeze drying, GMP was quantified by the Beer-Lambert law (section 6.3.4.5.2). Yields ranged between 70% and 80%.

6.8 General procedure for the synthesis of isotopically labelled H₂Fs

Chemo-enzymatic synthesis of 7,8-dihydrofolate (H₂F) was performed inside a LABstar glove box station (MBraun, Germany) equipped with a 50 mL falcon tube Thermomixer (Eppendorf), pH meter and syringe pump. Oxygen concentration was constantly kept below 0.5 ppm. Solutions were extensively degassed prior to their introduction into the glovebox system, and left to equilibrate to the inert atmosphere overnight before use. In a falcon tube, D-glucose (9 mg, 0.05 mmol), cystine (26 mg, 0.11 mmol) and PEP (62 mg, 0.3 mmol) were mixed in 5 mL of 100 mM Tris, 100 mM KCl, 10 mM MgCl₂, 2 mM GSH buffer at 37°C, and the pH was adjusted to 7.6 with NaOH_(aq). ATP (3 mg, 0.005 mmol) and NADP⁺ (0.8 mg, 0.001 mmol) were added together with PK (10 nmol), MK (10 nmol), (171) GRX2

(20 nmol), GR (5 nmol), G6PDH (5 nmol) and PRI (5 nmol). After adjusting the total volume of 10 mL with the reaction buffer, the enzymatic cascade was triggered by addition of HK (10 nmol) and left to react overnight (or until solid cystine was fully dissolved) at 37 °C. The day after, PRS (10 nmol), XGPRT (30 nmol) and GK (20 nmol) were added. The reaction was left to proceed for further 15 min in order to generate sufficient amounts of the intermediate PRPP *in situ*. Guanine (7.6 mg, 0.05 mmol) dissolved in 50 µL of 5 M KOH was diluted to 10 mL with deionized water and loaded in a 10 mL syringe. Alkaline guanine was then flowed into the reaction mixture at the rate of 0.2 mL/min (1 µmol/min). During guanine addition, the reaction vessel was agitated at 400 rpm. After 50 min, when addition of guanine was complete, the reaction mixture was allowed to proceed for further 10 min; the pH shifted from 7.6 to ~8.0. GTP-CH-I (100 nmol) and DHNTPase (25 nmol) were added and the reaction was left to proceed overnight protected from light. After the overnight reaction with GTP-CH-I and DHNTPase, ALP (15 nmol) was added and the reaction mixture incubated for 1 h and 30 min. The reaction mixture pH must be under strict control and never reach values below 7.0. This is to avoid pH-dependent degradation of 7,8-dihydropterin intermediates including the final product H₂F. Enzymes were removed by ultrafiltration using a 50 mL 10 kDa spin column (GE Healthcare Life Sciences). The filtrate was put in a clean 50 mL falcon tube, and a solution of ATP (6 mg, 0.01 mmol), MK (10 nmol), PK (10 nmol), 0.015 mmol of PEP (31 mg, 0.15 mmol) and pABA-Glu (16 mg, 0.06 mmol) was added to the main mixture making sure the pH was adjusted between 7.6 and 8.0 before addition. Then, DHNA (20 nmol), HPPK (20 nmol) and DHPS (30 nmol) were added, and the reaction mixture was left overnight. During H₂F formation, the reaction mixture turns faint yellow. The final product was purified from the crude mixture by anion

exchange chromatography. Briefly, the crude product was diluted to 200 mL with dH₂O. The diluted solution was put on ice and accurately protected from light, for being loaded on a ProPac SAX-10 preparative column (Fisher Scientific) equilibrated with 20 mM Tris buffer (pH 7.6). After loading, the column was washed with buffer until absorbance at 210 nm declined to the baseline. H₂F was thereafter eluted from the anion exchange column with a linear gradient from 0 to 400 mM NaCl over 60 min, following 7,8-dihydropterin absorbance at 330 nm. H₂F eluted after ~33 min. Fractions containing the product were merged. The H₂F solution was immediately put in a flask and the product (and other salts) precipitated with cold acetone. The acetone solution was left on ice for 10 min to ensure complete precipitation, and the solid was separated through centrifugation by collecting it in a 50 mL falcon tube. The faint yellow solid collected at the bottom of the falcon tube was gently dried from residual acetone using a stream of N₂. When sufficiently dry, the tube was put on ice and the pellet treated with a 1-2 mL of ice-cold 10% ascorbic acid (pH 2.8). While salts are dissolved in the ascorbic acid solution, H₂F remains insoluble and it can be therefore separated by centrifugation in a 1.5 mL Eppendorf tube. The solid was washed 3 times with ice-cold dH₂O and once with ice-cold acetone. Eventually, the acetone-washed product was dried under vacuum for 30 min and stored at -20 °C. The average overall yield was 30% (6.7 mg, 0.015 mmol).

6.9 Characterisation of isotopically labelled GMPs and H₂Fs

6.9.1 NMR spectroscopy

All NMR experiments were performed at 25 °C on a Bruker AVANCE III 600 MHz (¹H) spectrometer with a QCI-P cryoprobe. All samples were prepared in 10% deuterium oxide by dissolving samples with 0.1 M NaOH.

6.9.1.1 [1',2',3'4',5'-¹³C₅]-GMP

¹H NMR (600 MHz, 90% H₂O + 10% D₂O) δ 8.00 (s), 5.77 (1H, d, J_{C-H} = 164 Hz), 3.93 (5H, m) ppm. ¹³C NMR (150 MHz, 90% H₂O + 10% D₂O) δ 86.25 (d, J_{C-C} = 42.6 Hz), 84.45 (m), 74.23 (dd, J_{C-C} = 37, 5 Hz), 71.05 (t, J_{C-C} = 38 Hz), 63.77 (d, J_{C-C} = 43 Hz) ppm.

6.9.1.2 [1',2',3'4',5'-¹³C₅, 7-¹⁵N]-GMP

¹H NMR (600 MHz, 90% H₂O + 10% D₂O) δ 8.00 (d, 1H, $^2J_{N-H}$ = 10.8 Hz), 5.78 (1H, d, J_{C-H} = 165 Hz), δ 3.93 (5H, m) ppm. ¹³C NMR (150 MHz, 90% H₂O + 10% D₂O) δ 86.25 (d, J_{C-C} = 42.6 Hz), 84.45 (m), 74.23 (dd, J_{C-C} = 37, 5 Hz), 71.05 (t, J_{C-C} = 38 Hz), 63.77 (d, J_{C-C} = 43 Hz) ppm.

6.9.1.3 [1',2',3'4',5',8-¹³C₆, 7-¹⁵N]-GMP

¹H NMR (600 MHz, 90% H₂O + 10% D₂O) δ 8.06 (dd, 1H, $^1J_{C-H}$ = 205 Hz, $^2J_{N-H}$ = 11 Hz), δ 5.78 (1H, d, J_{C-H} = 169 Hz), δ 3.93 (5H, m) ppm. ¹³C NMR (150 MHz, 90% H₂O + 10% D₂O) δ 135.71 (s), 86.25 (d, J_{C-C} = 42.6 Hz), 84.45 (m), 74.23 (dd, J_{C-C} = 37, 5 Hz), 71.05 (t, J_{C-C} = 38 Hz), 63.77 (d, J_{C-C} = 43 Hz).

6.9.1.4 [2-¹³C]-GMP

¹H NMR (600 MHz, 90% H₂O + 10% D₂O) δ 8.04 (s), 5.77 (1H, d, J_{H-H} = 6 Hz), 4.31 (2H, dd, J_{H-H} = 3.4, 1.6 Hz), 4.21 (2H, m), 3.89 (1H, m) ppm. ¹³C NMR (150 MHz, 90% H₂O + 10% D₂O) δ 161.38 (s) ppm.

6.9.1.5 [5-¹⁵N]-H₂F

¹H NMR (600 MHz, 90% H₂O + 10% D₂O) δ 7.63 (2H, d, $J_{H-H} = 8.8$ Hz), 6.74 (2H, d, $J_{H-H} = 8.8$ Hz), 4.21 (1H, dd, $J_{H-H} = 9$ Hz, 5 Hz), 3.95 (2H, s), 3.87 (2H, s), 2.20 (2H, m), 1.98 (2H, m) ppm.

6.9.1.6 [6-¹³C]-H₂F

¹H NMR (600 MHz, 90% H₂O + 10% D₂O) δ 7.63 (2H, d, $J_{H-H} = 8.8$ Hz), 6.74 (2H, d, $J_{H-H} = 8.8$ Hz), 4.21 (1H, dd, $J_{H-H} = 9$ Hz, 5 Hz), 3.95 (2H, d, $^2J_{C-H} 6.1$ Hz), 3.87 (2H, d, $^2J_{C-H} 6.1$ Hz), 2.20 (2H, m), 1.98 (2H, m) ppm. ¹³C NMR (150 MHz, 90% H₂O + 10% D₂O) δ 152.07 (s) ppm.

6.9.1.7 [5-¹⁵N][6-¹³C]-H₂F

¹H NMR (600 MHz, 90% H₂O + 10% D₂O) δ 7.63 (2H, d, $J_{H-H} = 8.8$ Hz), 6.74 (2H, d, $J_{H-H} = 8.8$ Hz), 4.21 (1H, dd, $J_{H-H} = 9$ Hz, 5 Hz), 3.95 (2H, d, $^2J_{C-H} 5.8$ Hz), 3.87 (2H, d, $^2J_{C-H} 5.8$ Hz), 2.20 (2H, m), 1.98 (2H, m) ppm. ¹³C NMR (150 MHz, 90% H₂O + 10% D₂O) δ 152.08 (d, $J_{C-N} 7.0$ Hz) ppm.

6.9.1.8 [6,7,9-¹³C₃]-H₂F

¹H NMR (600 MHz, 90% H₂O + 10% D₂O) δ 7.63 (2H, d, $J_{H-H} = 8.8$ Hz), 6.74 (2H, d, $J_{H-H} = 8.8$ Hz), 6.74 (1H, s), 4.21 (1H, dd, $J_{H-H} = 9$, 5 Hz), 3.95 (2H, dd, $^1J_{C-H} = 132$ Hz, $^2J_{C-H} 6$ Hz), 3.87 (2H, dd, $^1J_{C-H} = 147$ Hz, $^2J_{C-H} 6$ Hz), 2.20 (2H, m), 1.98 (2H, m) ppm. ¹³C NMR (150 MHz, 90% H₂O + 10% D₂O) δ 152.05 (dd, $J_{C-C} = 52$, 40 Hz), 47.84 (d, $J_{C-C} = 52$ Hz), 47.84 (d, $J_{C-C} = 52$ Hz) ppm.

6.9.1.9 [5-¹⁵N][6,7,9-¹³C₃]-H₂F

¹H NMR (600 MHz, 90% H₂O + 10% D₂O) δ 7.63 (2H, d, *J*_{H-H} = 8.8 Hz), 6.74 (2H, d, *J*_{H-H} = 8.8 Hz), 4.21 (1H, dd, *J*_{H-H} = 9 Hz, 5 Hz), 3.95 (2H, dd, ¹*J*_{C-H} = 132 Hz, ²*J*_{C-H} 6 Hz), 3.87 (2H, dd, ¹*J*_{C-H} = 147 Hz, ²*J*_{C-H} 6 Hz), 2.20 (2H, m), 1.98 (2H, m) ppm. ¹³C NMR (150 MHz, 90% H₂O + 10% D₂O) δ 152.03 (ddd, *J*_{C-C} = 51, 40 Hz, *J*_{C-N} 7.2 Hz), 47.84 (d, *J*_{C-C} = 52 Hz), 47.84 (d, *J*_{C-C} = 52 Hz) ppm.

6.9.2 Liquid chromatography – high resolution mass spectrometry (LC-HRMS)

All LC-HRMS analyses were run on a Waters Synapt G2-Si time-of-flight mass spectrometer (Surrey, UK) equipped with a Acquity UPLC system.

6.10 Pre-steady state kinetics (PSSK) and heavy-atom kinetic isotope effect measurements on EcDHFR**6.10.1 Preparation of natural abundance H₂F for PSSK measurements**

Natural abundance H₂F was prepared with a modified version of the method described by Blakley (236). 8 g ascorbic acid were placed in a three-neck round bottom flask and dissolved with 80 mL dH₂O. pH was adjusted to 6.00 and the solution constantly purged with a stream of N₂ protected from light. 400 mg folic acid dissolved in 40 mL NaOH were added to the ascorbic acid solution, and after 5 min pH was re-adjusted to 6.00. The reaction mixture was put on ice under stirring for 5 min, and 4.4 g sodium dithionite were added. When sodium dithionite was completely dissolved, the reaction was allowed to proceed for 15 min. A fresh solution of 1 M HCl was added to the reaction mixture dropwise using a peristaltic

pump until pH drops to 2.8. H₂F will precipitate out from the solution. The precipitate is separated from the solution by centrifugation, and precipitated again in 10% sodium ascorbate as described before. To ensure sample homogeneity in PSSK measurements, H₂F is then purified by anion exchange chromatography following the same procedure described for isotopically labelled H₂Fs (section 6.8).

6.10.2 Single-turnover experiments

Single-turnover experiments were performed on an Applied Photophysics SX20/LED stopped-flow spectrophotometer (UK) optimized for measuring DHFR reaction rate through fluorescence resonance energy transfer (FRET) by exciting tryptophan residues at 292 nm, which were in turn exciting NADPH at 340 nm and measuring the subsequent emission at 450 nm. NADPH and H₂F concentrations were determined spectrophotometrically as described in section 6.3.4.5.2. Experiments were performed in 100 mM phosphate, 100 mM NaCl, 5 mM β-ME, pH 7.0. The buffer was filtered and extensively degassed before use. Solutions were constantly kept on ice and protected from light during measurements. EcDHFR (20 μM) was preincubated with NADPH (8 μM) for at least 5 min before measurements by rapidly mixing with H₂F (200 μM). Measurements were repeated at least three times. Rate constants were extrapolated by fitting the kinetic data to the equation for a triple-exponential decay using Applied Photophysics Pro-Data SX software. Isotopically labelled H₂Fs were checked by NMR before use.

6.10.3 Errors and their propagation

6.10.3.1 Standard deviation and standard error of the mean

Uncertainty for the measured pre-steady-state values are reported as standard deviation (σ) which is defined as:

$$\sigma = \sqrt{\frac{\sum (X - M)^2}{n}}$$

where X is the value of each measurement, M is the mean value of the sample and n is the total number of repetitions.

6.10.3.2 Propagation of uncertainty

Errors of the KIE data presented in this work were calculated using the error following propagation formula:

$$\Delta Z = \sqrt{(\Delta X)^2 + (\Delta Y)^2}$$

where X and Y represent the independently measured values, ΔZ and ΔY the uncertainty values for X and Y respectively.

7. REFERENCES

References

1. Definition of life in English. Oxford English Dictionary: Oxford University Press; 2016.
2. Snider MJ, Wolfenden R. The rate of spontaneous decarboxylation of amino acids. *J Am Chem Soc.* 2000;122(46):11507-8. doi: 10.1021/ja002851c
3. Bar-Even A, Noor E, Savir Y, Liebermeister W, Davidi D, Tawfik DS, et al. The moderately efficient Enzyme: evolutionary and physicochemical trends shaping enzyme parameters. *Biochemistry.* 2011;50(21):4402-10. doi: 10.1021/bi2002289
4. Imming P, Sinning C, Meyer A. Opinion - Drugs, their targets and the nature and number of drug targets. *Nat Rev Drug Discov.* 2006;5(10):821-34. doi: 10.1038/nrd2132
5. Hopkins AL, Groom CR. The druggable genome. *Nat Rev Drug Discov.* 2002;1(9):727-30. doi: 10.1038/nrd892
6. Brunton LL, Knollmann BrC, Hilal-Dandan R. Goodman & Gilman's The pharmacological basis of therapeutics. Thirteenth edition. ed. New York: McGraw Hill Medical; 2018.
7. Huggins DJ, Sherman W, Tidor B. Rational approaches to improving selectivity in drug design. *J Med Chem.* 2012;55(4):1424-44. doi: 10.1021/jm2010332
8. Waring MJ, Arrowsmith J, Leach AR, Leeson PD, Mandrell S, Owen RM, et al. An analysis of the attrition of drug candidates from four major pharmaceutical companies. *Nat Rev Drug Discov.* 2015;14(7):475-86. doi: 10.1038/nrd4609
9. Pauling L. Molecular architecture and biological reactions. *Chem Eng News.* 1946;24:1375-7.
10. Schramm VL. Transition States and transition state analogue interactions with enzymes. *Acc Chem Res.* 2015;48:1032-9. doi: 10.1021/acs.accounts.5b00002
11. Wolfenden R. Conformational aspects of inhibitor design: enzyme-substrate interactions in the transition state. *Bioorg Med Chem.* 1999;7:647-52.
12. Schramm VL. Enzymatic transition states, transition-state analogs, dynamics, thermodynamics, and lifetimes. *Annu Rev Biochem.* 2011;80:703-32. doi: 10.1146/annurev-biochem-061809-100742
13. Mahalingam AK, Axelsson L, Ekegren JK, Wannberg J, Kihlström J, Unge T, et al. HIV-1 protease inhibitors with a transition-state mimic comprising a tertiary alcohol: improved antiviral activity in cells. *J Med Chem.* 2010;53:607-15. doi: 10.1021/jm901165g
14. Brik A, Wong CH. HIV-1 protease: mechanism and drug discovery. *Org Biomol Chem.* 2003;1:5-14.
15. Yang H, Nkeze J, Zhao RY. Effects of HIV-1 protease on cellular functions and their potential applications in antiretroviral therapy. *Cell Biosci.* 2012;2:32. doi: 10.1186/2045-3701-2-32
16. Arts EJ, Hazuda DJ. HIV-1 antiretroviral drug therapy. *Cold Spring Harb Perspect Med.* 2012;2(4):a007161. doi: 10.1101/cshperspect.a007161
17. Kipp DR, Hirschi JS, Wakata A, Goldstein H, Schramm VL. Transition states of native and drug-resistant HIV-1 protease are the same. *Proc Natl Acad Sci USA.* 2012;109:6543-8. doi: 10.1073/pnas.1202808109
18. von Itzstein M, Wu WY, Kok GB, Pegg MS, Dyason JC, Jin B, et al. Rational design of potent sialidase-based inhibitors of influenza virus replication. *Nature.* 1993;363:418-23. doi: 10.1038/363418a0

References

19. von Itzstein M. The war against influenza: discovery and development of sialidase inhibitors. *Nat Rev Drug Discov*. 2007;6:967-74. doi: 10.1038/nrd2400
20. Chong AK, Pegg MS, Taylor NR, von Itzstein M. Evidence for a sialosyl cation transition-state complex in the reaction of sialidase from influenza virus. *Eur J Biochem*. 1992;207:335-43.
21. Kicska GA, Long L, Hörig H, Fairchild C, Tyler PC, Furneaux RH, et al. Immucillin H, a powerful transition-state analog inhibitor of purine nucleoside phosphorylase, selectively inhibits human T lymphocytes. *Proc Natl Acad Sci U S A*. 2001;98:4593-8. doi: 10.1073/pnas.071050798
22. Schramm VL. Development of transition state analogues of purine nucleoside phosphorylase as anti-T-cell agents. *Biochim Biophys Acta*. 2002;1587:107-17.
23. Stoeckler JD, Cambor C, Parks RE. Human erythrocytic purine nucleoside phosphorylase: reaction with sugar-modified nucleoside substrates. *Biochemistry*. 1980;19:102-7.
24. Cohen A, Gudas LJ, Ammann AJ, Staal GE, Martin DW. Deoxyguanosine triphosphate as a possible toxic metabolite in the immunodeficiency associated with purine nucleoside phosphorylase deficiency. *J Clin Invest*. 1978;61:1405-9. doi: 10.1172/JCI109058
25. Giblett ER, Ammann AJ, Wara DW, Sandman R, Diamond LK. Nucleoside-phosphorylase deficiency in a child with severely defective T-cell immunity and normal B-cell immunity. *Lancet*. 1975;1:1010-3.
26. Morris PE, Omura GA. Inhibitors of the enzyme purine nucleoside phosphorylase as potential therapy for psoriasis. *Curr Pharm Des*. 2000;6:943-59.
27. Gandhi V, Kilpatrick JM, Plunkett W, Ayres M, Harman L, Du M, et al. A proof-of-principle pharmacokinetic, pharmacodynamic, and clinical study with purine nucleoside phosphorylase inhibitor immucillin-H (BCX-1777, forodesine). *Blood*. 2005;106:4253-60. doi: 10.1182/blood-2005-03-1309
28. Balakrishnan K, Verma D, O'Brien S, Kilpatrick JM, Chen Y, Tyler BF, et al. Phase 2 and pharmacodynamic study of oral forodesine in patients with advanced, fludarabine-treated chronic lymphocytic leukemia. *Blood*. 2010;116:886-92. doi: 10.1182/blood-2010-02-272039
29. McNaught AD, Wilkinson A. IUPAC. Compendium of Chemical Terminology. 2 ed. Oxford: Blackwell Scientific Publications; 1997.
30. Maccoll A. Heavy-atom kinetic isotope effects. *Annu Rep Prog Chem, Sect A Inorg and Phys Chem*. 1974;71:77-101. doi: 10.1039/pr9747100077
31. Schramm VL. Enzymatic transition states and transition state analog design. *Annu Rev Biochem*. 1998;67:693-720. doi: 10.1146/annurev.biochem.67.1.693
32. Lewandowicz A, Schramm VL. Transition state analysis for human and *Plasmodium falciparum* purine nucleoside phosphorylases. *Biochemistry*. 2004;43:1458-68. doi: 10.1021/bi0359123
33. Geretti AM, Easterbrook P. Antiretroviral resistance in clinical practice. *Int J STD AIDS*. 2001;12:145-53. doi: 10.1258/0956462011916938
34. Weber IT, Agniswamy J. HIV-1 Protease: Structural Perspectives on Drug Resistance. *Viruses*. 2009;1:1110-36. doi: 10.3390/v1031110
35. Martinez-Cajas JL, Wainberg MA. Protease inhibitor resistance in HIV-infected patients: molecular and clinical perspectives. *Antiviral Res*. 2007;76:203-21. doi: 10.1016/j.antiviral.2007.06.010

References

36. Gershell LJ, Atkins JH. A brief history of novel drug discovery technologies. *Nat Rev Drug Discov.* 2003;2:321-7. doi: 10.1038/nrd1064
37. Schramm VL. Transition States, analogues, and drug development. *ACS Chem Biol.* 2013;8:71-81. doi: 10.1021/cb300631k
38. Pina AS, Hussain A, Roque AC. An historical overview of drug discovery. *Methods Mol Biol.* 2009;572:3-12. doi: 10.1007/978-1-60761-244-5_1
39. Sneader W. *Drug discovery: a history.* Chichester: Wiley; 2005.
40. Anderson AC. The process of structure-based drug design. *Chem Biol.* 2003;10:787-97.
41. Kapetanovic IM. Computer-aided drug discovery and development (CADD): in silico-chemico-biological approach. *Chem Biol Interact.* 2008;171:165-76. doi: 10.1016/j.cbi.2006.12.006
42. Murray CW, Rees DC. The rise of fragment-based drug discovery. *Nat Chem.* 2009;1:187-92. doi: 10.1038/nchem.217
43. Kaul PN. Drug discovery: past, present and future. *Prog Drug Res.* 1998;50:9-105.
44. Charlton PA, Young DW, Birdsall B, Feeney J, Roberts GCK. Stereochemistry of reduction of the vitamin folic acid by dihydrofolate reductase. *J Chem Soc, Perkin Trans 1.* 1985:1349-53. doi: 10.1039/p19850001349
45. Fox JT, Stover PJ, Litwack G. Folate-mediated one-carbon metabolism. *Folic Acid and Folates.* 2008;79:1-44. doi: 10.1016/S0083-6729(08)00401-9
46. Mentch SJ, Locasale JW. One-carbon metabolism and epigenetics: understanding the specificity. *Ann N Y Acad Sci.* 2016;1363:91-8. doi: 10.1111/nyas.12956
47. Locasale JW. Serine, glycine and one-carbon units: cancer metabolism in full circle. *Nat Rev Cancer.* 2013;13:572-83. doi: 10.1038/nrc3557
48. Yang M, Vousden KH. Serine and one-carbon metabolism in cancer. *Nat Rev Cancer.* 2016;16:650-62. doi: 10.1038/nrc.2016.81
49. Angelastro A, Dawson WM, Luk LYP, Loveridge EJ, Allemann RK. Chemoenzymatic Assembly of Isotopically Labeled Folates. *J Am Chem Soc.* 2017;139:13047-54. doi: 10.1021/jacs.7b06358
50. S. F, L. DL, D. MR, F. SR, A. WJ. Temporary Remissions in Acute Leukaemia in Children Produced by Folic Acid Antagonist, 4-Aminopteroyl-glutamic Acid (Aminopterin). *New Engl J Med.* 1948;238:787-93.
51. Hertz R, Bergenstal DM, Lipsett MB, Price EB, Hilbish TF. Chemotherapy of choriocarcinoma and related trophoblastic tumors in women. *JAMA.* 1958;168:845-54.
52. Li MC, Hertz R, Bergenstal DM. Therapy of choriocarcinoma and related trophoblastic tumors with folic acid and purine antagonists. *N Engl J Med.* 1958;259:66-74. doi: 10.1056/NEJM195807102590204
53. Nzila A. The past, present and future of antifolates in the treatment of *Plasmodium falciparum* infection. *J Antimicrob Chemother.* 2006;57:1043-54. doi: 10.1093/jac/dkl104
54. Curd FH, Davey DG, Rose FL. Studies on synthetic antimalarial drugs; some biguanide derivatives as new types of antimalarial substances with both therapeutic and causal prophylactic activity. *Ann Trop Med Parasitol.* 1945;39:208-16.

References

55. Falco EA, Goodwin LG, Hitchings GH, Rollo IM, Russell PB. 2:4-diaminopyrimidines- a new series of antimalarials. *Br J Pharmacol Chemother.* 1951;6:185-200.
56. Bushby SR, Hitchings GH. Trimethoprim, a sulphonamide potentiator. *Br J Pharmacol Chemother.* 1968;33:72-90.
57. Burchall JJ. The development of the diaminopyrimidines. *J Antimicrob Chemother.* 1979;5:3-14.
58. Takimoto CH. New Antifolates: Pharmacology and Clinical Applications. *Oncologist.* 1996;1:68-81.
59. Fleming GF, Schilsky RL. Antifolates: the next generation. *Semin Oncol.* 1992;19:707-19.
60. Zhao R, Goldman ID. Resistance to antifolates. *Oncogene.* 2003;22:7431-57. doi: 10.1038/sj.onc.1206946
61. Schweitzer BI, Dicker AP, Bertino JR. Dihydrofolate reductase as a therapeutic target. *FASEB J.* 1990;4:2441-52.
62. Estrada A, Wright DL, Anderson AC. Antibacterial Antifolates: From Development through Resistance to the Next Generation. *Cold Spring Harb Perspect Med.* 2016;6(8) doi: 10.1101/cshperspect.a028324
63. Blair JM, Webber MA, Baylay AJ, Ogbolu DO, Piddock LJ. Molecular mechanisms of antibiotic resistance. *Nat Rev Microbiol.* 2015;13:42-51. doi: 10.1038/nrmicro3380
64. Gregson A, Plowe CV. Mechanisms of resistance of malaria parasites to antifolates. *Pharmacol Rev.* 2005;57:117-45. doi: 10.1124/pr.57.1.4
65. Amyes SG, Towner KJ, Young HK. Classification of plasmid-encoded dihydrofolate reductases conferring trimethoprim resistance. *J Med Microbiol.* 1992;36:1-3. doi: 10.1099/00222615-36-1-1
66. Brumfitt W, Hamilton-Miller JM. Limitations of and indications for the use of cotrimoxazole. *J Chemother.* 1994;6:3-11.
67. Black RH, Ray AP. Experimental studies of the potentiation of proguanil and pyrimethamine by dapsone using *Plasmodium berghei* in white mice. *Ann Trop Med Parasitol.* 1977;71:131-9.
68. Matthews DA, Alden RA, Bolin JT, Freer ST, Hamlin R, Xuong N, et al. Dihydrofolate reductase: x-ray structure of the binary complex with methotrexate. *Science.* 1977;197:452-5.
69. Lerner MG, Bowman AL, Carlson HA. Incorporating dynamics in *E. coli* dihydrofolate reductase enhances structure-based drug discovery. *J Chem Inf Model.* 2007;47:2358-65. doi: 10.1021/ci700167n
70. Mauldin RV, Carroll MJ, Lee AL. Dynamic dysfunction in dihydrofolate reductase results from antifolate drug binding: modulation of dynamics within a structural state. *Structure.* 2009;17:386-94. doi: 10.1016/j.str.2009.01.005
71. Li X, Hilgers M, Cunningham M, Chen Z, Trzoss M, Zhang J, et al. Structure-based design of new DHFR-based antibacterial agents: 7-aryl-2,4-diaminoquinazolines. *Bioorg Med Chem Lett.* 2011;21:5171-6. doi: 10.1016/j.bmcl.2011.07.059
72. Lam T, Hilgers MT, Cunningham ML, Kwan BP, Nelson KJ, Brown-Driver V, et al. Structure-based design of new dihydrofolate reductase antibacterial agents: 7-(benzimidazol-1-yl)-2,4-diaminoquinazolines. *J Med Chem.* 2014;57:651-68. doi: 10.1021/jm401204g

References

73. Zolli-Juran M, Cechetto JD, Hartlen R, Daigle DM, Brown ED. High throughput screening identifies novel inhibitors of *Escherichia coli* dihydrofolate reductase that are competitive with dihydrofolate. *Bioorg Med Chem Lett*. 2003;13:2493-6.
74. Elowe NH, Blanchard JE, Cechetto JD, Brown ED. Experimental screening of dihydrofolate reductase yields a "test set" of 50,000 small molecules for a computational data-mining and docking competition. *J Biomol Screen*. 2005;10:653-7. doi: 10.1177/1087057105281173
75. Bolin JT, Filman DJ, Matthews DA, Hamlin RC, Kraut J. Crystal structures of *Escherichia coli* and *Lactobacillus casei* dihydrofolate reductase refined at 1.7 Å resolution. I. General features and binding of methotrexate. *J Biol Chem*. 1982;257:13650-62.
76. Bystroff C, Kraut J. Crystal structure of unliganded *Escherichia coli* dihydrofolate reductase. Ligand-induced conformational changes and cooperativity in binding. *Biochemistry*. 1991;30:2227-39.
77. Fierke CA, Johnson KA, Benkovic SJ. Construction and evaluation of the kinetic scheme associated with dihydrofolate reductase from *Escherichia coli*. *Biochemistry*. 1987;26:4085-92.
78. Sawaya MR, Kraut J. Loop and subdomain movements in the mechanism of *Escherichia coli* dihydrofolate reductase: crystallographic evidence. *Biochemistry*. 1997;36:586-603. doi: 10.1021/bi962337c
79. Venkitakrishnan RP, Zaborowski E, McElheny D, Benkovic SJ, Dyson HJ, Wright PE. Conformational changes in the active site loops of dihydrofolate reductase during the catalytic cycle. *Biochemistry*. 2004;43:16046-55. doi: 10.1021/bi048119y
80. Boehr DD, McElheny D, Dyson HJ, Wright PE. The dynamic energy landscape of dihydrofolate reductase catalysis. *Science*. 2006;313:1638-42. doi: 10.1126/science.1130258
81. Osborne MJ, Schnell J, Benkovic SJ, Dyson HJ, Wright PE. Backbone dynamics in dihydrofolate reductase complexes: role of loop flexibility in the catalytic mechanism. *Biochemistry*. 2001;40:9846-59.
82. Luk LY, Loveridge EJ, Allemann RK. Protein motions and dynamic effects in enzyme catalysis. *Phys Chem Chem Phys*. 2015;17:30817-27. doi: 10.1039/c5cp00794a
83. Stone SR, Morrison JF. Catalytic mechanism of the dihydrofolate reductase reaction as determined by pH studies. *Biochemistry*. 1984;23:2753-8.
84. Hecht D, Tran J, Fogel GB. Structural-based analysis of dihydrofolate reductase evolution. *Mol Phylogenet Evol*. 2011;61:212-30. doi: 10.1016/j.ympev.2011.06.005
85. Howell EE, Villafranca JE, Warren MS, Oatley SJ, Kraut J. Functional role of aspartic acid-27 in dihydrofolate reductase revealed by mutagenesis. *Science*. 1986;231:1123-8.
86. Bystroff C, Oatley SJ, Kraut J. Crystal structures of *Escherichia coli* dihydrofolate reductase: the NADP⁺ holoenzyme and the folate.NADP⁺ ternary complex. Substrate binding and a model for the transition state. *Biochemistry*. 1990;29:3263-77.
87. Shrimpton P, Allemann RK. Role of water in the catalytic cycle of *E. coli* dihydrofolate reductase. *Protein Sci*. 2002;11:1442-51. doi: 10.1110/ps.5060102
88. Wan Q, Bennett BC, Wilson MA, Kovalevsky A, Langan P, Howell EE, et al. Toward resolving the catalytic mechanism of dihydrofolate reductase using neutron and ultrahigh-resolution X-ray crystallography. *Proc Natl Acad Sci USA*. 2014;111:18225-30. doi: 10.1073/pnas.1415856111

References

89. Maharaj G, Selinsky BS, Appleman JR, Perlman M, London RE, Blakley RL. Dissociation constants for dihydrofolic acid and dihydrobiopterin and implications for mechanistic models for dihydrofolate reductase. *Biochemistry*. 1990;29:4554-60.
90. Chen YQ, Kraut J, Blakley RL, Callender R. Determination by Raman spectroscopy of the pKa of N5 of dihydrofolate bound to dihydrofolate reductase: mechanistic implications. *Biochemistry*. 1994;33:7021-6.
91. Cummins PL, Gready JE. Molecular dynamics and free energy perturbation study of hydride-ion transfer step in dihydrofolate reductase using combined quantum and molecular mechanical model. *Journal of Computational Chemistry*. 1998;19:977-88. doi: 10.1002/(SICI)1096-987X(199806)19:8<977::AID-JCC15>3.0.CO;2-4
92. Castillo R, Andres J, Moliner V. Catalytic mechanism of dihydrofolate reductase enzyme. A combined quantum-mechanical/molecular-mechanical characterization of transition state structure for the hydride transfer step. *J Am Chem Soc*. 1999;121:12140-7. doi: 10.1021/ja9843019
93. Cummins PL, Gready JE. Energetically most likely substrate and active-site protonation sites and pathways in the catalytic mechanism of dihydrofolate reductase. *J Am Chem Soc*. 2001;123:3418-28.
94. Ferrer S, Silla E, Tunon I, Marti S, Moliner V. Catalytic mechanism of dihydrofolate reductase enzyme. A combined quantum-mechanical/molecular-mechanical characterization of the N5 protonation step. *J Phys Chem B*. 2003;107:14036-41. doi: 10.1021/jp0354898
95. Rod TH, Brooks CL. How dihydrofolate reductase facilitates protonation of dihydrofolate. *J Am Chem Soc*. 2003;125:8718-9. doi: 10.1021/ja035272r
96. Liu CT, Francis K, Layfield JP, Huang X, Hammes-Schiffer S, Kohen A, et al. Escherichia coli dihydrofolate reductase catalyzed proton and hydride transfers: temporal order and the roles of Asp27 and Tyr100. *Proc Natl Acad Sci USA*. 2014;111:18231-6. doi: 10.1073/pnas.1415940111
97. Peracchi A. Enzyme catalysis: removing chemically 'essential' residues by site-directed mutagenesis. *Trends Biochem Sci*. 2001;26:497-503.
98. Cioni P, Strambini GB. Effect of heavy water on protein flexibility. *Biophys J*. 2002;82:3246-53. doi: 10.1016/S0006-3495(02)75666-X
99. Schowen KB, Schowen RL. Solvent isotope effects of enzyme systems. *Methods Enzymol*. 1982;87:551-606.
100. Curthoys NP, Rabinowitz JC. Formyltetrahydrofolate synthetase. Binding of folate substrates and kinetics of the reverse reaction. *J Biol Chem*. 1972;247(7):1965-71.
101. Kisliuk RL. The source of hydrogen for methionine methyl formation. *J Biol Chem*. 1963;238(1):397-400.
102. Matthews RG, Haywood BJ. Inhibition of pig liver methylenetetrahydrofolate reductase by dihydrofolate: some mechanistic and regulatory implications. *Biochemistry*. 1979;18(22):4845-51.
103. Matthews RG. Studies on the methylene/methyl interconversion catalyzed by methylenetetrahydrofolate reductase from pig liver. *Biochemistry*. 1982;21(17):4165-71.
104. Vanoni MA, Ballou DP, Matthews RG. Methylenetetrahydrofolate reductase. Steady state and rapid reaction studies on the NADPH-methylenetetrahydrofolate, NADPH-menadione, and methyltetrahydrofolate-menadione oxidoreductase activities of the enzyme. *J Biol Chem*. 1983;258(19):11510-4.

References

105. Vanoni MA, Matthews RG. Kinetic isotope effects on the oxidation of reduced nicotinamide adenine dinucleotide phosphate by the flavoprotein methylenetetrahydrofolate reductase. *Biochemistry*. 1984;23(22):5272-9. doi: 10.1021/bi00317a027
106. Vanoni MA, Lee S, Floss HG, Matthews RG. Stereochemistry of reduction of methylenetetrahydrofolate to methyltetrahydrofolate catalyzed by pig liver methylenetetrahydrofolate reductase. *J Am Chem Soc*. 1990;112(10):3987-92. doi: 10.1021/ja00166a040
107. Sumner JS, Matthews RG. Stereochemistry and mechanism of hydrogen transfer between NADPH and methylenetetrahydrofolate in the reaction catalyzed by methylenetetrahydrofolate reductase from pig liver. *J Am Chem Soc*. 1992;114(18):6949-56. doi: 10.1021/ja00044a001
108. Zydowsky TM, Courtney LF, Frasca V, Kobayashi K, Shimizu H, Yuen LD, et al. Stereochemical analysis of the methyl transfer catalyzed by cobalamin-dependent methionine synthase from *Escherichia coli* B. *Journal of the American Chemical Society*. 1986;108(11):3152-3. doi: 10.1021/ja00271a081
109. Tatum CM, Benkovic PA, Benkovic SJ, Potts R, Schleicher E, Floss HG. Stereochemistry of methylene transfer involving 5,10-methylenetetrahydrofolate. *Biochemistry*. 1977;16(6):1093-102. doi: 10.1021/bi00625a010
110. Pastore EJ, Friedkin M. The enzymatic synthesis of thymidylate. II. Transfer of tritium from tetrahydrofolate to the methyl group of thymidylate. *J Biol Chem*. 1962;237:3802-10.
111. Bruice TW, Santi DV. Secondary alpha-hydrogen isotope effects on the interaction of 5-fluoro-2'-deoxyuridylate and 5,10-methylenetetrahydrofolate with thymidylate synthetase. *Biochemistry*. 1982;21(26):6703-9.
112. Sliker LJ, Benkovic SJ. Synthesis of (6R,11S)- and (6R,11R)-5,10-methylene[11-1H,2H]tetrahydrofolate. Stereochemical paths of serine hydroxymethyltransferase, 5,10-methylenetetrahydrofolate dehydrogenase, and thymidylate synthetase catalysis. *J Am Chem Soc*. 1984;106(6):1833-8. doi: 10.1021/ja00318a049
113. Kouniga K, Vandervelde DG, Himes RH. ¹⁸Oxygen incorporation into inorganic phosphate in the reaction catalyzed by N^{5,10}-methenyltetrahydrofolate synthetase. *Febs Letters*. 1995;364(2):215-7. doi: 10.1016/0014-5793(95)00396-Q
114. Huang T, Schirch V. Mechanism for the coupling of ATP hydrolysis to the conversion of 5-formyltetrahydrofolate to 5,10-methenyltetrahydrofolate. *J Biol Chem*. 1995;270(38):22296-300.
115. Agrawal N, Mihai C, Kohen A. Microscale synthesis of isotopically labeled R-[6-^xH]N⁵,N¹⁰-methylene-5,6,7,8-tetrahydrofolate as a cofactor for thymidylate synthase. *Anal Biochem*. 2004;328(1):44-50. doi: 10.1016/j.ab.2004.01.029
116. Cocco L, Groff JP, Temple C, Montgomery JA, London RE, Matwiyoff NA, et al. Carbon-13 nuclear magnetic resonance study of protonation of methotrexate and aminopterin bound to dihydrofolate reductase. *Biochemistry*. 1981;20:3972-8.
117. Selinsky BS, Perlman ME, London RE, Unkefer CJ, Mitchell J, Blakley RL. ¹³C and ¹⁵N nuclear magnetic resonance evidence of the ionization state of substrates bound to bovine dihydrofolate reductase. *Biochemistry*. 1990;29:1290-6.
118. Connor MJ, Blair JA, Said H. Secondary isotope effects in studies using radiolabelled folate tracers. *Nature*. 1980;287(5779):253-4.
119. Gregory JF, Williamson J, Liao JF, Bailey LB, Toth JP. Kinetic model of folate metabolism in nonpregnant women consuming [2H₂]folic acid: isotopic labeling of

References

- urinary folate and the catabolite para-acetamidobenzoylglutamate indicates slow, intake-dependent, turnover of folate pools. *J Nutr.* 1998;128:1896-906.
120. Halsted CH, Villanueva JA, Devlin AM, Chandler CJ. Metabolic interactions of alcohol and folate. *J Nutr.* 2002;132(8 Suppl):2367S-72S.
121. Lin YM, Dueker SR, Follett JR, Fadel JG, Arjomand A, Schneider PD, et al. Quantitation of in vivo human folate metabolism. *Am J Clin Nutr.* 2004;80(3):680-91.
122. Obeid R, Kirsch SH, Dilmann S, Klein C, Eckert R, Geisel J, et al. Folic acid causes higher prevalence of detectable unmetabolized folic acid in serum than B-complex: a randomized trial. *Eur J Nutr.* 2016;55(3):1021-8. doi: 10.1007/s00394-015-0916-z
123. Kopp M, Morisset R, Koehler P, Rychlik M. Stable Isotope Dilution Assays for Clinical Analyses of Foliates and Other One-Carbon Metabolites: Application to Folate-Deficiency Studies. *PLOS ONE.* 2016;11(6):e0156610. doi: 10.1371/journal.pone.0156610
124. Girgis S, Suh JR, Jolivet J, Stover PJ. 5-Formyltetrahydrofolate regulates homocysteine remethylation in human neuroblastoma. *J Biol Chem.* 1997;272(8):4729-34.
125. Anguera MC, Suh JR, Ghandour H, Nasrallah IM, Selhub J, Stover PJ. Methenyltetrahydrofolate synthetase regulates folate turnover and accumulation. *J Biol Chem.* 2003;278(32):29856-62. doi: 10.1074/jbc.M302883200
126. Anderson B, Belcher EH, Chanarin I, Mollin DL. The urinary and faecal excretion of radioactivity after oral doses of 3H-folic acid. *Br J Haematol.* 1960;6:439-55.
127. Johns DG, Sperti S, Burgen AS. The metabolism of tritiated folic acid in man. *J Clin Invest.* 1961;40:1684-95. doi: 10.1172/JCI104391
128. Goresky CA, Watanbe H, Johns DG. The renal excretion of folic acid. *J Clin Invest.* 1963;42:1841-9. doi: 10.1172/JCI104868
129. Levitt M, Nixon PF, Pincus JH, Bertino JR. Transport characteristics of folates in cerebrospinal fluid; a study utilizing doubly labeled 5-methyltetrahydrofolate and 5-formyltetrahydrofolate. *J Clin Invest.* 1971;50(6):1301-8. doi: 10.1172/JCI106609
130. Halsted CH. The intestinal absorption of folates. *Am J Clin Nutr.* 1979;32(4):846-55.
131. Blocker DE, Thenen SW. Intestinal absorption, liver uptake, and excretion of ³H-folic acid in folic acid-deficient, alcohol-consuming nonhuman primates. *Am J Clin Nutr.* 1987;46(3):503-10.
132. Lakoff A, Fazili Z, Aufreiter S, Pfeiffer CM, Connolly B, Gregory JF, et al. Folate is absorbed across the human colon: evidence by using enteric-coated caplets containing ¹³C-labeled [6S]-5-formyltetrahydrofolate. *Am J Clin Nutr.* 2014;100(5):1278-86. doi: 10.3945/ajcn.114.091785
133. Weygand F, Schaefer G. Synthese von Foliinsäure-11-¹⁴C. *Naturwissenschaften.* 1951;38(18):432-3. doi: 10.1007/BF00630742
134. Weislogel O, Bond TJ. Studies on cofactor functions of folinic acid using radiolabeled compounds. *Arch Biochem Biophys.* 1960;89:221-4.
135. Ho PPK, Jones L. Enzymatic preparation of the (+),L-diastereoisomer of [methenyl-¹⁴C]-N⁵,N¹⁰-methenyltetrahydrofolic acid. *Biochim Biophys Acta.* 1967;148(3):622-8. doi: 10.1016/0304-4165(67)90035-9
136. Zakrzewski SF, Himberg JJ. Preparation of tritiated dihydrofolate and its use in the assay of dihydrofolate reductase. *Anal Biochem.* 1971;40(2):336-44.

References

137. Nixon PF, Bertino JR. Enzymic preparations of radiolabeled (+)-L-5-methyltetrahydrofolate and (+)-L-5-formyltetrahydrofolate. *Anal Biochem.* 1971;43(1):162-72. doi: 10.1016/0003-2697(71)90121-7
138. Curthoys NP, Scott JM, Rabinowitz JC. Folate coenzymes of *Clostridium acidurici*. The isolation of (l)-5,10-methenyltetrahydropteroyltriglutamate, its conversion to (l)-tetrahydropteroyltriglutamate and (l)-10-(¹⁴C)formyltetrahydropteroyltriglutamate, and the synthesis of (l)-10-formyl-(6,7-³H₂)tetrahydropteroyltriglutamate and (l)-(6,7-³H₂)tetrahydropteroyltriglutamate. *J Biol Chem.* 1972;247:1959-64.
139. Hachey DL, Palladino L, Blair JA, Rosenberg IH, Klein PD. Preparation of pteroylglutamic acid-3',5'-H₂ by acid catalyzed exchange with deuterium oxide. *J Labelled Comp Radiopharm.* 1978;14(4):479-86.
140. Horne DW, Briggs WT, Wagner C. Enzymic synthesis of (d)-L-5-methyltetrahydropteroylglutamate of high specific radioactivity. *Methods Enzymol.* 1980;66:545-7.
141. Pastore EJ. Folate and its reduced forms labeled with deuterium at carbon-7. *Methods Enzymol.* 1980;66:538-41.
142. Pastore EJ. N⁵-Formyltetrahydrofolate (citraovorum factor) labeled stereospecifically with deuterium or tritium at carbon-6. *Methods Enzymol.* 1980;66:541-5.
143. Plante LT, Williamson KL, Pastore EJ. Preparation of folic acid specifically labeled with carbon-13 in the benzoyl carbonyl. *Methods Enzymol.* 1980;66:533-5.
144. Gregory JF, Toth JP. Preparation of folic acid specifically labeled with deuterium at 3', 5' positions. *J Labelled Comp Radiopharm.* 1988;25(12):1349-59. doi: 10.1002/jlcr.2580251209
145. Gregory JF. Improved synthesis of [3',5'-(H₂)₂]folic acid - extent and specificity of deuterium labeling. *J Agric Food Chem.* 1990;38(4):1073-6. doi: 10.1021/jf00094a036
146. Cheung HTA, Birdsall B, Frenkiel TA, Chau DD, Feeney J. ¹³C NMR determination of the tautomeric and ionization states of folate in its complexes with *Lactobacillus casei* dihydrofolate reductase. *Biochemistry.* 1993;32:6846-54. doi: 10.1021/bi00078a007
147. Cowart M, Falzone CJ, Benkovic SJ. A new synthesis of double labeled [7,9-¹³C₂] folic acid. *J Labelled Comp Radiopharm.* 1994;34:67-71. doi: 10.1002/jlcr.2580340109
148. Dueker SR, Jones AD, Smith GM, Clifford AJ. Preparation of [2',3',5',6'-²H₄]pteroylglutamic acid. *J Labelled Comp Radiopharm.* 1995;36(10):981-91. doi: 10.1002/jlcr.2580361010
149. Pfeiffer CM, Gregory JF. Preparation of stable isotopically labeled folates for in vivo investigation of folate absorption and metabolism. *Methods Enzymol.* 1997;281:106-16.
150. Maunder P, Finglas P, Mallet A, Mellon F, Razzaque M, Ridge B, et al. The synthesis of folic acid, multiply labelled with stable isotopes, for bio-availability studies in human nutrition. *J Chem Soc, Perkin Trans 1.* 1999:1311-23. doi: 10.1039/a900944b
151. Freisleben A, Schieberle P, Rychlik M. Syntheses of labeled vitamers of folic acid to be used as internal standards in stable isotope dilution assays. *J Agric Food Chem.* 2002;50(17):4760-8. doi: 10.1021/jf025571k
152. Melse-Boonstra A, Verhoef P, West C, van Rhijn J, van Breemen R, Lasaroms J, et al. A dual-isotope-labeling method of studying the bioavailability of hexaglutamyl folic acid relative to that of monoglutamyl folic acid in humans by using multiple orally administered low doses. *Am J Clin Nutr.* 2006;84(5):1128-33.

References

153. Naponelli V, Hanson A, Gregory J. Improved methods for the preparation of [H-3]folate polyglutamates: biosynthesis with *Lactobacillus casei* and enzymatic synthesis with *Escherichia coli* folylpolyglutamate synthetase. *Anal Biochem.* 2007;371(2):127-34. doi: 10.1016/j.ab.2007.08.026
154. Weygand F, Schaefer G. Synthese von pteroyl-L-glutaminsäure[11C-14] (folinsäure-[11-C-14]). *Chem Ber.* 1952;85(4):307-14. doi: 10.1002/cber.19520850407
155. Weygand F, Mann HJ, Simon H. Synthese von pteroyl-L-glutaminsäure [2-C-14]. *Chem Ber.* 1952;85(5):463-5. doi: 10.1002/cber.19520850523
156. Saeed M, Tewson TJ, Erdahl CE, Kohen A. A fast chemoenzymatic synthesis of [¹¹C]-N⁵,N¹⁰-methylenetetrahydrofolate as a potential PET tracer for proliferating cells. A fast chemoenzymatic synthesis of [¹¹C]-N⁵,N¹⁰-methylenetetrahydrofolate as a potential PET tracer for proliferating cells. *Nucl Med Biol.* 2012;39:697-701. doi: 10.1016/j.nucmedbio.2011.12.003
157. De Brouwer V, Zhang GF, Storozhenko S, Straeten DV, Lambert WE. pH stability of individual folates during critical sample preparation steps in prevision of the analysis of plant folates. *Phytochem Anal.* 2007;18(6):496-508. doi: 10.1002/pca.1006
158. Dantola ML, Vignoni M, Capparelli AL, Lorente C, Thomas AH. Stability of 7,8-dihydropterins in air-equilibrated aqueous solutions. *Helv Chim Acta.* 2008;91:411-25. doi: 10.1002/hlca.200890046
159. Reed LS, Archer MC. Oxidation of tetrahydrofolic acid by air. *J Agric Food Chem.* 1980;28(4):801-5. doi: 10.1021/jf60230a044
160. Strandler HS, Patring J, Jägerstad M, Jastrebova J. Challenges in the determination of unsubstituted food folates: impact of stabilities and conversions on analytical results. *J Agric Food Chem.* 2015;63(9):2367-77. doi: 10.1021/jf504987n
161. Walker TE, Unkefer CJ, Ehlrer DS. The synthesis of carbon-13 enriched monosaccharides derived from glucose and mannose. *J Carbohydr Chem.* 1988;7:115-32.
162. Burg AW, Brown GM. The biosynthesis of folic acid. 8. Purification and properties of the enzyme that catalyzes the production of formate from carbon atom 8 of guanosine triphosphate. *J Biol Chem.* 1968;243:2349-58.
163. Gabelli SB, Bianchet MA, Xu W, Dunn CA, Niu ZD, Amzel LM, et al. Structure and function of the *E. coli* dihydroneopterin triphosphate pyrophosphatase: a Nudix enzyme involved in folate biosynthesis. *Structure.* 2007;15:1014-22. doi: 10.1016/j.str.2007.06.018
164. You C, Zhang YHP. Biomanufacturing by in vitro biosystems containing complex enzyme mixtures. *Process Biochem.* 2017;52:106-14.
165. Guo W, Sheng J, Feng X. In vitro metabolic engineering for biomanufacturing of high-value products. *Comput Struct Biotechnol J.* 2017;15:161-7.
166. Schultheisz HL, Szymczyna BR, Scott LG, Williamson JR. Pathway Engineered Enzymatic de novo Purine Nucleotide Synthesis. *ACS Chem Biol.* 2008;3:499-511.
167. Schultheisz HL, Szymczyna BR, Scott LG, Williamson JR. Enzymatic De Novo Pyrimidine Nucleotide Synthesis. *J Am Chem Soc.* 2011;133(2):297-304. doi: 10.1021/ja1059685
168. Chenault HK, Whitesides GM. Regeneration of nicotinamide cofactors for use in organic synthesis. *Appl Biochem Biotechnol.* 1987;14(2):147-97.
169. Chenault HK, Simon ES, Whitesides GM. Cofactor regeneration for enzyme-catalysed synthesis. *Biotechnol Genet Eng Rev.* 1988;6:221-70.

References

170. Zhao H, van der Donk WA. Regeneration of cofactors for use in biocatalysis. *Curr Opin Biotechnol.* 2003;14(6):583-9.
171. Gross A, Abril O, Lewis JM, Geresh S, Whitesides GM. Practical Synthesis of 5-Phospho-D-Ribosyl α -1-Pyrophosphate (PRPP): Enzymatic Routes from Ribose 5-Phosphate or Ribose. *J Am Chem Soc.* 1983;105:7428-35. doi: 10.1021/ja00363a037
172. Lee LG, Whitesides GM. Preparation of Optically Active 1,2-Diols and α -Hydroxy Ketones Using Glycerol Dehydrogenase as Catalyst: Limits to Enzyme-Catalyzed Synthesis due to Noncompetitive and Mixed Inhibition by Product. *J Org Chem.* 1986;51(1):25-36. doi: 10.1021/jo00351a005
173. Wong CH, McCurry SD, Whitesides GM. Practical enzymic syntheses of ribulose 1,5 biphosphate and ribose 5-phosphate. *J Am Chem Soc.* 1980;102(27):7938-9.
174. Boyer PD. The enzymes. Volume 11, Oxidation-reduction. Part A, Dehydrogenases (I), electron transfer (I). 3rd ed. New York ; London: Academic Press,; 1975.
175. Zhu L, Xu X, Wang L, Dong H, Yu B, Ma Y. NADP⁺-Preferring D-Lactate Dehydrogenase from *Sporolactobacillus inulinus*. *Appl Environ Microbiol.* 2015;81(18):6294-301. doi: 10.1128/AEM.01871-15
176. Riebel BR, Gibbs PR, Wellborn WB, Bommarius AS. Cofactor regeneration of both NAD(+) from NADH and NADP(+) from NADPH : NADH oxidase from *Lactobacillus sanfranciscensis*. *Adv Synth Catal.* 2003;345(6-7):707-12. doi: 10.1002/adsc.200303039
177. Wu X, Kobori H, Orita I, Zhang C, Imanaka T, Xing XH, et al. Application of a novel thermostable NAD(P)H oxidase from hyperthermophilic archaeon for the regeneration of both NAD and NADP . *Biotechnol Bioeng.* 2012;109(1):53-62. doi: 10.1002/bit.23294
178. Pham NH, Hollmann F, Kracher D, Preims M, Haltrich D, Ludwig R. Engineering an enzymatic regeneration system for NAD(P)H oxidation. *J Mol Catal B: Enzym.* 2015;120:38-46. doi: 10.1016/j.molcatb.2015.06.011
179. Angelastro A, Dawson WM, Luk YPL, Allemann RK. A versatile disulfide-driven recycling system for NADP⁺ with high cofactor turnover number. *ACS Catal.* 2017;7:1025-9.
180. Holmgren A, Johansson C, Berndt C, Lönn ME, Hudemann C, Lillig CH. Thiol redox control via thioredoxin and glutaredoxin systems. *Biochem Soc Trans.* 2005;33(6):1375-7. doi: 10.1042/BST20051375
181. Lillig CH, Berndt C, Holmgren A. Glutaredoxin systems. *Biochim Biophys Acta.* 2008;1780(11):1304-17. doi: 10.1016/j.bbagen.2008.06.003
182. Bushweller JH, Aslund F, Wüthrich K, Holmgren A. Structural and functional characterization of the mutant *Escherichia coli* glutaredoxin (C14----S) and its mixed disulfide with glutathione. *Biochemistry.* 1992;31(38):9288-93.
183. Vlamis-Gardikas A, Holmgren A. Thioredoxin and glutaredoxin isoforms. *Methods Enzymol.* 2002;347:286-96.
184. Luthman M, Holmgren A. Glutaredoxin from Calf Thymus - Purification to Homogeneity. *J Biol Chem.* 1982;257(12):6686-90.
185. Holmgren A, Aslund F. Glutaredoxin. *Methods Enzymol.* 1995;252:283-92.
186. Aslund F, Ehn B, Miranda-Vizuete A, Pueyo C, Holmgren A. Two additional glutaredoxins exist in *Escherichia coli*: glutaredoxin 3 is a hydrogen donor for ribonucleotide reductase in a thioredoxin/glutaredoxin 1 double mutant. *Proc Natl Acad Sci USA.* 1994;91(21):9813-7.

References

187. Chenas NK, Rakauskene GA, Kulis II. [The relation of glutathione reductase and diaphorase activity of glutathione reductase from *Saccharomyces cerevisiae*]. *Biokhimiia*. 1989;54(7):1090-7.
188. Vlamis-Gardikas A, Aslund F, Spyrou G, Bergman T, Holmgren A. Cloning, overexpression, and characterization of glutaredoxin 2, an atypical glutaredoxin from *Escherichia coli*. *J Biol Chem*. 1997;272(17):11236-43.
189. Massey V, Williams CH. On the reaction mechanism of yeast glutathione reductase. *J Biol Chem*. 1965;240(11):4470-80.
190. Holmgren A. Glutathione-dependent synthesis of deoxyribonucleotides. Purification and characterization of glutaredoxin from *Escherichia coli*. *J Biol Chem*. 1979;254(9):3664-71.
191. Cheng NH, Liu JZ, Brock A, Nelson RS, Hirschi KD. AtGRXcp, an Arabidopsis chloroplastic glutaredoxin, is critical for protection against protein oxidative damage. *J Biol Chem*. 2006;281(36):26280-8. doi: 10.1074/jbc.M601354200
192. Bandyopadhyay S, Starke DW, Mieyal JJ, Gronostajski RM. Thioltransferase (glutaredoxin) reactivates the DNA-binding activity of oxidation-inactivated nuclear factor I. *J Biol Chem*. 1998;273(1):392-7.
193. Davis DA, Newcomb FM, Starke DW, Ott DE, Mieyal JJ, Yarchoan R. Thioltransferase (glutaredoxin) is detected within HIV-1 and can regulate the activity of glutathionylated HIV-1 protease in vitro. *J Biol Chem*. 1997;272(41):25935-40.
194. Braasch I, Scharl M, Volff JN. Evolution of pigment synthesis pathways by gene and genome duplication in fish. *BMC Evol Biol*. 2007;7:74. doi: 10.1186/1471-2148-7-74
195. Kim H, Kim K, Yim J. Biosynthesis of drospterins, the red eye pigments of *Drosophila melanogaster*. *IUBMB Life*. 2013;65:334-40. doi: 10.1002/iub.1145
196. Basu P, Burgmayer SJ. Pterin chemistry and its relationship to the molybdenum cofactor. *Coord Chem Rev*. 2011;255:1016-38. doi: 10.1016/j.ccr.2011.02.010
197. Reader JS, Metzgar D, Schimmel P, de Crécy-Lagard V. Identification of four genes necessary for biosynthesis of the modified nucleoside queuosine. *J Biol Chem*. 2004;279:6280-5. doi: 10.1074/jbc.M310858200
198. Schwarz G, Mendel RR, Ribbe MW. Molybdenum cofactors, enzymes and pathways. *Nature*. 2009;460:839-47. doi: 10.1038/nature08302
199. Thöny B, Auerbach G, Blau N. Tetrahydrobiopterin biosynthesis, regeneration and functions. *Biochem J*. 2000;347:1-16.
200. White RH. Biosynthesis of the methanogenic cofactors. *Vitam Horm*. 2001;61:299-337.
201. Bacher A, Eberhardt S, Eisenreich W, Fischer M, Herz S, Illarionov B, et al. Biosynthesis of riboflavin. *Vitam Horm*. 2001;61:1-49.
202. Longhini AP, LeBlanc RM, Becette O, Salguero C, Wunderlich CH, Johnson BA, et al. Chemo-enzymatic synthesis of site-specific isotopically labeled nucleotides for use in NMR resonance assignment, dynamics and structural characterizations. *Nucleic Acids Res*. 2016;44(6):1-10. doi: 10.1093/nar/gkv1333
203. Duss O, Diarra Dit Konté N, Allain FH. Cut and paste RNA for nuclear magnetic resonance, paramagnetic resonance enhancement, and electron paramagnetic resonance structural studies. *Methods Enzymol*. 2015;565:537-62. doi: 10.1016/bs.mie.2015.05.029
204. Lu K, Miyazaki Y, Summers MF. Isotope labeling strategies for NMR studies of RNA. *J Biomol NMR*. 2010;46(1):113-25. doi: 10.1007/s10858-009-9375-2

References

205. Tolbert TJ, Williamson JR. Preparation of specifically deuterated RNA for NMR studies using a combination of chemical and enzymatic synthesis. *J Am Chem Soc.* 1996;118:7929-40. doi: 10.1021/ja961274i
206. Cromsigt J, Schleucher J, Gustafsson T, Kihlberg J, Wijmenga S. Preparation of partially H-2/C-13-labelled RNA for NMR studies. Stereo-specific deuteration of the H5'' in nucleotides. *Nucleic Acids Res.* 2002;30:1639-45. doi: 10.1093/nar/30.7.1639
207. LaFrancois CJ, Fujimoto J, Sowers LC. Synthesis and utilization of ¹³C(8)-enriched purines. *Nucleosides Nucleotides.* 1999;18:23-37.
208. Seela F, Ramzaeva N, Rosemeyer H. 7.1. Purines. In: Schaumann E, editor. *Houben-Weyl Methods of Organic Chemistry.* 4 ed. New York: Georg Thieme Verlag; 1997. p. 304-547.
209. Traube W. Ueber eine neue synthese des guanins und xanthins. *Chem Ber.* 1900;33:1371-83.
210. Sharma M, Alderfer JL, Box HC. Synthesis of morpholinium [¹³C] formate and its application in the synthesis of [8-¹³C] purine base. *J Labelled Comp Radiopharm.* 1983;20:1219-25.
211. Yamazaki A, Kumashiro I, Takenishi T. Synthesis of guanosine and its derivatives from 5-amino-1-beta-D-ribofuranosyl-4-imidazolecarboxamide. I. Ring closure with benzoyl isothiocyanate. *J Org Chem.* 1967;32:1825-8.
212. Yamazaki A, Okutsu M, Yamada Y. Synthesis of guanosine and its derivatives from 5-amino-1-beta-D-ribofuranosyl-e-imidazolecarboxamide. IV. A new route to guanosine via cyanamide derivative. *Nucleic Acids Res.* 1976;3:251-9.
213. Dawson W. Analysis of the transition state of dihydrofolate reductase Cardiff University; 2014.
214. Oeschger MP. Guanylate kinase from *Escherichia coli* B. *Methods Enzymol.* 1978;51:473-82.
215. Gräwert T, Fischer M, Bacher A. Structures and reaction mechanisms of GTP cyclohydrolases. *IUBMB Life.* 2013;65:310-22. doi: 10.1002/iub.1153
216. Schramek N, Bracher A, Bacher A. Ring opening is not rate-limiting in the GTP cyclohydrolase I reaction. *J Biol Chem.* 2001;276:2622-6. doi: 10.1074/jbc.M004912200
217. Schoedon G, Redweik U, Frank G, Cotton RG, Blau N. Allosteric characteristics of GTP cyclohydrolase I from *Escherichia coli*. *Eur J Biochem.* 1992;210:561-8.
218. McLennan AG. Folate synthesis: an old enzyme identified. *Structure.* 2007;15:891-2. doi: 10.1016/j.str.2007.07.002
219. Yim JJ, Brown GM. Characteristics of guanosine triphosphate cyclohydrolase I purified from *Escherichia coli*. *J Biol Chem.* 1976;251:5087-94.
220. Derrick JP. The structure and mechanism of 6-hydroxymethyl-7,8-dihydropterin pyrophosphokinase. *Vitam Horm.* 2008;79:411-33. doi: 10.1016/S0083-6729(08)00415-9
221. Richey DP, Brown GM. A comparison of the effectiveness with which p-aminobenzoic acid and p-aminobenzoylglutamic acid are used as substrate by dihydropteroate synthetase from *Escherichia coli*. *Biochim Biophys Acta.* 1970;222:237-9.
222. Shrimpton P, Mullaney A, Allemann RK. Functional role for Tyr 31 in the catalytic cycle of chicken dihydrofolate reductase. *Proteins.* 2003;51:216-23. doi: 10.1002/prot.10370

References

223. Rebelo J, Auerbach G, Bader G, Bracher A, Nar H, Hösl C, et al. Biosynthesis of pteridines. Reaction mechanism of GTP cyclohydrolase I. *J Mol Biol.* 2003;326:503-16.
224. Deng H, Callender R, Howell E. Vibrational structure of dihydrofolate bound to R67 dihydrofolate reductase. *J Biol Chem.* 2001;276:48956-60. doi: 10.1074/jbc.M105107200
225. Mönch S, Netzel M, Netzel G, Rychlik M. Quantitation of folates and their catabolites in blood plasma, erythrocytes, and urine by stable isotope dilution assays. *Anal Biochem.* 2010;398:150-60. doi: 10.1016/j.ab.2009.11.007
226. Gregory JF. Case study: folate bioavailability. *J Nutr.* 2001;131:1376S-82S.
227. Gregory JF, Quinlivan EP. In vivo kinetics of folate metabolism. *Annu Rev Nutr.* 2002;22:199-220. doi: 10.1146/annurev.nutr.22.120701.083554
228. de Ambrosis A, Vishnumohan S, Paterson J, Haber P, Arcot J. Relative bioavailability of ¹³C5-folic acid in pectin-coated folate fortified rice in humans using stable isotope techniques. *Eur J Clin Nutr.* 2017;71:103-6. doi: 10.1038/ejcn.2016.122
229. Mansoorabadi SO, Thibodeaux CJ, Liu HW. The diverse roles of flavin coenzymes - nature's most versatile thespians. *J Org Chem.* 2007;72:6329-42. doi: 10.1021/jo0703092
230. Noguchi Y, Ishii A, Matsushima A, Haishi D, Yasumuro K, Moriguchi T, et al. Isolation of Biopterin-alpha-glucoside from *Spirulina* (*Arthrospira*) *platensis* and Its Physiologic Function. *Mar Biotechnol* (NY). 1999;1:207-10.
231. Syn CK, Swarup S. A scalable protocol for the isolation of large-sized genomic DNA within an hour from several bacteria. *Anal Biochem.* 2000;278:86-90. doi: 10.1006/abio.1999.4410
232. Swanwick RS, Maglia G, Tey LH, Allemann RK. Coupling of protein motions and hydrogen transfer during catalysis by *Escherichia coli* dihydrofolate reductase. *Biochem J.* 2006;394:259-65. doi: 10.1042/BJ20051464
233. Bradford MM. A rapid and sensitive method for the quantitation of microgram quantities of protein utilizing the principle of protein-dye binding. *Anal Biochem.* 1976;72:248-54.
234. Rippa M, Giovannini PP, Barrett MP, Dallochio F, Hanau S. 6-Phosphogluconate dehydrogenase: the mechanism of action investigated by a comparison of the enzyme from different species. *Biochim Biophys Acta.* 1998;1429(1):83-92.
235. Bracher A, Eisenreich W, Schramek N, Ritz H, Gotze E, Herrmann A, et al. Biosynthesis of pteridines - NMR studies on the reaction mechanisms of GTP cyclohydrolase I, pyruvoyltetrahydropterin synthase, and sepiapterin reductase. *J Biol Chem.* 1998;273(43):28132-41. doi: 10.1074/jbc.273.43.28132
236. Blakley RL. Crystalline dihydropteroylglutamic acid. *Nature.* 1960;188:231-2. doi: 10.1038/188231a0

8. APPENDICES

8.1 Appendix 1. High-resolution mass spectrometry data

8.1.1 HRMS of isotopically labelled guanosine monophosphates

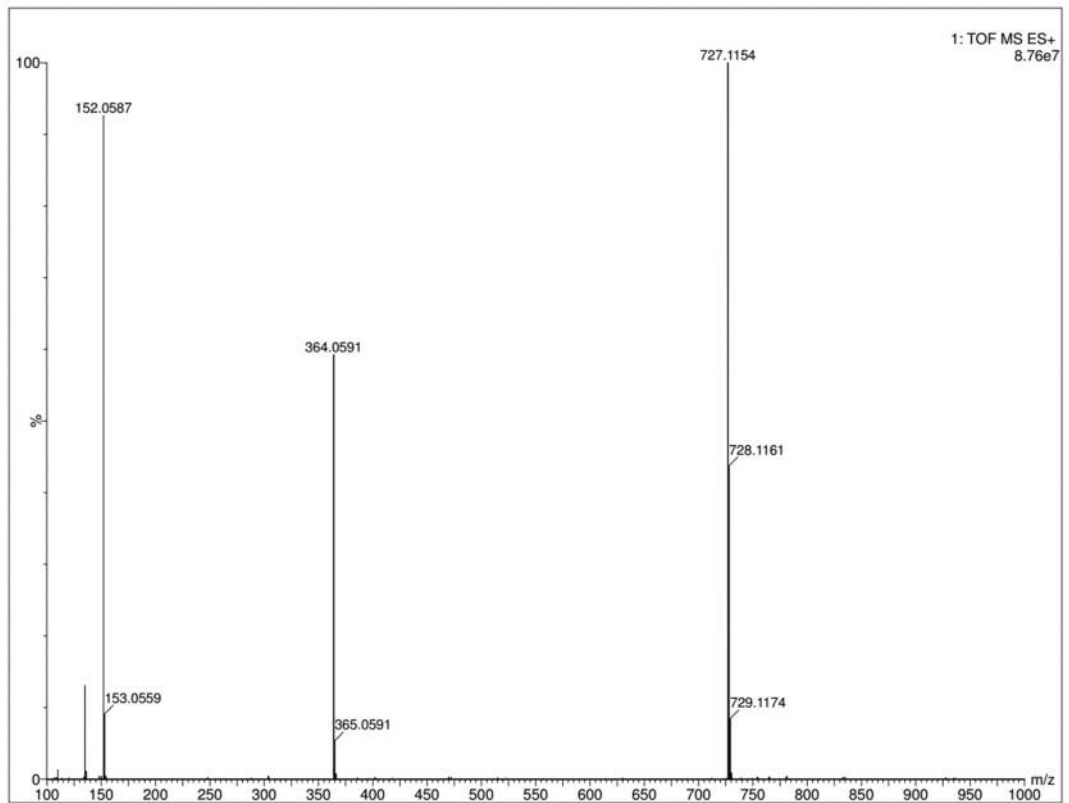


Figure A.1. Positive TOF HRMS of natural abundance GMP.

Appendices

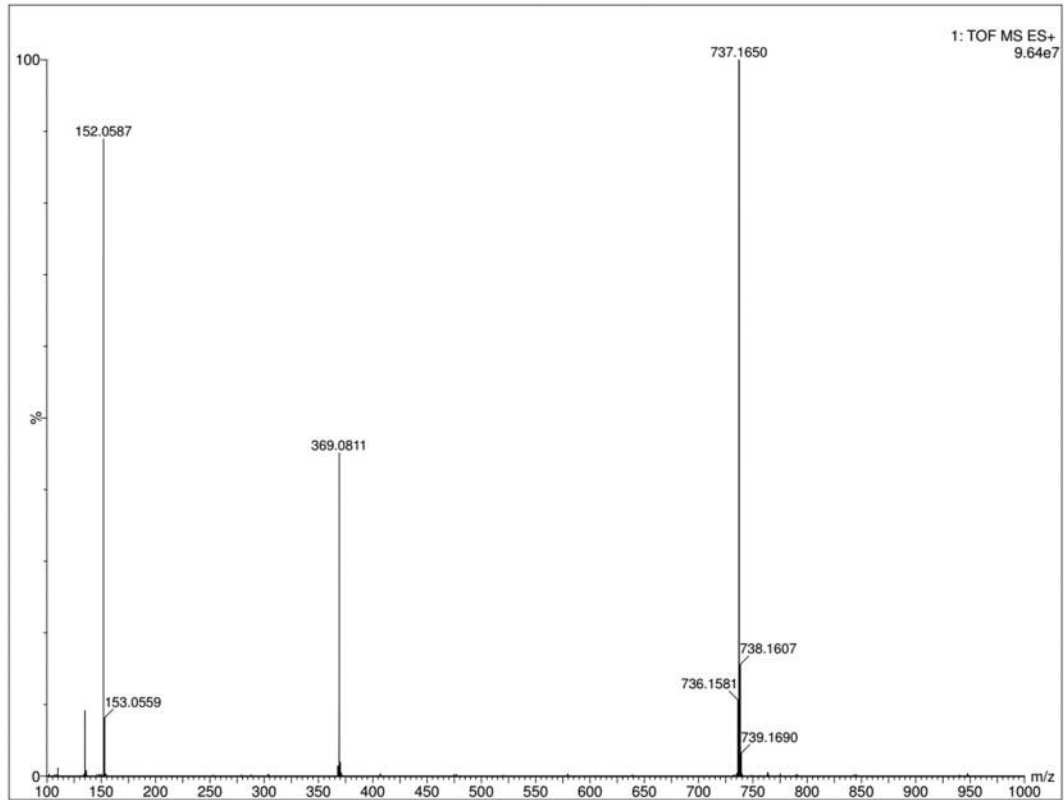


Figure A.2. Positive TOF HRMS of [1',2',3',4',5'-¹³C₅]-GMP.

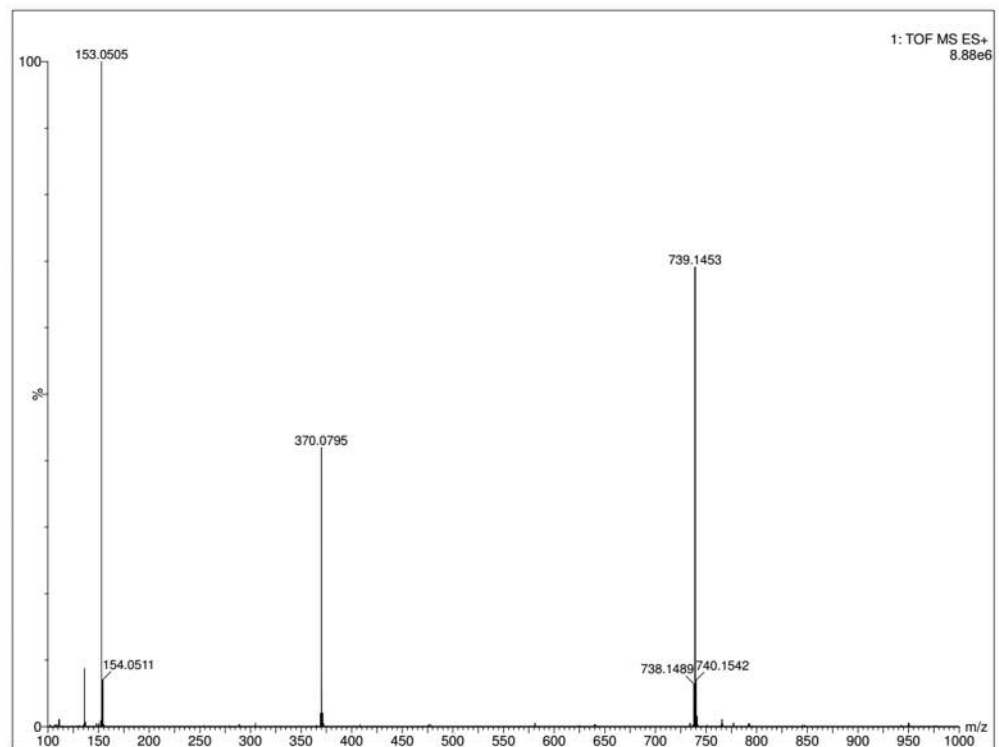


Figure A.3. Positive TOF HRMS of [1',2',3',4',5',8-¹³C₆,7-¹⁵N]-GMP.

Appendices

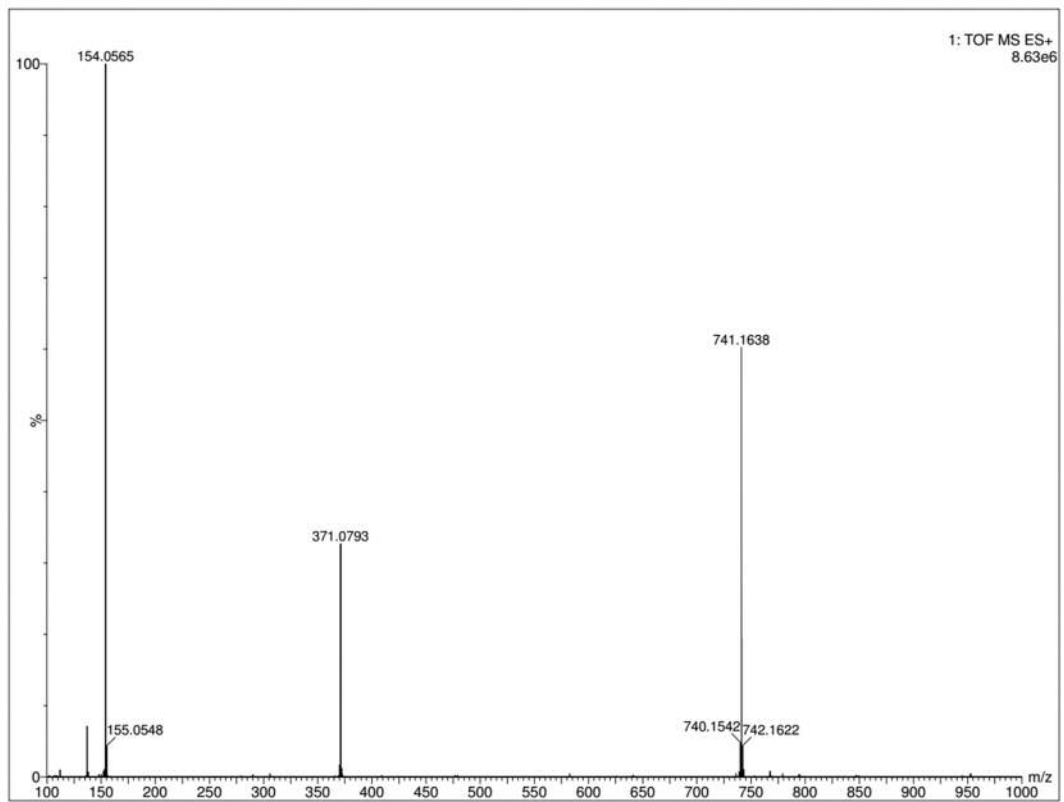


Figure A.4. Positive TOF HRMS of [1',2',3',4',5'-¹³C₅,7-¹⁵N]-GMP

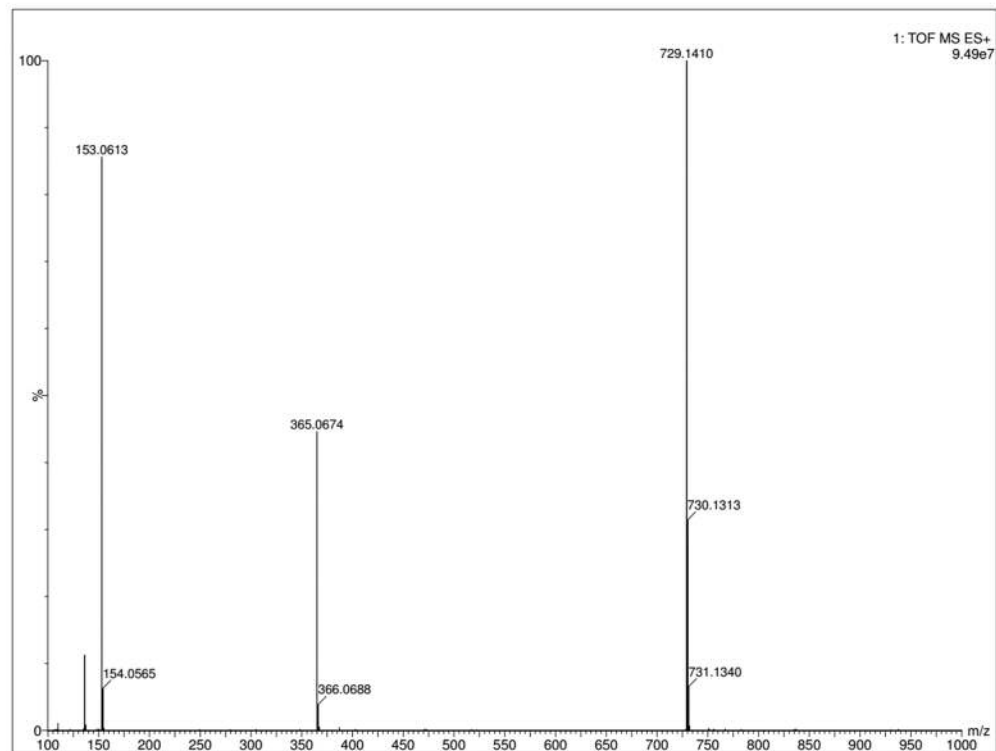


Figure A.5. Positive TOF HRMS of [2-¹³C]-GMP.

8.1.2. HRMS of isotopically labelled dihydrofolates

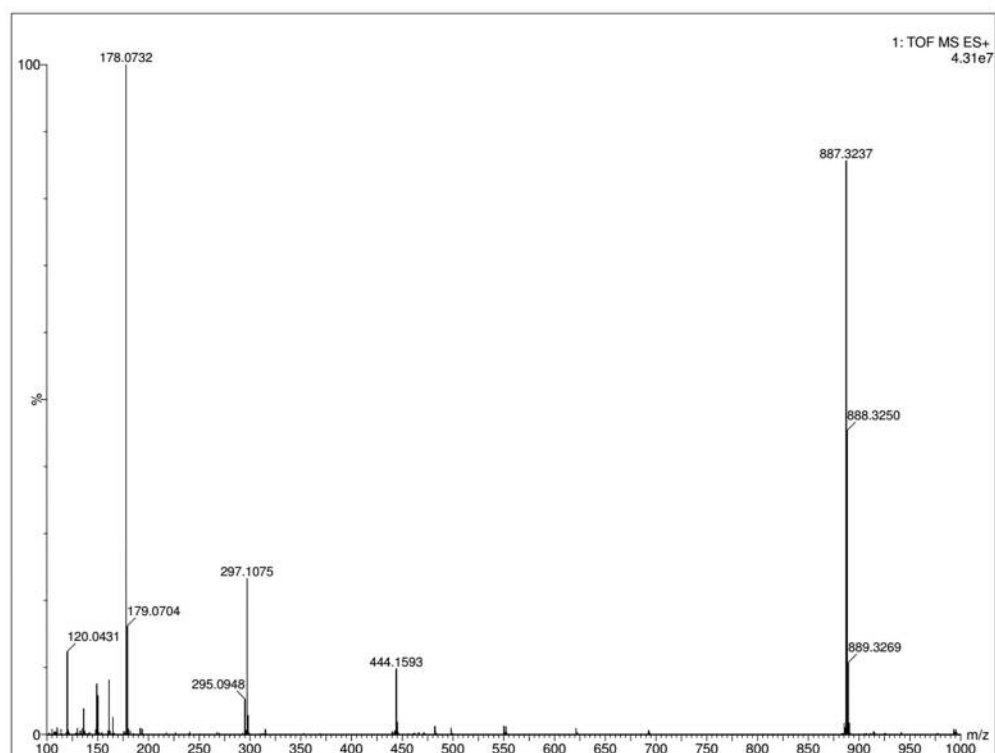


Figure A.6. Positive TOF HRMS of natural abundance H₂F.

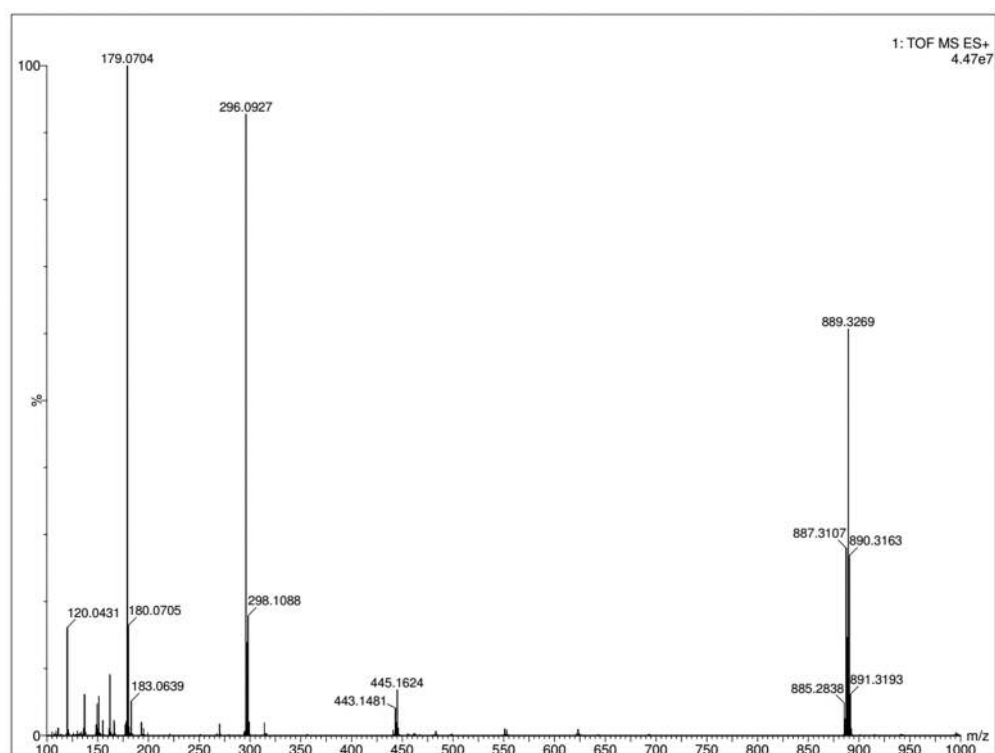


Figure A.7. Positive TOF HRMS of [5-¹⁵N]-H₂F.

Appendices

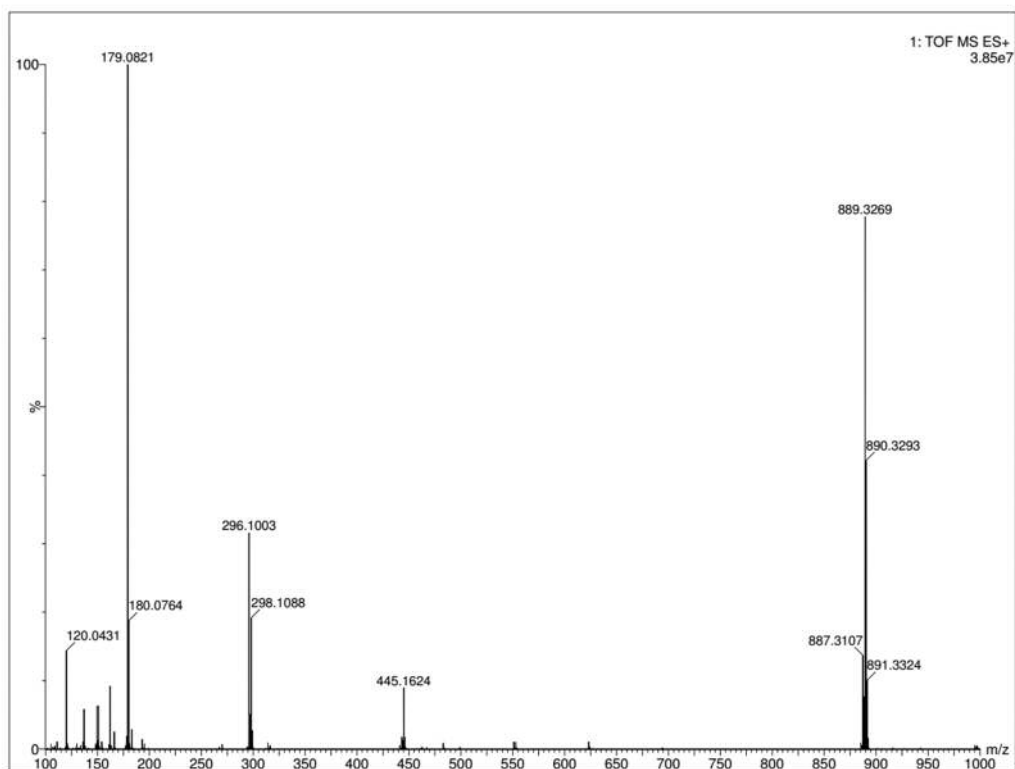


Figure A.8. Positive TOF HRMS of [6-¹³C]-H₂F.

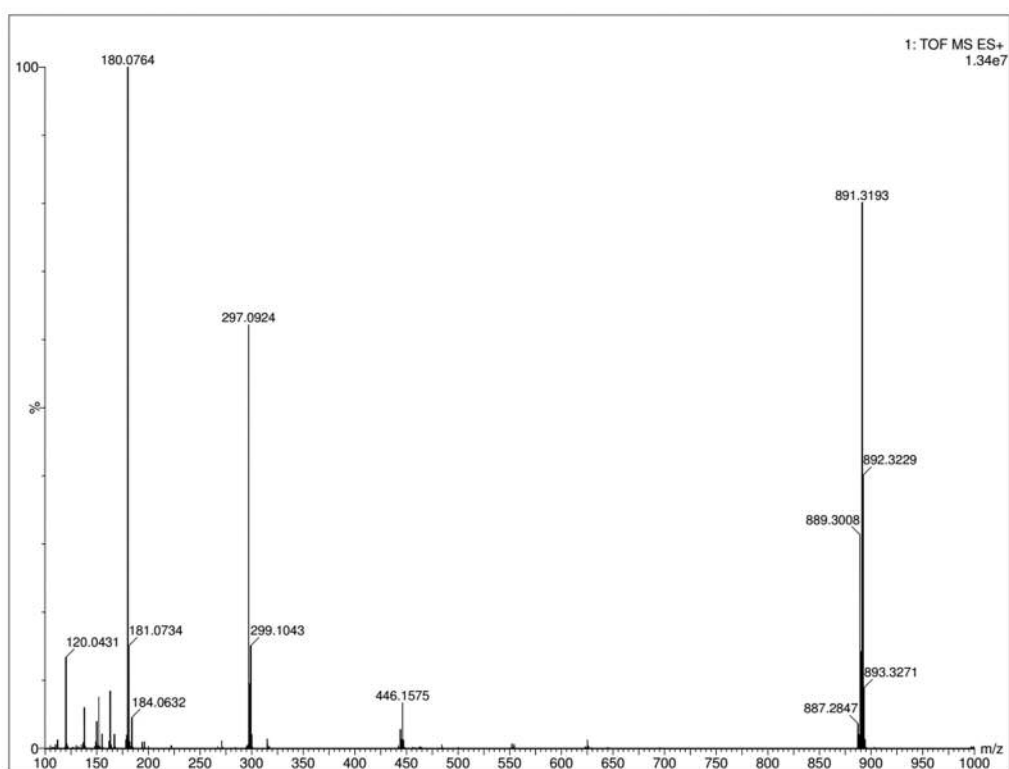


Figure A.9. Positive TOF HRMS of [6-¹³C,5-¹⁵N]-H₂F.

Appendices

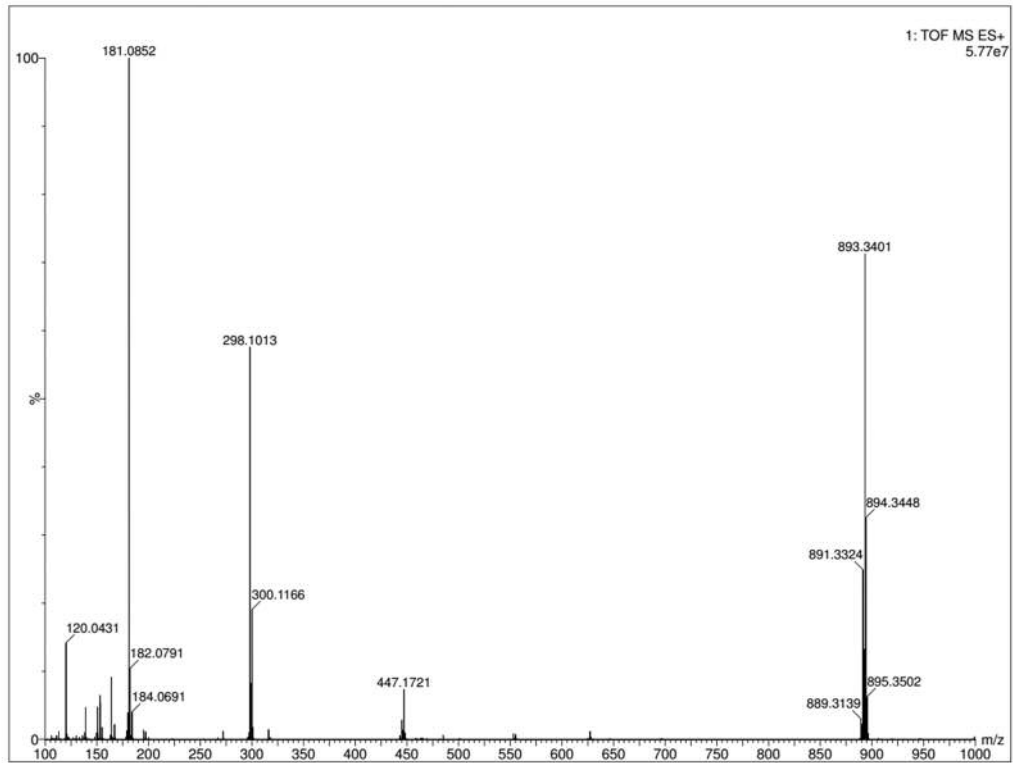


Figure A.10. Positive TOF HRMS of [6,7,9-¹³C₃]-H₂F

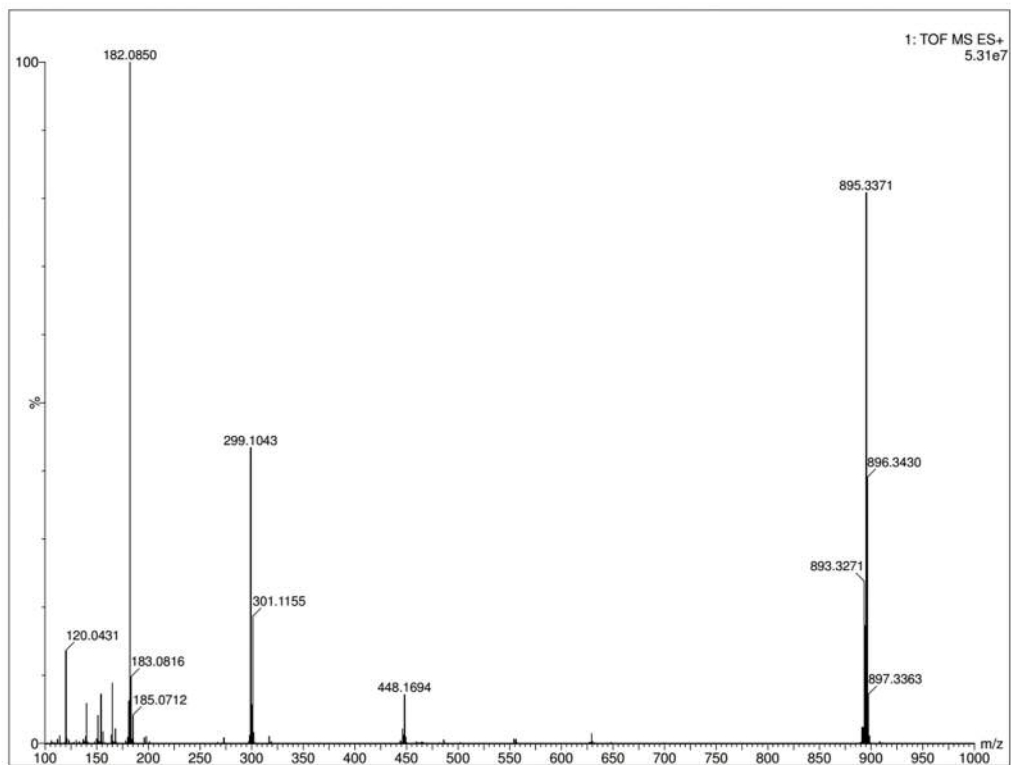


Figure A.11. Positive TOF HRMS of [6,7,9-¹³C₃,5-¹⁵N]-H₂F.

8.2. Appendix 2. Pre-steady state kinetic data

Table A.1. Pre-steady-state kinetic data for determining ^{15}N -KIE on EcDHFR using [5- ^{15}N]- H_2F .

$T(^{\circ}\text{C})$	$k_{\text{H}}^{14\text{N}} (\text{s}^{-1})$	$k_{\text{H}}^{15\text{N}} (\text{s}^{-1})$
5	83.229 ± 1.045	83.560 ± 1.089
10	107.963 ± 1.250	108.400 ± 1.461
15	144.056 ± 0.793	144.200 ± 0.059
20	182.443 ± 1.595	182.500 ± 0.630
25	228.902 ± 1.297	230.300 ± 1.634
30	281.197 ± 3.883	281.200 ± 4.868
35	338.237 ± 3.005	338.000 ± 4.395

Table A.2. Pre-steady-state kinetic data for determining ^{13}C -KIE on EcDHFR using [6- ^{13}C]- H_2F .

$T(^{\circ}\text{C})$	$k_{\text{H}}^{12\text{C}} (\text{s}^{-1})$	$k_{\text{H}}^{13\text{C}} (\text{s}^{-1})$
5	93.397 ± 0.675	91.717 ± 0.547
10	120.504 ± 0.916	118.407 ± 0.900
15	157.535 ± 0.568	155.171 ± 0.822
20	195.551 ± 1.346	191.540 ± 2.143
25	246.174 ± 0.894	239.506 ± 1.501
30	286.3681 ± 1.587	279.970 ± 2.968
35	357.173 ± 0.965	347.012 ± 3.773

Table A.3. Pre-steady-state kinetic data for determining ^{15}N , ^{13}C -KIE on EcDHFR using $[5\text{-}^{15}\text{N}][6\text{-}^{13}\text{C}]\text{-H}_2\text{F}$.

T(°C)	$k_{\text{H}}^{14\text{N},12\text{C}}$ (s⁻¹)	$k_{\text{H}}^{15\text{N},13\text{C}}$ (s⁻¹)
5	94.208 ± 0.724	92.336 ± 0.685
10	121.883 ± 1.000	119.133 ± 0.680
15	157.775 ± 1.032	155.535 ± 1.162
20	198.094 ± 1.152	195.862 ± 0.720
25	241.495 ± 1.111	237.226 ± 0.806
30	282.080 ± 0.760	279.100 ± 2.41
35	351.533 ± 3.340	339.801 ± 4.247

8.3 Appendix 3. Additional SDS-PAGE analyses

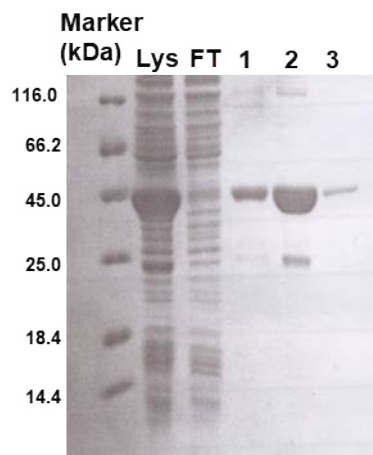


Figure A.12. SDS-PAGE of purified PRS (MW = 34,2 kDa; fractions 1-3) compared to cell lysate (Lys) before and after (FT) purification.

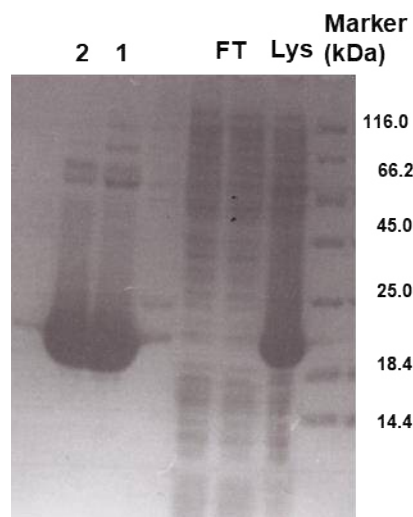


Figure A.13. SDS-PAGE of purified XGPRT (MW = 16,8 kDa; fractions 1-2) compared to cell lysate (Lys) before and after (FT) purification.

Appendices

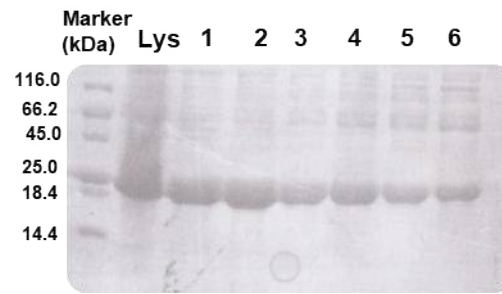


Figure A.14. SDS-PAGE of purified GTP-CH-I (MW = 24,8 kDa; fractions 1-6) compared to cell lysate (Lys) after size exclusion chromatography.

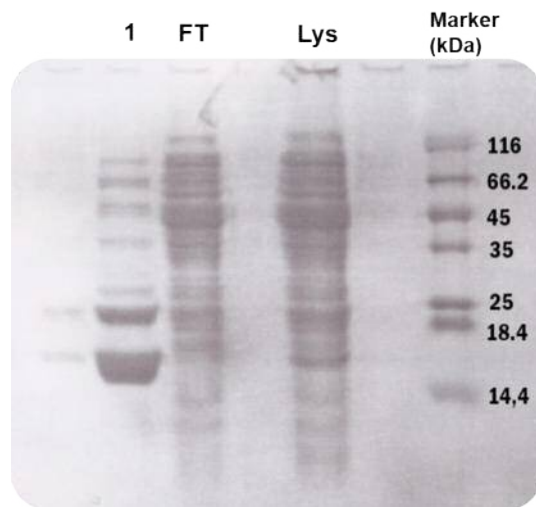


Figure A.15. SDS-PAGE of purified DHNA (MW = 13,6 kDa; fractions 1) compared to cell lysate (Lys) before and after (FT) purification.

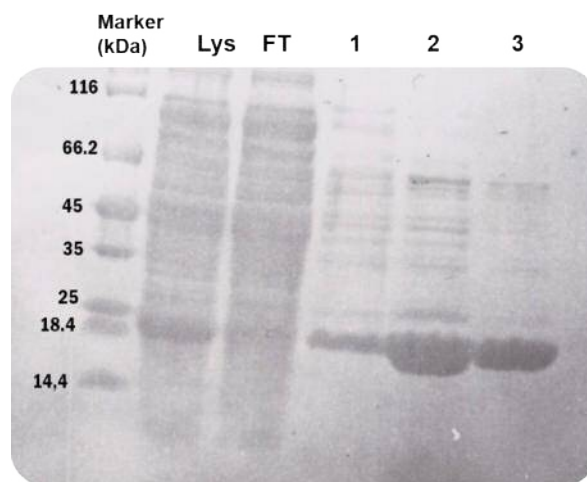


Figure A.16. SDS-PAGE of purified HPPK (MW = 18,1 kDa; fractions 1-3) compared to cell lysate (Lys) before and after (FT) purification.

Appendices

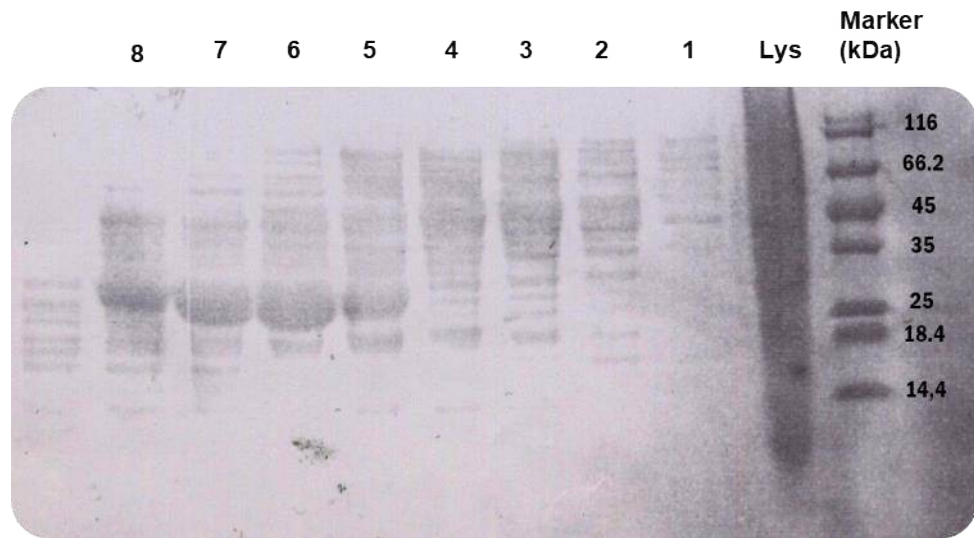
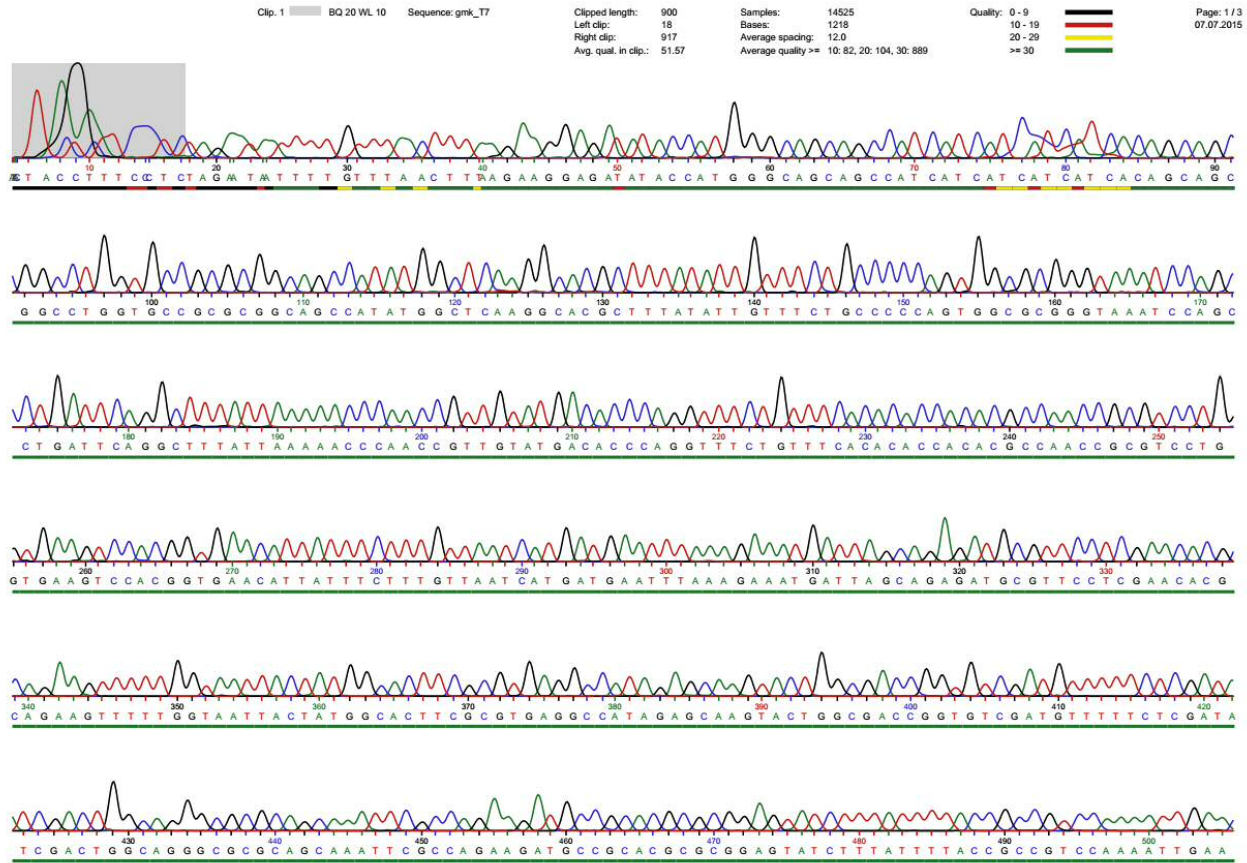


Figure A.17. SDS-PAGE of purified DHPS (MW = 30,6 kDa; fractions 5-8) compared to cell lysate (Lys) after size exclusion chromatography.

Appendices



Appendices

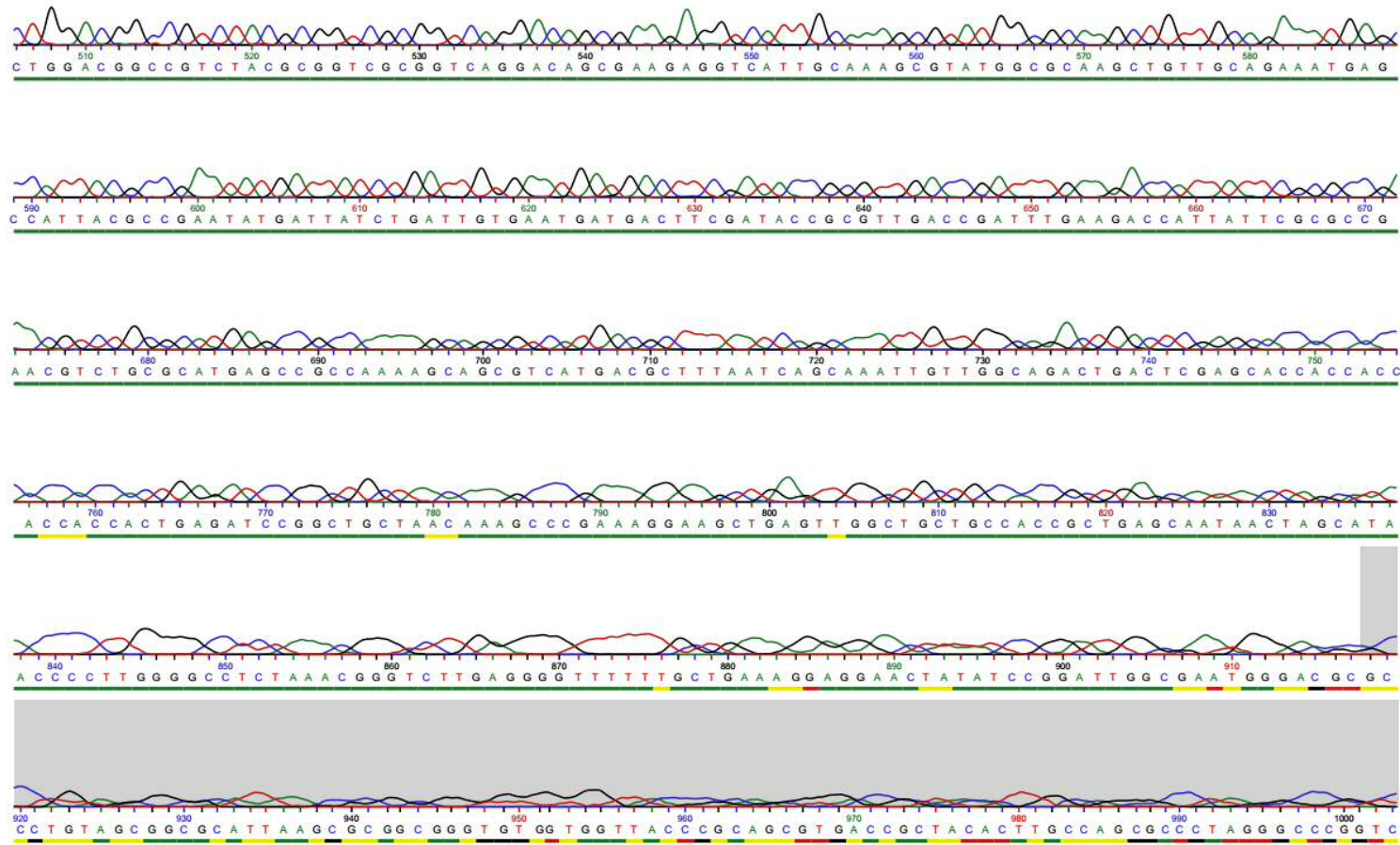
Clip. 1 BQ 20 WL 10 Sequence: gmk_T7

Clipped length: 900
Left clip: 18
Right clip: 917
Avg. qual. in clip.: 51.57

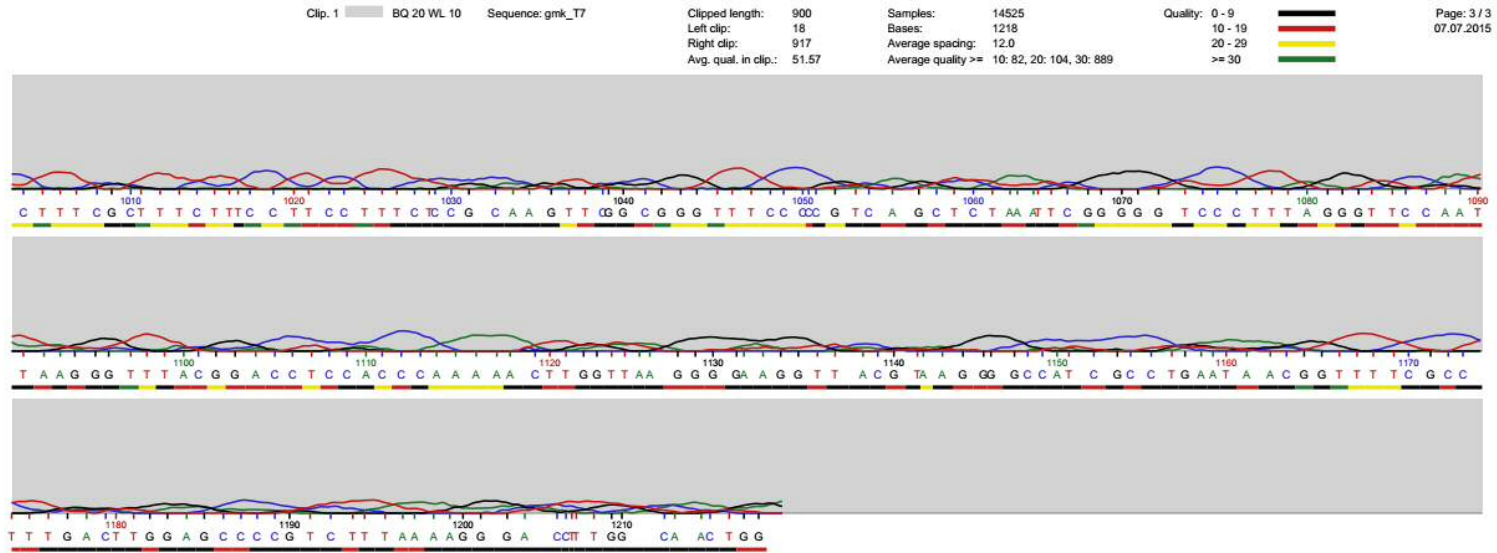
Samples: 14525
Bases: 1218
Average spacing: 12.0
Average quality >= 10: 82, 20: 104, 30: 889

Quality: 0 - 9
10 - 19
20 - 29
>= 30

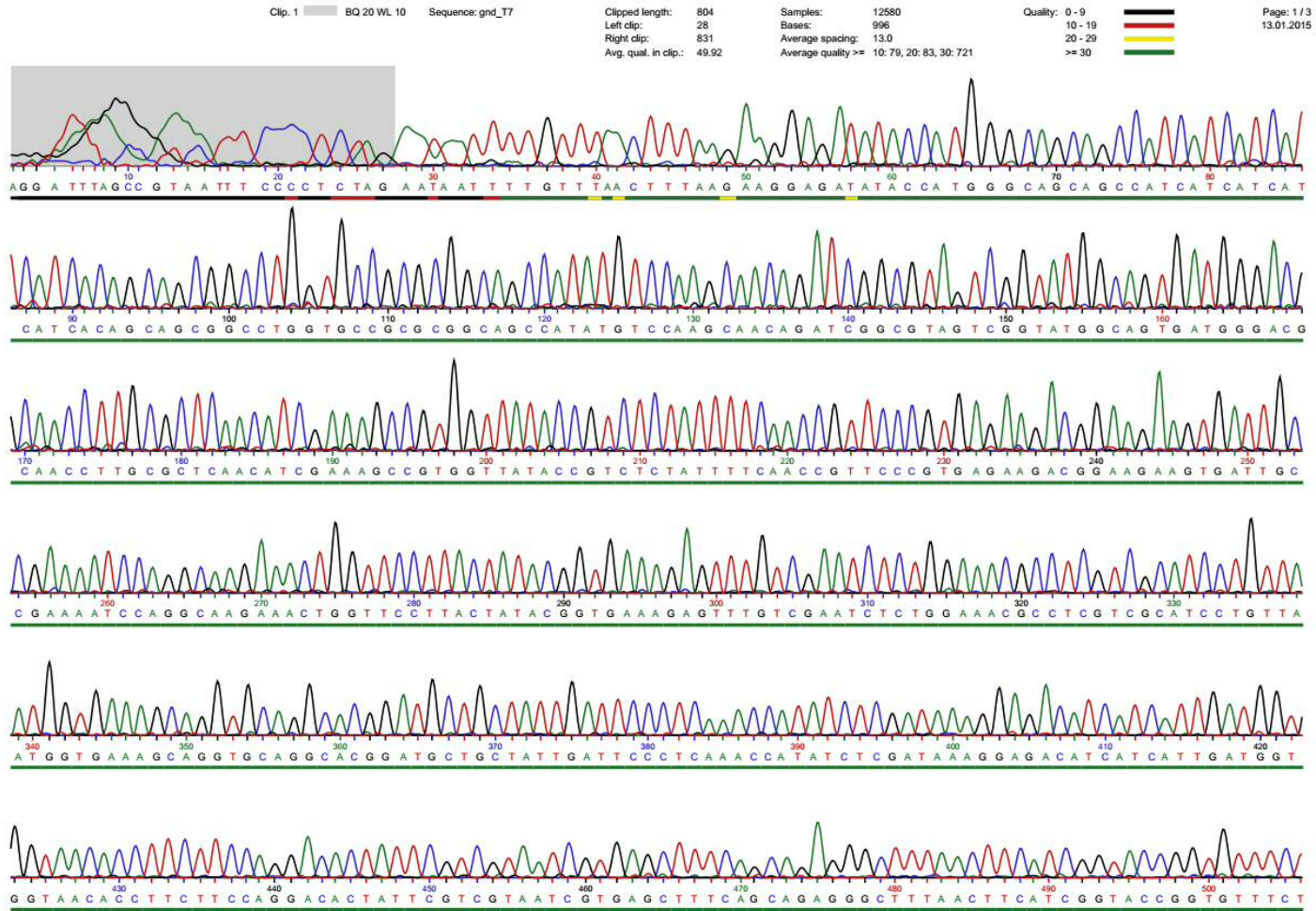
Page: 2 / 3
07.07.2015



Appendices



Appendices



Appendices

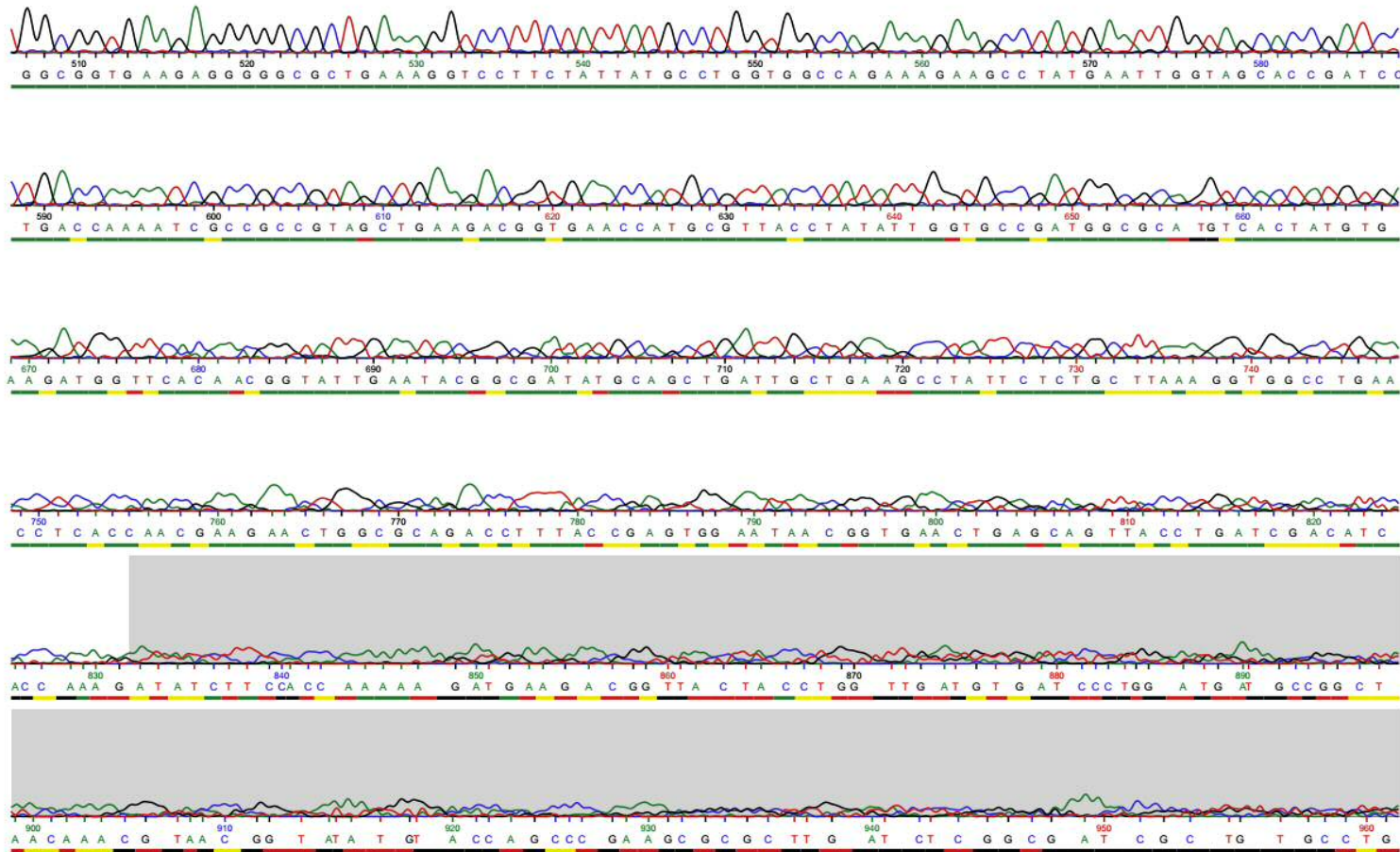
Clip. 1 BQ 20 WL 10 Sequence: gnd_T7

Clipped length: 804
Left clip: 28
Right clip: 831
Avg. qual. in clip.: 49.92

Samples: 12580
Bases: 996
Average spacing: 13.0
Average quality >= 10: 79, 20: 83, 30: 721

Quality: 0 - 9
10 - 19
20 - 29
>= 30

Page: 2 / 3
13.01.2015



Appendices

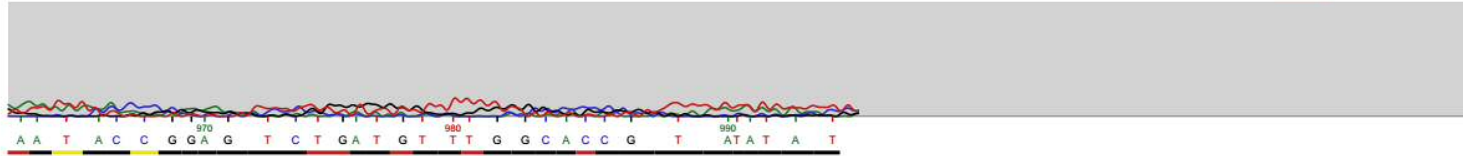
Clip. 1 BQ 20 WL 10 Sequence: gnd_T7

Clipped length: 804
Left clip: 28
Right clip: 831
Avg. qual. in clip.: 49.92

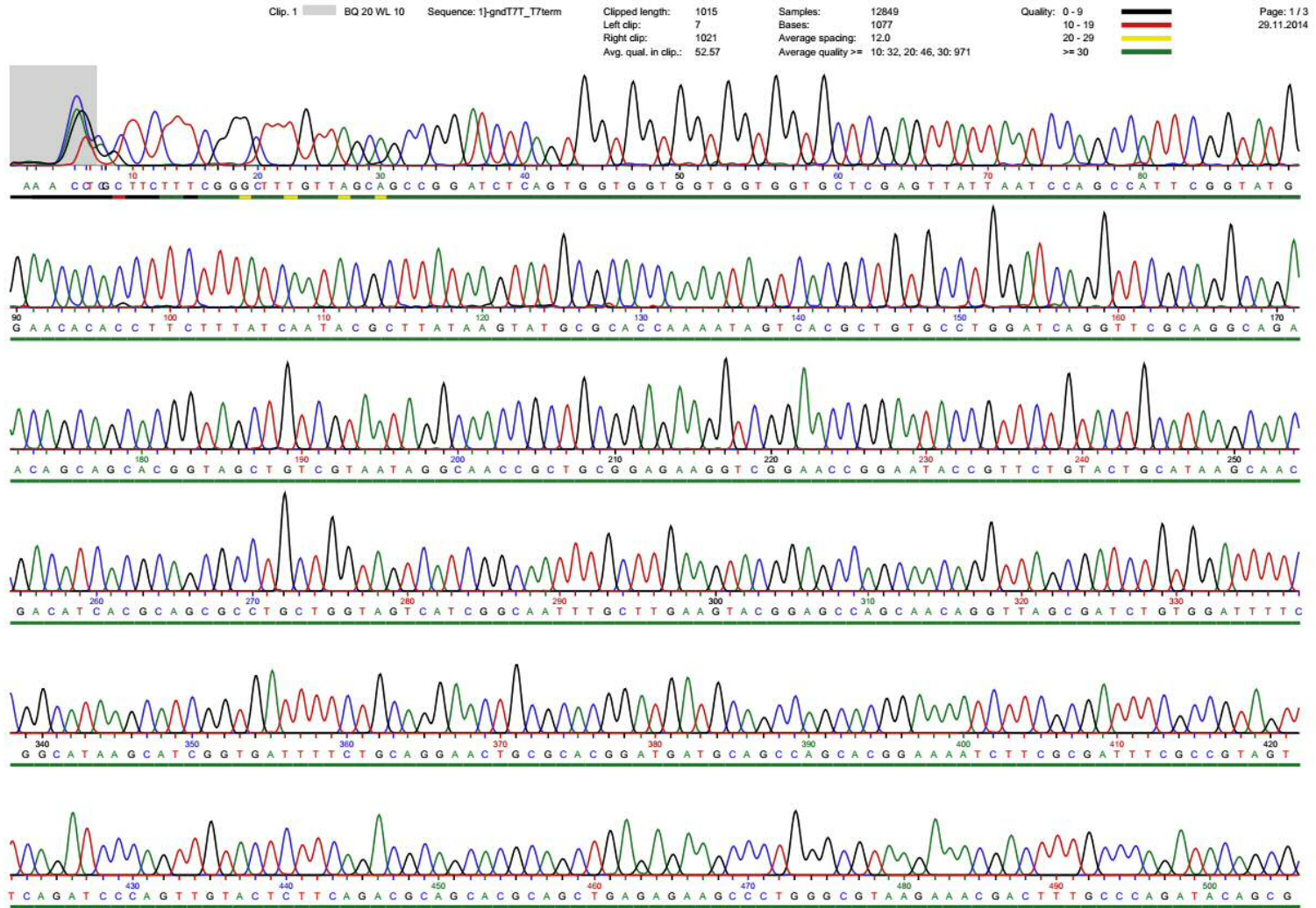
Samples: 12580
Bases: 996
Average spacing: 13.0
Average quality >= 10: 79, 20: 83, 30: 721

Quality: 0 - 9
10 - 19
20 - 29
>= 30

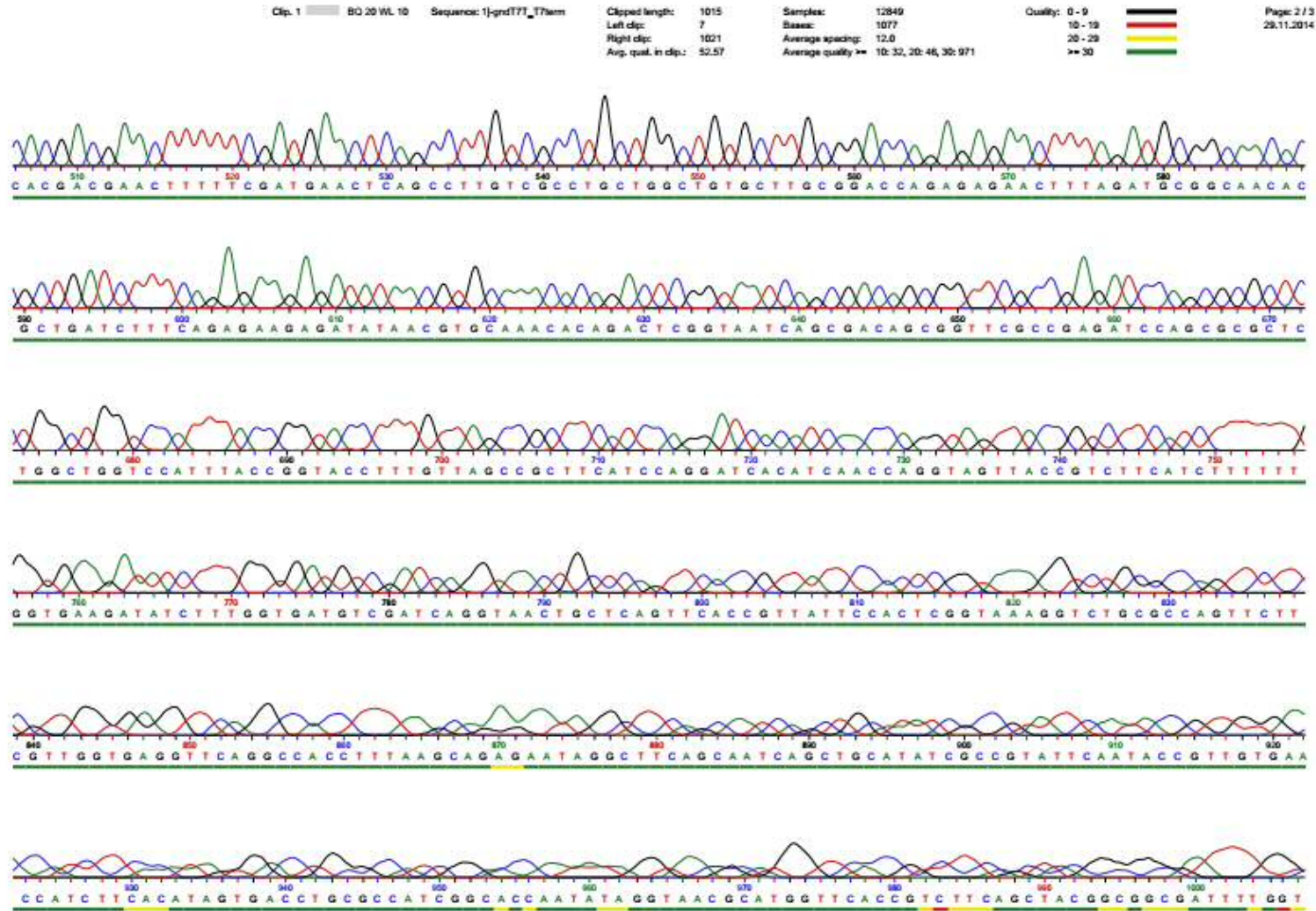
Page: 3 / 3
13.01.2015



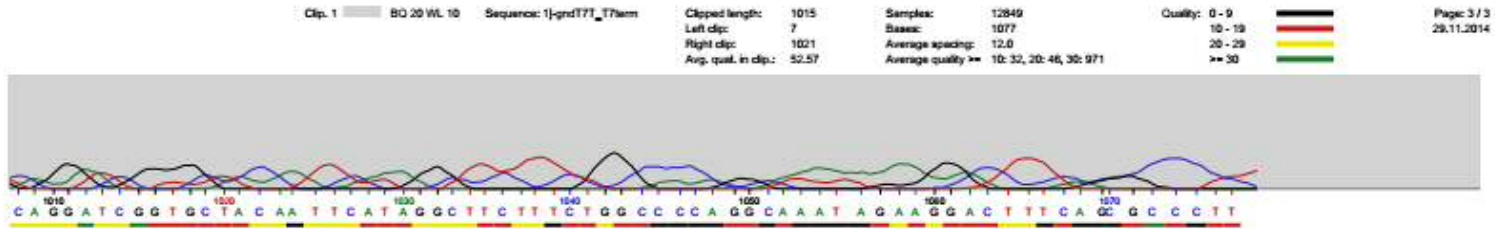
Appendices



Appendices



Appendices



8.4.3 Sequencing of *grxB*

>grxB_T7 -- 33..766 of sequence

```
TTTTGTTTAACTTTAAGAAGGAGGATATACCATGGGCAGCAGCCATCATCATCATCACAGCAGCGGCCTGGTGCCGCGCGGC  
AGCCATATGAAGCTATACATTTACGATCACTGCCCTTACTGCCTCAAAGCCC GCATGATTTTCGGCCTGAAAAATATCCCCGTCGA  
ATTACATGTTCTGCTCAACGACGACGCAGAAACACCCACCCGGATGGTTCGGTCAAAAACAGGTTCCATTCTGCAAAAAGATGAC  
AGCCGCTATATGCCAGAAAGCATGGACATCGTTCACTATGTCGATAAACTCGACGGCAAACCGTTACTGACCGGCAAACGTTCCC  
CTGCCATTGAAGAGTGGCTGCGCAAGGTCAATGGCTACGCCAACAACTGCTGTTGCCGCGTTTTTGCCAAATCGGCATTTGATGA  
GTTTTCTACTCCCGCCGCGCGCAAATATTTTCGTGACAAGAAAGAGGCCAGCGCGGGTAATTTTGCCGACCTGCTGGCCCACTCT  
GACGGTCTGATTAAGAATATCAGCGATGATTTACGTGCGCTGGACAACTGATCGTCAAACCGAACGCCGTGAATGGCGAACTTT  
CGGAAGATGATATTCAGCTATTCCTGCTACTGCGTAATCTGACGCTGGTAGCCGGAATTA ACTGGCCAAGCCGCGTTGCTGATTA  
CCGCGATAATATGGCGAAAACAGACACAAATCAAATTTGTTATCATCAATGGC
```


Appendices

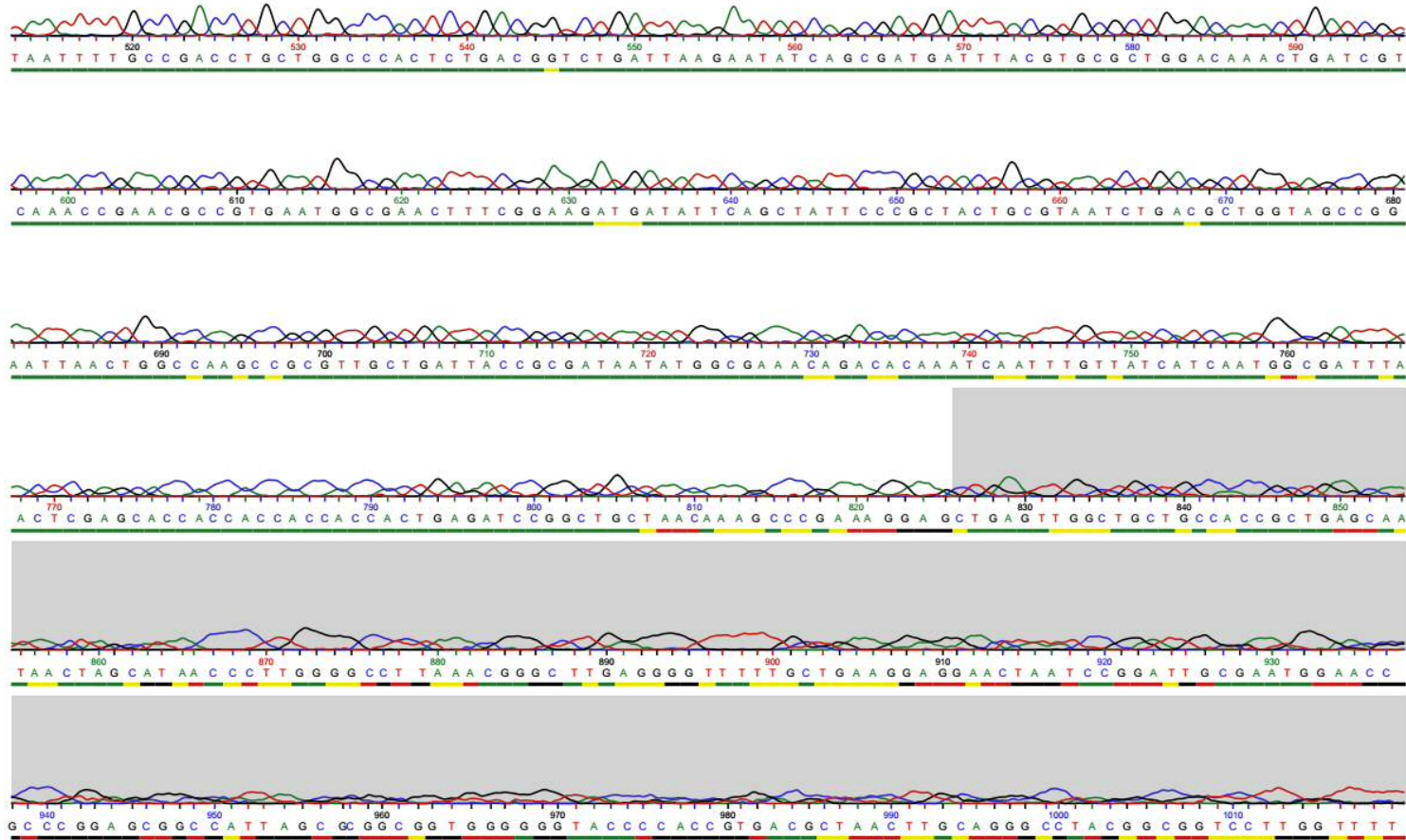
Clip. 1 BQ 20 WL 10 Sequence: gnrB_T7

Clipped length: 743
Left clip: 83
Right clip: 825
Avg. qual. in clip.: 50.1

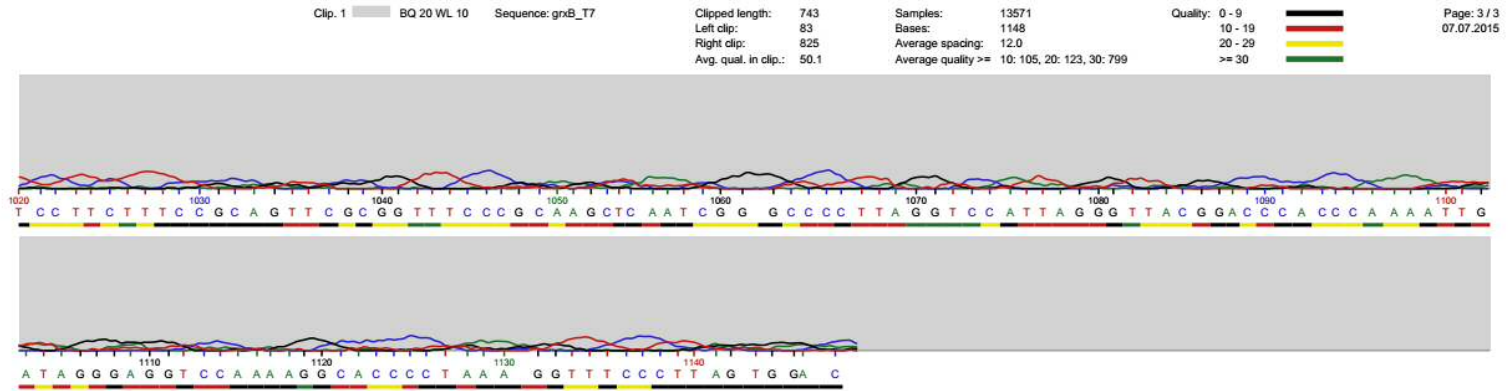
Samples: 13571
Bases: 1148
Average spacing: 12.0
Average quality >=: 10: 105, 20: 123, 30: 799

Quality: 0 - 9
10 - 19
20 - 29
>= 30

Page: 2 / 3
07.07.2015



Appendices

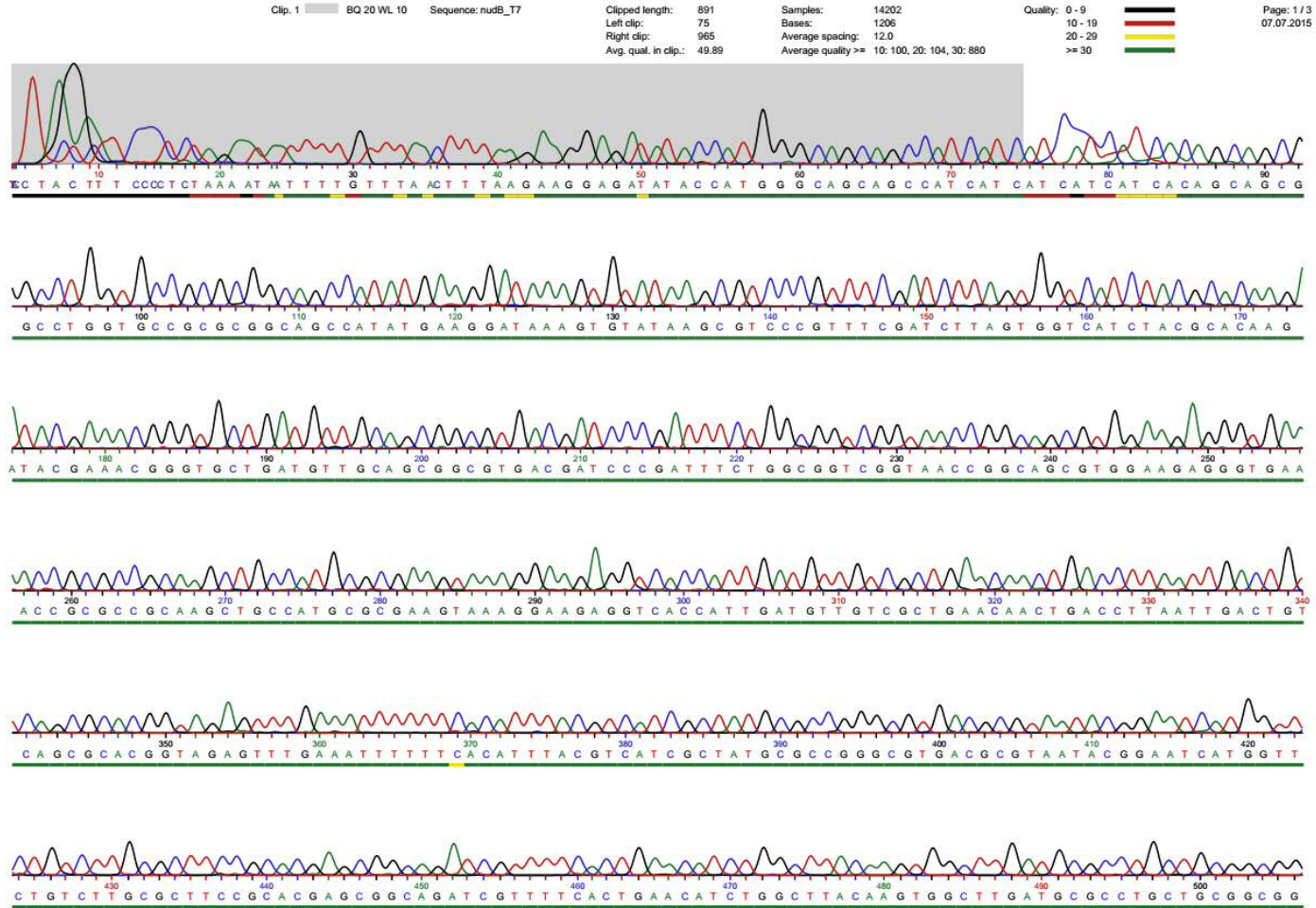


8.4.4 Sequencing of *nudB*

>nudB[3]_T7

AAATAATTTTGTTTAACTTTAAGAAGGAGATATACCATGGGCAGCAGCCATCATCATCATCACAGCAGCGGCCTGGTGCCGCG
CGGCAGCCATATGAAGGATAAAGTGTATAAGCGTCCCGTTTCGATCTTAGTGGTCATCTACGCACAAGATACGAAACGGGTGCTG
ATGTTGCAGCGGCGTGACGATCCCGATTTCTGGCGGTCGGTAACCGGCAGCGTGGAAGAGGGTGAAACCGCGCCGCAAGCTGC
CATGCGCGAAGTAAAGGAAGAGGTCACCATTGATGTTGTCGCTGAACAACCTGACCTTAATTGACTGTCAGCGCACGGTAGAGTTT
GAAATTTTTTTCACATTTACGTCATCGCTATGCGCCGGGCGTGACGCGTAATACGGAATCATGGTTCTGTCTTGCGCTTCCGCACGA
GCGGCAGATCGTTTTTCACTGAACATCTGGCTTACAAGTGGCTTGATGCGCCTGCTGCGGCGGCGCTCACTAAGTCCTGGAGCAA
CCGGCAGGCGATTGAACAGTTTGTAAATTAACGCTGCCTGACTCGAGCACCACCACCACCACCTGAGATCCGGCTGCTAACAAA
GCCCGAAAGGAAGCTGAGTTGGCTGCTGCCACCGCTGAGCAATAACTAGCATAACCCCTTGGGGCCTCTAAACGGGTCTTGAGG
GGTTTTTTGCTGAAAGGAGGAACTATATCCGGATTGGCGAATGGGACGCGCCCTGTAGCGGCGCATTAAACCGCGGC

Appendices



Appendices

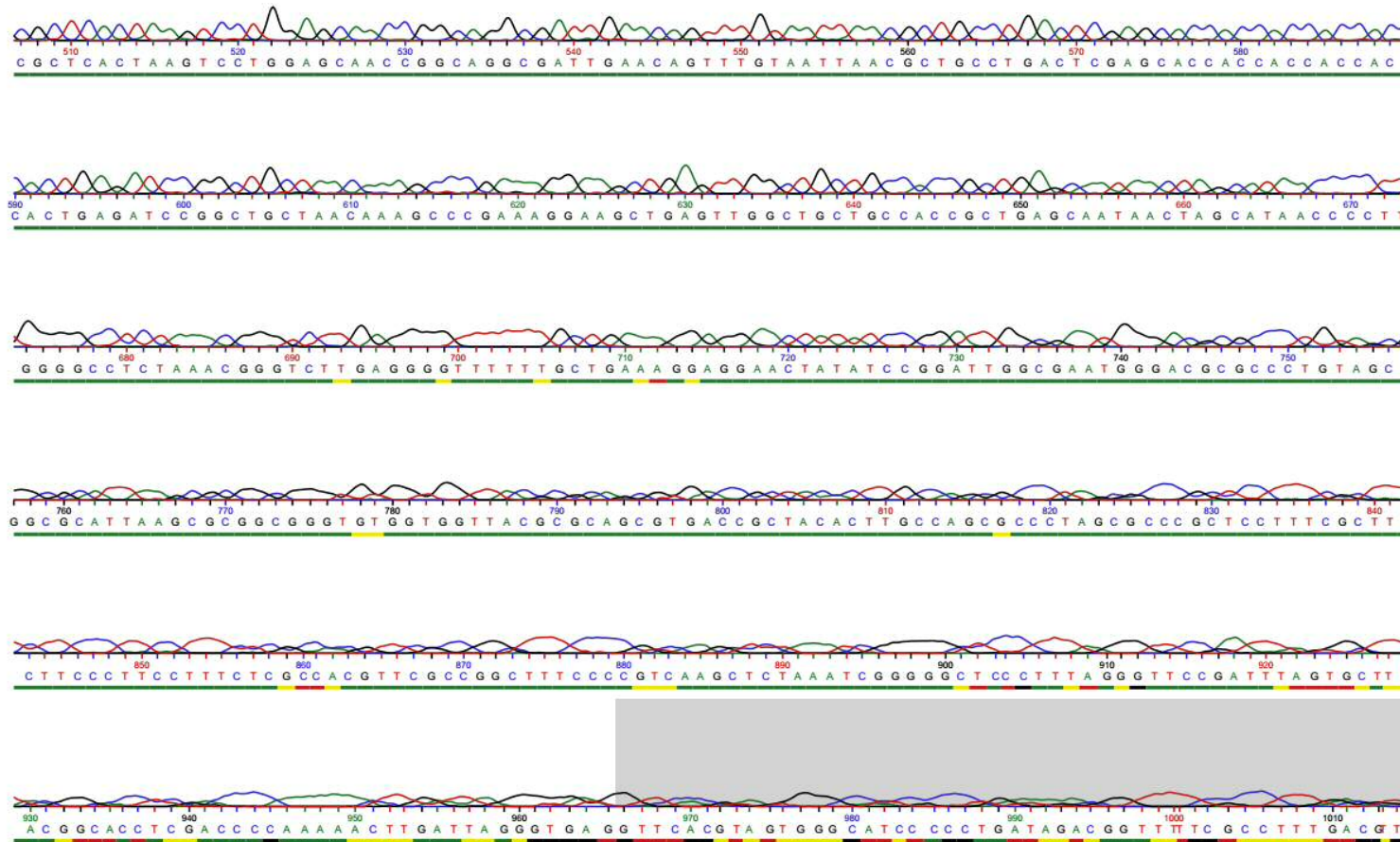
Clip. 1 BQ 20 WL 10 Sequence: nudB_T7

Clipped length: 891
Left clip: 75
Right clip: 965
Avg. qual. in clip.: 49.89

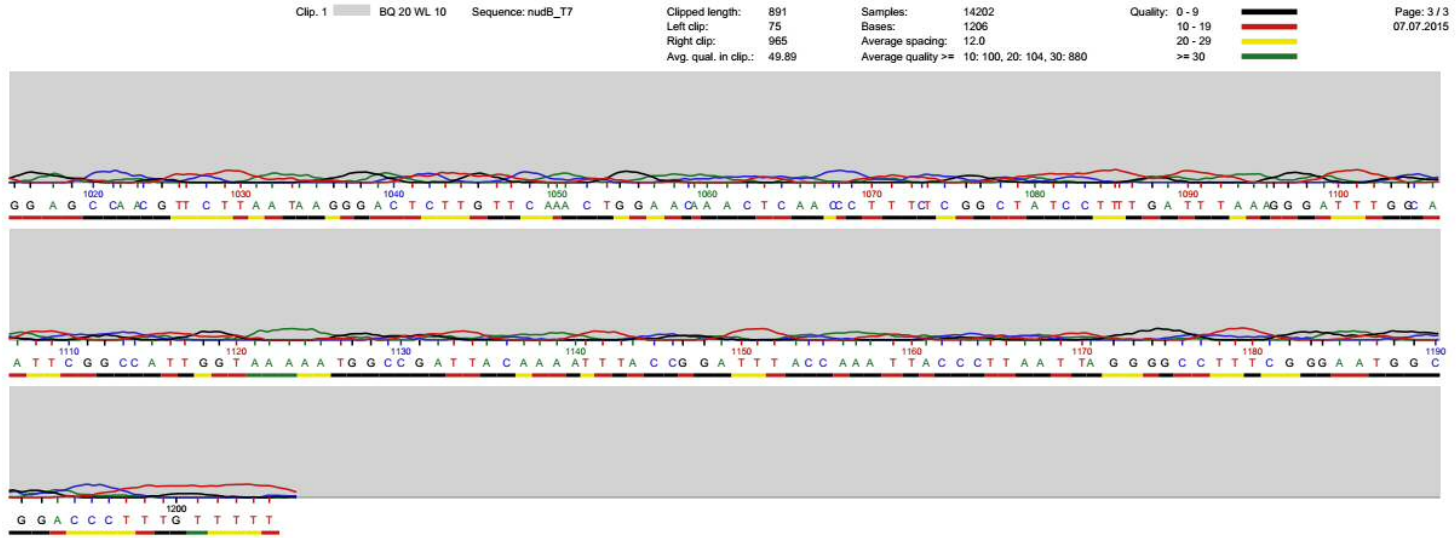
Samples: 14202
Bases: 1206
Average spacing: 12.0
Average quality >= 10: 100, 20: 104, 30: 880

Quality: 0 - 9
10 - 19
20 - 29
>= 30

Page: 2 / 3
07.07.2015



Appendices



8.5 Appendix 5. Published articles

A Versatile Disulfide-Driven Recycling System for NADP⁺ with High Cofactor Turnover Number

Antonio Angelastro, William M. Dawson,[†] Louis Y. P. Luk, and Rudolf K. Allemann^{*†}

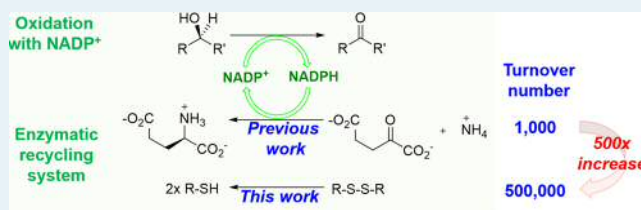
School of Chemistry and Cardiff Catalysis Institute, School of Chemistry, Cardiff University, Park Place, Cardiff CF10 3AT, United Kingdom

Supporting Information

ABSTRACT: NADP⁺-dependent enzymes are important in many biocatalytic processes to generate high-value chemicals for the pharmaceutical and food industry; hence, a cost-effective, efficient, and environmentally friendly recycling system for the relatively expensive and only marginally stable enzyme cofactor NADP⁺ offers significant benefits. NADP⁺ regeneration schemes have previously been described, but their application is severely limited by the low total turnover

numbers (TTN) for the cofactor. Here, we report a glutathione-based recycling system that combines glutaredoxin from *E. coli* (EcGRX) and the glutathione reductase from *S. cerevisiae* (ScGR) for NADP⁺ regeneration. This system employs inexpensive latent organic disulfides such as oxidized cysteine or 2-hydroxyethyl disulfide (HED) as oxidizing agents and allows NADP⁺ recycling under both aerobic and anaerobic conditions with a TTN in excess of 5×10^5 , indicating that each regeneration cycle is 99.9998% selective toward forming the cofactor. Accordingly, for each 1 mol of product generated, less than \$0.05 of cofactor is needed. Finally, the EcGRX/ScGR pair is compatible with eight enzymes in the guanosine monophosphate (GMP) biosynthetic pathway, giving the corresponding isotopically labeled nucleotide in high yield. The glutathione-based NADP⁺ recycling system has potential for biocatalytic applications in academic and industrial settings.

KEYWORDS: biocatalysis, biosynthesis, cofactor/coenzyme recycling, enzyme oxidation, biotechnology



INTRODUCTION

Refining the performance of enzyme-catalyzed redox processes remains at the frontier of biocatalysis research^{1,2} and is of central importance to the development of sustainable chemical production processes.³ Oxidoreductases are a large group of enzymes,⁴ which due to their good catalytic efficiency, general applicability, and nontoxic nature have been used widely in industrial processes, ranging from kilogram-scale chiral resolutions⁵ to intricate syntheses of pharmaceuticals.^{6,7} Since oxidoreductases almost exclusively require the use of structurally complex and expensive cofactors such as nicotinamide adenine dinucleotide phosphate NADP(H), cost-efficient recycling schemes have been developed. Currently, there are a number of in situ enzymatic systems that efficiently recycle NADPH, including engineered glucose/glucose 6-phosphate dehydrogenase,^{8,9} formate dehydrogenase,^{10,11} and phosphite dehydrogenase.¹² These recycling schemes have been extensively used in NADPH-dependent enzymatic reductions, such as the production of the HMG-CoA reductase inhibitor atorvastatin.⁶ On the other hand, the current options for the regeneration of the corresponding oxidized cofactor NADP⁺ are limited,¹³ even though enzymatic oxidation processes play an important role in contemporary synthetic chemistry and should be fully integrated into chemical manufacturing.^{14–23} Hence, there is a pressing need for the design of a flexible, noninterfering NADP⁺ recycling system.^{24–27}

The industrial relevance of any cofactor-regenerating scheme is primarily assessed by its total turnover number (TTN), which is defined as the total number of moles of product formed per mole of cofactor.^{2,28,29} While the minimal TTN required for each specific cofactor depends on its cost and the value of the product yielded from the biocatalytic process, it is generally anticipated that the TTN should fall in the range of 10^4 – 10^6 to be economically viable on an industrial scale.^{2,28,29} This generalization is applicable to the use of NADP⁺; its current cost is ~\$22k per mole (Table S1 in the Supporting Information) and it cannot be used as a stoichiometric reagent for large-scale synthetic reactions. Additionally, in order to be practical, the cofactor-recycling process needs to be specific yet compatible with the designed chemical reactions. Enzymes are often characterized by high chemical selectivity and specificity, and they are biodegradable, so that enzymatic methods to regenerate a cofactor have significant advantages.²⁹ Therefore, it is perhaps surprising that there are only a few published enzymatic NADP⁺ recycling schemes, but all of these have drawbacks that limit their applications. The glutamate dehydrogenase (GDH) system is the most widely used method to regenerate NADP⁺ (Figure 1).^{25,30–32} In this system, a stoichiometric amount of ammonium α -ketoglutarate is

Received: October 26, 2016

Revised: December 3, 2016

Published: December 19, 2016

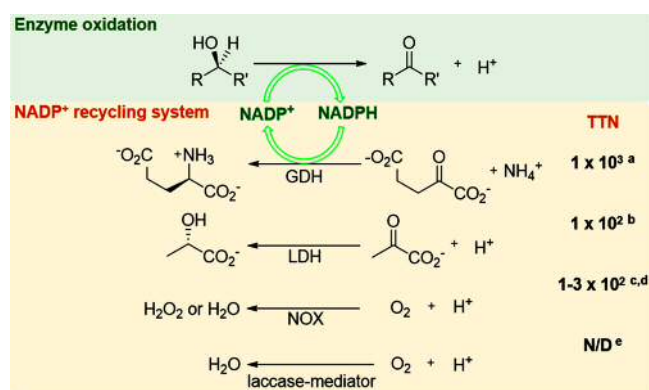


Figure 1. Currently available NADP^+ -recycling systems and their corresponding total turnover number (TTNs): glutamate dehydrogenase (GDH), lactate dehydrogenase (LDH), NADPH oxidase (NOX) and laccase/mediator system. N/D = not determined. For a–e see refs 25 and 34–37, respectively.

converted to glutamate to regenerate the oxidized cofactor. A major drawback of this system is the modest activity of GDH whose maximum steady-state turnover number of approximately 40 s^{-1} restricts the maximal TTN to less than 1×10^3 ,^{25,33} significantly lower than the value required for an economically viable process. Furthermore, α -ketoglutarate contains a highly electrophilic carbonyl group that is prone to cross reaction with other components of the system, resulting in the production of unwanted byproduct(s); in addition, the byproduct glutamate has been shown to complicate product isolation.²⁹ Consequently, other regeneration schemes, including the D-lactate dehydrogenase (LDH),³⁴ NADPH oxidase (NOX),^{35,36} and the laccase/mediator system,³⁷ have been developed. The calculated TTNs of the LDH and NOX systems are rather low, however, and range from 1×10^2 to 3×10^2 ,^{35,36} whereas the laccase/mediator system has not been optimized for NADP^+ and its TTN has not been determined.³⁷ Moreover, both NOX and the laccase/mediator system are oxygen-dependent and hence not suitable for most anaerobic biocatalysts such as cytochrome P450 dependent enzymes. Hence, a recycling system that uses simple, inert, latent oxidizing reagents and is characterized by high TTNs is urgently required.

In nature, NADP^+ can be generated by coupling to enzymatic disulfide bond reduction.³⁸ One major example of this

chemistry is the glutathione (GSH) reductase system, which plays an essential role in maintaining a reducing environment within the cell.³⁹ In plants, mammals, some bacteria, and archaea, this system is composed of a pair of enzymes, glutaredoxin (GRX) and glutathione reductase (GR), and a pair of redox reagents, glutathione (GSH) and its oxidized counterpart GSSG.⁴⁰ GRX contains catalytic cysteine residue(s), which are used to reduce organic disulfide bonds.^{41,42} The resulting oxidized disulfides within the active site of GRX are then recycled by reduced glutathione to regenerate the enzyme in its reducing form (Figure 2A). In turn, to maintain a sufficient pool of glutathione, GSSG is reduced by GR, an enzymatic process that oxidize a stoichiometric amount of NADPH to NADP^+ (Figure 2B).

The glutathione coupling system presents itself as an ideal surrogate for a NADP^+ recycling system. Glutathione and its oxidized counterpart are relatively inert in comparison to oxygen and α -ketoglutarate and are thus more compatible with most biocatalytic processes. Importantly, while GR is directly responsible for generating NADP^+ , GRX is capable of generating GSSG by reducing a wide range of disulfide species from oxidized proteins to small, inexpensive organic molecules such as 2-hydroxyethyl disulfide (HED or oxidized β -mercaptoethanol) and cystine (Figure 2A).^{43,44} Such substrate promiscuity can be exploited in that the oxidizing agent can be carefully chosen to suit a particular transformation and complications in product isolation can be minimized. The reduced thiol byproduct (e.g., β -mercaptoethanol and cysteine) will also protect the substrates and biocatalysts from oxidative damages. This system requires the use of two cooperating enzymes, and it provides clear competitive advantages over what is offered by all of the currently used systems.

We have developed a glutathione-based recycling system that employs the enzymes GR and GRX and is capable of using small, latent organic disulfides as oxidizing reagents to regenerate NADP^+ with a maximal TTN in excess of 5×10^5 , a value noticeably higher than those of the existing NADP^+ recycling system and acceptable at an industrial standard. This system is compatible with various enzymes and can be used to generate important sugar intermediates such as 6-phosphoglucuronate (6-PG), ribulose 5-phosphate (Ru5P), and GMP.

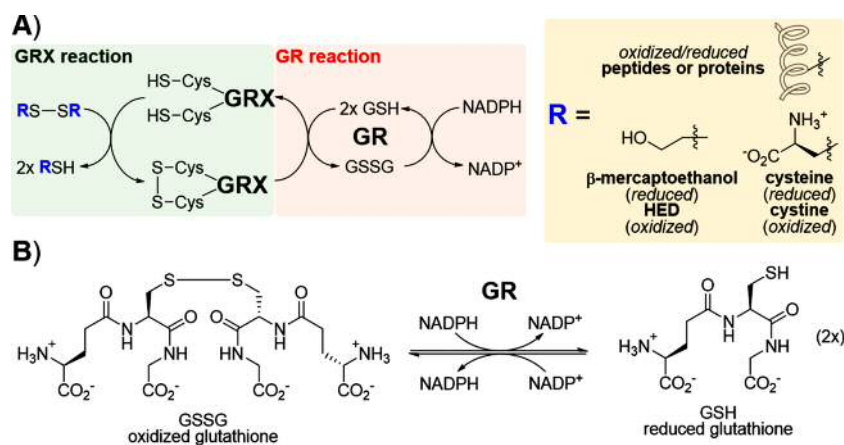


Figure 2. (A) Coupling of the glutaredoxin (GRX) and glutathione reductase (GR) reactions and (B) the disulfide bond reduced in the GR reaction.

RESULTS AND DISCUSSION

Glutathione reductase from *S. cerevisiae* (ScGR) and glutaredoxin 2 from *E. coli* (EcGRX2) were chosen to construct a glutathione recycling system.^{45–48} ScGR is commercially available at a reasonable price with a relatively high turnover number k_{cat} of 240 s⁻¹ at pH 7.0,⁴⁶ while recombinant EcGRX2 can be produced in large quantities by expression in *E. coli* (Table S2 in the Supporting Information),⁴⁷ which yields an enzyme with a high k_{cat} value (~ 550 s⁻¹).⁴⁷ On the basis of their kinetic parameters, the functional pair of EcGRX2 and ScGR should recycle NADP⁺ 8.64×10^5 times within 1 h, resulting in a high TTN.

Oxidized sugar intermediates are often used in both traditional chemoenzymatic synthesis and contemporary synthetic biology developments.^{31,32,49–52} Hence, the efficiency of the ScGR/EcGRX2 recycling system was tested for the production of 6-phosphogluconate (6-PG), a common intermediate in glucose-utilizing metabolic pathways such as the pentose-phosphate⁵³ and Entner–Doudoroff pathways.⁵⁴ To this end D-glucose was incubated with the commercially available enzymes hexokinase (HK), which catalyzes the addition of phosphate to C-6 of D-glucose, and glucose 6-phosphate dehydrogenase (G6PDH) (Figure 3). The gluta-

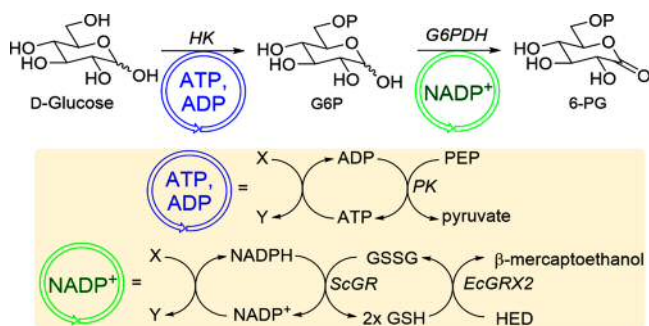


Figure 3. Conversion of D-glucose to 6-phosphogluconate by hexokinase (HK) and glucose 6-phosphate dehydrogenase (G6PDH). The ATP/ADP and NADP⁺ recycling systems are composed of pyruvate kinase (PK), glutathione reductase (ScGR), and glutaredoxin (EcGRX2).

thione coupling enzymes ScGR and EcGRX2, the recycling reagent GSH, and the latent oxidizing reagent HED were added to regenerate NADP⁺. A downfield shift from ~ 96 and 92 ppm (64% β and 36% α anomer, respectively) of the resonance of C-1 to ~ 178 ppm in the ¹³C NMR spectrum showed that the substrate was efficiently converted to 6-PG (Figure S1 in the Supporting Information). The maximum TTN achieved with the enzyme pair ScGR/EcGRX2 recycling system was 5×10^5 (Table S3 in the Supporting Information), which together with the low cost of HED (\$3.27 per mole) shows that ScGR/EcGR can form a NADP⁺ recycling system that is commercially viable on an industrial scale. This system is also compatible with pyruvate kinase, which is used to recycle ATP in the first step of the pathway.⁵⁰ Cystine, though sparingly soluble, can also act as a latent oxidizing agent; it efficiently recycled NADP⁺ and converted glucose to 6PG (see Supporting Information).

To further examine the potential of the ScGR/EcGRX2 recycling system, an additional NADP⁺-dependent enzyme, 6-phosphogluconate dehydrogenase (6-PGDH), on the pathway to guanosine monophosphate (GMP) was added (Figure 4). 6-PGDH catalyzes the conversion of 6-PG to ribulose 5-

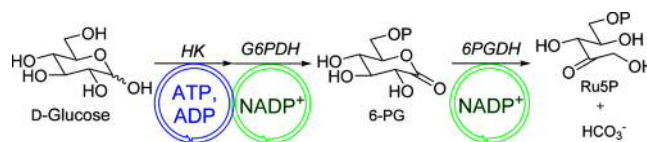


Figure 4. Conversion of D-glucose to ribulose 5-phosphate (Ru5P) by hexokinase (HK), glucose 6-phosphate dehydrogenase (G6PDH), and 6-phosphogluconate dehydrogenase (6PGDH). Details of the ATP and NADP⁺ recycling systems are described in Figure 3 and in the text.

phosphate (Ru5P).⁵³ Two characteristic downfield chemical shifts corresponding to C-2 of Ru5P (δ 213 ppm) and the byproduct bicarbonate (δ 160 ppm) indicated complete oxidative decarboxylation (Figure S2 in the Supporting Information).

The ScGR/EcGRX2 recycling system was then combined with eight enzymes to produce in a one-pot reaction ¹³C-labeled GMP,^{31,32,49} which is used in many biochemical studies, including structural and functional analysis of RNA^{51,55,56} and metabolomic investigations.^{57–59} The above Ru-5P biosynthetic pathway was extended by incorporating phosphoriboisomerase (PRI) and ribose-phosphate pyrophosphokinase (PRS), which catalyze the isomerization of Ru-5P and the addition of pyrophosphate to the C-1 position, respectively (Figure 5). The resulting intermediate phosphoribose pyrophosphate (PRPP) is chemically labile at room temperature and was transformed into GMP in situ with xanthine-guanine phosphoribosyl transferase (XGPRT). Guanine is only sparingly soluble at neutral pH, and while it has been suggested previously that the reaction can proceed as a slurry,⁴⁹ the heterogenous nature of the reaction led to poor reproducibility and increased reaction times of up to 1 day. Hence, guanine was dissolved at increased pH (50 mM KOH), where it shows good solubility, and added in a dropwise fashion to the reaction mixture. Under these conditions 70–80% GMP (Figure S3 in the Supporting Information) was reproducibly obtained within 2 h from D-glucose. Because PRPP formation requires ATP, which is converted to AMP as the byproduct, myokinase (MK) was included to generate ADP, which is subsequently converted to ATP in a PK-catalyzed reaction that uses phosphoenol pyruvate (PEP) as the phosphate donor. Together, this work illustrated that ScGR/EcGRX2 pair is compatible with eight enzymes, including six biosynthetic enzymes and two ATP-recycling enzymes.

CONCLUSIONS

Developing an efficient and highly compatible NADP⁺ recycling process is an essential step toward integrating enzymatic oxidation into the production of high-value chemicals.^{14,15} With small, inert organic disulfides as oxidizing agents, the ScGR/EcGRX2 pair can regenerate NADP⁺ up to 5×10^5 times, well in excess of the best TTNs of 1×10^3 reported so far.²⁵ Accordingly, each cycle of regeneration is 99.9998% selective for the formation of the active cofactor. With such selectivity, the cost of NADP⁺ can be reduced to < \$0.05 per mole of product formed. In practice, the ScGR/EcGRX2 pair was shown to be compatible with several biosynthetic enzymes, including ATP-recycling kinases, in the production of crucial synthons such as 6-PG, 5RuP, and GMP. This system also offers an attractive synthetic pathway for the production of isotopically labeled compounds. In addition, GRX is able to produce useful “byproducts” such as β -mercaptoethanol, which can protect enzymes, reagents, and

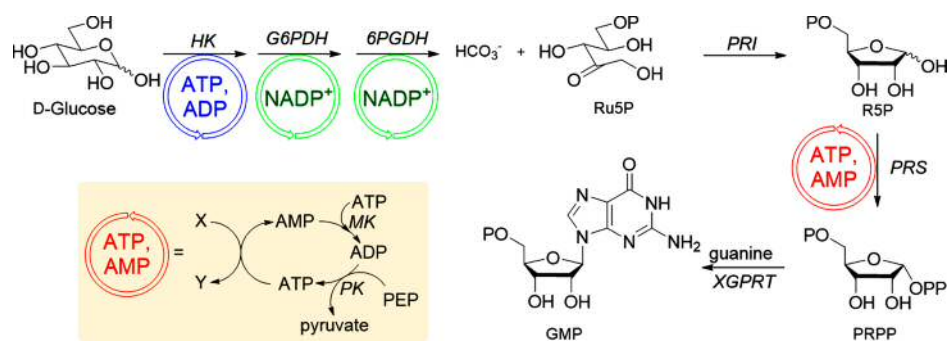


Figure 5. Conversion of D-glucose to GMP by hexokinase (HK), glucose 6-phosphate dehydrogenase (G6PDH), 6-phosphogluconate dehydrogenase (6PGDH), phosphoribose isomerase (PRI), ribose-phosphate pyrophosphokinase (PRS) and xanthine-guanine phosphoribosyl transferase (XGPRT). The ATP/AMP recycling system composed of myokinase (MK), pyruvate kinase (PK), and phosphoenol pyruvate (PEP) is illustrated. The ATP/ADP and NADP⁺ recycling systems are described in Figure 3 and in the text.

products from unwanted oxidative damage. GRX has previously been shown to enhance protein stability by preventing proteins from oxidative misfolding and aggregation.^{60–62} The system developed here is atom efficient in that there are reagents serving more than one role. Finally, unlike other NADP⁺ recycling schemes, including the NOX and laccase/mediator systems, the ScGR/EcGRX2 pair is oxygen-independent and is functional in aerobic as well as anaerobic environments and is therefore compatible with oxygen-sensitive biocatalysts such as P450s. The ScGR/EcGRX2 based NADP⁺ recycling systems is superior to all existing methods for cofactor regeneration and offers many advantages for commercial and academic users.

■ ASSOCIATED CONTENT

● Supporting Information

The Supporting Information is available free of charge on the ACS Publications website at DOI: 10.1021/acscatal.6b03061.

Full experimental procedures and tabulated experimental data for TTN (PDF)

■ AUTHOR INFORMATION

Corresponding Author

*E-mail for R.K.A.: allemanrk@cf.ac.uk.

ORCID

William M. Dawson: 0000-0003-2710-6879

Rudolf K. Allemann: 0000-0002-1323-8830

Present Address

[†]School of Chemistry, University of Bristol, Cantock's Close, Bristol BS8 1TS, United Kingdom.

Notes

The authors declare no competing financial interest.

■ ACKNOWLEDGMENTS

The authors thank Dr. James R. Williamson at the Scripps Research Institute for his kind gift of the *prsA* gene in a pET22-HT plasmid. This work was supported by Cardiff University through a President's Research Scholarship to A.A. and the UK's Biotechnology and Biological Sciences Research Council (BBSRC) through grants BB/J005266/1 and BB/L020394/1 to R.K.A.

■ REFERENCES

(1) Gamemara, D. *Redox biocatalysis: fundamentals and applications*, 1st ed.; Wiley: Hoboken, NJ, 2013.

(2) Zhao, H.; van der Donk, W. A. *Curr. Opin. Biotechnol.* **2003**, *14*, 583–589.

(3) Sheldon, R. A. *Chem. Soc. Rev.* **2012**, *41*, 1437–1451.

(4) Wu, H.; Tian, C. Y.; Song, X. K.; Liu, C.; Yang, D.; Jiang, Z. Y. *Green Chem.* **2013**, *15*, 1773–1789.

(5) Huisman, G. W.; Liang, J.; Krebber, A. *Curr. Opin. Chem. Biol.* **2010**, *14*, 122–129.

(6) Ma, S. K.; Gruber, J.; Davis, C.; Newman, L.; Gray, D.; Wang, A.; Grate, J.; Huisman, G. W.; Sheldon, R. A. *Green Chem.* **2010**, *12*, 81–86.

(7) Liang, J.; Lalonde, J.; Borup, B.; Mitchell, V.; Mundorff, E.; Trinh, N.; Kochrekar, D. A.; Cherat, R. N.; Pai, G. G. *Org. Process Res. Dev.* **2010**, *14*, 193–198.

(8) Wong, C. H.; Whitesides, G. M. *J. Am. Chem. Soc.* **1981**, *103*, 4890–4899.

(9) Wong, C. H.; Drueckhammer, D. G.; Sweers, H. M. *J. Am. Chem. Soc.* **1985**, *107*, 4028–4031.

(10) Seelbach, K.; Riebel, B.; Hummel, W.; Kula, M. R.; Tishkow, V. I.; Egorov, A. M.; Wandrey, C.; Kragl, U. *Tetrahedron Lett.* **1996**, *37*, 1377–1380.

(11) Hoelsch, K.; Sührer, I.; Heusel, M.; Weuster-Botz, D. *Appl. Microbiol. Biotechnol.* **2013**, *97*, 2473–2481.

(12) Woodyer, R.; van der Donk, W. A.; Zhao, H. *Biochemistry* **2003**, *42*, 11604–11614.

(13) Rodriguez, C.; Gotor, V. *Curr. Org. Chem.* **2012**, *16*, 2525–2541.

(14) Hollmann, F.; Arends, I. W. C.; Buehler, K.; Schallmeyer, A.; Bühler, B. *Green Chem.* **2011**, *13*, 226–265.

(15) Robins, K.; Osorio-Lozada, A. *Catal. Sci. Technol.* **2012**, *2*, 1524–1530.

(16) Wong, C. M.; Wong, K. H.; Chen, X. D. *Appl. Microbiol. Biotechnol.* **2008**, *78*, 927–938.

(17) Bučko, M.; Gemeiner, P.; Schenk Mayerová, A.; Krajčovič, T.; Rudroff, F.; Mihovilovič, M. D. *Appl. Microbiol. Biotechnol.* **2016**, *100*, 6585–6599.

(18) Schmidt, S.; Scherkus, C.; Muschiol, J.; Menyes, U.; Winkler, T.; Hummel, W.; Gröger, H.; Liese, A.; Herz, H. G.; Bornscheuer, U. T. *Angew. Chem., Int. Ed.* **2015**, *54*, 2784–2787.

(19) Knaus, T.; Mutti, F. G.; Humphreys, L. D.; Turner, N. J.; Scrutton, N. S. *Org. Biomol. Chem.* **2015**, *13*, 223–233.

(20) Mutti, F. G.; Knaus, T.; Scrutton, N. S.; Breuer, M.; Turner, N. J. *Science* **2015**, *349*, 1525–1529.

(21) Brummund, J.; Sonke, T.; Müller, M. *Org. Process Res. Dev.* **2015**, *19*, 1590–1595.

(22) Braun, M.; Link, H.; Liu, L.; Schmid, R. D.; Weuster-Botz, D. *Biotechnol. Bioeng.* **2011**, *108*, 1307–1317.

(23) Jiao, X. C.; Zhang, Y. J.; Chen, Q.; Pan, J.; Xu, J. H. *Catal. Sci. Technol.* **2016**, *6*, 7094–7100.

(24) Hoyos, P.; Sinisterra, J. V.; Molinari, F.; Alcantara, A. R.; De Maria, P. D. *Acc. Chem. Res.* **2010**, *43*, 288–299.

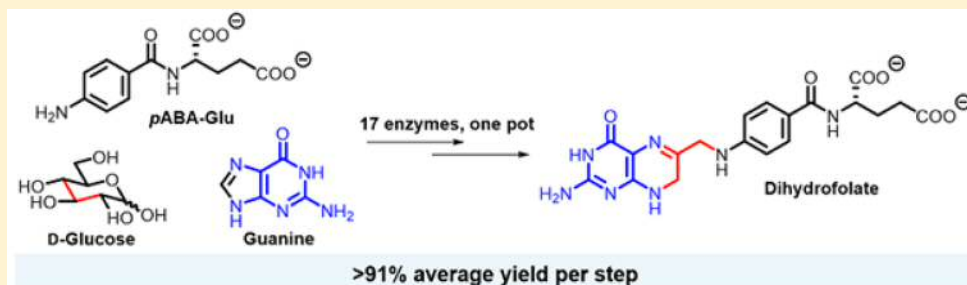
- (25) Wong, C. H.; McCurry, S. D.; Whitesides, G. M. *J. Am. Chem. Soc.* **1980**, *102*, 7938–7939.
- (26) Romano, D.; Villa, R.; Molinari, F. *ChemCatChem* **2012**, *4*, 739–749.
- (27) Patel, R. N. *ACS Catal.* **2011**, *1*, 1056–1074.
- (28) Chenault, H. K.; Whitesides, G. M. *Appl. Biochem. Biotechnol.* **1987**, *14*, 147–197.
- (29) Chenault, H. K.; Simon, E. S.; Whitesides, G. M. *Biotechnol. Genet. Eng. Rev.* **1988**, *6*, 221–270.
- (30) Lee, L. G.; Whitesides, G. M. *J. Org. Chem.* **1986**, *51*, 25–36.
- (31) Schultheisz, H. L.; Szymczyna, B. R.; Scott, L. G.; Williamson, J. R. *ACS Chem. Biol.* **2008**, *3*, 499–511.
- (32) Schultheisz, H. L.; Szymczyna, B. R.; Scott, L. G.; Williamson, J. R. *J. Am. Chem. Soc.* **2011**, *133*, 297–304.
- (33) Boyer, P. D. *The enzymes*, 3rd ed.; Academic Press: New York, London, 1975; Vol. 11, Oxidation-reduction Part A, Dehydrogenases (I), electron transfer (I).
- (34) Zhu, L.; Xu, X.; Wang, L.; Dong, H.; Yu, B.; Ma, Y. *Appl. Environ. Microbiol.* **2015**, *81*, 6294–6301.
- (35) Riebel, B. R.; Gibbs, P. R.; Wellborn, W. B.; Bommarius, A. S. *Adv. Synth. Catal.* **2003**, *345*, 707–712.
- (36) Wu, X.; Kobori, H.; Orita, I.; Zhang, C.; Imanaka, T.; Xing, X. H.; Fukui, T. *Biotechnol. Bioeng.* **2012**, *109*, 53–62.
- (37) Pham, N. H.; Hollmann, F.; Kracher, D.; Preims, M.; Haltrich, D.; Ludwig, R. *J. Mol. Catal. B: Enzym.* **2015**, *120*, 38–46.
- (38) Holmgren, A.; Johansson, C.; Berndt, C.; Lönn, M. E.; Hudemann, C.; Lillig, C. H. *Biochem. Soc. Trans.* **2005**, *33*, 1375–1377.
- (39) Sies, H. *Free Radical Biol. Med.* **1999**, *27*, 916–921.
- (40) Lillig, C. H.; Berndt, C.; Holmgren, A. *Biochim. Biophys. Acta, Gen. Subj.* **2008**, *1780*, 1304–1317.
- (41) Bushweller, J. H.; Aaslund, F.; Wüthrich, K.; Holmgren, A. *Biochemistry* **1992**, *31*, 9288–9293.
- (42) Vlamis-Gardikas, A.; Holmgren, A. *Methods Enzymol.* **2002**, *347*, 286–296.
- (43) Luthman, M.; Holmgren, A. *J. Biol. Chem.* **1982**, *257*, 6686–6690.
- (44) Holmgren, A.; Aslund, F. *Methods Enzymol.* **1995**, *252*, 283–292.
- (45) Aslund, F.; Ehn, B.; Miranda-Vizuete, A.; Pueyo, C.; Holmgren, A. *Proc. Natl. Acad. Sci. U. S. A.* **1994**, *91*, 9813–9817.
- (46) Chenas, N. K.; Rakauskene, G. A.; Kulis, I. I. *Biokhimiia* **1989**, *54*, 1090–1097.
- (47) Aslund, F.; Spyrou, G.; Bergman, T.; Holmgren, A. *J. Biol. Chem.* **1997**, *272*, 11236–11243.
- (48) Massey, V.; Williams, C. H. *J. Biol. Chem.* **1965**, *240*, 4470–4480.
- (49) Tolbert, T. J.; Williamson, J. R. *J. Am. Chem. Soc.* **1996**, *118*, 7929–7940.
- (50) Gross, A.; Abril, O.; Lewis, J. M.; Geresh, S.; Whitesides, G. M. *J. Am. Chem. Soc.* **1983**, *105*, 7428–7435.
- (51) Longhini, A. P.; LeBlanc, R. M.; Becette, O.; Salguero, C.; Wunderlich, C. H.; Johnson, B. A.; D'Souza, V. M.; Kreutz, C.; Dayie, T. K. *Nucleic Acids Res.* **2016**, *44*, e52.
- (52) Zhu, Z.; Kin Tam, T.; Sun, F.; You, C.; Percival Zhang, Y. H. *Nat. Commun.* **2014**, *5*, 3026.
- (53) Stincone, A.; Prigione, A.; Cramer, T.; Wamelink, M. M. C.; Campbell, K.; Cheung, E.; Olin-Sandoval, V.; Gruning, N. M.; Kruger, A.; Alam, M. T.; Keller, M. A.; Breitenbach, M.; Brindle, K. M.; Rabinowitz, J. D.; Ralser, M. *Biol. Rev.* **2015**, *90*, 927–963.
- (54) Conway, T. *FEMS Microbiol. Lett.* **1992**, *103*, 1–28.
- (55) Duss, O.; Diarra Dit Konté, N.; Allain, F. H. *Methods Enzymol.* **2015**, *565*, 537–562.
- (56) Lu, K.; Miyazaki, Y.; Summers, M. F. *J. Biomol. NMR* **2010**, *46*, 113–125.
- (57) Bracher, A.; Eisenreich, W.; Schramek, N.; Ritz, H.; Gotze, E.; Herrmann, A.; Gutlich, M.; Bacher, A. *J. Biol. Chem.* **1998**, *273*, 28132–28141.
- (58) Illarionova, V.; Eisenreich, W.; Fischer, M.; Haussmann, C.; Romisch, W.; Richter, G.; Bacher, A. *J. Biol. Chem.* **2002**, *277*, 28841–28847.
- (59) Bracher, A.; Fischer, M.; Eisenreich, W.; Ritz, H.; Schramek, N.; Boyle, P.; Gentili, P.; Huber, R.; Nar, H.; Auerbach, G.; Bacher, A. *J. Biol. Chem.* **1999**, *274*, 16727–16735.
- (60) Cheng, N. H.; Liu, J. Z.; Brock, A.; Nelson, R. S.; Hirschi, K. D. *J. Biol. Chem.* **2006**, *281*, 26280–26288.
- (61) Bandyopadhyay, S.; Starke, D. W.; Mieryl, J. J.; Gronostajski, R. M. *J. Biol. Chem.* **1998**, *273*, 392–397.
- (62) Davis, D. A.; Newcomb, F. M.; Starke, D. W.; Ott, D. E.; Mieryl, J. J.; Yarchoan, R. *J. Biol. Chem.* **1997**, *272*, 25935–25940.

Chemoenzymatic Assembly of Isotopically Labeled Folates

Antonio Angelastro, William M. Dawson,[†] Louis Y. P. Luk, E. Joel Loveridge,[‡] and Rudolf K. Allemann^{*†}

School of Chemistry, Cardiff University, Park Place, Cardiff CF10 3AT, United Kingdom

Supporting Information



ABSTRACT: Pterin-containing natural products have diverse functions in life, but an efficient and easy scheme for their in vitro synthesis is not available. Here we report a chemoenzymatic 14-step, one-pot synthesis that can be used to generate ¹³C- and ¹⁵N-labeled dihydrofolates (H₂F) from glucose, guanine, and *p*-aminobenzoyl-L-glutamic acid. This synthesis stands out from previous approaches to produce H₂F in that the average yield of each step is >91% and it requires only a single purification step. The use of a one-pot reaction allowed us to overcome potential problems with individual steps during the synthesis. The availability of labeled dihydrofolates allowed the measurement of heavy-atom isotope effects for the reaction catalyzed by the drug target dihydrofolate reductase and established that protonation at N5 of H₂F and hydride transfer to C6 occur in a stepwise mechanism. This chemoenzymatic pterin synthesis can be applied to the efficient production of other folates and a range of other natural compounds with applications in nutritional, medical, and cell-biological research.

INTRODUCTION

Pterin is a common motif found in natural products. Folate, the essential vitamin that fuels the one-carbon cycle for the biosynthesis of nucleotide and amino acid building blocks, was one of the first natural products found to contain pterin.^{1,2} The metabolic importance of pterins is illustrated by their integration into enzyme cofactors such as molybdopterin and tetrahydrobiopterin.^{3–5} Pterin natural products are also used as pigments in the butterflies *Catopsilia argante* and *Appias nero*,⁶ whereas biopterin- α -glucoside serves as a natural sunscreen that protects cellular contents from photoinduced damage in photosynthetic cyanobacteria.⁷

5,6,7,8-Tetrahydrofolic acid (H₄F), which in addition to the pterin ring system contains *p*-aminobenzoic acid (*p*ABA) and L-glutamic acid (Glu), is required for the biosynthesis of metabolites that are key for cell survival and replication.² A one-carbon unit in different oxidation states can be added at N5 and/or N10 of H₄F and used to produce metabolites such as thymidylate, purines, glycine, serine, and S-adenosylmethionine (SAM) (Figure 1).⁸ Because of the central importance of folate biochemistry for cell replication and survival, dihydrofolate reductase (DHFR), thymidylate synthase (TS), and serine hydroxymethyltransferase (SHMT) have long been exploited as important drug targets in the treatment of bacterial infections,⁹ malaria,^{10,11} and cancer,^{12,13} and the DHFR-targeting drugs trimethoprim, proguanil, pyrimethamine, and methotrexate are

listed as essential medicines by the World Health Organization (WHO).¹⁴ Nevertheless, as with many clinically used drugs, resistance to antifolates has begun to emerge,^{15–17} and investigation of the enzymes of the one-carbon cycle is an important part of inhibitor design strategies.¹⁸

Detailed mechanistic insight into enzyme-catalyzed reactions is often obtained by isotopic labeling and measurement of kinetic isotope effects (KIEs)^{19–22} or spectroscopic analysis.^{23,24} Information derived from regio- and stereospecific substrate labeling has been used to design inhibitors with dissociation constants in the micro- to picomolar range.²⁵ However, the use of these techniques to investigate folate-dependent enzymes is hindered by the absence of a general and efficient method to specifically label atoms of the pterin ring system, particularly at N5, C6, C7, and C9, which are directly linked to the chemistry of the catalyzed reactions. Folate and its derivatives can be synthesized by connecting the pterin, *p*ABA, and glutamate groups in sequential order,²⁶ and several synthetic strategies to incorporate an isotopic label into pterin in a regiospecific manner have been reported.^{27–30} Pterins have been synthesized by condensing guanidine or dihydroxyacetone with the respective heterocyclic starting materials, and N5-, C2-, and C6-labeled folates have been made previously.^{27,28} However, because symmetric

Received: June 19, 2017

Published: August 18, 2017

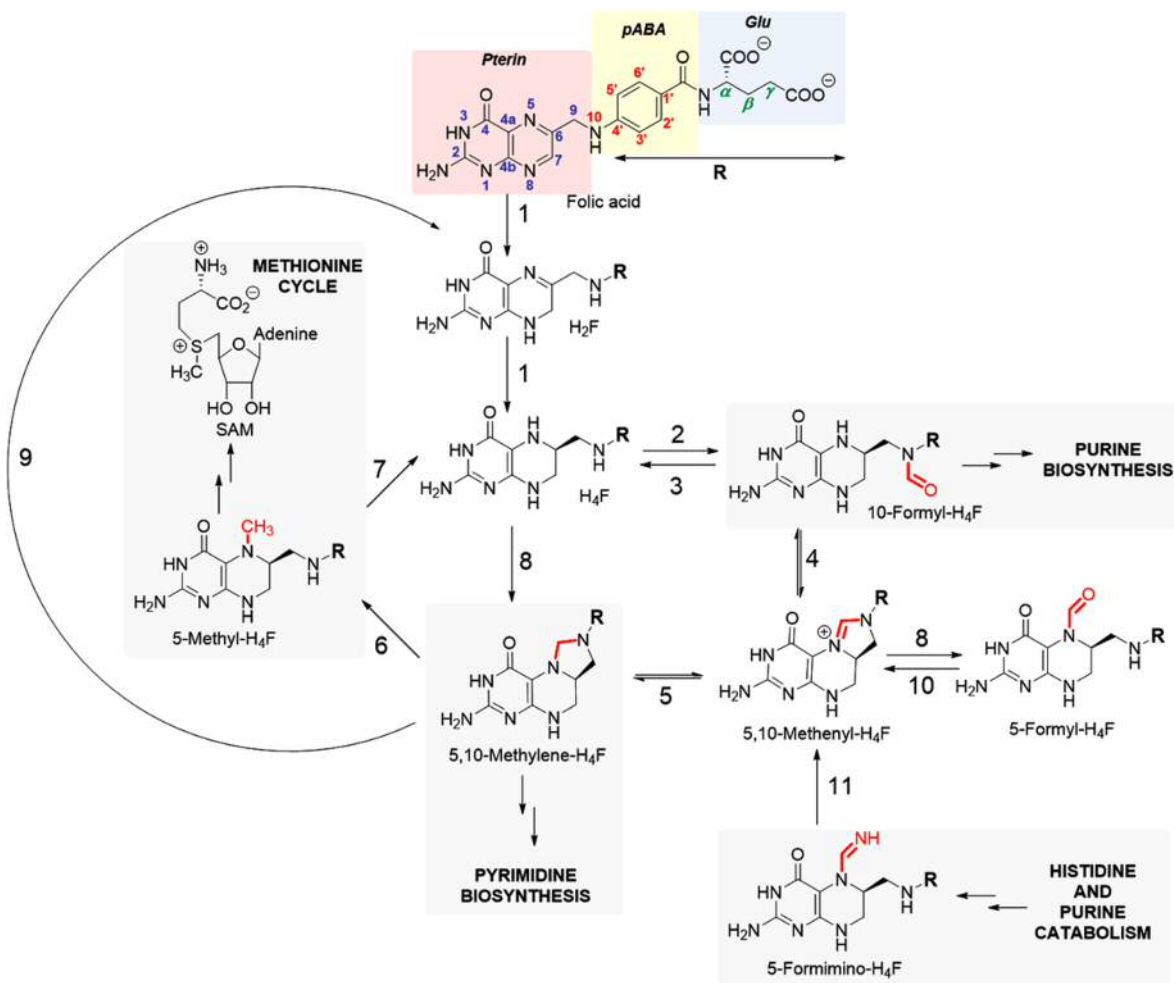


Figure 1. Folate coenzymes in one-carbon metabolism. Folic acid is converted to 7,8-dihydrofolic acid (H_2F) and 5,6,7,8-tetrahydrofolic acid (H_4F). One-carbon units attached to H_4F are highlighted. Abbreviations: 1, dihydrofolate reductase (DHFR); 2, 10-formyl- H_4F synthetase (FTHFS); 3, 10-formyl- H_4F dehydrogenase (FDH); 4, 5,10-methenyl- H_4F cyclohydrolase (MTHFC); 5, 5,10-methylene- H_4F dehydrogenase (MTHFD); 6, 5,10-methylene- H_4F reductase (MTHFR); 7, methionine synthase (MS); 8, serine hydroxymethyltransferase (SHMT); 9, thymidylate synthase (TS); 10, 5,10-methenyl- H_4F synthetase (MTHFS); 11, 5-formimino- H_4F cyclodeaminase (FTCD); SAM, S-adenosylmethionine.

reagents are used in these syntheses, regioselective isotope labeling of C7 and C9 cannot easily be achieved.^{28,30} In all cases, the yields of labeled folate or derivatives are low (<5% overall yield), and the procedures depend on multiple purification steps. Chemoenzymatic strategies have also been described,^{31–33} whereby H_4F was condensed with ^{11}C -formaldehyde or ^{14}C -formic acid to yield the corresponding isotopically labeled [^{11}C]5,10-methylene- H_4F , [^{14}C]5-formyl- H_4F , and [^{14}C]10-formyl- H_4F . However, a general and efficient method to label the pterin ring in folates has never been developed.

In nature, the pterin ring in folate is formed from guanosine triphosphate (GTP) in one biochemical step catalyzed by GTP cyclohydrolase (GTP-CH),^{34,35} an enzyme found in all kingdoms of life ranging from archaeobacteria, insects, plants to humans. In all GTP-CH-catalyzed reactions, GTP is converted to a pterin via a set of tandem reactions that have no equivalent in organic chemistry. GTP cyclohydrolase I (GTP-CH-I) catalyzes the formation of 7,8-dihydropterin triphosphate (DHNTTP) from GTP by mediating four distinct chemical reactions (Figure S1): hydrolysis of the purine ring yielding an *N*-formyl intermediate, *N*-deformylation, a stereospecific Amadori rearrangement of the ribose moiety, and ring closure to form the pterin.^{36–38} Because no symmetric reagent is used in this

reaction, GTP-CH-I can be used to synthesize the pterin ring system of folate with heavy isotopes incorporated regio- and stereoselectively.³⁹ It is therefore surprising that GTP-CH-I has not been used in any *in vitro* enzymatic pathway to synthesize folates. Perhaps the low catalytic turnover ($k_{cat} = 0.05 s^{-1}$)⁴⁰ and the rather low stability of the product 7,8-dihydropterin⁴¹ toward oxygen and light have limited the use of GTP-CH-I in synthesis.

Here we report a 14-step one-pot chemoenzymatic synthesis of 7,8-dihydrofolic acid (H_2F) that exploits the well-established procedures to isotopically label GTP^{39,42,43} by using GTP-CH-I to site-specifically isotope-label pterins. The low enzymatic activity and product instability of GTP-CH-I were addressed by enzymatic coupling. By means of our methodology, H_2F enriched with stable isotopes at N5 and C6 could be synthesized efficiently in pure form in >30% yield from isotopically enriched D-glucose and guanine. Given the high degree of purity and isotopic enrichment (>97%; see the Supporting Information), heavy-atom KIEs could be measured to investigate the mechanism of the *Escherichia coli* DHFR (EcDHFR)-catalyzed reduction of H_2F to H_4F .

RESULTS AND DISCUSSION

In Vitro Synthesis of Folate. The biosynthetic pathway to folate in *E. coli* uses the building blocks D-glucose, guanine, and

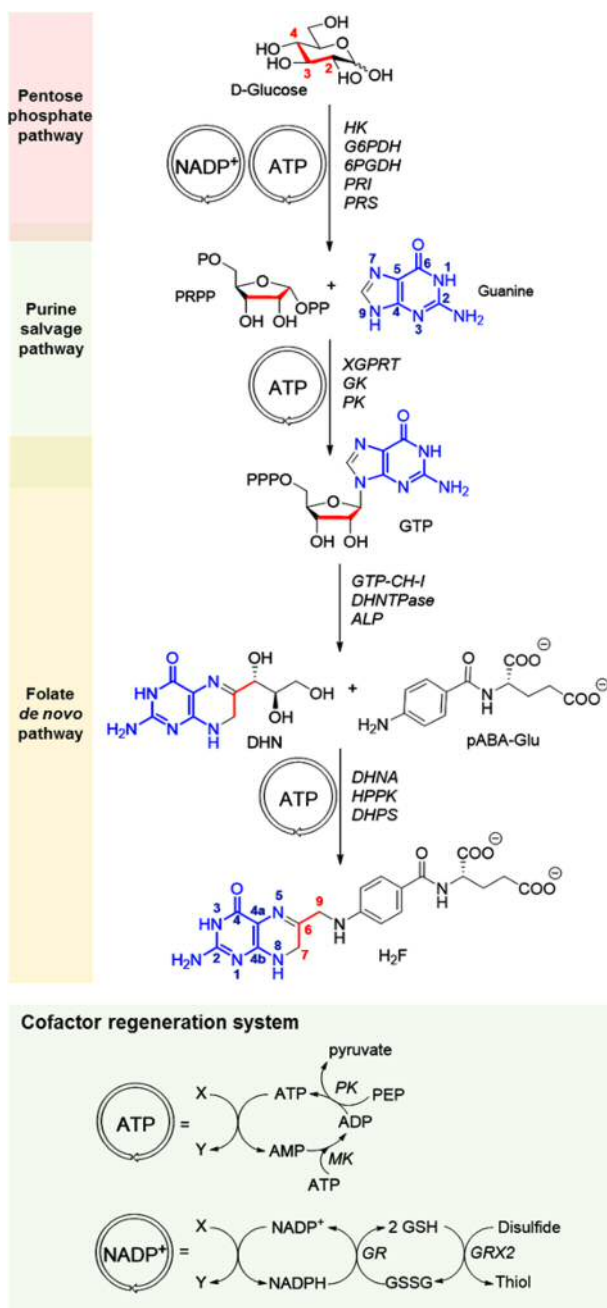


Figure 2. Strategy for the synthesis of 7,8-dihydrofolate (H_2F). Guanosine triphosphate (GTP) was made via the pentose phosphate and purine salvage pathways under hexokinase (HK), glucose 6-phosphate dehydrogenase (G6PDH), 6-phosphogluconate dehydrogenase (6PGDH), phosphoriboisomerase (PRI), ribose-phosphate pyrophosphokinase (PRS), xanthine guanine phosphoribosyl transferase (XGPRT), guanylate kinase (GK), and pyruvate kinase (PK) catalysis. In the folate de novo pathway, GTP is converted to 7,8-dihydroneopterin (DHN) under catalysis by GTP cyclohydrolase I (GTP-CH-I), 7,8-dihydroneopterin pyrophosphatase (DHNTase), and alkaline phosphatase (ALP); DHN is then converted to H_2F under catalysis by dihydroneopterin aldolase (DHNA), 6-hydroxymethyl 7,8-dihydropterin pyrophosphokinase (HPPK), and dihydropteroyl synthase (DHPS). The additional enzymes myokinase (MK), glutathione reductase (GR), and glutaredoxin 2 (GRX2) are used for the regeneration of ATP and $NADP^+$.^{44,45} The pterin atoms of H_2F derived from glucose (red) and guanine (blue) are highlighted. Details of each biosynthetic step are described in Figure S2.

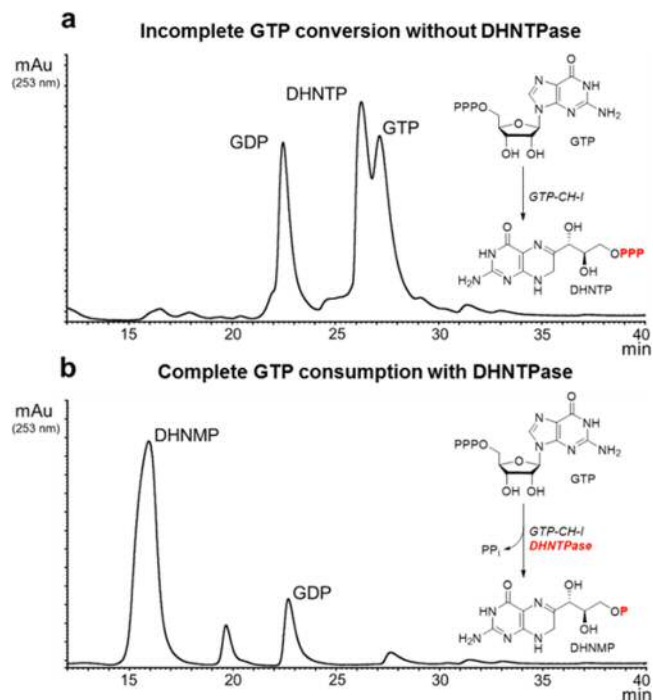


Figure 3. Conversion of guanosine triphosphate (GTP) into 7,8-dihydroneopterin triphosphate (DHNTp) and monophosphate (DHNMP). Shown are anion-exchange chromatography analyses of GTP incubated for 2 h at 37 °C with (a) GTP cyclohydrolase I (GTP-CH-I), which shows partial conversion to DHNTp, and (b) both GTP-CH-I and 7,8-dihydroneopterin triphosphate pyrophosphohydrolase (DHNTase), resulting in essentially complete conversion to DHNMP. Production of guanosine diphosphate (GDP) is most likely due to the nonenzymatic hydrolysis of GTP during incubation.

p-aminobenzoyl-L-glutamate (*p*ABA-Glu). In the biosynthetic scheme of H_2F (Figure 2), C2, C3, and C4 of glucose correspond to C7, C6, and C9 of H_2F and N1, C2, N3, C4, C5, C6, N7, and N9 of guanine correspond to N3, C2, N1, C4b, C4a, C4, N5, and N8 in H_2F . GTP is the key intermediate in this synthetic pathway, connecting the purine salvage pathway to de novo folate biosynthesis. Accordingly, a minimum of 14 enzymes need to be assembled *in vitro* to produce H_2F .

The GTP biosynthetic pathway is composed of enzymes from the pentose phosphate and purine salvage pathways (Figures 2 and S2). D-Glucose serves as the starting material, which is transformed into phosphoribose pyrophosphate (PRPP) in five steps that are catalyzed by hexokinase (HK), glucose 6-phosphate dehydrogenase (G6PDH), 6-phosphogluconate dehydrogenase (6PGDH), phosphoriboisomerase (PRI), and ribose-phosphate pyrophosphokinase (phosphoribosylpyrophosphate synthetase, PRS).⁴⁴ PRPP is then combined with guanine to form GMP under xanthine guanine phosphoribosyl transferase (XGPRT) catalysis. The resulting GMP is converted to the corresponding nucleotide triphosphate in reactions catalyzed by guanylate kinase (GK) and pyruvate kinase (PK). Since HK and GK use ATP as the phosphate source, PK can also function as the recycling enzyme. On the other hand, PRS uses ATP as the pyrophosphate source, so myokinase (MK) was included to regenerate ATP from AMP.⁴⁵ A significant amount of $NADP^+$ is also needed for GTP biosynthesis. Hence, the recently developed glutathione reductase (GR)/glutaredoxin 2 (GRX2) recycling system was used to regenerate the oxidized cofactor.⁴⁴ The GR/GRX2 system uses disulfides like 2-hydroxyethyl

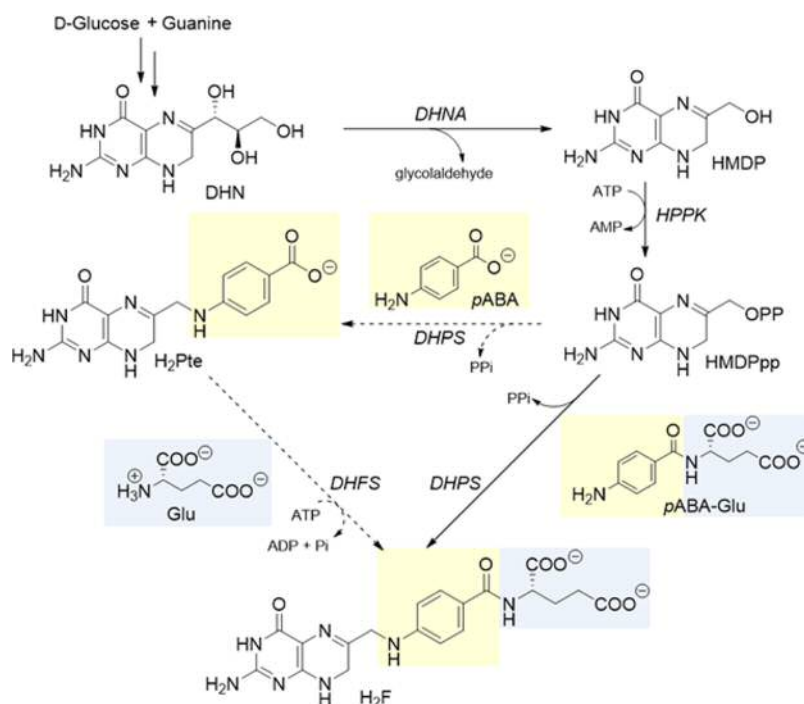


Figure 4. Conversion of 7,8-dihydroneopterin (DHN) to dihydrofolate (H_2F). Dihydroneopterin aldolase (DHNA) catalyzes the transformation of DHN to 6-hydroxymethyl-7,8-dihydropterin (HMDP), which is pyrophosphorylated by 6-hydroxymethyl 7,8-dihydropterin pyrophosphokinase (HPPK). The resulting 6-hydroxymethyl-7,8-dihydropterin pyrophosphate (HMDPpp) is converted to H_2F by dihydropterate synthase (DHPS), whose promiscuity allows the use of preassembled *pABA*-Glu as the substrate and the omission of dihydrofolate synthase (DHFS) in the *in vitro* synthetic pathway.

disulfide (HED or oxidized β -mercaptoethanol) or cystine as regenerating reagents and produces thiols as useful byproducts that protect the enzymes and intermediates from oxidative damage.

The conversion of GTP to DHNTP by GTP-CH-I marks the entry point of the folate *de novo* pathway. It has been reported that potassium and magnesium ions are positive allosteric effectors that can increase the rate of the GTP-CH-I reaction up to 5-fold.⁴⁶ The addition of these cations, however, was insufficient, as the reaction was found to be incomplete, giving a poor yield of DHNTP (Figure 3a). In folate *de novo* biosynthesis, dephosphorylation of DHNTP to 7,8-dihydroneopterin monophosphate (DHNMP) by DHNTP pyrophosphohydrolase (DHNTPase) is the biochemical step followed by the GTP-CH-I reaction (Figure 2).^{47,48} Knockout of the DHNTPase gene significantly impairs folate metabolism in *E. coli*,⁴⁸ which suggests that DHNTP phosphohydrolysis is a key regulatory step in folate metabolism. In other words, the activity of GTP-CH-I is most likely inhibited by its own product, DHNTP, which therefore needs to be immediately converted to DHNMP in order to sustain the activity of GTP-CH-I. In the presence of DHNTPase, GTP-CH-I showed a marked rate enhancement (Figure S3), with nearly complete conversion of GTP and a high yield of DHNMP (Figure 3b).

Additional enzymes are needed to convert DHNMP into folate. To the best of our knowledge, the natural enzyme responsible for the conversion of DHNMP to 7,8-dihydroneopterin (DHN) is unknown,^{37,48} and alkaline phosphatase (ALP) was used instead as a surrogate. DHN is subjected to a retro-aldol reaction catalyzed by dihydroneopterin aldolase (DHNA) to yield 6-hydroxymethyl-7,8-dihydropterin (HMDP),^{49,50} which then reacts with ATP in the presence of 6-hydroxymethyl 7,8-dihydropterin pyrophosphokinase (HPPK) (Figure 4).⁵¹

In *E. coli*, the resulting intermediate, 6-hydroxymethyl-7,8-dihydropterin pyrophosphate (HMDPpp), is first condensed with *pABA* and then with glutamate, catalyzed by dihydropterate synthase (DHPS)⁵² and dihydrofolate synthase (DHFS),⁵³ respectively, to finally generate H_2F . However, DHPS accepts preassembled *pABA*-Glu as a substrate,⁵⁴ so DHFS is not required in the *in vitro* reaction. The entire H_2F synthetic pathway requires only one purification step of the product, but ALP needs to be removed by ultrafiltration prior to the addition of DHNA, HPPK, and DHPS because the phosphatase can also catalyze the phosphorolysis of ATP and HMDPpp. Two additional modifications were made to further improve the overall yield. A N_2 -filled glovebox system was used because all reduced pterin-containing compounds, DHNTP, DHNMP, DHN, HMDP, HMDPpp, and the final product H_2F , are oxygen-sensitive.⁴¹ Also, cystine was found to be the preferred reagent over HED for the $NADP^+$ regeneration system operated by GR and GRX2. Perhaps β -mercaptoethanol made from the reduction of HED interferes with other enzymatic reactions, such as the chelation of Zn^{2+} in GTP-CH-I. The total turnover numbers for the regeneration of ATP from ADP by pyruvate kinase and from AMP by pyruvate kinase/myokinase are both ~ 100 ,⁵⁵ while the total turnover number for our GR/GRX2-based $NADP^+$ recycling system can reach 5×10^5 .⁴⁴ In general, a typical biosynthetic cascade produced 6.6 mg of H_2F from 9 mg of glucose in an overall yield of 30%, i.e., the average yield of each chemical transformation is in excess of 91%.

Synthesis of Selectively Labeled Folates. Five isotopically labeled H_2F s were synthesized using the newly developed *in vitro* pathway (Figure 5a). Liquid chromatography–high-resolution mass spectrometry (LC-HRMS) analysis of $[6-^{13}C]H_2F$, produced from $[3-^{13}C]D$ -glucose, showed an increase of ~ 1 amu; ^{13}C NMR spectroscopy revealed a singlet at 152 ppm.

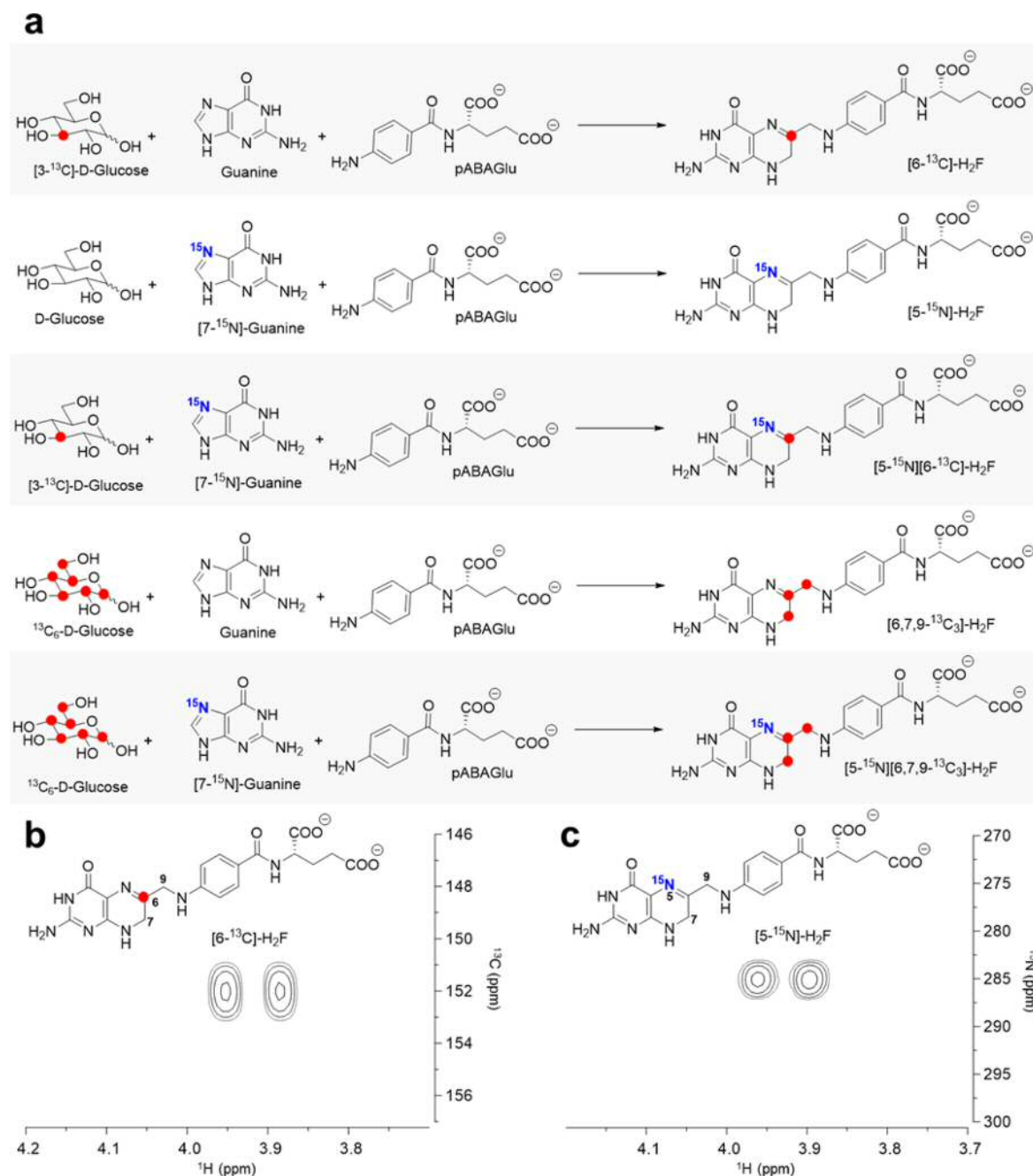


Figure 5. H₂Fs labeled with stable isotopes on the pterin ring system. (a) Patterns of isotopic distribution are determined by the starting material isotopic enrichment used during H₂F biosynthetic assembly. (b) ¹H,¹³C HMBC and (c) ¹H,¹⁵N HMBC spectra of [6-¹³C]H₂F and [5-¹⁵N]H₂F. Protons attached to C7 (3.95 ppm) and C9 (3.87 ppm) correlate to C6 (152 ppm) or N5 (285 ppm). ¹H NMR spectra of all compounds and additional 2D NMR characterization of [5-¹⁵N][6-¹³C]H₂F, [6,7,9-¹³C₃]H₂F and [5-¹⁵N][6,7,9-¹³C₃]H₂F are reported in Figures S12–S15. HRMS data for all of the compounds are given in Table S3 and Figures S16–S21. Isotopic enrichment was calculated to be at least 97% from the mass spectrometric data (as illustrated in Figures S22–S24).

Additionally, long-range coupling between 6-¹³C and protons on C7 and C9 of [6-¹³C]H₂F were observed in the ¹H,¹³C HMBC spectrum (Figure 5b).

To incorporate an ¹⁵N label into the pterin moiety at N5, [7-¹⁵N]guanine was used. The resulting product showed ~1 amu increase in LC-HRMS analysis and an ¹⁵N signal at 285 ppm coupling to C7 and C9 protons in the ¹H,¹⁵N HMBC spectrum (Figure 5c).

When [3-¹³C]D-glucose and [7-¹⁵N]guanine were combined to produce [5-¹⁵N][6-¹³C]H₂F, a mass increase of ~2 amu was measured. The ¹³C NMR spectrum showed a doublet at 152 ppm

with a coupling constant ¹J_{CN} of 7.5 Hz; long-range coupling between the protons on C7 and C9 was observed in the ¹H,¹³C HMBC and ¹H,¹⁵N HMBC spectra (see the Supporting Information), indicating that both N5 and C6 of H₂F were isotopically enriched.

Similarly, [6,7,9-¹³C₃]H₂F and [5-¹⁵N][6,7,9-¹³C₃]H₂F were synthesized from ¹³C₆-D-glucose and [7-¹⁵N]guanine, and their identities were confirmed by HRMS and NMR spectroscopy (see the Supporting Information).

Heavy-Atom Kinetic Isotope Effects on the Reaction Catalyzed by EcDHFR. The preparation of ¹³C- and ¹⁵N-labeled

dihydrofolates allowed the measurement of heavy-atom isotope effects for the reactions catalyzed by dihydrofolate reductase (DHFR), a key enzyme in one-carbon metabolism and a validated target for the treatment of bacterial infections, malaria, and cancer.⁵⁶ DHFR catalyzes the reduction of H₂F to H₄F via transfer of the pro-*R* hydride from C4 of NADPH to the *Re* face on C6 accompanied by protonation of N5 of H₂F (Figure 6).^{57,58}

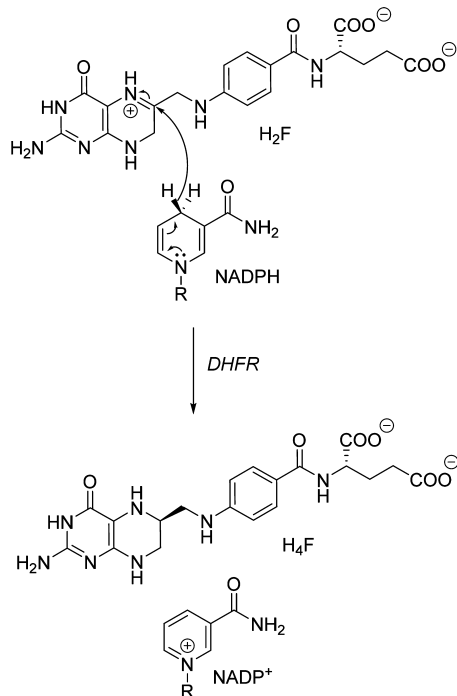


Figure 6. Reduction of 7,8-dihydrofolate (H₂F) to 5,6,7,8-tetrahydrofolate (H₄F) catalyzed by dihydrofolate reductase (DHFR).

Several aspects of the reaction mechanism warrant additional investigation. In particular, the transition state structure and the order of chemical transformation events have not been fully determined.^{59,60} The active site of DHFR provides a favorable environment for protonation of N5 by elevating the pK_a from 2.6 to 6.5 and using an active-site water as the proton source.^{61,62} Solvent and hydrogen KIE measurements combined with site-directed mutagenesis have suggested a stepwise mechanism in which protonation precedes hydride transfer.^{63,64} However, D₂O increases the viscosity of the reaction buffer relative to H₂O,^{65,66} and site-directed modification can alter the catalytic behavior of an enzyme.⁶⁷ Thus, additional mechanistic investigations are needed to establish the order of events. Since isotopic substitution does not alter the chemistry of the reaction but only the kinetics, [6-¹³C]H₂F and [5-¹⁵N]H₂F were used to measure the ¹⁵N and ¹³C heavy-atom kinetic isotope effects. Pre-steady-state kinetic measurements at 15 °C by fluorescence resonance energy transfer from the active-site tryptophan in DHFR to the reduced cofactor yield first-order hydride transfer rate constants with an accuracy of up to 0.7% (Figures S25–S27 and Table S4). While a ¹³C KIE of 1.015 ± 0.006 was observed for the reduction of [6-¹³C]H₂F, the corresponding ¹⁵N KIE for [5-¹⁵N]H₂F was essentially unity (0.999 ± 0.006) under the same conditions. To confirm this finding, [5-¹⁵N][6-¹³C]H₂F was used to probe both positions at the same time, and the measured value for the corresponding multiple heavy-atom KIE was 1.014 ± 0.008, which is statistically identical to that obtained when the substrate was labeled with ¹³C only.

The observed ¹⁵N KIE on hydride transfer indicates that protonation of N5 is not isotopically sensitive, likely because it is not rate-limiting under pre-steady-state conditions (as the reaction is essentially irreversible,⁵⁸ the observed KIE will tend to unity rather than to the equilibrium isotope effect).²² On the other hand, the measured ¹³C KIE indicates that the hydride transfer step is rate-determining. This strongly suggests a stepwise mechanism. If the protonation and hydride transfer steps were concerted, ¹⁵N- and ¹³C-labeled H₂Fs should both yield measurable KIEs;^{19,21,22} this interdependence may also lead to an additive effect in the multiple heavy-atom isotope effect measurement with the double-labeled substrate.^{19,21,22} In other words, our results suggest that the pre-steady-state kinetic measurement at pH 7.0 reveals only the step of hydride transfer because protonation of N5 is in rapid equilibrium and the ensemble of reaction-ready conformations is mostly populated with protonated H₂F. Importantly, these results confirm the validity of previous solvent KIE and site-directed mutagenesis studies, which also concluded that the sequence of chemical events (protonation and hydride transfer) is distinct and strictly ordered.^{64,68} Overall, the results provided here strongly support a mechanism where protonation and hydride transfer are independent of each other and occur in a stepwise fashion.

CONCLUSIONS

Dihydrofolate was produced enzymatically in an easy one-pot, high-yielding reaction sequence from glucose, guanine, and *p*ABA-Glu that required only a single purification step. Potential problems with individual steps during the synthesis could be overcome through the use of a one-pot reaction. This methodology can be used to generate dihydrofolates labeled in specific positions with stable isotopes with average overall yields of >30%, facilitating many applications in cell biology and mechanistic enzymology.^{27–29,61,69,70} For the first time, heavy-atom KIEs for the DHFR-catalyzed reduction of H₂F could be measured to provide strong support for a stepwise reduction of the substrate in which protonation at N5 and hydride transfer from C4 of the NADPH to C6 of protonated dihydrofolate proceed independently. This chemoenzymatic pterin synthesis can be integrated into other enzymatic procedures to generate folate derivatives^{31,32} and other high-value natural products that are not easily accessible by conventional synthesis.⁷¹ It can be applied to nutritional, medical, and cell-biological research to address questions of in vivo bioavailability and to explore the kinetics of folate metabolism in intact cells and organisms.^{70,72–76}

ASSOCIATED CONTENT

Supporting Information

The Supporting Information is available free of charge on the ACS Publications website at DOI: 10.1021/jacs.7b06358.

Full experimental procedures and supplementary figures and tables (PDF)

AUTHOR INFORMATION

Corresponding Author

*allemanrk@cardiff.ac.uk

ORCID

William M. Dawson: 0000-0003-2710-6879

E. Joel Loveridge: 0000-0002-8528-4019

Rudolf K. Allemann: 0000-0002-1323-8830

Present Addresses

[†]W.M.D.: School of Chemistry, University of Bristol, Cantock's Close, Bristol BS8 1TS, United Kingdom.

[‡]E.J.L.: Department of Chemistry, Swansea University, Singleton Park, Swansea SA2 8PP, United Kingdom.

Notes

The authors declare no competing financial interest.

ACKNOWLEDGMENTS

We are grateful to Dr. James R. Williamson (Scripps Research Institute) for his gift of *prsA*. The help of Dr. Rob Jenkins and Mr. Thomas Williams with mass spectrometry is gratefully acknowledged. This work was supported by Cardiff University through a President's Research Scholarship to A.A. and the UK's Biotechnology and Biological Sciences Research Council (BBSRC) through Grants BB/J005266/1 and BB/L020394/1 to R.K.A.

REFERENCES

- Hoffbrand, A. V.; Weir, D. G. *Br. J. Haematol.* **2001**, *113*, 579–589.
- Fox, J. T.; Stover, P. J. *Vitam. Horm.* **2008**, *79*, 1–44.
- Basu, P.; Burgmayer, S. J. *Coord. Chem. Rev.* **2011**, *255*, 1016–1038.
- Schwarz, G.; Mendel, R. R.; Ribbe, M. W. *Nature* **2009**, *460*, 839–847.
- Thöny, B.; Auerbach, G.; Blau, N. *Biochem. J.* **2000**, *347*, 1–16.
- Pfleiderer, W. *Adv. Exp. Med. Biol.* **1993**, *338*, 1–16.
- Noguchi, Y.; Ishii, A.; Matushima, A.; Haishi, D.; Yasumuro, K.; Moriguchi, T.; Wada, T.; Kodaera, Y.; Hiroto, M.; Nishimura, H.; Sekine, M.; Inada, Y. *Mar. Biotechnol.* **1999**, *1*, 207–210.
- Ducker, G. S.; Rabinowitz, J. D. *Cell Metab.* **2017**, *25*, 27–42.
- Murima, P.; McKinney, J. D.; Pethe, K. *Chem. Biol.* **2014**, *21*, 1423–1432.
- Nzila, A.; Ward, S. A.; Marsh, K.; Sims, P. F.; Hyde, J. E. *Trends Parasitol.* **2005**, *21*, 292–298.
- Nzila, A.; Ward, S. A.; Marsh, K.; Sims, P. F.; Hyde, J. E. *Trends Parasitol.* **2005**, *21*, 334–339.
- Locasale, J. W. *Nat. Rev. Cancer* **2013**, *13*, 572–583.
- Yang, M.; Vousden, K. H. *Nat. Rev. Cancer* **2016**, *16*, 650–662.
- WHO Model Lists of Essential Medicines, 19th ed.; World Health Organization: Geneva, Switzerland, 2015.
- Zhao, R.; Goldman, I. D. *Oncogene* **2003**, *22*, 7431–7457.
- Müller, I. B.; Hyde, J. E. *Mol. Biochem. Parasitol.* **2013**, *188*, 63–77.
- Sköld, O. Sulfonamides and Trimethoprim. In *Antimicrobial Drug Resistance*; Mayers, D. L., Ed.; Humana Press: New York, 2009; Vol. 1, pp 259–269.
- Copeland, R. A.; Harpel, M. R.; Tummino, P. J. *Expert Opin. Ther. Targets* **2007**, *11*, 967–978.
- Cleland, W. W. *Arch. Biochem. Biophys.* **2005**, *433*, 2–12.
- Vardi-Kilshtain, A.; Nitoker, N.; Major, D. T. *Arch. Biochem. Biophys.* **2015**, *582*, 18–27.
- Cook, P. F. *Isot. Environ. Health Stud.* **1998**, *34*, 3–17.
- O'Leary, M. H. *Annu. Rev. Biochem.* **1989**, *58*, 377–401.
- Wharton, C. W. *Nat. Prod. Rep.* **2000**, *17*, 447–453.
- Palmer, A. G. *Acc. Chem. Res.* **2015**, *48*, 457–65.
- Schramm, V. L. *Acc. Chem. Res.* **2015**, *48*, 1032–1039.
- Maunder, P.; Finglas, P.; Mallet, A.; Mellon, F.; Razzaque, M.; Ridge, B.; Vahteristo, L.; Witthoft, C. *J. Chem. Soc., Perkin Trans. 1* **1999**, 1311–1323.
- Cocco, L.; Groff, J. P.; Temple, C.; Montgomery, J. A.; London, R. E.; Matwiyoff, N. A.; Blakley, R. L. *Biochemistry* **1981**, *20*, 3972–3978.
- Selinsky, B. S.; Perlman, M. E.; London, R. E.; Unkefer, C. J.; Mitchell, J.; Blakley, R. L. *Biochemistry* **1990**, *29*, 1290–1296.
- Cheung, H. T. A.; Birdsall, B.; Frenkiel, T. A.; Chau, D. D.; Feeney, J. *Biochemistry* **1993**, *32*, 6846–6854.
- Cowart, M.; Falzone, C. J.; Benkovic, S. J. *J. Labelled Compd. Radiopharm.* **1994**, *34*, 67–71.
- Saeed, M.; Tewson, T. J.; Erdahl, C. E.; Kohen, A. *Nucl. Med. Biol.* **2012**, *39*, 697–701.
- Curthoys, N. P.; Scott, J. M.; Rabinowitz, J. C. *J. Biol. Chem.* **1972**, *247*, 1959–1964.
- Moran, R. G.; Keyomarsi, K.; Colman, P. D. *Methods Enzymol.* **1986**, *122*, 309–312.
- Gräwert, T.; Fischer, M.; Bacher, A. *IUBMB Life* **2013**, *65*, 310–322.
- Fischer, M.; Thöny, B.; Leimkühler, S. The biosynthesis of folate and pterins and their enzymology. In *Comprehensive Natural Products II*; Mander, L.; Liu, H.-W., Eds.; Elsevier: Oxford, U.K., 2010; Vol. 7, pp 599–648.
- Rebello, J.; Auerbach, G.; Bader, G.; Bracher, A.; Nar, H.; Hösl, C.; Schramek, N.; Kaiser, J.; Bacher, A.; Huber, R.; Fischer, M. *J. Mol. Biol.* **2003**, *326*, 503–516.
- Burg, A. W.; Brown, G. M. *Chem. Commun.* **1968**, *243*, 2349–2358.
- Yim, J. J.; Brown, G. M. *J. Biol. Chem.* **1976**, *251*, 5087–5094.
- Illarionova, V.; Eisenreich, W.; Fischer, M.; Haussmann, C.; Romisch, W.; Richter, G.; Bacher, A. *J. Biol. Chem.* **2002**, *277*, 28841–28847.
- Schramek, N.; Bracher, A.; Bacher, A. *J. Biol. Chem.* **2001**, *276*, 2622–2626.
- Dantola, M. L.; Vignoni, M.; Capparelli, A. L.; Lorente, C.; Thomas, A. H. *Helv. Chim. Acta* **2008**, *91*, 411–425.
- Schultheisz, H. L.; Szymczyna, B. R.; Scott, L. G.; Williamson, J. R. *ACS Chem. Biol.* **2008**, *3*, 499–511.
- Tolbert, T. J.; Williamson, J. R. *J. Am. Chem. Soc.* **1996**, *118*, 7929–7940.
- Angelastro, A.; Dawson, W. M.; Luk, Y. P. L.; Allemann, R. K. *ACS Catal.* **2017**, *7*, 1025–1029.
- Gross, A.; Abril, O.; Lewis, J. M.; Geresh, S.; Whitesides, G. M. *J. Am. Chem. Soc.* **1983**, *105*, 7428–7435.
- Schoedon, G.; Redweik, U.; Frank, G.; Cotton, R. G.; Blau, N. *Eur. J. Biochem.* **1992**, *210*, 561–568.
- Suzuki, Y.; Brown, G. M. *J. Biol. Chem.* **1974**, *249*, 2405–2410.
- Gabelli, S. B.; Bianchet, M. A.; Xu, W.; Dunn, C. A.; Niu, Z. D.; Amzel, L. M.; Bessman, M. J. *Structure* **2007**, *15*, 1014–1022.
- Mathis, J. B.; Brown, G. M. *J. Biol. Chem.* **1970**, *245*, 3015–3025.
- Wang, Y.; Li, Y.; Yan, H. *Biochemistry* **2006**, *45*, 15232–15239.
- Derrick, J. P. *Vitam. Horm.* **2008**, *79*, 411–433.
- Weisman, R. A.; Brown, G. M. *J. Biol. Chem.* **1964**, *239*, 326–331.
- Griffin, M. J.; Brown, G. M. *J. Biol. Chem.* **1964**, *239*, 310–316.
- Richey, D. P.; Brown, G. M. *Biochim. Biophys. Acta, Gen. Subj.* **1970**, *222*, 237–239.
- Chenault, H. K.; Simon, E. S.; Whitesides, G. M. *Biotechnol. Genet. Eng. Rev.* **1988**, *6*, 221–270.
- Schweitzer, B. I.; Dicker, A. P.; Bertino, J. R. *FASEB J.* **1990**, *4*, 2441–2452.
- Charlton, P. A.; Young, D. W.; Birdsall, B.; Feeney, J.; Roberts, G. C. K. *J. Chem. Soc., Perkin Trans. 1* **1985**, 1349–1353.
- Fierke, C. A.; Johnson, K. A.; Benkovic, S. J. *Biochemistry* **1987**, *26*, 4085–4092.
- Shrimpton, P.; Allemann, R. K. *Protein Sci.* **2002**, *11*, 1442–1451.
- Shrimpton, P.; Mullaney, A.; Allemann, R. K. *Proteins: Struct., Funct., Genet.* **2003**, *51*, 216–223.
- Chen, Y. Q.; Kraut, J.; Blakley, R. L.; Callender, R. *Biochemistry* **1994**, *33*, 7021–7026.
- Wan, Q.; Bennett, B. C.; Wilson, M. A.; Kovalevsky, A.; Langan, P.; Howell, E. E.; Dealwis, C. *Proc. Natl. Acad. Sci. U. S. A.* **2014**, *111*, 18225–18230.
- Stone, S. R.; Morrison, J. F. *Biochemistry* **1984**, *23*, 2753–2758.
- Liu, C. T.; Francis, K.; Layfield, J. P.; Huang, X.; Hammes-Schiffer, S.; Kohen, A.; Benkovic, S. J. *Proc. Natl. Acad. Sci. U. S. A.* **2014**, *111*, 18231–18236.
- Cioni, P.; Strambini, G. B. *Biophys. J.* **2002**, *82*, 3246–3253.
- Schowen, K. B.; Schowen, R. L. *Methods Enzymol.* **1982**, *87*, 551–606.
- Peracchi, A. *Trends Biochem. Sci.* **2001**, *26*, 497–503.

- (68) Loveridge, E. J.; Behiry, E. M.; Swanwick, R. S.; Allemann, R. K. *J. Am. Chem. Soc.* **2009**, *131*, 6926–6927.
- (69) Deng, H.; Callender, R.; Howell, E. *J. Biol. Chem.* **2001**, *276*, 48956–48960.
- (70) Mönch, S.; Netzel, M.; Netzel, G.; Rychlik, M. *Anal. Biochem.* **2010**, *398*, 150–160.
- (71) McCarty, R. M.; Somogyi, A.; Lin, G.; Jacobsen, N. E.; Bandarian, V. *Biochemistry* **2009**, *48*, 3847–3852.
- (72) Gregory, J. F., III; Williamson, J.; Liao, J.-F.; Bailey, L. B.; Toth, J. *P. J. Nutr.* **1998**, *128*, 1896–1906.
- (73) Gregory, J. F., III. *J. Nutr.* **2001**, *131*, 1376S–1382S.
- (74) Gregory, J. F., III; Quinlivan, E. P. *Annu. Rev. Nutr.* **2002**, *22*, 199–220.
- (75) Kopp, M.; Morisset, R.; Koehler, P.; Rychlik, M. *PLoS One* **2016**, *11*, e0156610.
- (76) de Ambrosis, A.; Vishnumohan, S.; Paterson, J.; Haber, P.; Arcot, J. *Eur. J. Clin. Nutr.* **2017**, *71*, 103–106.